uOttawa

L'Université canadienne
Canada's university

FACULTÉ DES ÉTUDES SUPÉRIEURES ET POSTOCTORALES

uOttawa

L'Université canadienne
Canada's university

FACULTY OF GRADUATE AND POSDOCTORAL STUDIES

Jessie Anne Blake

AUTEUR DE LA THÈSE / AUTHOR OF THESIS

Ph.D. (Chemistry)

GRADE / DEGREE

Faculty of Science – Department of Chemistry

FACULTÉ, ÉCOLE, DÉPARTEMENT / FACULTY, SCHOOL, DEPARTMENT

The Development of a Novel Photolabile Protecting Group Based on Xanthone Acetic Acid Photodecarboxylation for Corneal Drug Delivery

TITRE DE LA THÈSE / TITLE OF THESIS

Juan C. Scaiano

DIRECTEUR (DIRECTRICE) DE LA THÈSE / THESIS SUPERVISOR

CO-DIRECTEUR (CO-DIRECTRICE) DE LA THÈSE / THESIS CO-SUPERVISOR

Robert Ben

Robert Crutchley

Linda Johnston

Peter Wan (University of Victoria)

Gary W. Slater

Le Doyen de la Faculté des études supérieures et postdoctorales / Dean of the Faculty of Graduate and Postdoctoral Studies

The Development of a Novel Photolabile Protecting Group based on Xanthone Acetic Acid Photodecarboxylation for Corneal Drug Delivery

Jessie A. Blake

Thesis submitted to the Faculty of Graduate & Postdoctoral Studies
University of Ottawa
in partial fulfillment of the requirements for the
Ph. D. degree in the
Ottawa-Carleton Chemistry Institute

uOttawa

Candidate

Supervisor

Jessie A. Blake

J.C. Scaiano

Your file Votre référence
ISBN: 978-0-494-73923-5
Our file Notre référence
ISBN: 978-0-494-73923-5

Abstract

This thesis describes the development of a new photolabile protecting group. It spans the detailed characterisation of the photochemical mechanism to the application of this group towards a novel drug delivery method.

Photolabile protecting groups (PPGs) are essentially molecules (usually organic) that can be attached to another molecule of interest (often termed the 'effector') in a way that masks the activity of this second molecule. Upon excitation, the effector is released through a photochemical reaction allowing the rapid and controlled introduction of a high effector concentration. PPGs have been used in a wide variety of applications where either spatial or temporal control is desired. These include numerous dynamic biological studies, photolithography, and solid state synthesis to name a few.

The photochemical mechanism that forms the basis of our new PPG is the photodecarboxylation of 2-xanthone acetic acid. Using a number of steady state and time resolved techniques, we have established that decarboxylation proceeds from the singlet excited state of 2- and 4-xanthone acetic acids (2-XAA and 4-XAA) yielding a short-lived carbanion intermediate. Interestingly, in a stark example of the ortho-meta effect, 3-xanthone acetic acid (3-XAA) is photostable. The carbanion generated from either 2- or 4-XAA is formed efficiently and is subsequently protonated very rapidly ($\tau < 20$ ns) in aqueous solution. With proper substitution,

this reactive carbanion can be harnessed to eliminate anionic leaving groups on the subnanosecond timescale.

Both the release rate and efficiency of our PPGs represent a significant improvement over conventional PPGs. Additionally, the photochemistry of release is remarkably clean and the UVA absorption of the xanthone chromophore is quite high. For this reason, we have applied our new PPG to the development of a novel drug delivery method based on photorelease, a field that has not yet been greatly explored. More specifically, we have demonstrated the release of acyclovir, an antiviral commonly used for the treatment of ocular herpes simplex virus (HSV-1). We have also shown the ability of our PPG-acyclovir conjugate to suppress viral proliferation in corneal cells upon UVA irradiation.

Acknowledgements

I have been blessed with so many wonderful people in my life and I will be forever grateful to them.

Thanks first to my mom for always encouraging me to be the best person I can be, words cannot express all that I want to say. I am who I am today because of you.

Thanks to the rest of my family, to my dad and brother, my grandparents and Aunt Tam and all the other Findlays and Blakes. Your love and belief in me has given me so much strength. Thanks also to the Billones for your love over the past few years. Grazie.

Thanks to my adopted family, Keith Ingold. Keith you have truly led me down this path, first by igniting the research spark, then by giving me the confidence I needed to pursue a PhD, pointing me in the right direction (towards Tito) and supporting me through it all. I owe so much to you.

Thanks of course to Tito Scaiano for the opportunity to work on this exciting project and for all you have taught me about chemistry, research and life. I have always admired both your brilliance and your humanity.

I have thanked my two greatest mentors but as everyone knows behind every great man there is a greater woman, so thank you Cairine and Elda. You have both been wonderful beacons of positivity, always welcoming, always supportive.

Thanks once more to Tito for bringing together such an amazing group of

people. During my years in the group I have made many great friendships that I hope will last a lifetime. First to Matt Lukeman, you have evolved from a mentor into one of my dearest friends and I hope you know how much you and your ladies (Nicole, Anna and Kate) mean to me. Mathieu, you were honestly one of the deciding factors for me joining the group because as soon as I met you I knew we would be great friends. You'll always be that third leg of the tripod. Michelle, although we never really worked together you have mentored me in so many ways and I will always value our friendship. Carolina, what can I say to tell you how wonderful I think you are? I always wished we had overlapped for more time. To my two deskmates, Kathy Sarah and Laetitia, thanks for putting up with me and being great friends despite my mess. To the Matts (Yorke and Decan), you always made it fun to come to work. To my readers (Kathy, Kathy Sarah, Maria, Kevin, Laetitia, Matt Y., Matt D., Paul), thanks for all of your comments, you have all been great co-workers and awesome friends. To many other co-workers and friends (Belinda, Colleen, Raquel, Claudio and the rest of the Scaiano mafia, past and present), work didn't feel so much like work with all of you around.

Thanks also to the many friends I have made outside of the Scaiano group, especially the members of the CGSA (Joseph, Nathalie, Joffré, Heather and Rachel), the Accomodators, formerly UOCSJE (Joseph, Mathieu L., Roger, Hasan and Charles), and the RSD. Some of my best memories in Ottawa involve all of you.

Finally, thank you Paul for being with me through this whole journey, first as a friend, then as a partner. Your love has seen me through the best and the worst of times and I only hope I can do the same for you. I'm so glad I met you.

Table of Contents

List of Abbreviations

ACV	acyclovir
ATP	adenosine triphosphate
Boc	*tert*-butyloxycarbonyl
CNB	α-carboxy-2-nitrobenzyl ester
DMF	dimethylformamide
DMSO	dimethylsulfoxide
EDG	electron donating group
E_T	triplet energy
EtOAc	ethyl acetate
EWG	electron withdrawing group
F	fluorescence
fs	femtosecond
FWHM	full width half maximum
GC	gas chromatography
GM	Goeppert Mayer (unit for the two photon absorption cross section)
HCEC	human corneal epithelial cells
HMN	hydroxymethylnaphthalene
HPLC	high performance liquid chromatography
HSV	herpes simplex virus
IC	internal conversion
ISC	intersystem crossing
L	leaving group
LFP	laser flash photolysis

MO	molecular orbital
ms	millisecond
MS	mass spectroscopy
MTT	3-(4,5-dimethylthiazol-2-yl)-2,5-diphenyltetrazolium
nm	nanometre
NMR	nuclear magnetic resonance spectroscopy
NOS	nitric oxide synthase
NP	nanoparticle
NPE	nitrophenylethyl
$\mathbf{n_{photolysed}}$	number of moles photolysed
ns	nanosecond
NSAID	non-steroidal anti-inflammatory drug
***o*NB**	*ortho*-nitrobenzyl
PB	phosphate buffer solution
PBS	phosphate buffer saline
PDC	photodecarboxylation
PFU	plaque forming unit
***p*HP**	*p*-hydroxyphenacyl
PPG	photolabile protecting group
ps	picosecond
***p*TsOH**	*para*-toluenesulfonic acid
Q	quencher
RT	retention time
RT-PCR	real time polymerase chain reaction
$\mathbf{S_1}$	lowest energy singlet excited state
$\mathbf{T_1}$	lowest energy triplet excited state

TDA-1	tris-[2-(2-methoxy-ethoxy)-ethyl]-amine
THF	tetrahydrofuran
TPE	two photon excitation
TR-FTIR	time resolved fourier transform infrared spectroscopy
UV-Vis	ultraviolet-visible
UVA	ultraviolet radiation ranging from 320 nm – 400 nm
UVB	ultraviolet radiation ranging from 280 nm – 320 nm
VR	vibrational relaxation
XAA	xanthone acetic acid
XPA	xanthone propionic acid, also used as the abbreviation for the xanthone propionic acid based PPG
YAG	ytterium-argon-garnate
ΔE_{ST}	singlet-triplet energy gap
ΔOD	change in absorbance from the probe beam, before and after laser excitation
ε	molar absorption coefficient
λ	wavelength
μs	microsecond
τ	lifetime
Φ_i	quantum yield of process i

List of Figures

List of Schemes

List of Tables

1. Photolabile Protecting Groups: An Introduction

Graphical Abstract

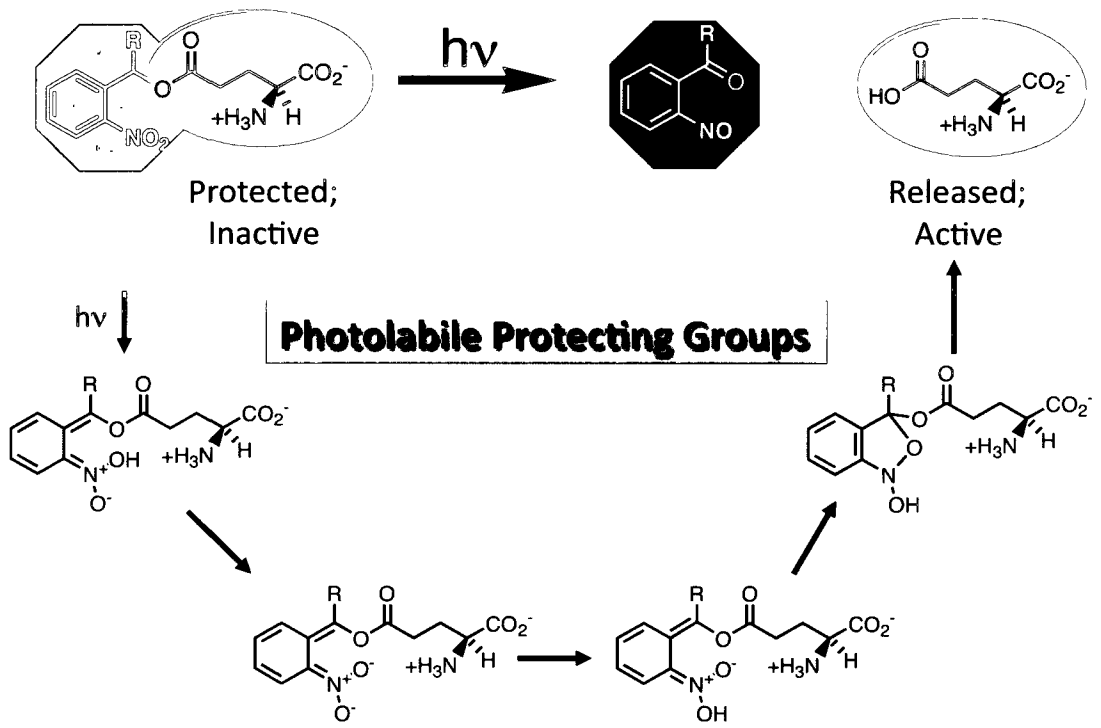

1.1 Photolabile Protecting Groups

Photolabile protecting groups (PPGs), also commonly known as 'photocages', 'photoremovable protecting groups', or simply 'photo protecting groups', are essentially photo-reactive moieties that can be attached to some active molecule in a way that quenches the activity of that molecule. Upon irradiation with light of an appropriate wavelength, the active form is released through a photochemical reaction. While PPGs were originally used as protecting groups in organic synthesis,[1, 2] their most common application today is in the study of dynamic biological processes. More specifically, these groups can be used to rapidly introduce a concentration jump of some active biological molecule (*e.g.* a neurotransmitter) allowing the dynamic study of events that follow. The application of PPGs to the study of signaling events in biology was pioneered by Kaplan, Forbush and Hoffmann in 1978 with 'caged' ATP (adenosine triphosphate) using *o*-nitrobenzyl as the caging group (**1**).[3] Kaplan *et al.* were also the first to apply the term 'caging'. Although somewhat misleading - active molecules are not really inside a molecular cage – the usage of this term is now too common to be avoided.

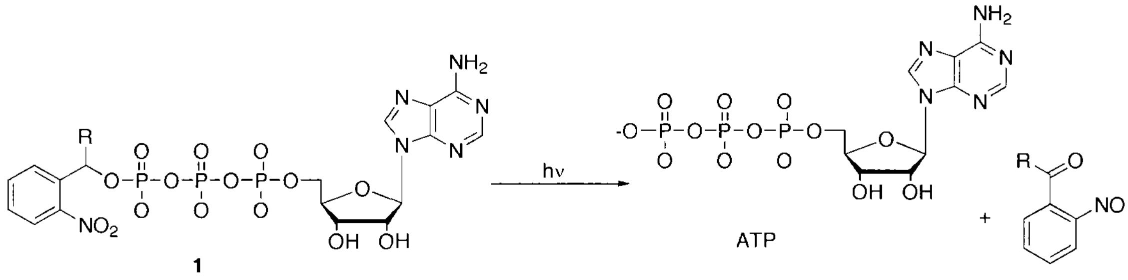

Scheme 1-1. Photochemical release of ATP from *o*NB-ATP (**1**).[3] R = H, Me This group was initially used by Kaplan *et al.* to study the erythrocytic Na:K ion pump.

A helpful list of criteria for good PPGs was recently outlined by Pelliciolli and Wirz.[4] These include:

1) *Clean and efficient photochemistry.* Ideally, the only photochemical path will be the one that leads to release of the active molecule and this will occur with a high quantum yield ($\Phi_{release}$, a measure of photochemical efficiency).

2) *High absorption coefficient at wavelengths above 300 nm.* This is particularly significant for biological applications since light with wavelengths below 300 nm is likely to be absorbed by, and may cause damage to, the biological environment.

3) *Non-interfering photoproducts.* The photoproduct(s) formed (apart from the released active group) should not interfere with either the photochemistry or the environment. That is, there should be no toxicity or activity of the photoproduct(s) and ideally, they should be transparent so as to avoid any screening effects. This latter point is particularly challenging since it requires a significant change in the chromophore following release. With respect to interference with the environment, formation of free radicals and other reactive species should be avoided.

4) *Fast release rate.* For time resolved studies, the release rate should exceed the rate of the response investigated.

5) *Solubility.* Caged compounds must be soluble in the experimental medium (usually water at pH 7.4 for biological applications) and be able to pass biological barriers.

6) *Low background activity.* The caged compound should be inactive and thermally stable in the experimental medium so that only light activation induces a significant change in signal molecule concentration and activity.

It is important to realize that no system will fully satisfy each criterion. Of the PPGs available, each has certain advantages and disadvantages (*vide infra*) so it is necessary to choose a PPG based on the specific requirements of each application. For example, the use of PPGs in synthesis does not require a nanosecond release time, and toxicity is only important insofar as the toxicity during the time period of the application. While many PPGs have been introduced since the first *o*NB group, there is still plenty of room for newcomers with improved characteristics. In addition, there remain particular challenges in the field. High among these are the efficient release of poor leaving groups (RO-, RHN-, RS-) and the ability to release with two photon excitation.

Another important consideration is the photochemical dependence on environment and the released group. Since the mechanism leading to release often

proceeds through multiple intermediates (both excited state and ground state) the solvent, pH and presence of other reactive substrates could very well influence the outcome of the photochemistry.[4] For example, a proton transfer step will be highly influenced by pH, while a radical intermediate may react with oxygen. For this reason, it is beneficial to know the photochemical mechanism in detail so that the usefulness in a particular application can be better predicted.

1.2 Examples of PPGs

Due to their accessibility and history, *o*-nitrobenzyl (*o*NB) PPGs and derivatives of this group are by far the most commonly used PPG. The photochemistry of the *o*NB group is based on phototautomerization of *o*-nitrobenzyl compounds (Scheme 1-2, left).[5] Excitation of the caged compound (Scheme 1-2, **2**) leads to hydrogen abstraction followed by cyclization to the ground state *aci*-nitro intermediate **3**. Ring opening of **3** yields an unstable intermediate that will eliminate the leaving group, thus yielding the final nitroso photoproduct **4** and the released leaving group LH.

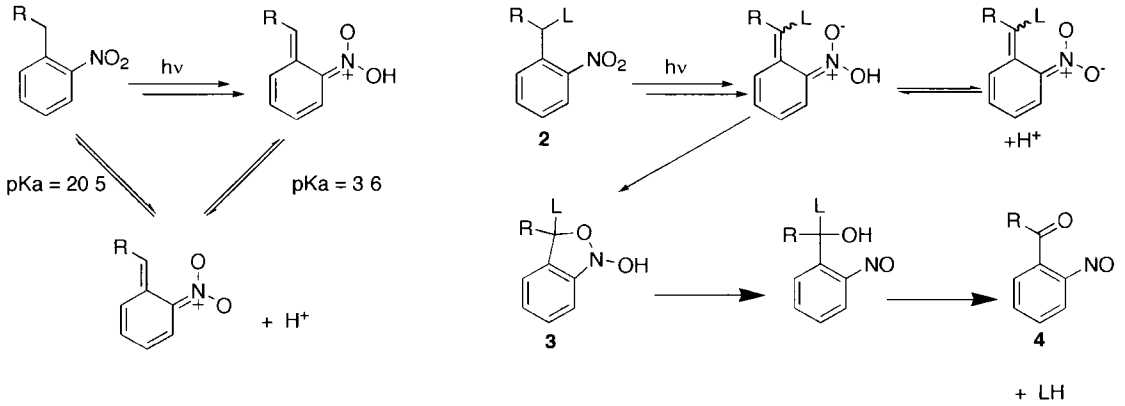

Scheme 1-2. Left: Phototautomerization of the *o*-nitrobenzyl group. Right: Release of a leaving group (L) from the *o*NB PPG.

As previously mentioned, the first example of a 'caged' compound was Kaplan's *o*NB-ATP. For this example, at pH > 6.5, the rate determining step is the ground state ring opening decay of **3**.[6, 7] Intermediate **3** is easily monitored thanks to a strong absorption around 400 nm, thus providing a way to measure the rate of release. However, for other leaving groups, or under different conditions (lower pH, lower temperature, non-aqueous solvent), subsequent steps might be much slower, meaning the release rate cannot always be measured by monitoring the *aci*-nitro (**3**) signal.[4] The only way to truly measure the release rate (without a detailed investigation into the decay rates of each intermediate as was performed by Wirz *et al.* for *o*NB-ATP and *o*NB-OCH_3)[6] is to monitor the rate of photoproduct formation. This can often be difficult in the absence of a characteristic signal and techniques are limited, though time-resolved fourier transform infrared spectroscopy (TR-FTIR) is thought to be promising.[8]

The complexity and variability of the release mechanism is an often-

overlooked disadvantage of the *o*NB group. Other disadvantages include the production of a strongly absorbing toxic nitroso photoproduct (**4**), only a moderate quantum yield (Φ = 0.04 - 0.2 at pH 7, depending on released group) and frequently slow release rates that depend on the released group. Nonetheless, there are many commercially available *o*NB 'caged' compounds and numerous derivatives have been developed with improved properties. For example, α-carboxy-2-nitrobenzyl ester (CNB, **5,** Chart 1-1) exhibits a higher $\Phi_{release}$ and greater thermal stability at physiological pH;[9] nitrophenylethyl (NPE, **6,** Chart 1-1) has a faster release rate and a less toxic photoproduct; derivative **7** (Chart 1-1) includes a substituent that traps the nitroso photoproduct;[10] and introduction of the nitrodibenzofuran chromophore (**8,** Chart 1-1) increases absorption at wavelengths above 300 nm, improves $\Phi_{release}$ and opens up the possibility for two photon excitation[11]. Because of the availability and research precedence for *o*NB it is easy to see why this group is still the most popular choice for biologists and biochemists; however, there remains a great deal of room for chemists to improve on the tools available.

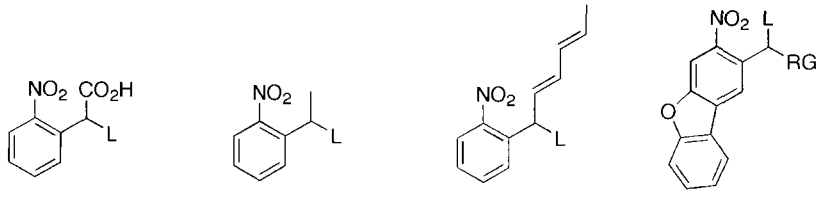

5 6 7 8

Chart 1-1.

One group with advantageous characteristics is the *p*-hydroxyphenacyl PPG (*p*HP, Scheme 1-3, **9**) which is synthetically accessible, soluble and stable in aqueous media, reacts with a fast release rate and reasonable quantum yield (0.1 to 0.4) and produces a non-toxic, blue-shifted photoproduct. However, the product distribution depends on the released group as well as the solvent and the absorption coefficient is low for wavelengths above 320 nm.[12] In an attempt to improve the absorption characteristics, 3,5-dimethoxy-*p*HP (Scheme 1-3, **10**) was synthesized. This compound absorbs well above 400 nm but the quantum yield of release dropped to 0.03-0.04.[13]

Another interesting group, because of the potential for two photon excitation, is the coumarin PPG (**11**). This group absorbs into the visible and releases carboxylic acids, phosphates, cyclic nucleotides and amino acids rapidly and with a quantum yield up to 0.25.[14-16]

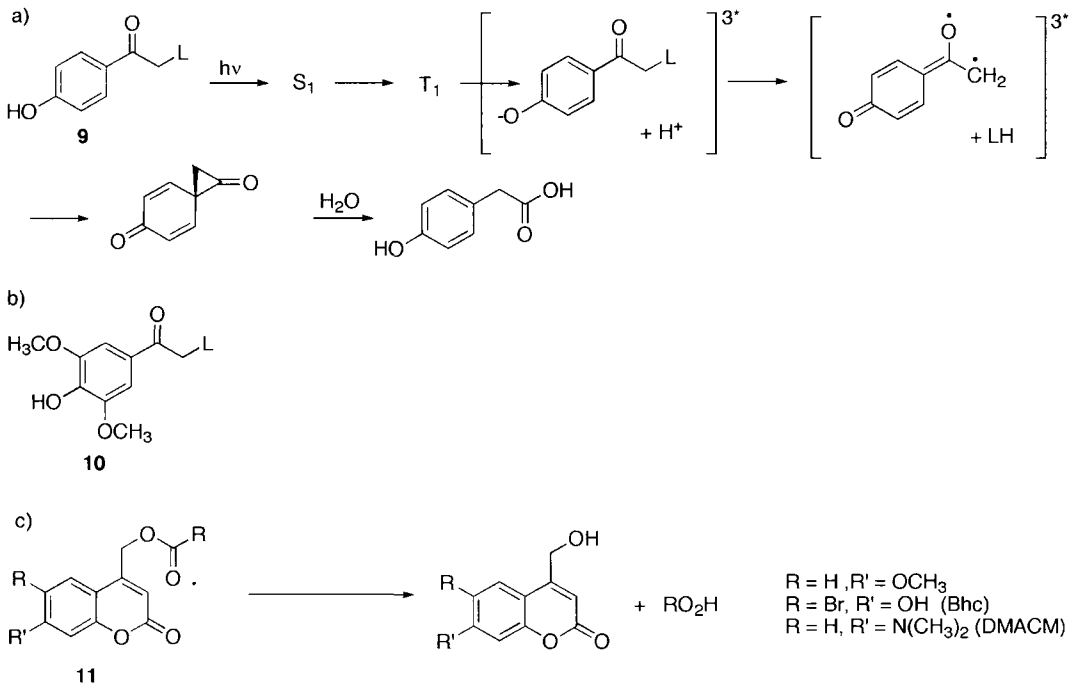

Scheme 1-3. a) Mechanism of photorelease from *p*HP. b) Structure of a *p*HP derivative with improved absorption characteristics but lower $\Phi_{release}$. c) Photorelease from methoxycoumarins.

While many other PPGs exist, each with varying advantages and disadvantages, I will not attempt to review them all here. Instead, I direct the reader to some very thorough and interesting reviews.[4, 14, 15]

1.3 Applications of PPGs

1.3.1 PPGs and Dynamic Biological Studies

While theoretically PPGs could be applied anywhere spatiotemporal control is desired, their most common application remains in the field of biological signaling. In terms of caged small molecules, ATP is still one of the most common,[16] an observation that is not surprising given the vast number of dynamic physiological processes ATP hydrolysis takes part in.

Amino acids, glutamate in particular, are also commonly used to study neuronal signaling events; events that are the basis for information to be received, stored, and processed by the central nervous system.[17, 18] Three classes of glutamate-gated ion channel receptors are involved in postsynaptic signal transduction; the AMPA, the kainate and the NMDA receptors.[19] The use of caged glutamate has led to an improved understanding of how these receptors operate and therefore a better understanding of neuronal networks in general. For example, Li *et al.* have used CNB-glutamate (described as having a fast release rate, $t_{1/2}$ = 21 μs)[20] to study the channel-opening kinetics of GluR6,[21] (a kainate receptor channel) as well as GluR2Q_{flip} and GluR1Q_{flip} (both AMPA receptor channels).[22, 23] Figure 1-1 shows a typical measure of whole cell current from the opening of the GluR1Q_{flip} channel initiated by the laser flash photolysis of caged glutamate. By measuring this signal at various concentrations of released glutamate they were able to extract the opening and closing kinetics (k_{open} = 2.9 x 10^4 s^{-1} and k_{close} = 2.1 x 10^3 s^{-1}) for the

receptor channel. I will not go through the details of the kinetic analysis, but only wish to point out that this time resolved data is only possible because glutamate was released within microseconds (i.e. instantaneous with respect to k_{open} and k_{close}).

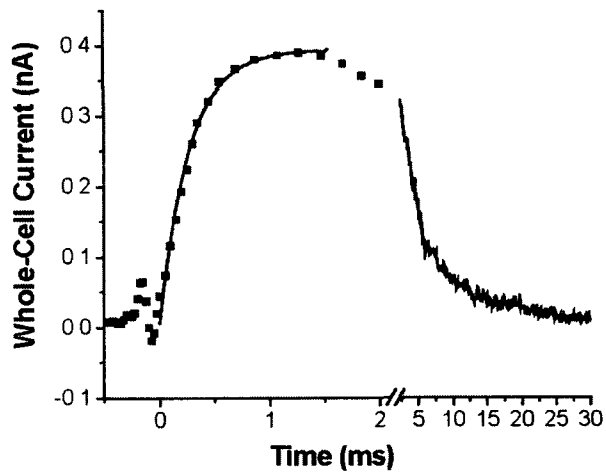

Figure 1-1. Whole cell current from the opening of the GluR1Q_{flip} channel initiated by the laser flash photolysis of caged glutamate at time 0. Reproduced from ref. 23.

Other examples using 'caged' glutamate take adavantage of the spatial resolution possible with PPGs to map out the locations of neurons connected to a single cell by generating an action potential in that cell.[24] The use of PPGs in this application (as compared with imaging neuronal tracers) allows for functional, rather than just physical, mapping. The level of spatial resolution available with two photon excitation, allowing the experimentalist to excite a single neuron, has been invaluable to this field.

Additional commonly caged small molecules include other neurotransmitters like serotonin[25], steroids, second messengers, sugars and lipids.[26] Besides small

molecule signaling, PPGs have been used to study peptide signaling, protein folding,[27] and gene expression.[28, 29]

1.3.2 PPGs and the Synthesis of Biological Molecules

PPGs found their origin as protecting groups in organic synthesis[1] where the main advantage over other protecting groups is a deprotection mechanism typically orthogonal to any other chemistry in solution. Essentially, they provide an alternative for molecules that are sensitive to other deprotection conditions. More recently, this same advantage has been applied in the solid phase synthesis of peptides, oligonucleotides and DNA and the fabrication of arrays of these biological molecules.[30-32]

1.3.3 PPGs and Drug Delivery

The use of PPGs in the field of drug delivery has been quite limited thus far. The only examples, other than the work that will be presented in this thesis, use caged derivatives of a nitric oxide synthase (NOS) inhibitor, 1400W (Bhc-1400W, Chart 1-2),[33, 34] or caged NO[35] for the control of NO levels, which has been identified as a possible strategy to combat several diseases.

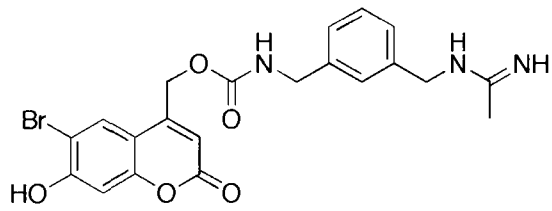

Bhc-1400W

Chart 1-2.

1.4 Tools Used for Studying PPGs

1.4.1 Photochemistry Primer

The essence of chemistry is an understanding of competing processes; when a molecule is placed in a certain environment, the essential questions are: what pathways are available to it, how will they compete with each other and how can the competition be influenced? In photochemistry and photophysics, the relevant pathways are best illustrated in a Jablonski diagram (Figure 1-2). When an organic molecule absorbs light it is excited to an electronically excited state. Given that the vast majority of ground states are singlet, and absorption occurs without change in multiplicity, this initial state is typically of singlet multiplicity (S_n). Most commonly, the molecule will relax to the lowest singlet excited state (S_1) through vibrational relaxation (VR) and internal conversion (IC). From S_1 it can relax to the ground state (S_0) through a non-radiative pathway (IC and VR), or a radiative pathway (fluorescence), or it can convert to a triplet state *via* intersystem crossing (ISC) followed by either non-radiative relaxation to S_0 or radiative phosphorescence. Two additional pathways for the molecule not included in Figure 1-2 are the reactive pathway and the quenching pathway (*i.e.* reaction or energy transfer with a ground state molecule quencher Q), which can occur from S_0, S_1 or T_1, and rarely from higher excited states.

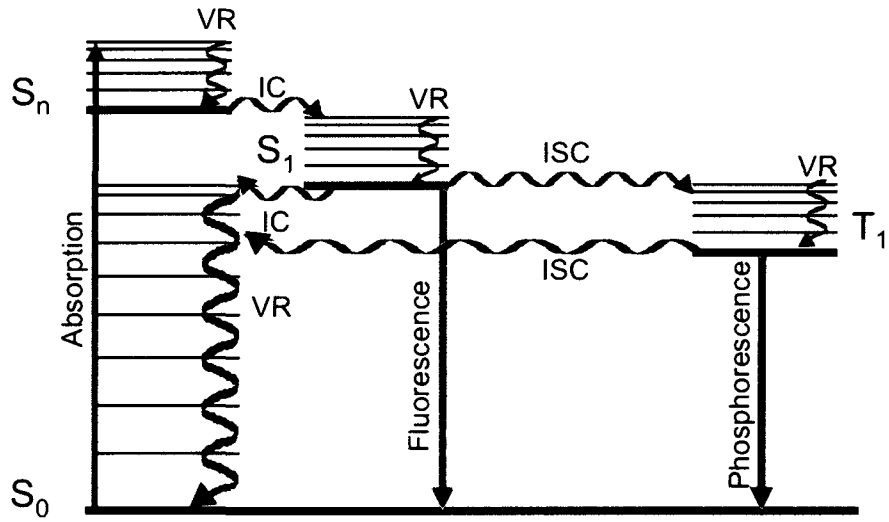

Figure 1-2. Jablonski Diagram showing absorption and non-reactive excited state processes fluorescence, phosphorescence, vibrational relaxation (VR), internal conversion (IC), intersystem crossing (ISC). Radiative processes are shown as straight arrows while non-radiative processes are depicted with wavy arrows.

An important equation stemming from the consideration of competing pathways is that of quantum yield (Φ). By definition a photochemical or photophysical quantum yield for a particular path is the yield of that path per photon absorbed (Equation 1-1). Thus, a photorelease quantum yield is equal to the number of moles of compound released per mole of photons absorbed.

$$\Phi_i = \frac{\#\ of\ events\ (i)}{\#\ of\ photons\ absorbed} \tag{1-1}$$

Since the competition of each pathway from a particular state is dictated by the rate of that pathway, the quantum yield can also be expressed in terms of rate constants. Equation 1-2 expresses this for any unimolecular process occurring from S_1

assuming all excited molecules initially go through S_1. Here k_i is the rate constant of process i, Σk is the sum of all rate constants for processes occurring from S_1 and τ_S is the singlet state lifetime.

$$\Phi_i = \frac{k_i}{\sum k} = \frac{k_i}{k_{IC} + k_{ISC} + k_F + k_{rxn} + k_q[Q]} = k_i \tau_s \qquad (1\text{-}2)$$

The typical timescale for each photophysical process is shown in Figure 1-3 making it evident why the majority of photochemical processes occur from either the lowest singlet or triplet excited state: vibrational relaxation and internal conversion are too fast for most reactions to compete, so it is only S_1 and T_1 that are long-lived enough for any reaction to occur. The lowest triplet state in particular can be particularly long-lived owing to a forbidden transition back to the ground state.

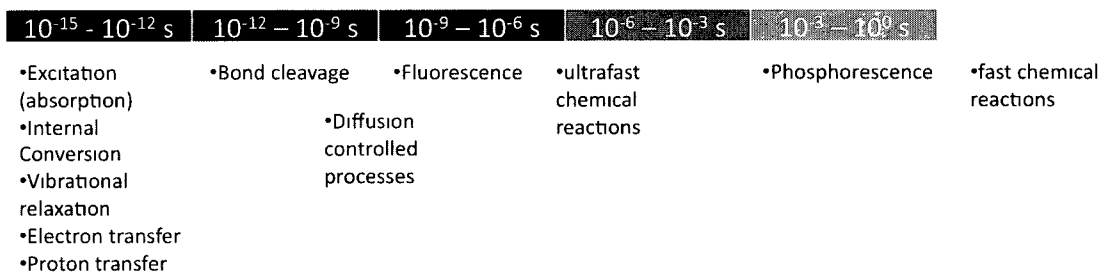

Figure 1-3. Timescales and corresponding photochemical and photophysical processes.

When discussing photochemical reaction mechanisms, it is also important to consider the molecular orbitals involved as they will often dictate the type of reaction an excited molecule will undergo. While multiple transitions are possible

for any one chromophore, for reactivity considerations we are mostly interested in transitions to the S_1 and T_1 states. The most common transitions in organic photochemistry, and the ones relevant to this work, can be described either as π,π^* (refering to the excitation of an electron from a ground state π molecular orbital to an antibonding π^* molecular orbital) or as n,π^* (refering to excitation from a non-bonding ground state orbital to an antibonding π^* orbital). The nature of the lowest energy transition will have a large effect on the reactivity of the excited state. This is best illustrated using two simple examples, formaldehyde and ethylene (Figure 1-4). Excitation of the lowest energy transition for formaldehyde promotes an electron from the nonbonding orbital localised on the oxygen to the π system of the C=O resulting in an electrophilic oxygen with alkoxyl radical character. For this reason, many n,π^* excited ketones like benzophenone will undergo reactions typical of alkoxyl radicals (e.g. hydrogen abstraction). Conversely, the lowest energy excitation of ethylene results in a more delocalised excitation which can lead to cis-trans isomerization for substituted ethylene.

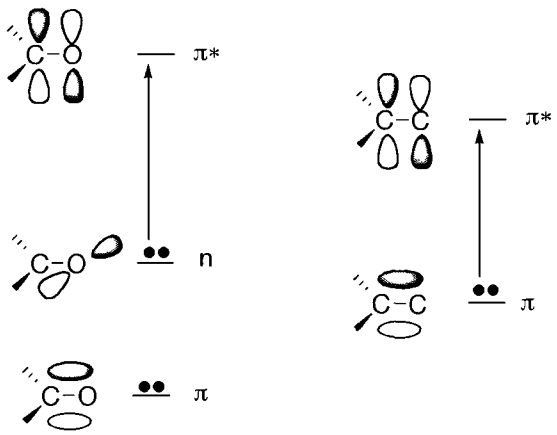

Figure 1-4. Illustration of the lowest energy excitations for formaldehyde (left) and ethylene (right).

In addition to understanding the molecular orbitals involved in a transition, it is also important to know whether the reactive excited state is singlet or triplet and how readily these states can interconvert since the chemistry of each state can vary dramatically. Triplet states are more often associated with radical reactions while singlet states usually lead to heterolytic processes (assuming photochemistry occurs). The rate constant for intersystem crossing from S_1 to T_1 (or from T_1 to S_1) is generally much higher when the energy gap between the two states (ΔE_{ST}) is low. To understand some of the factors influencing the size of ΔE_{ST} we turn once more to Figure 1-4. The energy of each state is comprised of the zero order energy E_0 (the one electron approximation) and matrix elements that describe the electron repulsion energies that split the S_1 and T_1 states.

$$E(S_1) = E_0 + K + J \tag{1-3}$$

$$E(T_1) = E_0 + K - J \tag{1-4}$$

Where K is the matrix element that measures the electron repulsion due to Coulombic interactions and J is the matrix element that measures the electron repulsion due to electron exchange (N.B. both K and J > 0). From Equations 1-3 and 1-4 we can derive Equation 1-5 for the energy gap between S_1 and T_1.

$$\Delta E_{ST} = E(S_1) - E(T_1) = 2J \qquad (1\text{-}5)$$

Two results follow from this: i) since J must be positive, S_1 is always higher in energy than T_1 and ii) since J is proportional to the overlap integral between the two orbitals involved in the transition, transitions with higher overlap will have higher ΔE_{ST}. As is obvious in Figure 1-4, the overlap for a π, π^* transition is significantly higher than for an n, π^* transition. We observe this effect experimentally by comparing the singlet-triplet energy gaps for different molecules, for example ΔE_{ST} for formaldehyde is 40 kJ/mole while that of ethylene is 290 kJ/mole.[36]

Many of the concepts outlined above will return in later chapters because the question of how efficient release from a PPG can be is really a question of how well the release pathway is able to compete with all other pathways available to the excited molecule. As I will describe in Chapter 2, the question of multiplicity (i.e. singlet *vs.* triplet) for the photochemistry in this thesis is particularly relevant because we attribute the reactivity to a singlet state and this is unusual for an aromatic ketone.

1.4.2 Laser Flash Photolysis

Time resolved tools like laser flash photolysis (LFP) are invaluable for a detailed study of photochemical release mechanisms. This section will give an overview of the techniques used in our lab. In general, an excited state is generated with a short light pulse. The transients that form can then be monitored in a time resolved manner using absorption or emission spectroscopies. The transients observed may either be excited state (e.g. T_1 of the initially excited molecule) or ground state intermediates (e.g. a radical cation formed from the excited state); the only requirements being that the transient absorbs or emits in a measurable region and lives long enough to be observed. In order to determine the rate of release from a PPG it is necessary to either monitor the growth of the released molecule or identify the longest lived transient in the release mechanism and monitor the decay of this transient (i.e. the rate determining step).

Nanosecond laser flash photolysis (ns LFP) was first developed in the late 1960s by Lindqvist.[37] This technique relies on the excitation of a ground state molecule by short laser pulses (*ca.* 5-10 ns) followed by the observation of transient absorption or emission. What is measured is a change in optical density (ΔOD) over time, reflecting changes in transmitted light from the probe beam before (I_0) and after (I_t) laser excitation (Equation 1-6). The experimental set up is shown in Figure 1-5 (a).

$$\Delta OD = -\log\left(\frac{I_t}{I_0}\right) \tag{1-6}$$

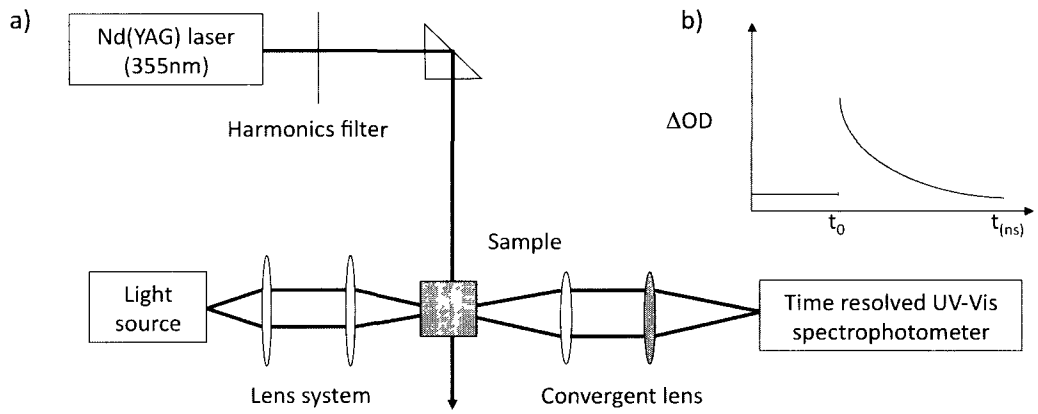

Figure 1-5. a) Schematic diagram of a ns Laser flash photolysis (LFP) system. b) Typical data recorded for a decaying (absorbing) transient

In our system the light source is a xenon lamp, allowing us to monitor from *ca.* 250 nm up to 800 nm. For kinetic data a monitoring wavelength is pre-selected and the ΔOD at this wavelength is monitored following the laser pulse. In the fortunate case where transient spectra do not completely overlap in time and wavelength, it is possible to acquire growth and decay traces for any transient that absorbs or emits between 250 and 800 nm on a timescale of 10 ns – 100 ms (Figure 1-5 (b)). Such a trace can then be fitted with the appropriate kinetics to obtain the lifetime(s) of the transient(s). It is also possible to measure a full transient spectrum by pre-selecting time windows of the decay (or growth) to monitor while changing the monitoring wavelength in a stepwise manner (Figure 1-6).

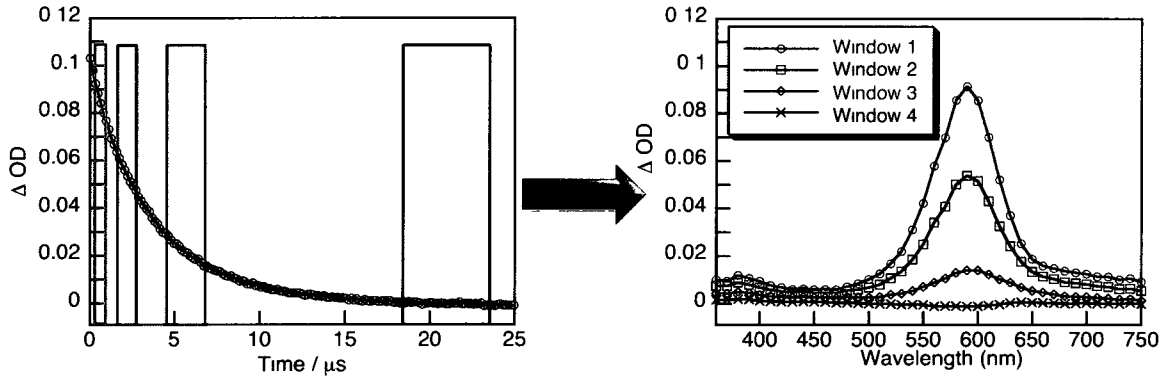

Figure 1-6. An illustration of how a spectrum is constructed from time resolved data.

Transients are typically assigned based on the signal wavelength and lifetime obtained as described above, but also based on quenching behaviour. For example, triplet states can be quenched by a ground state molecule (quencher, Q) with a triplet state that has an energy below that of the triplet being quenched (i.e. ΔE (Q) < ΔE(X)). Many such quenchers with known low-lying triplets are known and are commonly used to assign signals suspected to be triplets.

Given the importance of understanding the mechanism of photochemical release from a PPG, we have adopted a very mechanistic-based approach to the design and study of our novel PPG. The concepts outlined here will return in subsequent chapters (particularly Chapter 2) as I discuss our detailed photochemical studies.

1.5 Summary

This section was meant to give the reader a taste for some of the challenges and possibilities in the field of photolabile protecting groups. While not a thorough review of the field by any means, a number of PPGs were presented with their respective advantages and disadvantages. A variety of current applications were also presented with the aim of showing the broad scope of this field.

In the following chapters I will describe our efforts towards the development and application of a new photolabile protecting group. Chapter 2 pertains to the detailed mechanistic studies of the parent photochemistry for our new PPG, that is, the photodecarboxylation of 2-xanthone acetic acid. Chapter 3 reports the release of some simple groups from the 2-xanthone acetic acid derived PPG and the important photochemical parameters of such release. In Chapter 4 I outline our attempts to incorporate a handle into the PPG that could be used for attachment to a surface as well as an investigation into the photochemical effects of altering the xanthone chromophore. Chapter 5 describes the application of our new PPG towards a corneal drug delivery application, focusing mainly on the synthesis required for this application and the release in solution. Some preliminary results of drug release in a corneal cell model are also presented.

As a final note for this chapter, I have already mentioned that *o*NB derived PPGs remain the most widely used mainly due to availability and precedence. As chemists developing new tools for the biologist's toolbox, we might hope the

scientists using the tools would venture out of the safe zone. However, we should demand the same creativity of ourselves. Many reports of novel PPGs demonstrate the release of glutamate or glycine or other well established groups because it is known that these molecules are of interest to biologists and biochemists. As a result there are at least 19 reported PPGs for glutamate alone.[38]

For many areas of research, some of the most interesting developments stem from collaboration between disciplines. I hope that the reader will find the work described in this thesis to be such a case. We have both designed a novel photolabile protecting group (Chapters 2 and 3) and applied it in a novel way with the help of collaborators from the University of Ottawa Eye Institute (Chapter 5).

1.6 References

1. Pillai, V. N. R., Photoremovable protecting groups in organic synthesis. *Synthesis* **1980**, 1-26.

2. Hoffmann, N., Photochemical reactions as key steps in organic synthesis. *Chem. Rev.* **2008,** *108* (3), 1052-1103.

3. Kaplan, J. H.; Forbush, B.; Hoffman, J. F., Rapid photolytic release of adenosine 5'-triphosphate from a protected analog - utilization by Na-K pump of human red blood-cell ghosts. *Biochemistry* **1978,** *17* (10), 1929-1935.

4. Pelliccioli, A. P.; Wirz, J., Photoremovable protecting groups: reaction mechanisms and applications. *Photochem. Photobiol. Sci.* **2002,** *1* (7), 441-458.

5. Schwörer, M.; Wirz, J., Photochemical reaction mechanisms of 2-nitrobenzyl compounds in solution I. 2-nitrotoluene: Thermodynamic and kinetic parameters of the aci-nitro tautomer. *Helv. Chim. Acta* **2001,** *84* (6), 1441-1458.

6. Il'ichev, Y.; Schworer, M.; Wirz, J., Photochemical Reaction Mechanisms of 2-Nitrobenzyl Compounds: Methyl Ethers and Caged ATP. *J. Am. Chem. Soc* **2004,** *126* (14), 4581-4595.

7. Walker, J. W.; Reid, G. P.; McCray, J. A.; Trentham, D. R., Photolabile 1-(2-Nitrophenyl)ethyl Phosphate Esters of Adenine Nucleotide Analogues. Synthesis and Mechanism of Photolysis. *J. Am. Chem. Soc.* **1988,** *110*, 7170-7177.

8. Givens, R.; Kotala, M. B.; Lee, J.-I., Mechanistic Overview of Phototriggers and Cage Release. In *Dynamic Studies in Biology*, Goeldner, M.; Givens, R., Eds. Wiley-VCH: Weinheim, 2005; pp 95-129.

9. Grewer, C.; Jager, J.; Carpenter, B. K.; Hess, G. P., A new photolabile precursor of glycine with improved properties: A tool for chemical kinetic investigations of the glycine receptor. *Biochemistry* **2000,** *39* (8), 2063-2070.

10. Pirrung, M. C.; Rok, L.; Park, K.; Springer, J. B., Pentadienylnitrobenzyl and Pentadienylnitropiperonyl Photochemically Removable Protecting Groups. *J. Org. Chem.* **1999,** *64*, 5042-5047.

11. Momotake, A.; Lindegger, N.; Niggli, E.; Barsotti, R. J.; Ellis-Davies, G. C. R., The nitrodibenzofuran chromophore: a new caging group for ultra-efficient photolysis in living cells. *Nat. Meth.* **2006,** *3* (1), 35-40.

12. Park, C. H.; Givens, R. S., New photoactivated protecting groups .6. *p*-hydroxyphenacyl: A phototrigger for chemical and biochemical probes. *J. Am. Chem. Soc.* **1997,** *119* (10), 2453-2463.

13. Conrad, P. G.; Givens, R. S.; Weber, J. F. W.; Kandler, K., New phototriggers: Extending the *p*-hydroxyphenacyl π-π* absorption range. *Org. Lett.* **2000,** *2* (11), 1545-1547.

14. Mayer, G.; Heckel, A., Biologically active molecules with a "light switch". *Angew. Chem. Int. Edit.* **2006,** *45* (30), 4900-4921.

15. Lee, H.-M.; Larson, D. R.; Lawrence, D. S., Illuminating the Chemistry of Life: Design, Synthesis, and Applications of "Caged" and Related Photoresponsive Compounds. *ACS Chem. Biol.* **2009,** *4* (6), 409-427.

16. Goeldner, M.; Givens, R., *Dynamic Studies in Biology*. Wiley-VCH: Weinheim, 2005; Vol. 1.

17. Callaway, E. M.; Yuste, R., Stimulating neurons with light. *Curr. Opin. Neurobiol.* **2002,** *12* (5), 587-592.

18. Hess, G. P., Photochemical Release of Neurotransmitters. In *Dynamic Studies in Biology*, Goeldner, M.; Givens, R., Eds. Wiley-VCH: Weinheim, 2005; pp 205-231.

19. Corrie, J. E. T., Photoremovable Protecting Groups Used for the Caging of Biomolecules. In *Dynamic Studies in Biology*, Goeldner, M.; Givens, R., Eds. Wiley-VCH: Weinheim, 2005; pp 1-94.

20. Cheng, Q.; Steinmetz, M. G.; Jayaraman, V., Photolysis of γ-(α-carboxy-2-nitrobenzyl)-L-glutamic acid investigated in the microsecond time scale by time-resolved FTIR. *J. Am. Chem. Soc.* **2002,** *124* (26), 7676-7677.

21. Li, G.; Oswald, R. E.; Niu, L., Channel-opening kinetics of GluR6 kainate receptor. *Biochemistry* **2003,** *42* (42), 12367-12375.

22. Li, G.; Pei, W. M.; Niu, L., Channel-opening kinetics of $GluR2Q_{flip}$ AMPA receptor: A laser-pulse photolysis study. *Biochemistry* **2003,** *42* (42), 12358-12366.

23. Li, G.; Niu, L., How fast does the $GluR1Q_{flip}$ channel open? *J. Biol. Chem.* **2004,** *279* (6), 3990-3997.

24. Gillespie, D. C.; Kim, G.; Kandler, K., Caged Neurotransmitters for Probing Neuronal Circuits, Neuronal Integration and Synaptic Plasticity. In *Dynamic Studies in Biology*, Goeldner, M.; Givens, R., Eds. Wiley-VCH: Weinheim, 2005; pp 232-251.

25. Breitinger, H.-G. A.; Wieboldt, R.; Ramesh, D.; Carpenter, B. K.; Hess, G. P., Synthesis and characterization of photolabile derivatives of serotonin for chemical kinetic investigations of the serotonin 5-HT_3 receptor. *Biochemistry* **2000,** *39*, 5500-5508.

26. Dorman, G.; Prestwich, G. D., Using photolabile ligands in drug discovery and development. *Trends Biotechnol.* **2000,** *18* (2), 64-77.

27. Hansen, K. C.; Rock, R. S.; Larsen, R. W.; Chan, S. I., A method for photoinitating protein folding in a nondenaturing environment. *J. Am. Chem. Soc.* **2000,** *122* (46), 11567-11568.

28. Monroe, W. T.; McQuain, M. M.; Chang, M. S.; Alexander, J. S.; Haselton, F. R., Targeting expression with light using caged DNA. *J. Biol. Chem.* **1999,** *274* (30), 20895-20900.

29. Cruz, F. G.; Koh, J. T.; Link, K. H., Light-activated gene expression. *J. Am. Chem. Soc.* **2000,** *122* (36), 8777-8778.

30. Fodor, S. P. A.; Read, J. L.; Pirrung, M. C.; Stryer, L.; Lu, A. T.; Solas, D., Light-Directed, Spatially Addressable Parallel Chemical Synthesis. *Science* **1991,** *251* (4995), 767-773.

31. Chee, M.; Yang, R.; Hubbell, E.; Berno, A.; Huang, X. C.; Stern, D.; Winkler, J.; Lockhart, D. J.; Morris, M. S.; Fodor, S. P. A., Accessing genetic information with high-density DNA arrays. *Science* **1996,** *274* (5287), 610-614.

32. Alvarez, K.; Vasseur, J.-J.; Beltran, T.; Imbach, J.-L., Photocleavable Protecting Groups as Nucleobase Protections Allowed the Solid-Phase Synthesis of Base-Sensitive SATE-Prooligonucleotides. *J. Org. Chem.* **1999,** *64*, 6319-6328.

33. Montgomery, H. J.; Perdicakis, B.; Fishlock, D.; Lajoie, G. A.; Jervis, E.; Guillemette, J. G., Photo-Control of nitric oxide synthase activity using a caged isoform specific inhibitor. *Bioorg. Med. Chem.* **2002,** *10*, 1919-1927.

34. Perdicakis, B.; Montgomery, H. J.; Abbott, G. L.; Fishlock, D.; Lajoie, G. A.; Guillemette, J. G.; Jervis, E., Photocontrol of nitric oxide production in cell culture using a caged isoform selective inhibitor. *Bioorg. Med. Chem.* **2005,** *13* (1), 47-57.

35. Yip, K.-P., Flash photolysis of caged nitric oxide inhibits proximal tubular fluid reabsorption in free-flow nephron. *Am. J. Physiol. Reg. I.* **2005,** *289*, 620-626.

36. Turro, N. J.; Ramamurthy, V.; Scaiano, J. C., *Modern Molecular Photochemistry of Organic Molecules*. University Science Books: Sausalito, California, 2010.

37. Lindqvist, L., Utilisation d'un Laser à Émission Ultraviolette Pulse en Photolyse-éclairs: Étude de L'Etat Triplet de l'Acridine. *C. R. Hebd. Séances Acad. Sci., Ser. C 1966* (263), 852-854.

38. Based on the combined search results from Scifinder Scholar and Web of Science, verifying 19 individual PPGs.

2. Xanthone Acetic Acid: A PPG Precursor[1]

Graphical Abstract

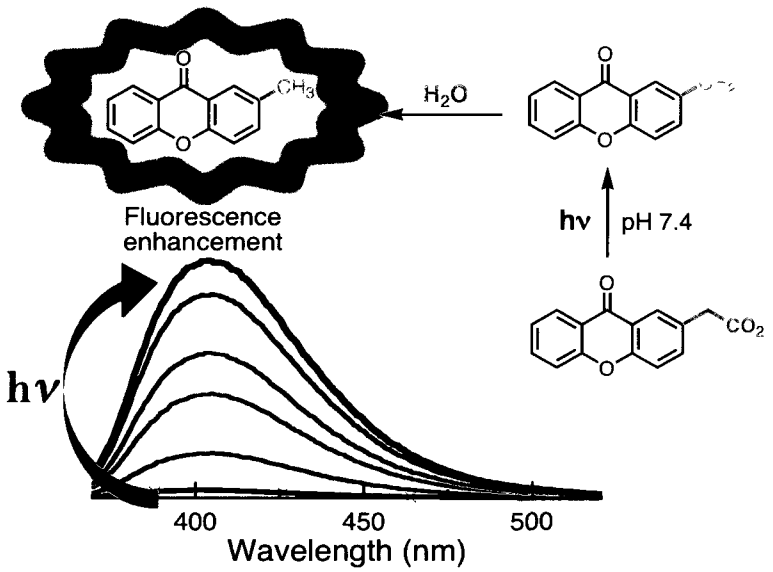

2.1 Introduction: Photodecarboxylation of aryl acetic acids

A number of aryl acetic acids possessing electron-withdrawing substituents on the aromatic ring are known to undergo efficient photodecarboxylation in neutral aqueous solution to give benzylic carbanion intermediates, which typically are rapidly protonated to give the corresponding aryl alkane (Scheme 2-1).[2, 3]

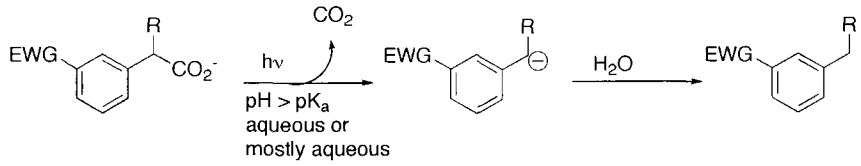

EWG	R	Φ_{PDC}	Ref.
NO_2	H	0.6	4, 5
PhCO	H	0.66	6
CH_3CO	H	0.60	7
PhCO	CH_3	0.75	8, 9
CF_3	H	0.46	10

Scheme 2-1. General photodecarboxylation (PDC) of electron poor arylacetic acids.

The photodecarboxylation process appears to be general for various electron withdrawing groups (EWGs) in either *meta* or *para* substitution positions, although higher reactivities are usually encountered for those with the EWG positioned *meta* to the acetic acid function when compared to those with a *para* arrangement. This phenomenon is an example of the '*meta* effect' that was first proposed by Zimmerman to explain the photoinduced hydrolysis of benzyl acetates, and can be readily rationalized using the results of molecular orbital (MO) calculations.[11] In general, substituents (either EDG or EWG) have their highest impact on the meta and ortho positions in the excited state. This is contrary to the familiar ground state

substituent effect for which EDGs and EWGs have a stronger effect on the *para* and *ortho* positions.

The photochemistry of ketoprofen (**1**) in particular has received a great deal of attention, in part because of its role as a potent non-steroidal anti-inflammatory drug (NSAID) with observed phototoxicity, and in part because the benzophenone chromophore is a favourite among photochemists.

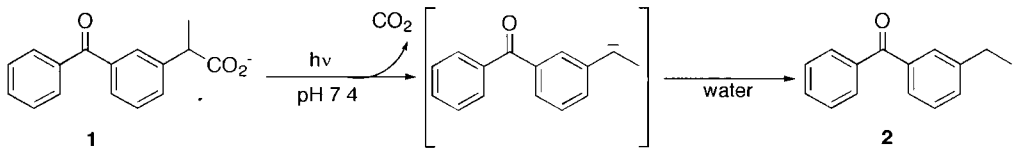

Scheme 2-2. Photodecarboxylation of ketoprofen (**1**) (pH > pK_a)

The mechanism of photodecarboxylation from ketoprofen has been a source of interest for almost two decades. Costanzo *et al.* first reported this reaction in 1989.[8] They observed a photodecarboxylation quantum yield (Φ_{PDC}) of 0.75 in phosphate buffer at pH 7.4. When solutions were deaerated, the only photoproduct observed was 3-ethylbenzophenone (**2**). When oxygen was present in solutions, although the quantum yield remained the same, trace amounts of oxidation products were also observed. This, and the fact that benzophenone photochemistry typically generates radical intermediates, led to the initially proposed mechanism which involved electron ejection followed by loss of CO_2 to generate a benzylic radical intermediate.[12]

Both Martínez and Scaiano[9] and Monti et al.[13] observed a solvated electron signal during ns laser flash photolysis (LFP), but power dependence studies showed that the ejected electron is formed through a biphotonic mechanism independent of the other transient observed (λ_{max} ~ 600 nm). The ejected electron mechanism accounts for at most 8 % of the reaction pathway upon laser excitation[9] and likely does not occur at all under steady state conditions.

It has since been established that the key intermediate involved is a carbanion (as shown in Scheme 2-2), possibly with some diradical anion character. The carbanion intermediate which is readily detected due to a characteristic absorbance at ~600 nm is formed monophotonically within the laser pulse. In water, it is rapidly protonated with a lifetime of approximately 200 ns to give (**2**)[14] while in dry, basic THF it can live many minutes at room temperature.[15] The oxidation photoproducts initially observed most likely arise from reaction of the carbanion with oxygen. This intermediate is consistent with a number of ionic reactions that ketoprofen derivatives will undergo upon excitation, including intramolecular substitution[16] and elimination,[17] the latter of which forms the basis for our novel PPG and will be discussed further in Chapter 3.

While the carbanion intermediate is well accepted for ketoprofen, the multiplicity of its precursor is less settled. Both singlet and triplet mediated mechanisms have been proposed[12, 13, 18-21] although a singlet mediated mechanism is more consistent with the carbanion intermediate in Scheme 2-2, since the triplet

manifold would favour a biradical intermediate. Research in the Scaiano group has favoured a singlet pathway primarily based on the observation of the triplet state of ketoprofen and the carbanion intermediate simultaneously by LFP. However, these studies were performed in mixtures of organic solvents with water, in contrast with the pure aqueous environment in which most of the ketoprofen reactions have been examined.

2.2 Photochemistry of xanthone acetic acids (XAA) at pH > pK_a[22]

A singlet mechanism represents unusual photochemistry for benzophenones, which normally are dominated by triplet processes because of very rapid intersystem crossing (although other examples of singlet-state reactivity are emerging).[23] A major difficulty in unequivocally establishing the multiplicity of photodecarboxylation from **1** results from the fact that derivatives of benzophenone are not fluorescent, which makes it difficult to gather information on the singlet excited state. In order to provide insight into the photodecarboxylation mechanism we decided to study the acetic acids of xanthone. Xanthone is structurally very similar to benzophenone, but is fluorescent in aqueous solutions (due in part to the much higher oscillator strength of the $S_0 \leftarrow S_1$ transition).[24] To this end, we chose to prepare and study 2-, 3-, and 4-xanthone acetic acids (**3** – **5** in Chart 2-1 respectively). The photodecarboxylation of **5** in aqueous solutions exposed to ambient light was previously observed during studies of its antitumour activity.[25]

However, prior to the work presented here, little idea as to the efficiency of the photochemistry and no mechanistic information was known.

The differing substitution of **3** – **5** was expected to provide mechanistic insight: if the mechanism proceeded *via* direct bond heterolysis (*i.e.* direct carbanion formation, singlet mechanism), then the reaction efficiency should be highly dependent on the excited state electronics at the benzylic position, and derivatives with acetic acids substituted *meta* to the electron withdrawing ketone (**3** and **5**) would be expected to show higher reactivity than **4** according to Zimmerman's *meta* effect. Alternatively, if reaction proceeded by electron transfer as has been proposed for a triplet mediated mechanism, the substitution should have little effect on the reaction efficiency, since both the separation distance and the oxidation potentials of the donor and acceptor are similar for all three derivatives.

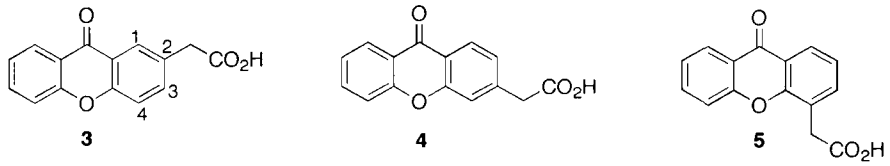

Chart 2-1.

We are also interested in **3** – **5** as possible new photolabile protecting group (PPG) precursors. A new type of PPG based on the photodecarboxylation of ketoprofen was initially developed by Lukeman and Scaiano.[17] The photoprocesses of **3** and **5** reported here suggest that these moieties may have improved spectral properties over ketoprofen in relation to their use in PPG design. Likely the most

important of these improved properties is the large increase in absorption coefficient at wavelengths above 300 nm. As the reader may recall from Chapter 1, this is particularly important for biological applications in order to avoid damage to the biological environment. This aspect will be discussed further in Chapter 3. In this chapter I will describe the synthesis and detailed photochemistry and photophysics of 2, 3, and 4-xanthone acetic acids (**3**, **4**, and **5**).

2.2.1 Synthesis

Derivatives **3** - **5** were initially prepared by Ullmann-type coupling of the appropriate hydroxyphenylacetic acid and *o*-iodobenzoic acid, followed by acid catalyzed ring closure (Scheme 2-3) according to literature procedure[26] with an overall yield of ~30%. We were able to improve the overall yield of **3** to 40% by starting with 4-hydroxyphenylacetate ethyl ester rather than 4-hydroxyphenylacetic acid.

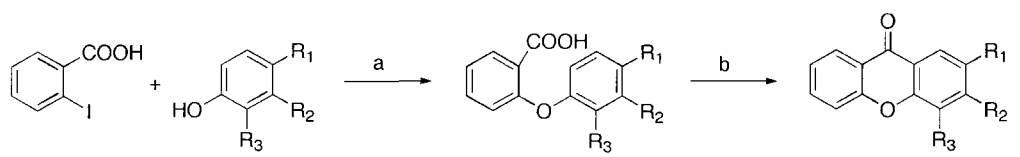

	R_1	R_2	R_3
3	CH_2CO_2H	H	H
4	H	CH_2CO_2H	H
5	H	H	CH_2CO_2H
6	CH_3	H	H
7	H	H	CH_3

Scheme 2-3. Ullmann-type coupling synthesis of xanthone derivatives **3** – **7**. (a) CuCl/TDA-1/Cs_2CO_3 b) H_2SO_4/85°C

Methyl derivatives **6** and **7** were prepared in the same fashion from 2- or 4-cresol. Derivatives **9** and **10**, which will also be discussed in this chapter, were synthesized by generating the carbanion of the methyl ester of **3** in THF using LDA and methylating this position with iodomethane (Scheme 2-4).

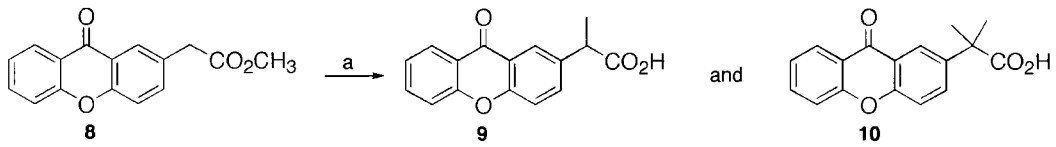

Scheme 2-4. Synthesis of xanthone derivatives **9** and **10**. (a) i) LDA/THF ii) CH_3I iii) 0.1 M KOH/CH_3CN

2.2.2 Photochemistry of 2-, 3-, and 4-xanthone acetic acids (3 – 5)

Compounds **3** – **5** in aqueous buffer (pH 7.4) exhibit a desirable improvement over ketoprofen in their absorbance above 300 nm, as seen in Figure 2-1. The spectra are very similar for all three xanthone derivatives and all show the characteristic $\pi^*\leftarrow\pi$ absorption band with a maximum near 350 nm. The molar absorbance coefficients at their band maxima for **3**, **4**, and **5** are 5600, 7900, and 8100 $M^{-1}cm^{-1}$ respectively, representing an approximate 40-fold absorption enhancement over **1**. Molar absorption coefficients at other relevant wavelengths are shown in Table 2-1.

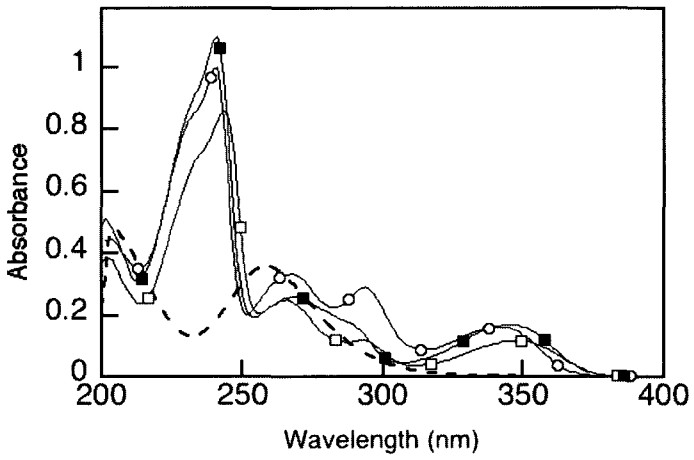

Figure 2-1. Absorption spectra of **1**(---), **3**(□), **4**(O), **5**(■) 2x10^{-5} M in pH 7.4 phosphate buffer.

Table 2-1. Molar absorption coefficients (ε, $M^{-1}cm^{-1}$) for **3–5** in pH 7.4 phosphate buffer.

	ε_{243nm}	$\varepsilon_{337\ nm}$[a]	ε (λ_{max})	λ_{max} (nm)	$\varepsilon_{355\ nm}$[b]
3	40500	4800	5600	347	5000
4	48300	7700	7900	341	4600
5	51700	7300	8100	348	6400

(a) N_2 laser excitation wavelength. (b) YAG laser excitation wavelength.

The photochemistry of **3** – **5** was investigated in aqueous solution in order to ascertain whether they are capable of undergoing photodecarboxylation to give carbanion intermediates as efficiently as ketoprofen (**1**). Irradiation of an 8 mM sample of **3** in buffered aqueous solution (Luzchem LZC-ORG photoreactor, 10 UVA lamps, pH 7.4, nitrogen bubbled) for 3 minutes resulted in its clean transformation to 2-methylxanthone (**6**, Scheme 2-5) in ~30 % yield. This reaction was conveniently followed by ^{1}H NMR, with irradiation leading to the growth of a characteristic singlet at 2.5 ppm, assigned to the methyl group of **6**, at the expense of

the singlet at 3.8 ppm, assigned to the methylene protons of **3** (Figure 2-3). Extensive irradiation (30 minutes) of **3** resulted in complete conversion to **6**, with no other products observed by ^{1}H NMR, HPLC-UV or GC-MS analysis. Remarkably, this photochemistry was equally clean in aerated and deaerated solutions. Irradiation of **5** under the same conditions gave 4-methylxanthone (**7**) as the only observable product (Scheme 2-5). Exclusive photogeneration of **6** and **7** on irradiation of **3** and **5** respectively is consistent with a heterolytic mechanism in which only carbanion intermediates are formed. In addition, since ketoprofen photodecarboxylation under air leads to two minor photoproducts that are attributed to reaction of the carbanion with oxygen, the absence of equivalent photoproducts from xanthone acetic acid in aerated solutions suggests a very short lifetime of the xanthone acetic acid carbanion. This is consistent with laser flash photolysis experiments where we were unable to observe the carbanion intermediate (*vide infra*).

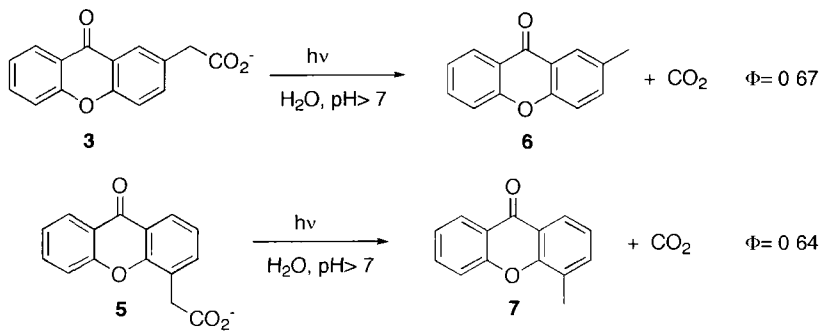

Scheme 2-5. Photodecarboxylation of 2- and 4-xanthone acetic acid (**3** and **5**).

Reaction quantum yields for the decarboxylation of **3** – **5** were initially measured by ^{1}H NMR using the analogous reaction of ketoprofen as a secondary reference standard (Φ = 0.75 at pH 7.4)[8]. Both **3** and **5** show a photodecarboxylation efficiency (Φ = 0.67 and 0.64 respectively) that is close to that of ketoprofen, demonstrating that the addition of the bridging oxygen does not significantly perturb the photochemistry. Simultaneous irradiation in either H_2O or D_2O, both with 0.1 M KOH, demonstrates no solvent isotope effect on the quantum yield of photodecarboxylation.

To our surprise, irradiation of **4** did not give any decarboxylation products, and even with extended photolysis complete recovery of starting material was realized. Such stark contrast in photodecarboxylation reactivity between positional isomers is rare; for the related 3- and 4-benzoylphenylacetic acids,[6] and for 3- and 4-nitrophenyl acetic acids,[4] the difference in photodecarboxylation efficiency between isomers is very small. We propose that both the high reactivity of **3** and **5** and the low reactivity of **4** are a result of Zimmerman's *meta* effect. That is, for **3** and **5** the enhanced electron-withdrawing ability of the ketone *meta* to the benzylic site in both of these isomers helps stabilize carbanion formation. The ketone is substituted *para* to the benzylic carbon in **4**, so the effect is absent in this case. Instead, the electron-donating ether oxygen is *meta* to the benzylic site in **4** which would actually destabilize carbanion formation. A similar effect is expected for *ortho* substituents on an aromatic ring. For this reason it was initially surprising

that **3** and **5** exhibit similar quantum yields despite the electron donating (deactivating) oxygen *ortho* to the benzylic position in **5**. While MO calculations for xanthone (Figure 2-2) confirm the electronic effect (i.e. the electron density at position 2 is lower than position 4 in the excited state), the longer singlet state lifetime of **5** (*vide infra*, Table 2-2) actually implies lower reactivity. The rate constant for singlet decarboxylation can be estimated using Equation 2-1 giving values of k_{PDC} equal to 8.5 x 10^6 s^{-1} for **3** and of 6.4 x 10^6 s^{-1} for **5** (see Table 2-2) consistent with MO expectation of a somewhat lower reactivity for **5**.

$$k_{PDC} = \frac{\Phi_{PDC}}{\tau_s} \qquad (2\text{-}1)$$

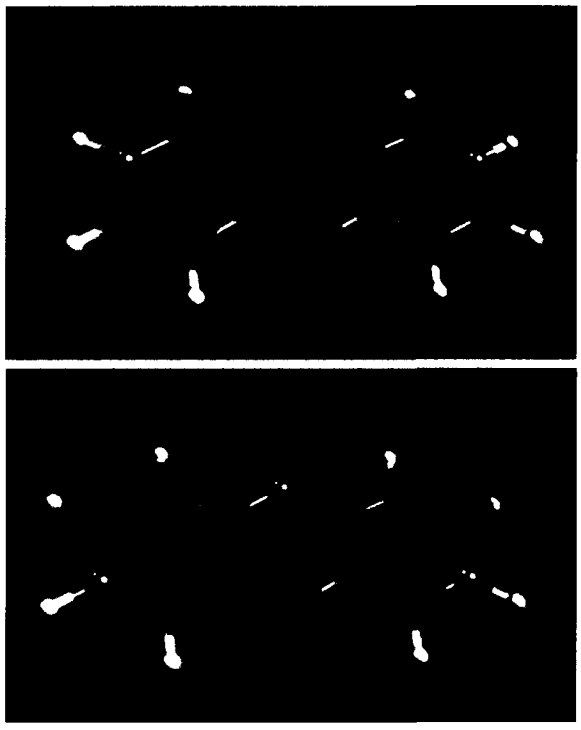

Figure 2-2. Pictorial representation of the LUMO (top) and HOMO (bottom) of xanthone, approximating the transition to the first singlet excited state. Calculated using AM1 Argus Labs 4.

To provide additional evidence of the intermediacy of carbanion intermediates in the photodecarboxylation of **3** and **5**, solutions of each were irradiated in H_2O and D_2O (containing 0.1 M KOH), and the photolysates were analyzed by ^1H NMR. Irradiation of **3** or **5** in D_2O solution gave the corresponding α-deuteromethylxanthone (**6-D** or **7-D**) with a small amount of **6-H** or **7-H**, (presumably due to the addition of KOH) as the only products observable by ^1H NMR. The α-deuteromethylxanthones were easily recognizable by ^1H NMR, since the CH_2D signal exhibits the characteristic triplet and integrates for 2 hydrogens relative to the aromatic signals of **6-D** or **7-D**. In addition, the CH_2D frequency is

slightly upfield from the corresponding methylxanthone CH_3 frequency (Figure 2-3). Since D_2O is a very poor deuterium atom donor, but an excellent D^+ source, these results support the intermediacy of a carbanion rather than a radical.

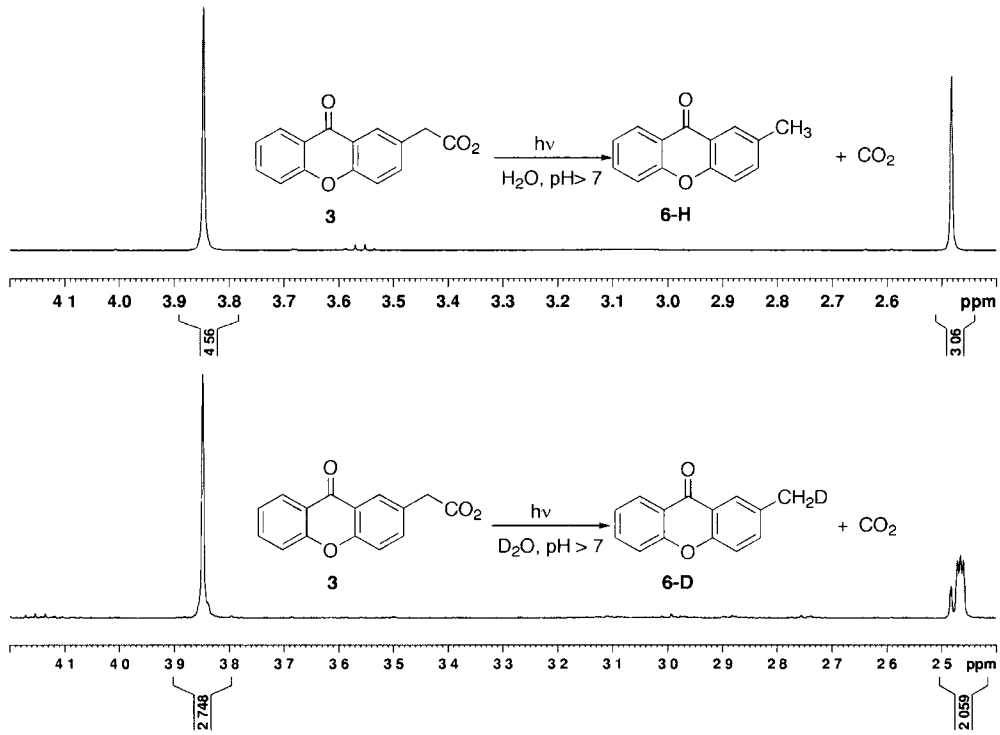

Figure 2-3. ^1H NMR spectra of **3** (8 mM) irradiated in H_2O with 0.1 M KOH (top) and **3** irradiated in D_2O with 0.1 M KOH (bottom). Samples were irradiated simultaneously with UVA light. The bottom spectrum shows formation of **6-H** (singlet) in addition to **6-D** (triplet), presumably due to the presence of residual (and more reactive) H_2O.

In subsequent experiments it was often necessary to use acetonitrile as a co-solvent due to the very poor water solubility of **6** and **7**. As such we wanted to determine if there was a significant effect from the cosolvent on the photodecarboxylation quantum yield. Initial comparison of **2** in either pure phosphate buffer (pH 7.4) or phosphate buffer with acetonitrile (1:1, v/v) showed a

slight solvent dependence on the extent of photodecarboxylation as measured by ^{1}H NMR of extracted photolysates. In order to determine if this difference was significant, the Φ_{PDC} for **3** in either pure buffer or buffer with acetonitrile with and without $N_{2(g)}$ purging was determined by HPLC quantification of triplicate samples, using ketoprofen as an actinometer. The quantum yields for each condition were found to be 0.64 ± 0.06 in pure buffer under air, 0.62 ± 0.07 in pure buffer under nitrogen, 0.68 ± 0.06 in buffer with acetonitrile under air, and 0.65 ± 0.08 in buffer with acetonitrile under nitrogen; all within error of each other. Additionally, irradiation of either **3** or **5** in both pH 7.4 phosphate buffer and in 0.1 M KOH gave identical yields of photoproduct, thus ruling out an effect of the buffer or pH in this range, at least on the photodecarboxylation yield.

Table 2-2. Photochemical Parameters for **3** – **7** in pH 7.4 phosphate buffer.

	Φ_{PDC}	Φ_F[a]	τ_S (ns)	k_F (ns^{-1})	τ_T (ns)[b]	Relative triplet yield
3	0.67 (0.64±0.06)[c]	0.0077	0.079	0.098	5400	0.4
4	<0.01	0.044	0.73	0.061	4500	1.1
5	0.64	0.010	0.10	0.097	6600	0.3
6	-	0.24	4.8	0.051	9500	1.0
7	-	0.15	3.9	0.039	6200	(1.0)[d]

[a]Measured for at least two concentrations (4 to 17 x 10^{-6} M). [b]Lifetimes of **3** – **5** are consistent for 2.0 x 10^{-6} and 5.0 x 10^{-6} M. At higher concentration (10.0 x 10^{-6}) the lifetime is shorter likely due to self-quenching of the triplet. The lifetimes of **6** and **7** were measured at 5.0 x 10^{-6} M. [c]Measured by HPLC-UV. Error based on a 95% confidence interval using student's t test. [d]Used as a reference for relative triplet yields.

2.2.3 Fluorescence

Xanthone and its derivatives are weakly fluorescent in solution, and the dependence of the fluorescence on the nature of the solvent has been well studied.[27, 28] Thus we expected that fluorescence spectroscopy could be a versatile tool in the study of the photodecarboxylation reaction of **3** and **5**. Xanthone acetic acids **3**, **4** and **5** showed weak fluorescence emission with λ_{max} at 410, 390 and 405 nm respectively in neutral phosphate buffer solution (absorbance = 0.1 or 0.05 at λ_{ex}). Photoproducts **6** and **7** have dramatically larger fluorescence quantum yields relative to their parent acids (Table 2-2). As such, the fluorescence signal from aqueous solutions of **3** or **5** can be observed to increase rapidly with irradiation (Figure 2-4). Solutions of **3** experience a 30-fold enhancement in fluorescence emission following 60 s of exposure to the UVA output of a hand-held TLC lamp (λ_{max} = 368 nm, 6.2 Watt m^{-2}, FWHM = 16 nm). Solutions of **5** experience a 15-fold enhancement. No fluorescence enhancement was observed for irradiation of the solution of **4**; instead a small decrease in fluorescence intensity was observed after several minutes of irradiation, probably resulting from inefficient photodegradation of the starting xanthone.

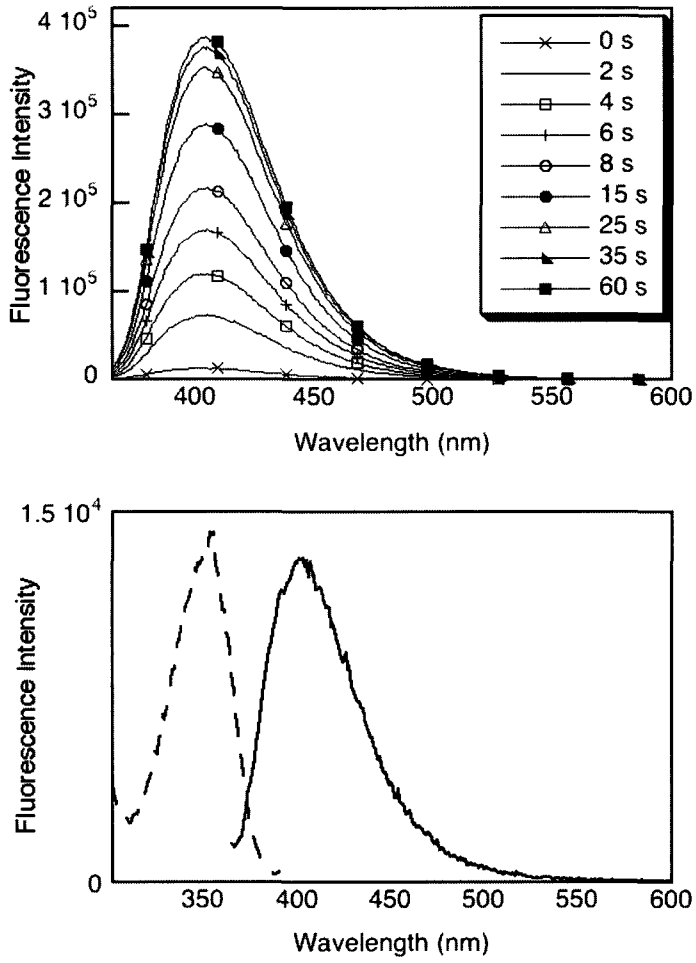

Figure 2-4. Top: Fluorescence increase with irradiation of 0.02 mM **3** in pH 7.4 phosphate buffer. Bottom: Excitation and emission spectra of **3** (may contain some **6** since the excitation beam of the fluorimeter induces photodecarboxylation).

We have measured the fluorescence lifetimes for reactive xanthone derivatives **3** and **5** as well as photostable **4**, **6** and **7** (Figure 2-5, Table 2-2). Using the measured fluorescence quantum yields (Φ_F) and singlet state lifetimes (τ_S), a fluorescence rate constant (k_F) can be calculated for **3** – **7** using Equation 2-2.

$$\Phi_F = \frac{k_F}{k_s} = k_F \tau_s \qquad (2\text{-}2)$$

Since k_F is calculated to be roughly the same for each of our xanthone derivatives, but the reactive **3** and **5** have much shorter singlet state lifetimes, there must be an additional deactivation process occurring from the singlet excited states of **3** and **5**. We attribute this process to singlet state photodecarboxylation.

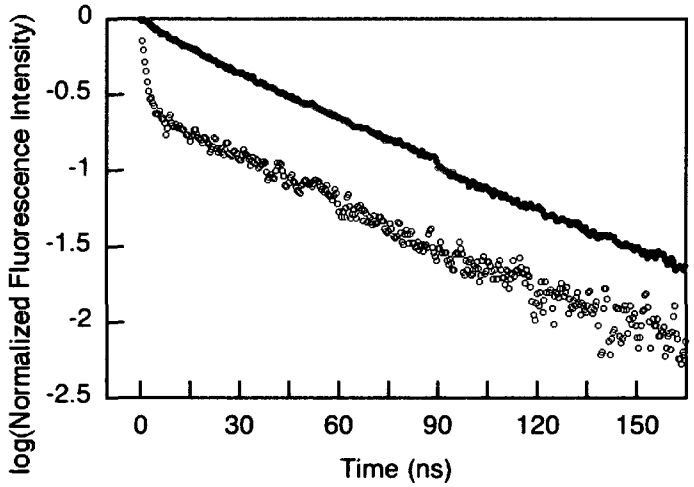

Figure 2-5. Semi-log plot for the decay of fluorescence from **5** (o) and **7** (•). The trace denoted by o decays with two components. The shorter of these two is assigned to **5** while the longer component corresponds to the fluorescence decay of a small amount of **7**. Time constants were obtained by fitting the trace after deconvoluting the laser pulse.

The observed fluorescence increase may also serve as a valuable 'reporting' tool since fluorescence increases dramatically with photorelease, thus having the potential to be used as a mapping tool in biological systems. This strategy has been applied in a limited number of other photocaging examples.[29]

2.2.4 Nanosecond Laser Flash Photolysis (LFP)

In the hope of observing the carbanion intermediates produced on photodecarboxylation of **3** and **5**, we employed nanosecond laser flash photolysis (LFP). The transient spectra of **3**, **4**, and **5** (Figure 2-6) contained broad absorption bands in the 450-750 nm range centered at 580, 600, and 585 nm respectively and in all cases decayed with clean first order kinetics. The transients produced from **3** - - **5** upon 355 nm excitation showed similar lifetimes of ~5 μs (Table 2-2) in N_2 saturated solutions. These transient absorption spectra are similar in λ_{max}, spectral width, and lifetime to the triplet-triplet absorption of the parent xanthone.[30, 31] When solutions were saturated with oxygen, similar transient absorption spectra were obtained, although the transient lifetime was reduced to 0.4, 0.2, and 0.3 μs for **3**, **4**, and **5** respectively. Since oxygen is well known to be an effective quencher of triplet states, we propose that the long-lived signals we see from **3** – **5** are due to triplet-triplet absorptions.

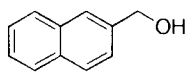

HMN

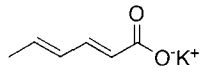

Potassium sorbate

Chart 2-2.

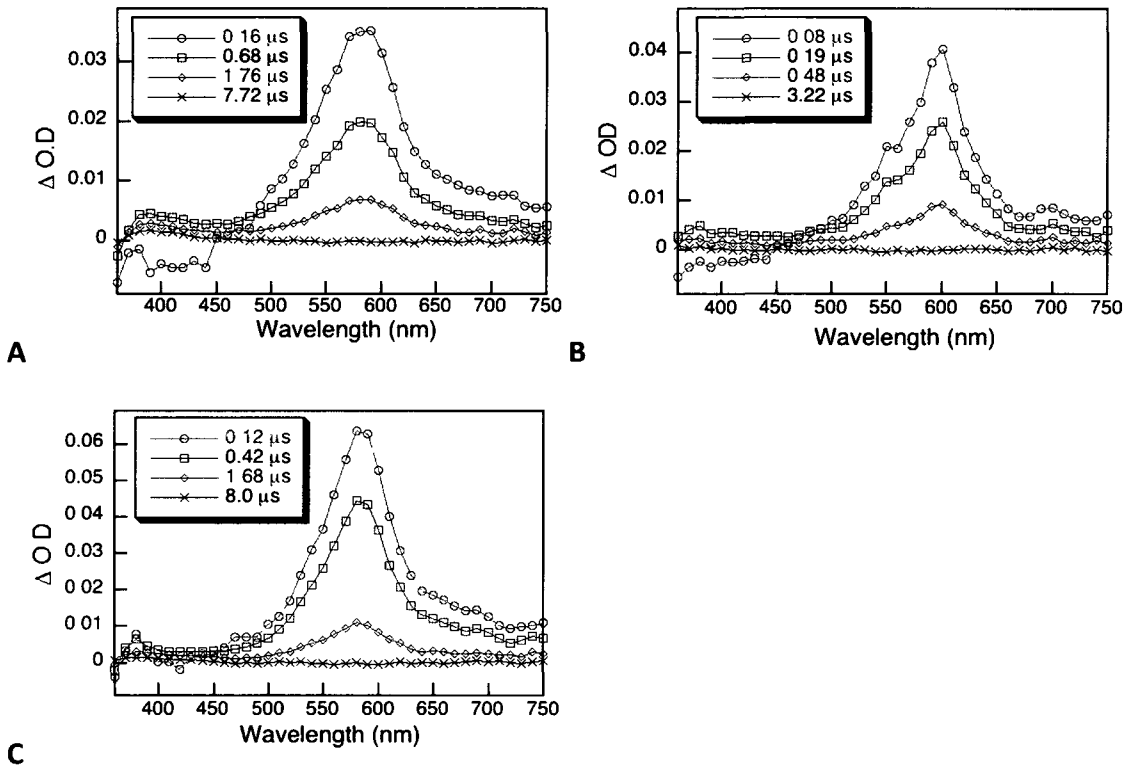

Figure 2-6. Time resolved absorption spectra of **3** (A), **4** (B), and **5** (C) in 0.1 M KOH solution purged with nitrogen. Solutions of **3** and **5** were flowed during data acquisition. Negative ΔO.D. values at the shortest timescale are due to fluorescence.

To confirm this assignment, we employed other triplet quenchers including 1-hydroxymethylnaphthalene (HMN) and potassium sorbate (Chart 2-2). Addition of HMN to solutions of **3** - **5** led to an increase in the decay rate constant for their respective triplet signals along with a growth at ~420 nm, which is characteristic of the triplet signal of the naphthalene chromophore.[32] This result is strong support for our assignment of the observed transients from **3** - **5** as triplet states, since quenching of triplets by HMN will produce a naphthalene triplet signal. Because the naphthalene triplet at 420 nm appears as a growth, we can be confident that the signal is not due to direct excitation of the HMN (which in any case does not absorb

at the excitation wavelength of 355 nm). Addition of increasing amounts of HMN to a solution of **4** allowed us to produce a quenching plot, whose slope gave a bimolecular quenching rate constant (k_q) of 4.4 x 10^9 $M^{-1}s^{-1}$ according to Equation 2-3.

$$k = k_0 + k_q[Quencher] \tag{2-3}$$

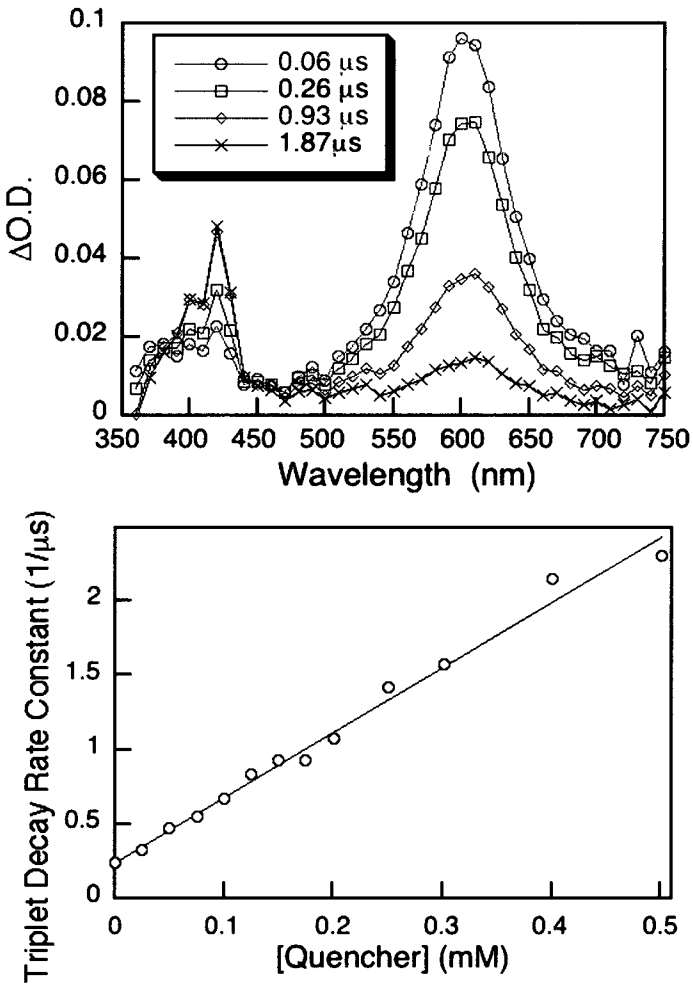

Figure 2-7. Quenching of $\mathbf{4}^{3*}$ by hydroxymethylnaphthalene (HMN). Top: Time resolved absorption spectrum of **4** with HMN showing HMN^{3*} (420 nm) and $\mathbf{4}^{3*}$ (600 nm). Bottom: Quenching plot for the dependence of the first order decay rate constant from the signal at 600 nm on the concentration of HMN.

On a first approximation we assume that the triplet states of **3** – **7** have similar absorption coefficients and thus the triplet signal intensities for matched samples can be used as a measure of the triplet yield. These values are shown in the last column of Table 2-2; they are consistent with the fluorescence data, *i.e.,* molecules **3** and **5**, with highly reactive (decarboxylating) singlets produce lower yields of the relative triplet state.

We also used potassium sorbate, a conjugated diene, to quench the triplets we observed on LFP of **3** – **5**. Efficient quenching was observed upon addition of sorbate and by varying the sorbate concentration we were able to produce the quenching plot shown in Figure 2-8. The quenching plot showed a linear correlation, and the slope indicated a bimolecular quenching rate constant of 2.7 x 10^9 $M^{-1}s^{-1}$. Due to the high solubility of potassium sorbate in water we were able to use sufficiently large concentrations to quench the triplet signal from **3** – **5** entirely. We were hoping that by completely quenching the triplet, we might detect a carbanion signal that had previously been obscured by the much larger triplet signal. On addition of 50 mM potassium sorbate we were unable to detect any transient absorption by LFP (Figure 2-8, bottom), suggesting that the carbanion lifetime is too short for us to detect within the time resolution of our instrument (~20 ns).[33]

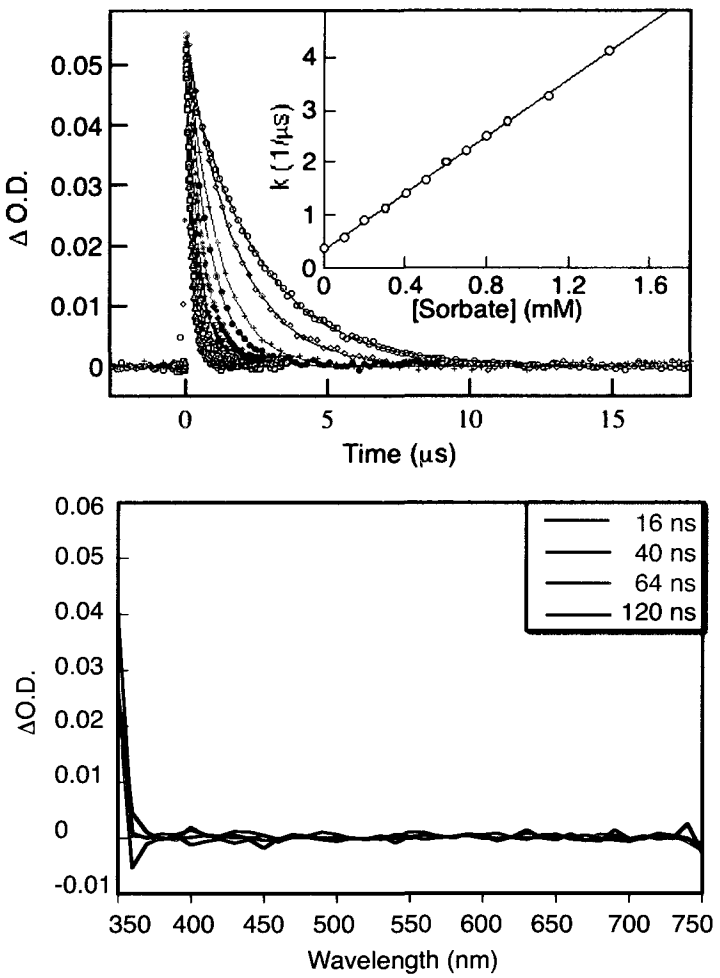

Figure 2-8. Top: Quenching by sorbate of transient decays for 0.08 mM **4** in deaerated pH 7.4 phosphate buffer/acetonitrile (80:20). Inset: rate constant of each decay (for the signal at 600 nm) as a function of sorbate concentration. Bottom: Time resolved absorption spectrum of **3** with 50 mM sorbate in pH 7.4 buffer.

With the knowledge that addition of 50 mM potassium sorbate to solutions of **3** – **5** leads to >95 % quenching of the photogenerated triplet states, we repeated the product studies with potassium sorbate to see if quenching the triplets would affect product yields. Solutions of **3** in pH 7.4 phosphate buffer with and without 50 mM sorbate were irradiated simultaneously in a carousel and the photoproducts were

analyzed. We found that the presence of sorbate had no effect whatsoever on product yields. This is strong evidence that the photodecarboxylation of **3** occurs *exclusively* from the singlet excited state and that the triplet state does not play a measurable role in the photodecarboxylation mechanism. To further confirm this multiplicity of the reaction, we irradiated **3** in phosphate buffer 1:1 with either acetonitrile or acetone (UVB, 3 min.). If the reaction proceeded from the triplet we would expect a higher yield for the solution with acetone since acetone is a known triplet sensitizer. Instead, we observed higher conversion for the solution with acetonitrile (30% *vs.* 20%). This difference is likely due to screening of the light by acetone.

We attempted to increase the lifetime of the carbanion produced on photodecarboxylation of **3** so that we could characterize it by LFP. We decided to substitute the benzylic carbon of **3** with alkyl groups, a strategy that was previously successful in prolonging the lifetimes of similar carbanions from ketoprofen due to steric shielding by the alkyl groups.[14] To this end, we prepared mono- and dimethylated derivatives **9** and **10**. LFP of these analogues in 0.1 M KOH, or D_2O with NaH, both with 50 mM sorbate to remove the triplet signal, failed to produce any detectable signal. It would seem from our results that the carbanion intermediates from **3** and **5** are very short lived, and that the lifetime enhancement provided by the benzylic alkyl groups was too modest to enable us to detect their absorption.

2.2.5 Two photon excitation

Given the recent interest in two photon excitation (TPE) for many applications including photolabile protecting groups, we were interested in measuring a two photon excitation cross-section for the xanthone acetic acid derivatives. The process of TPE involves initial excitation with one photon to a virtual excited state (τ ~ 1 fs) followed by promotion to a real singlet excited state by the second photon. As such, the requirements for TPE include a one photon absorbance at one half the wavelength of the two photon excitation wavelength and a high intensity light source (typically a femtosecond laser) so that the photon flux is high enough to excite the virtual state. As a consequence of the high flux required, TPE only occurs at the focal point of the laser. This is the source of the higher degree of spatial control compared to one photon excitation.

Taking advantage of the fluorescence increase with photodecarboxylation, we monitored the fluorescence from a solution of **5** in phosphate buffer (pH 7.4) placed in the focal point of our ps laser (532 nm). Spectra were measured at intervals of 2000 shots up to 10000 shots. No change at all was observed.

A subsequent collaboration with Prof. Tim Dore yielded much more promising results. Using with a fs-pulsed and mode-locked Ti:Sapphire laser (Chameleon Ultra II, Coherent) with 700 nm light at a power of 250 mW as the excitation source and monitoring both the disappearance of **3** and the appearance of **6** by HPLC, he was

able to measure a TPE action cross-section (δ_u) of 2.1 GM.[34] The same cross section was also obtained for the photodecarboxylation of **5**. This value is a product of the two photon absorbance cross-section (δ_a, related to the probability that two photons will be absorbed and analogous to the one photon value ε) and the quantum yield of the photochemical reaction. It has been proposed that for PPG applications, δ_u should be at least 0.1 GM,[35] over an order of magnitude lower than the value measured for photodecarboxylation from **3** and **5**. In fact, the value of 2.1 GM is one of the largest reported for photochemistry relating to a PPG.

2.3 Photodecarboxylation of xanthone acetic acid (XAA) at pH < pK_a

Other substituted arylacetic acids have exhibited interesting pH dependent photochemistry. Typically the Φ_{PDC} is highest when the pH is well above the pK_a of the carboxylic acid and drops off as the pK_a is approached indicating that photodecarboxylation occurs from the carboxylate form. While for some derivatives the quantum yield drops to 0 at low pH where the carboxylate is protonated,[2, 4, 5] for others,[7] it plateaus indicating an acid catalysed photodecarboxylation. That is, there is an alternative photodecarboxylation pathway from the acid form that is facilitated by transient protonation. Derivatives **3** and **5** appear to belong to this latter category.

Simultaneous irradiation of either **3** or **5** over a range of pH exhibited the dependence shown in Figure 2-9 with a significant amount of photodecarboxylation occuring even at low pH. It was confirmed by NMR and GC/MS that only the photodecarboxylation photoproducts, **6** and **7** respectively, were formed. Interestingly, in methanol under the same irradiation conditions **3** is photostable. Further investigation with 0.1 M HCl (or DCl) solutions either in H_2O or D_2O revealed a solvent isotope effect of 1.3 for the photodecarboxylation of **3**.

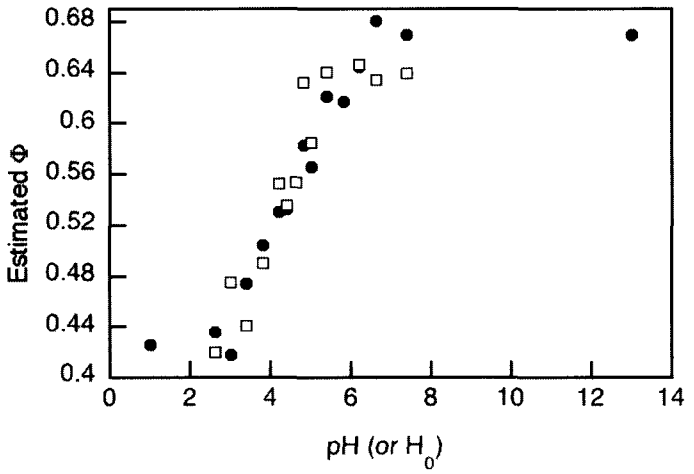

Figure 2-9. pH dependence of Φ_{PDC} for **3** (•) and **5** (□). Values are estimated based on one measure of photochemical conversion for each pH point and referenced to the quantum yield at determined at pH 7.4.

Given that fluorescence has been such a valuable tool for studying these systems, we tried to measure the singlet state lifetimes of **3** – **7** at pH 1.0 (where **3** – **5** should be entirely in the acid form). However, we were unable to measure a detectable fluorescence signal. With steady state fluorescence measurement of **5** and the corresponding photoproduct **7** we found the fluorescence of both to be significantly quenched at this pH (Figure 2-10).

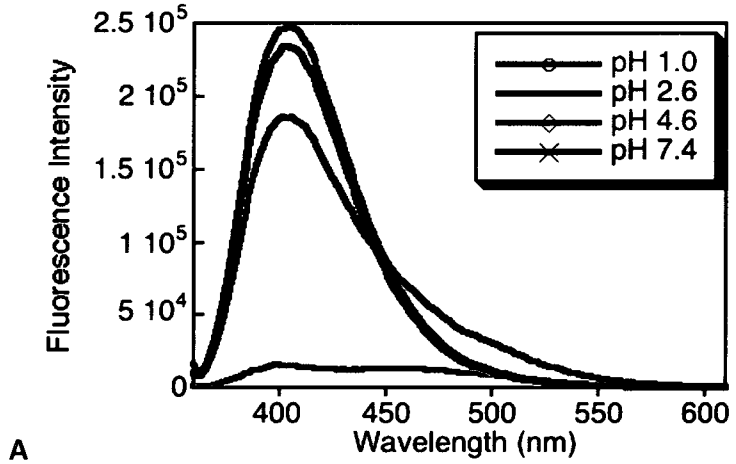

A

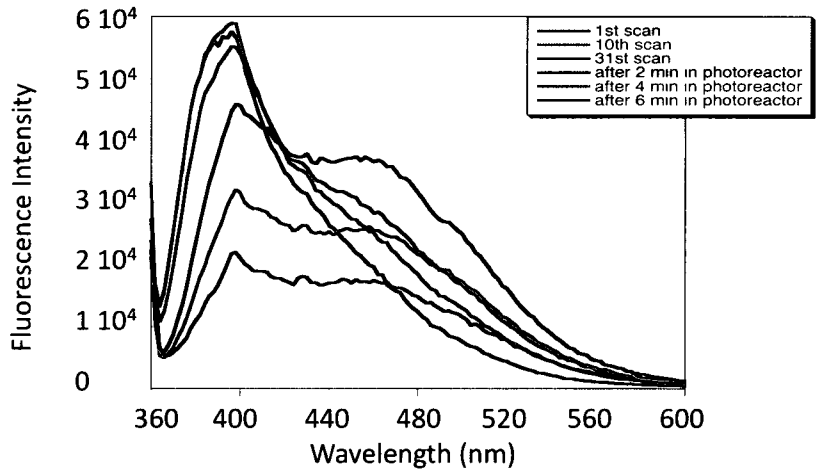

B

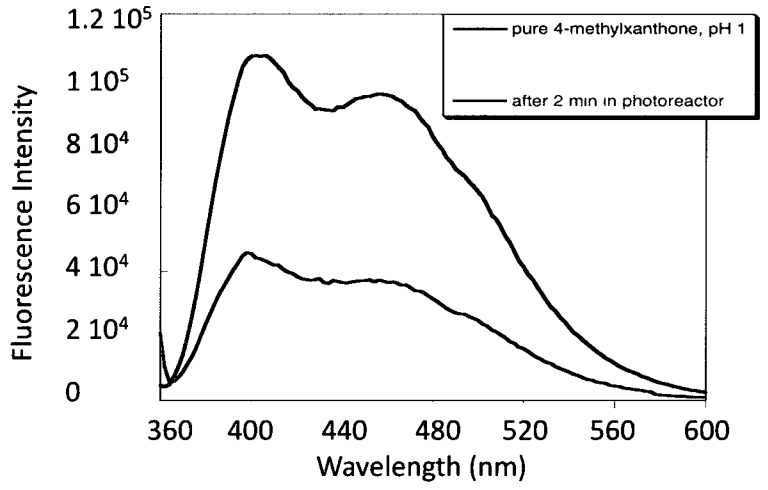

C

Figure 2-10. **A**: pH dependence for fluorescence of **5**. **B**: Fluorescence of **5** with irradiation in 0.1 M HCl. **C**: Fluorescence of **7** in 0.1 M HCl.

Huck *et al.* observed a very similar pH dependence of PDC quantum yield for *m*-acetylphenylacetic acid.[7] They proposed protonation of the reactive excited state, thus generating an even stronger electron withdrawing group, followed by decarboxylation with concerted loss of the carboxylic proton to water (Scheme 2-5). This would certainly fit with our observed solvent isotope effect at low pH.

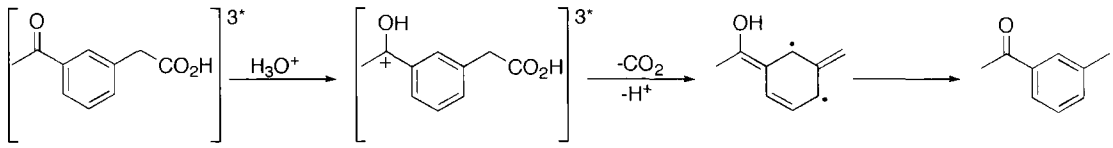

Scheme 2-6. Proposed mechanism for PDC from *m*-acetylphenylacetic acid at low pH.[7]

Our fluorescence studies suggest that the singlet excited states of **3** and **5** are protonated at low pH and so we initially thought the reactive excited state may still be the singlet. However, we could not rule out the possibility that the triplet state is also protonated, particularly given that Ramseier *et al.* have demonstrated that aromatic ketones are readily photoprotonated *via* the triplet excited state.[36] To determine the multiplicity, we irradiated solutions of **3** in 0.1 M aqueous HCl with acetonitrile (1:1) with and without 50 mM sorbic acid, the same experiment that established singlet mediated photochemistry at pH 7.4. This time, there was a very significant effect on the photochemical quantum yield. In the absence of the triplet quencher sorbic acid, the conversion was 22 % while in the presence of sorbic acid the conversion was only 5%. This strongly supports a triplet mediated mechanism at low pH.

2.4 Summary

Irradiation of **3** and **5** in aqueous and deuterated aqueous solutions gave products consistent with exclusive formation of a carbanion intermediate *via* photodecarboxylation, and the fluorescence and quenching experiments support a singlet pathway when pH > pK_a. We were able to directly detect strong triplet signals for **3** – **5** by LFP, indicating that intersystem crossing is significant. However, our quenching studies with sorbate allow us to conclude that the photodecarboxylation pathway is independent of this triplet formation. Our inability to detect a carbanion signal *via* LFP of **3**, **5**, and alkyl derivatives of **3** (**9** and **10**) and our inability to trap the intermediate carbanions with oxygen indicate that the carbanions produced are very reactive, much more so than the carbanion derived from ketoprofen. Since the carbanion intermediates produced on irradiation of **3**, **9**, and **10** were all too short-lived for us to observe by LFP, we can estimate an upper limit of 20 ns for their lifetimes, which gives us pseudo-first order protonation rate constants of $\geq 5 \times 10^7\ s^{-1}$.

If we assume that the carbanion intermediate is in its ground state before being protonated (i.e. that decarboxylation is not adiabatic), a higher reactivity for the carbanions derived from **3** and **5** as compared with that derived from ketoprofen is not entirely surprising considering the effect of the ether oxygen of xanthone on the ground state carbanion. This ether oxygen is positioned *para* and *ortho* in **3** and **5** respectively. As such, the electron donating effect is expected to be

strong in the ground state and would destabilize the ground state carbanion. In general, if we consider the energy surfaces of this type of photodecarboxylation reactions, *meta* substitution (being stronger in the excited state) will determine the excited state barrier towards carbanion formation. *Ortho* and *para* substitution (being stronger in the ground state) will determine the ground state barrier to protonation. Therefore, in both **3** and **5** there should be a lowered barrier to carbanion formation (resulting in a higher quantum yield) and and lowered barrier to protonation (since the carbanion intermediate would be raised in energy).

With regards to the potential for this photochemistry to be used in the development of a photolabile protecting group, we have a very reactive carbanion intermediate that is formed rapidly and efficiently. In the following chapter I will describe how we make use of this intermediate to release small molecules. Given the high efficiency, short timescale and the high UVA absorption, this photochemistry is very promising for PPG application. The high TPE action cross-section is also quite exciting since the ability to release in this way is very desirable and it would seem that PPGs based on either **3** or **5** should do so efficiently.

2.5 Experimental

All ^{1}H NMR and ^{13}C NMR spectra were recorded at room temperature on Bruker AVANCE 300, 400, or 500 instruments. Chemical shifts are reported relative to internal TMS. Melting points were determined on a Melt-Temp II aparatus from Laboratory Devices. Column chromatography employed Merck silica gel 230-400 mesh. Water was purified through a Millipore MilliQ system. Acetonitrile was HPLC grade. All other solvents are reagent grade from Aldrich and used as received except for THF, which was distilled over Na metal. All chemicals were purchased from Aldrich. Copper (I) chloride was recrystallized from concentrated hydrochloric acid, all others were used as received. The synthetic protocols for **3 – 7** were adapted from Rewcastle *et al.*[26]

2.5.1 Synthesis

(9-Oxo-9*H*-xanthen-2-yl)-acetic acid (3) [30087-31-1] To a flame dried 250 mL round bottom flask was added 2-iodobenzoic acid (5.47 g, 22.6 mmol), 4-hydroxyphenylacetic acid (4.81 g, 31.6 mmol), Cs_2CO_3 (28.0 g, 85.9 mmol), and dioxane (100 mL). This heterogeneous solution was stirred under an argon atmosphere at room temperature. After 10 minutes, tris-[2-(2-methoxy-ethoxy)-ethyl]-amine (TDA-1) (0.87 mL, 2.7 mmol) and CuCl (0.27 g, 2.7 mmol) were added. The mixture was brought to reflux under an argon atmosphere with stirring and left to reflux 20 hr. Following this period, the reaction was allowed to cool to room temperature. The solvent was then removed under reduced pressure. The

remaining solid was dissolved in 100 mL 0.1 M NaOH and filtered. The green filtrate was transferred to a separatory funnel, acidified with 1.0 M HCl and extracted with 3 × 30 mL ethyl acetate. The combined organic layers were dried with $MgSO_4$, filtered, and the solvent was removed under reduced pressure to yield an orange oil. Concentrated sulfuric acid (12 mL) was added to the oil in a 50 mL round bottom flask. This solution was heated to 85°C with stirring for 1 hr. After cooling to room temperature, the mixture was poured over ice. Once the ice had melted, the solution was transferred to a separatory funnel with water and extracted with 3 × 30 mL ethyl acetate. The organic layers were combined and dried with $MgSO_4$, filtered, and the solvent was removed under reduced pressure to give a brown solid. The solid was recrystallized twice from hot toluene to give a white crystalline solid (1.70 g, 6.7 mmol, 30%). m.p. 223°C, turns brown (lit. 224-226°C). ^{1}H-NMR and ^{13}C-NMR are in good agreement with those reported.[26] ^{1}H NMR (500 MHz, DMSO-d6) δ (ppm) 3.79 (2H, s), 7.49 (1H, t, J= 7.5 Hz), 7.64 (1H, d, J= 8.6 Hz), 7.68 (1H, d, J= 8.4 Hz), 7.78 (1H, dd, J_1= 8.6 Hz, J_2= 2.2 Hz), 7.88 (1H, td, J_1= 7.8 Hz, J_2= 1.7 Hz), 8.09 (1H, d, J= 2.0 Hz), 8.21 (1H, dd, J_1= 8.0 Hz, J_2= 1.6 Hz), 12.5 (1H, s). ^{13}C NMR (125 MHz, DMSO-d6) δ (ppm) 40.2, 118.4, 118.6, 121.1, 121.4, 124.7, 126.4, 126.7, 131.8, 135.9, 137.4, 154.8, 155.9, 172.9, 176.3. EI (MS) m/z (%) 254.06, (52.8) (M^+ - $C_{15}H_{10}O_4$); 209.06, (100) (M^+ - $C_{14}H_9O_2$); 161.99, (8.2); 152.06, (8.8). HRMS for $C_{15}H_{10}O_4$ [M^+] calculated 254.0579, found 254.0562.

4-7 were prepared in the same way as **3** with similar yields using 3-hydroxyphenylacetic acid, 2-hydroxyphenylacetic acid, 4-methylphenol, and 2-methylphenol in place of 4-hydroxyphenylacetic acid.

(9-Oxo-9*H*-xanthen-3-yl)-acetic acid (4) [118537-75-0] m.p. 224°C, turns brown (lit. 227.5-228.5°C). ^{1}H-NMR and ^{13}C-NMR are in good agreement with those reported.[26] ^{1}H NMR (500 MHz, DMSO-d6) δ (ppm) 3.81 (2H, s), 7.36 (1H, dd, J_1= 8 Hz, J_2= 1 Hz), 7.44 (1H, td, J_1= 8 Hz, J_2= 1 Hz), 7.56 (1H, s), 7.61 (1H, d, J= 8 Hz), 7.83 (1H, td, J_1= 8Hz, J_2= 1 Hz), 8.10 (1H, d, J= 8 Hz), 8.15 (1H, dd, J_1= 8 Hz, J_2= 1 Hz). ^{13}C NMR (125 MHz, DMSO-d6) δ (ppm) 40.8, 118.5, 119.0, 120.0, 121.5, 124.6, 126.1, 126.3 (2C), 135.7, 143.7, 155.7, 155.9, 172.1, 176.0. HRMS for $C_{15}H_{10}O_4$ [M^+] calculated 254.0579, found 254.0554.

(9-Oxo-9*H*-xanthen-4-yl)-acetic acid (5) [35614-21-2] m.p. 216°C, turns brown (lit. 214-215°C). ^{1}H-NMR and ^{13}C-NMR are in good agreement with those reported.[26] ^{1}H NMR (500 MHz, DMSO-d6) δ (ppm) 3.97 (2H, s), 7.43 (1H, t, J= 7.6 Hz), 7.49 (1H, t, J= 7.5 Hz), 7.62 (1H, d, J= 8.0 Hz), 7.81 (1H, dd, J_1= 7.3 Hz, J_2= 1.4 Hz), 7.88 (1H, td, J_1= 7.7 Hz, J_2= 1.6 Hz), 8.11 (1H, dd, J_1= 8.0 Hz, J_2= 1.6 Hz), 8.19 (1H, dd, J_1= 8.0 Hz, J_2= 1.4 Hz) ^{13}C NMR (125 MHz, DMSO-d6) δ (ppm) 35.2, 118.5, 121.2, 121.3, 124.2, 124.9, 125.1, 125.4, 126.3, 136.0, 137.3, 154.2, 155.6, 172.3, 176.4. EI (MS) m/z (%) 254.06, (61.5) (M^+ - $C_{15}H_{10}O_4$); 209.06, (100) (M^+ - $C_{14}H_9O_2$); 161.99, (18.4); 152.06, (8.1); 142.99, (14.7). HRMS for $C_{15}H_{10}O_4$ [M^+] calculated 254.0579, found 254.0554.

2-Methyl-xanthen-9-one (6) [6280-45-1] m.p. 122°C. (lit. 122°C) ^{1}H-NMR and ^{13}C-NMR are in good agreement with those reported.[37] EI (MS) m/z (%) 210.07, (100) (M^+ - $C_{14}H_{10}O_2$); 181.06, (32.2); 161.99, (8.1); 152.06, (5.7); 142.99, (5.9). HRMS for $C_{14}H_{10}O_2$ [M^+] calculated 210.0681, found 210.0662.

4-methyl-xanthen-9-one (7) [5396-28-1] m.p. 125-126°C. (lit. 127°C) . ^{1}H-NMR and ^{13}C-NMR are in good agreement with those reported.[37] ^{1}H NMR (500 MHz, DMSO-d6) δ (ppm) 2.46 (3H, s), 7.29 (1H, t, *J*= 7 Hz), 7.43 (1H, t, *J*= 7 Hz), 7.60 (1H, d, *J*= 8 Hz), 7.65 (1H, d, *J*= 7 Hz), 7.81 (1H, td, J_1= 8 Hz, J_2= 1Hz), 7.95 (1H, d, *J*= 8 Hz), 8.12 (1H, dd J_1= 8 Hz, J_2= 1 Hz). ^{13}C NMR (125 MHz, DMSO-d6) δ (ppm) 176.5, 155.7, 154.1, 136.3, 135.6, 127.4, 126.2, 124.6, 124.0, 123.8, 121.2, 121.1, 118.6, 15.6. EI (MS) m/z (%) 210.07, (100) (M^+ - $C_{14}H_{10}O_2$); 181.06, (31.2); 161.99, (3.6); 152.06, (8.1); 142.99, (2.4). HRMS for $C_{14}H_{10}O_2$ [M^+] calculated 210.0681, found 210.0666

9H-Xanthene-2-acetic acid, 9-oxo-, methyl ester (8) [78096-25-0] To a round bottom flask containing 40 mL methanol and 2 mL conc. H_2SO_4 was added **3** (1.19 g, 4.68 mmol). The solution was brought to reflux and kept there for 2 hr. at which point the solution was cooled to room temperature and filtered. The solid was dissolved in CH_2Cl_2 and washed with water. The organic layer was dried ($MgSO_4$) and concentrated *in vacuo* to give **8** as a white solid (1.21 g, 4.52 mmol, 96%). ^{1}H NMR (400 MHz, $CDCl_3$) δ (ppm) 3.72 (3H, s, -CH_3), 3.77 (2H, s, -CH_2-), 7.39 (2H, t, J=7.6 Hz), 7.51-7.48 (2H, m), 7.74-7.67 (2H, m), 8.22 (1H, d, *J*= 2.4 Hz), 8.34 (1H, dd, J_1= 18 Hz, J_2= 1.6 Hz).

9H-Xanthene-2-acetic acid, α-methyl-9-oxo- (9) [30087-33-3] A stirred solution of **8** (1.07 g, 3.99 mmol) in dry THF was cooled in a dry ice/acetone bath (-78°C) under a nitrogen atmosphere. To this was added LDA freshly prepared from diisopropylamine and standardized *n*-BuLi (2.5 M, 4.39 mmol). After 30 min., once the blue colour of the carbanion had evolved, iodomethane (5.99 mmol) was added. The solution was allowed to warm gradually to room temperature. The reaction was quenched with water and transferred to a separatory funnel with ethyl acetate for extraction. Organic layers were washed with $NaHCO_3$, dried over $MgSO_4$ and concentrated under vacuum. Recrystallization from hot ethanol yielded 9H-Xanthene-2-acetic acid, α-methyl-9-oxo-, methyl ester as a white solid. This solid was dissolved in CH_3CN and 0.1 M KOH (1:1) and stirred for 2 hr. The reaction solution was then washed with CH_2Cl_2, acidified with 10% HCl and extracted with 3 x 25 mL EtOAc. The combined organics were dried with $MgSO_4$, filtered and the solvent was removed under vacuum yielding pure **9**. ^1H NMR (400 MHz, DMSO-d6) δ (ppm) 1.46 (3H, d, J=7 Hz), 3.93 (1H, q, J= 7 Hz), 7.49 (1H, dt, J_1= 7 Hz, J_2= 1 Hz), 7.7 (2H, m), 7.8-7.9 (2H, m), 8.10 (1H, d, J= 2 Hz), 8.2 (dd, J_1= 8 Hz, J_2= 1 Hz). DEPTQ ^{13}C NMR (100 MHz, DMSO-d6) δ 18.52, (CH_3), 43.96 (CH), 118.22 (CH), 118.43 (CH), 120.87 (C), 121.05 (C), 124.21 (CH), 124.39 (CH), 126.03 (CH), 135.11 (CH), 135.57 (CH), 137.45 (C), 154.57 (C), 155.60 (C), 175.12 (C=O), 175.97 (C=O). HRMS for $C_{14}H_{10}O_2$ [M^+] calculated 268.0736, found 268.0729.

9H-Xanthene-2-acetic acid, α,α-dimethyl-9-oxo- (10) [40575-81-3] **8** (0.11 g, 0.41 mmol) was dissolved in 10 mL DMSO. After purging with nitrogen gas, crushed KOH (0.2 g) was added. Once the blue colour of the carbanion evolved, excess CH_3I was added and the solution was stirred under nitrogen gas for 3 hr. The reaction was quenched with 1% HCl and extracted with CH_2Cl_2. The combined organic layers were washed thoroughly with 1% HCl, dried (over $MgSO_4$) and concentrated *in vacuo* to give an oil that was further purified by flash chromatography (100 g silica, 25% ethyl acetate in hexanes). The methyl ester was deprotected using the same method as for **11** and **17** was obtained as a white solid. ^1H NMR (400 MHz, $CDCl_3$) δ 8.35 (2H), 7.71 (2H), 7.47 (2H), 7.38 (1H), 3.68 (3H), 1.68 (6H).

2.5.2 Absorption Coefficients

The values in Table 2-1 were measured in 0.1 M pH 7.4 phosphate buffer. At least 8 absorbance measurements were taken for concentrations ranging from 2.6 x 10^{-6} M to 2.1 x 10^{-5} M in quartz cells with a pathlength of 1.00 cm. Plots of absorbance *vs.* concentration were linear within this region.

2.5.3 Product Studies

Solutions of **3** – **5** (8 mM in the specified solvent) in quartz test tubes were irradiated in a Luzchem ORG photoreactor equipped with 8 lamps (4 bulbs on each side of the photoreactor, either UVA or UVB) in a merry-go-round apparatus for 3 min. (or 30 min. for exhaustive irradiation). Following irradiation, the contents of each tube were acidified with 1.0 M HCl and extracted with CH_2Cl_2 or ethyl acetate.

The recovered white solid from each sample was dissolved in DMSO-d6 or acetone-d6 and analyzed by ^{1}H and ^{13}C NMR. Xanthone acetic acids **3** and **5** were easily distinguished from their respective photoproducts in the ^{1}H NMR spectra based on the aromatic region, which is quite clean, and additionally in the case of **5**, based on the methyl protons. For **3**, the methyl protons are obscured by the DMSO signal. Irradiation of **6** and **7** followed the same procedure except the photolyses were followed by thin layer chromatography and GC/MS.

Solvent isotope effects were measured by irradiating solutions of **3** in H_2O with 0.1 M KOH, D_2O with 0.1 M KOH, H_2O with 0.1 M HCl, and D_2O with 0.1 M DCl for 2, 3, 4, and 5 minutes. Acetonitrile with acetic acid was then added to each solution to a total composition of 80% CH_3CN 15% H_2O 5% acetic acid. The % conversion was determined by HPLC analysis. The solvent isotope effect at each pH was determined as the ratio of two slopes (*i.e.* H_2O:D_2O) for the number of moles photolysed ($n_{photolysed}$) *vs.* irradiation time.

The photodecarboxylation quantum yields for **3** under different conditions were determined as follows. Solutions of **3** (2.1 mM in phosphate buffer solution (PB) and in PB/CH_3CN 1/1 (v/v)) and **1** (2.1 mM in PB) were prepared and 2 mL of each were added to quartz test tubes then capped with rubber septa. For **3**, 12 tubes were prepared: triplicate tubes of each PB under air, PB deaerated with nitrogen gas, PB/CH_3CN 1/1 (v/v) under air and PB/CH_3CN 1/1 (v/v) deaerated with nitrogen gas. All 12 tubes with 4 tubes containing 2 mL of 2.1 mM ketoprofen

in deaerated PB were irradiated for 3 min. in a merry-go-round apparatus within a Luzchem photoreactor with 2 UVB lamps per side. After irradiation 6.00 mL of an internal standard solution (0.21 mM 9-hydroxyfluorene in CH_3CN) was added to each tube and the contents were diluted to 20 % PB 80 % CH_3CN with 0.1% acetic acid for HPLC analysis.

2.5.4 HPLC Analysis

High performance liquid chromatography (HPLC) was performed using an Agilent 1100 Series apparatus (G1379A Degasser, G1312A Binary Pump, G1387A Autosampler, G1315B Diode Array Detector). Separations were achieved on a reversed-phase C-18 column (Zorbax SB C-18 4.6 mm x 25 cm) at room temperature.

The mobile phase, flowing at a rate of 0.25 mL/min., consisted of 85 % acetonitrile and 15% water with 0.1% acetic acid added to improve peak shape. The injection volume was 10.0 μL. Absorbance signals were monitored at 254 nm using 500 nm as a baseline reference. Quantification was based on peak area using a calibration curve constructed by analyzing standard samples with the identical HPLC method. 9-Hydroxyfluorene was used as an internal standard added to both the analysed and the calibration samples. The exception to this was the kinetic solvent effect measurements. In this case, quantification was based on a ratio of starting material area to product area. Since only one photoproduct is formed and there is no change in absorption with photolysis, this method is valid.

2.5.5 Fluorescence Spectroscopy

All solutions under study were thoroughly deaerated with dry nitrogen prior to fluorescence measurements. Steady state fluorescence spectra were collected with a luminescence spectrometer from Photon Technology International. Time-resolved studies were made with the third harmonic of a Continuum PY-61 Nd:YAG laser (λ_{ex} = 355 nm, FWHM = 35 ps, pulse energy = 4 mJ), using a Hamamatsu C4334 streak camera for luminescence detection.

Fluorescence quantum yields for **4**, **6** and **7** were measured using at least 3 multiple trials with quinine bisulfate in 1.0 N H_2SO_4 (at a matched absorbance) as a reference. Measurements were taken for at least two different concentrations in order to rule out self-quenching. Because of the limited solubility of **6** and **7** in water, a sample of each was left to stir overnight in pH 7.4 phosphate buffer. These saturated solutions were then filtered and the filtrate concentration was adjusted to the desired absorbance.

It was not possible to determine the quantum yield for **3** *and* **5** *in the same* way because the acids decarboxylate with the excitation beam of the fluorimeter. Instead, the quantum yields were estimated for these two compounds based on the increase in fluorescence with irradiation of the acids assuming that the initial scan is pure acid and the final scan (determined by successive unchanging scans) is pure methylxanthone.

2.5.6 Nanosecond Laser Flash Photolysis

The laser flash photolysis system is a customized system using Luzchem software. Kinetics and spectra were obtained by exciting with the third harmonic of a Surelite Nd:YAG laser generating pulses at 355 nm of 8 ns duration and 8 mJ output. The data were acquired and analyzed with a customized Luzchem Research LFP-111 apparatus with an orthogonal pump/probe configuration. The probe source was a ceramic xenon lamp coupled to quartz fiber-optical cables. The laser pulse and the LFP-111 system were synchronized with a Tektronix TDS 2012B digitizer, operating in pre-trigger mode. The signals from a compact Hamamatsu photomultiplier were initially captured by the Tektronix digitizer and transferred to a computer for data analysis and archiving.

Spectra and kinetic experiments of **4** employed 7x7 mm^2 quartz cells with static solution while experiments with **3** and **5** employed 7x7 mm^2 quartz flow cells with solutions flowed at a high rate with constant bubbling of either nitrogen or oxygen as specified. Lifetimes of the triplet signal for **3** – **5** were measured both for solutions with A = 0.15 and A = 0.30. Spectra and quenching studies were measured for solutions with A = 0.30. For all LFP studies, 20% acetonitrile was used as a cosolvent.

2.6 References

1. Blake, J. A.; Gagnon, E.; Lukeman, M.; Scaiano, J. C., Photodecarboxylation of xanthone acetic acids: C-C bond heterolysis from the singlet excited state. *Org. Lett.* **2006,** *8* (6), 1057-1060.

2. Budac, D.; Wan, P., Photodecarboxylation: mechanism and synthetic utility. *J. Photochem. Photobiol. A: Chem.* **1992,** *67* (2), 135-166.

3. Lukeman, M., Photodecarboxylation of Arylacetic Acids. In *CRC Handbook of Photochemistry*, 3rd ed.; CRC Press: Boca Raton, 2010.

4. Margerum, J. D.; Petrusis, C. T., The Photodecarboxylation of Nitrophenylacetate Ions. *J. Am. Chem. Soc.* **1969,** *91* (10), 2467-2472.

5. Wan, P.; Muralidharan, S., Structure and Mechanism in the Photo-Retro-Aldol Type Reactions of Nitrobenzyl Derivatives. Photochemical Heterolytic Cleavage of C-C Bonds. *J. Am. Chem. Soc.* **1988,** *110*, 4336-4345.

6. Xu, M.; Wan, P., Efficient photodecarboxylation of aroyl-substituted phenylacetic acids in aqueous solution: a general photochemical reaction. *Chem. Commun.* **2000**, 2147-2148.

7. Huck, L. A.; Xu, M.; Forest, K.; Wan, P., Efficient photodecarboxylation of 3- and 4-acetylphenylacetic acids in aqueous solution. *Can. J. Chem.* **2004,** *82*, 1760-1768.

8. Costanzo, L. L.; De Guidi, G.; Condorelli, G.; Cambria, A.; Fama, M., Molecular mechanism of drug photosensitization. II. Photohemolysis sensitized by ketoprofen. *Photochem. Photobiol.* **1989,** *50* (3), 359-365.

9. Martinez, L. J.; Scaiano, J. C., Transient Intermediates in the Laser Flash Photolysis of Ketoprofen in Aqueous Solutions: Unusual Photochemistry for the Benzophenone Chromophore. *J. Am. Chem. Soc.* **1997,** *119* (45), 11066-11070.

10. Burns, M. D.; Lukeman, M., Efficient photodecarboxylation of trifluoromethyl-sustituted phenylacetic and mandelic acids. *Photochem. Photobiol.* **2009, In Press**.

11. Zimmerman, H. E., The Meta Effect in Organic Photochemistry: Mechanistic and Exploratory Organic Photochemistry. *J. Am. Chem. Soc.* **1995,** *117* (35), 8988-8991.

12. Bosca, F.; Miranda, M. A.; Carganico, G.; Mauleon, D., Photochemical and Photobiological properties of ketoprofen associated with the benzophenone chromophore. *Photochem. Photobiol.* **1994,** *60*, 96-101.

13. Monti, S.; Sortino, S.; De Guidi, G.; Marconi, G., Photochemistry of 2-(3-benzoylphenyl)propionic acid (ketoprofen). Part 1. A picosecond and nanosecond time resolved study in aqueous solution. *J. Chem. Soc., Faraday Trans.* **1997,** *93* (13), 2269-2275.

14. Cosa, G.; Llauger, L.; Scaiano, J. C.; Miranda, M. A., Absolute Rate Constants for Water Protonation of 1-(3-Benzoylphenyl)alkyl Carbanions. *Org. Lett.* **2002,** *4* (18), 3083-3085.

15. Laferrière, M.; Sanramé, C. N.; Scaiano, J. C., A Remarkably Long-Lived Benzyl Carbanion. *Org. Lett.* **2004,** *6* (6), 873-875.

16. Llauger, L.; Miranda, M. A.; Cosa, G.; Scaiano, J. C., Comparative study of the reactivities of substituted 3-(benzoylphenyl)benzyl carbanions in water and DMSO. *J. Org. Chem.* **2004,** *69*, 7066-7071.

17. Lukeman, M.; Scaiano, J. C., Carbanion-Mediated Photocages: Rapid and Efficient Photorelease with Aqueous Compatibility. *J. Am. Chem. Soc.* **2005,** *127* (21), 7698-7699.

18. Cosa, G.; Lukeman, M.; Scaiano, J. C., How Drug Photodegradation Studies Led to the Promise of New Therapies and Some Fundamental Carbanion Reaction Dynamics along the Way. *Acc. Chem. Res.* **2009,** *42* (5), 599-607.

19. Musa, K. A. K.; Matxain, J. M.; Erikkson, J. A., The mechanism of photoinduced decomposition of ketoprofen. *J. Med. Chem.* **2007,** *50*, 1735-1743.

20. Suzuki, T.; Okita, T.; Osanai, Y.; Ichimure, T., Reaction dynamics of excited 2-(3-benzoylphenyl)propionic acid (ketoprofen) with histidine. *J. Phys. Chem. B.* **2008,** *112*, 15212-15216.

21. Chuang, Y. P.; Xue, J.; Du, Y.; Li, M.; An, H.-Y.; Phillips, D. L., Time-resolved resonance raman and density functional theory investigation of the photochemistry of (S)-ketoprofen. *J. Phys. Chem. B.* **2009,** *113*, 10530-10539.

22. The pKa of xanthone acetic acid is estimated to be ~ 5 based on Figure 2-9.

23. Yamaji, M.; Susumu, I.; Nakajima, S.; Akiyama, K.; Tobita, S.; Marciniak, B., Photoinduced ω-Bond Dissociation in the Higher Excited Singlet (S_2) and Lowest Triplet (T_1) States of a Benzophenone Derivative in Solution. *J. Phys. Chem. A.* **2005,** *109*, 3843-3848.

24. Turro, N. J.; Ramamurthy, V.; Scaiano, J. C., *Modern Molecular Photochemistry of Organic Molecules*. University Science Books: Sausalito, California, 2010.

25. Rewcastle, G. W.; Kestell, P.; Baguley, B. C.; Denny, W. A., Light-Induced

Breakdown of Flavone Acetic Acid and Xanthenone Analogues in Solution. *J. Natl. Cancer Inst.* **1990,** *82* (6), 528-529.

26. Rewcastle, G. W.; Atwell, G. J.; Baguley, B. C.; Calveley, S. B.; Denny, W. A., Potential antitumour agents. 58. Synthesis and structure-activity relationships of substituted xanthenone-4-acetic acids active against the codon 38 tumor in vivo. *J. Med. Chem.* **1989,** *32* (4), 793-799.

27. Abdullah, K. A.; Kemp, T. J., Solvatochromic Effects in the Fluorescence and Triplet-Triplet Absorption Spectra of Xanthone, Thioxanthone and *N*-Methylacridone. *J. Photochem.* **1986,** *32*, 49-57.

28. Scaiano, J. C.; Weldon, D.; Pliva, C. N.; Martínez, L. J., Photochemistry and Photophysics of 1-Azaxanthone in Organic Solvents. *J. Phys. Chem. A.* **1998,** *102*, 6898-6903.

29. Majjigapu, J. R. R.; Kurchan, A. N.; Kottani, R.; Gustafson, T. P.; Kutateladze, A. G., Release and Report: A New Photolabile Caging System with a Two-Photon Fluorescence Reporting Function. *J. Am. Chem. Soc.* **2005,** *127* (36), 12458-12459.

30. Scaiano, J. C., Solvent effects in the photochemistry of xanthone. *J. Am. Chem. Soc.* **1980,** *102* (26), 7747.

31. Evans, C. H.; Prud'homme, N.; King, M.; Scaiano, J. C., Calibration of the triplet-triplet absorption of xanthone as a microenvironment sensor. *J. Photochem. Photobiol. A: Chem.* **1999,** *121*, 105-110.

32. Grabner, G.; Rechthaler, K.; Mayer, B.; Köhler, G., Solvent Influences on the Photophysics of Naphthalene: Fluorescence and Triplet State Properties in Aqueous Solutions and in Cyclodextrin Complexes. *J. Phys. Chem. A.* **2000,** *104* (7), 1365-1376.

33. The resolution for non fluorescent molecules is more like 10 ns, however the fluorescence from these xanthone derivatives obscures the signal below 20 ns.

34. The unit of a two photon absorption cross section is the Goeppert-Mayer, named after Maria Goeppert-Mayer who first predicted the possibility of two photon absorption. 1 GM = 10^{-50} cm^4 s $photon^{-1}$.

35. Furuta, T.; Wang, S.; Dantzker, J. L.; Dore, T. M.; Bybee , W. J.; Callaway, E. M.; Denk, W.; Tsien, R. Y., Brominated 7-hydroxycoumarin-4-ylmethyls: Photolabile protecting groups with biologically useful cross-sections for two photon photolysis. *PNAS* **1999,** *96*, 1193-1200.

36. Ramseier, M.; Senn, P.; Wirz, J., Photohydration of Benzophenone in Aqueous Acid. *J. Phys. Chem. A.* **2003,** *107* (18), 3305-3315.

37. Pickert, M.; Frahm, A. W., Substituted Xanthones as Antimycobacterial Agents, Part 1: Synthesis and Assignment of $^{1}H/^{13}C$ NMR Chemical Shifts. *Arch. Pharm. Pharm. Med. Chem.* **1998,** *331* (5), 177-192.

3. A New Carbanion-Mediated Photolabile Protecting Group[1]

Graphical Abstract

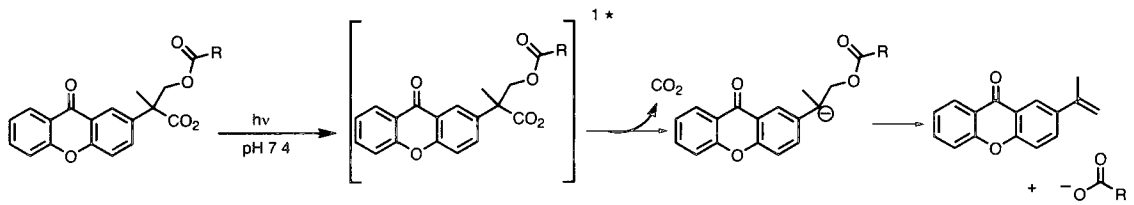

$\Phi \bullet \varepsilon \sim 2700\ M^{-1}cm^{-1}$

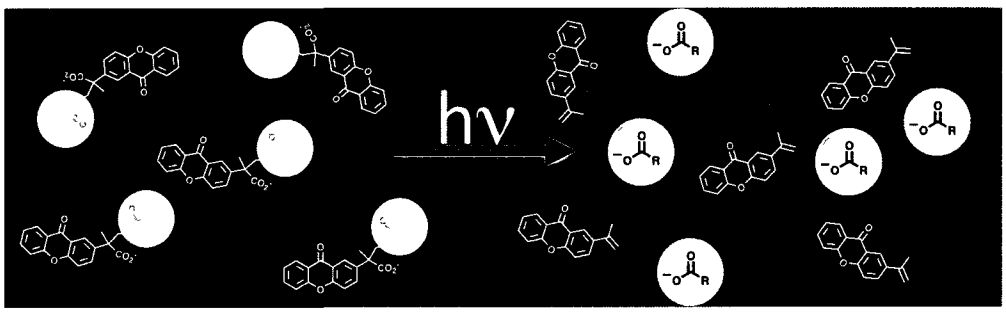

3.1 Introduction: Harnessing the efficiency of ketoprofen

The photodecarboxylation of ketoprofen (**1**) discussed in Chapter 2 is a well known example of highly efficient photochemistry. Recall that **1** photodecarboxylates with Φ_{PDC} = 0.75 generating a carbanion that is protonated rapidly (τ = 200 ns).[2] Considering that this quantum yield is remarkably high, it would be nice to find a way to take advantage of the efficiency. The ketoprofenate PPG (**2**) developed by Lukeman and Scaiano did just that; this PPG is a derivative of ketoprofen that contains leaving groups positioned β to the carboxylate group (and β to the incipient carbanion).[3] For **2a–f**, the photogenerated carbanion has an additional elimination pathway available that effectively competes with protonation by water (Scheme 3-1). For those derivatives possessing good leaving groups (**2a–e**), protonation by water is not observed, and only rapid elimination to release the leaving group takes place. Rate constants for this release are estimated to be greater than 10^8 s^{-1}.[3] Submicrosecond release of a primary alcohol was also achieved using this strategy (with **2f**), although protonation by water reduced the elimination yield to ~20% for this derivative.

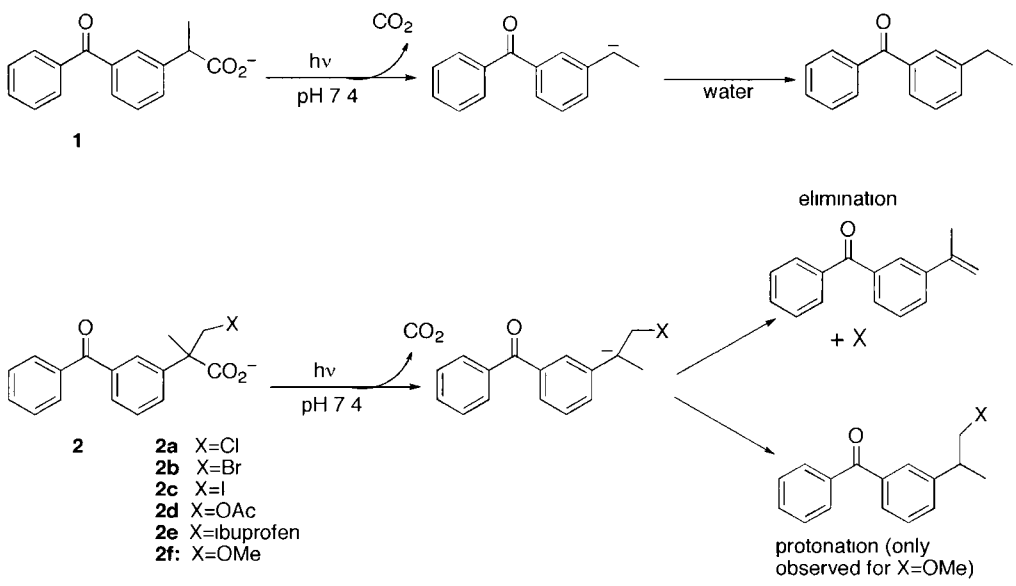

Scheme 3-1. Top: Ketoprofen photodecarboxylation. Bottom: Ketoprofenate PPG release mechanism.

Although the ketoprofenate PPG offers many advantages, one limitation stems from its poor absorption above 300 nm, a consideration that is particularly important for use in biological systems since wavelengths in the UVB region (280-320 nm) will cause extensive photodamage to cells. The ketoprofenate PPG is based on the benzophenone chromophore whose longest absorption wavelength band at $\lambda \sim 340$ nm has a very low extinction coefficient because it arises from a forbidden n,π^* transition.[4] We recognized that the structurally related xanthone chromophore has much higher absorption above 300 nm, and might therefore be a better choice for the design of a next-generation carbanion-mediated PPG. Xanthone (and thioxanthone) has been the chromophore of choice in a limited number of new PPGs.[5, 6] While these examples share the advantages of xanthone absorption

spectroscopy with our contribution they operate *via* a completely different mechanism to the photorelease described here. In both previous examples xanthone is used simply as a sensitizer for electron transfer.

Having established that **3** and **5** are efficient photochemical sources of carbanion intermediates (Chapter 2), we then sought to harness this reactivity to effect photorelease of anionic leaving groups

3.2 Synthesis

3.2.1 Synthesis of photolabile protected molecules

Recall from Chapter 2 that xanthone acetic acids **3** and **5** photodecarboxylate with quantum yields of 0.67 and 0.64 respectively while **4** is photostable under the same conditions. With this in mind we could design a PPG based on either **3** or **5** (or both), however we chose to focus on **3** due to the slightly higher quantum yield.

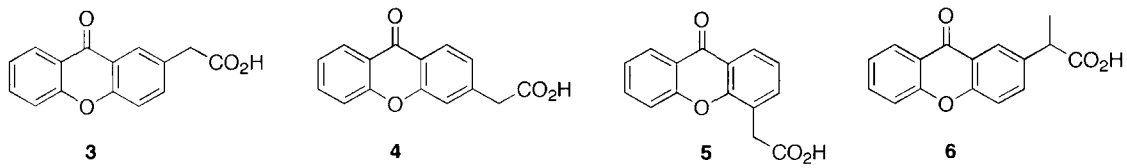

Chart 3-1.

Also as described in Chapter 2, the methyl group of **6** which is lacking in **3**, appears to have no significant effect on the photochemistry of these compounds. We did however find this methyl group to be essential in subsequent synthetic steps. Without it, the addition of a leaving group at the methyl position simply led to thermal elimination (Scheme 3-2). It soon became obvious that **6** would be a common synthetic intermediate enroute to our desired PPG. This lead to an improved synthesis of **6**, as compared with that described in Chapter 2.

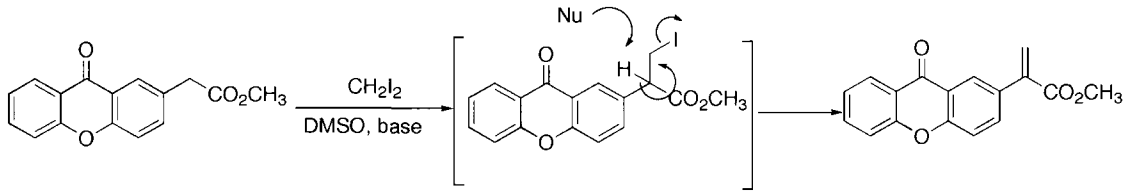

Scheme 3-2. Thermal elimination of iodide during the attempted synthesis of "photocaged" iodide.

Since a significant amount of desired product was typically lost in the methylation of xanthone acetic acids (initial synthetic route to **6**, see Chapter 2) and since it was impossible to carry out such methylations on a large scale due to the poor solubility of xanthone compounds, we chose to methylate the hydroxyphenylacetic acid precursor instead (**7**, Scheme 3-3). This required initial methyl ester protection of the carboxylic acid and protection of the phenol with allyl bromide, both very simple and high yielding reactions. Methylation of **8** was achieved in high yield using potassium hydride in dry THF followed by addition of iodomethane. Deprotection of the phenol gave **10**, the required starting material for construction of the xanthone derivative **6**. The synthesis of **6** was achieved by a modified Ulmann coupling using the same method described in Chapter 2 for 2-,3-, and 4-xanthoneacetic acids (**3**–**5**) which itself was an adaptation from a synthesis reported by Rewcastle et al.[7]

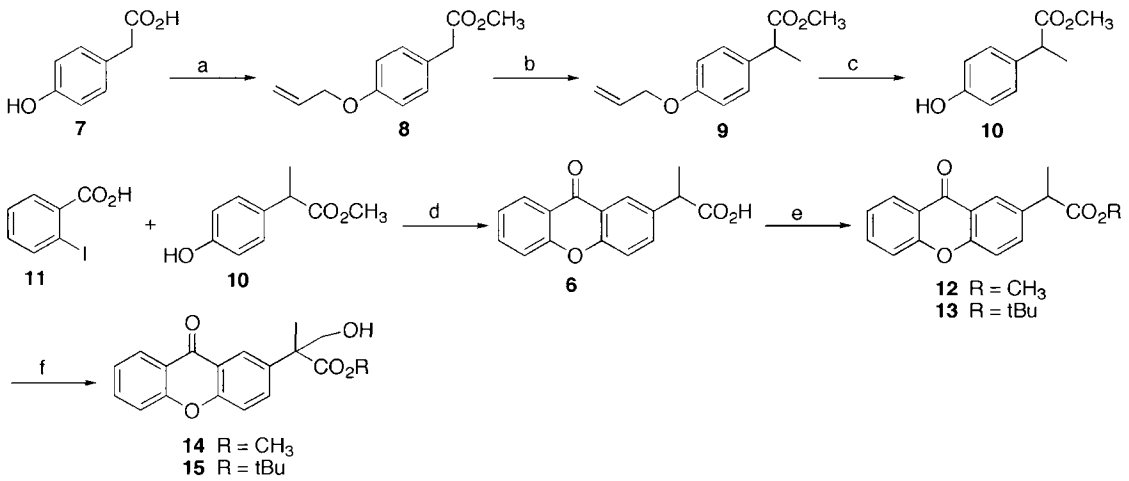

Scheme 3-3. Synthesis of our xanthonate photocaging group. (a) i) 5% H_2SO_4/CH_3OH/reflux (74%); ii) CH_2CHCH_2Br/K_2CO_3/DMF (93%) (b) i) KH/THF/-78°C ii) CH_3I (74%); (c) Pd(C)/*p*TsOH/CH_3OH (d) i) CuCl/TDA-1/Cs_2CO_3/Dioxane ii) H_2SO_4/85°C (50% from **9**); (e) **12**: 5% H_2SO_4/MeOH/reflux (94%); **13**: Boc_2O, DMAP/*t*BuOH (64%); (f) $(CH_2O)_n/K_2CO_3$/DMSO (94%). Overall yield ~ 15 %

Since the ring closing conditions also hydrolysed the methyl ester, the carboxylic acid of **6** needed to be reprotected. At this stage the choice of protection group depended on subsequent steps. Derivative **12** was used whenever possible due to the ease of protection and deprotection steps and since the yield of subsequent reactions were typically lower with **13**, likely due to steric hindrance from the *t*-butyl group. For the equivalent ketoprofen derivatives hydroxymethylation was accomplished with a complicated, low yielding set up involving the introduction of formaldehyde gas to a flask containing protected ketoprofen and LDA in dry THF.[3] Formaldehyde was generated by heating paraformaldehyde in a flask that was connected to the flask containing ketoprofen through a tygon tube. For the synthesis of **14** and **15** we developed a much easier synthesis. Hydroxymethylation

of **12** and **13** was accomplished in high yield simply by addition of paraformaldehyde to a solution of either **12** or **13** in DMSO saturated with nitrogen gas and K_2CO_3 yielding **14** and **15** respectively. Thorough purging with nitrogen was essential for high product yields likely because of competing oxidation reactions. The *in situ* addition of paraformaldehyde to the original reaction in THF with LDA was not possible because paraformaldehyde addition also introduces a small amount of water. In our new DMSO synthesis, K_2CO_3 acts both as the base and as a drying agent. Derivatives **14** and **15** served essentially as the photolabile protecting group since a number of molecules can be synthetically attached to the alcohol.

As proof of concept examples, we synthesized derivatives **17** and **20** which we hoped would release acetate and aniline (*via* the carbamate, *vide infra*) respectively. These two molecules were chosen because the functional groups involved (carboxylic acid and amine) are commonly found in biological molecules. For the synthesis of **17**, the deprotected intermedate **16** was treated with acetic anhydride, a simple and high yielding reaction. Synthesis of **19** was achieved by the very slow addition of aniline to 1/3 equivalent of triphosgene with triethylamine in dichloromethane, followed by the addition of one equivalent of **14**. Slow addition of the amine was essential to avoid the formation of byproduct **18**. Deprotection of **19** yielded the final product, **20**. To add a note on terminology, since the photolabile protecting group is based on xanthone propionic acid, we abbreviate this PPG as

XPA; therefore **17** can be referred to as XPA-OAc and **20** as XPA-OC(O)NHPh.

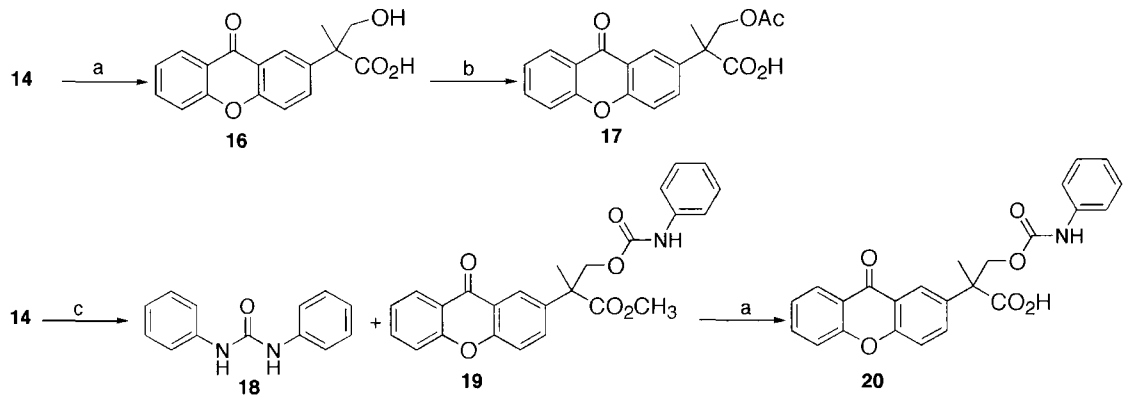

Scheme 3-4. Synthesis of photocaged acetate and aniline. (a) CH_3CN/0.1M KOH (96%); (b) pyridine/acetic anhydride (72%); (c) triphosgene/aniline/Et_3N/CH_2Cl_2

In order to test the limits of photorelease from the XPA PPG we also synthesized XPA-OCH_3 (**22**, Scheme 3-5) which we hoped would release methanol as was previously achieved with the ketoprofen based PPG. This was accomplished by alkylation of the carbanion of **12** using iodomethylmethyl ether followed by deprotection of the methyl ester to yield **22,** very similar to the method used to synthesize the equivalent ketoprofenate 'caged' methoxide.[3]

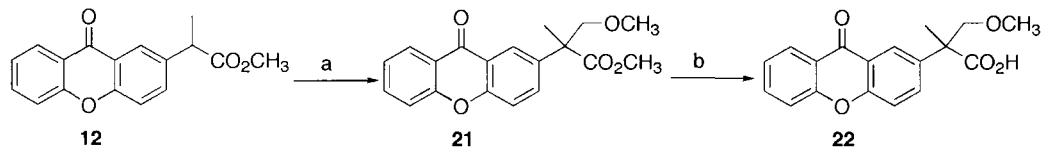

Scheme 3-5. Synthesis of photocaged methoxide. (a) i) LDA/THF/-78°C ii) CH_3OCH_2I (24%); (b) CH_3CN/0.1M KOH

We had hoped to demonstrate the release of a biologically relevant molecule by attaching glutamate to our XPA PPG. To do this we chose a glutamate derivative

with one carboxylate group protected by a *t*-butyl group and the amine protected with a boc group (Scheme 3-6). Our hope was that, following attachment to **15**, the Boc group and both t-butyl groups in **23** could be removed in one step. Unfortunately, while we were able to synthetically attach a protected glutamate (**23**), the structure did not survive the deprotection conditions when the reaction was left long enough to remove both t-butyl groups.

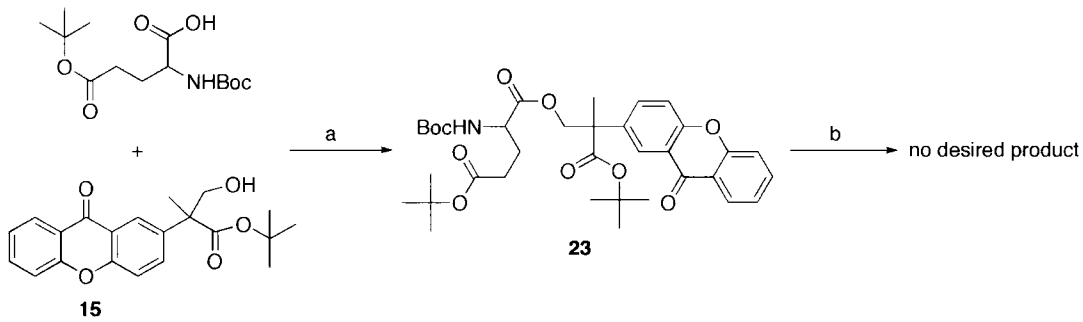

Scheme 3-6. Attempted synthesis of XPA-glutamate. The synthesis of **23** was successful, but the end product (with both t-butyl and Boc protecting groups removed) was not obtained. (a) EDCI/DMAP/CH_2Cl_2 (83%); (b) TFA/CH_2Cl_2

3.2.2 Characterization

The products reported here have been characterized by ^1H and ^{13}C (DEPTQ) NMR as well as high resolution mass spectrometry. ^1H NMR in particular was very useful for confirming of the xanthone derivatives; for one, the aromatic protons were all very well resolved which often allowed for an estimation of product yield in crude mixtures. Also, the methylene proton shifts of **14–23** are very characteristic. They are all split due to the adjacency of a chiral centre and the frequency of each is fairly sensitive to the group attached to the adjacent oxygen atom, that is, the

'photocaged' group.

All derivatives synthesized maintained the desirable absorption characteristics of the xanthone chromophore. The absorption coefficient (ε) for the lowest energy band of **17** was determined to be 6960 $M^{-1}cm^{-1}$ with λ_{max} = 347 nm. For **20** and **22**, too little material was synthesized to accurately determine ε, but for each derivative, it is expected to be similar.

3.3 Release

3.3.1 Results

As I have previously mentioned, **17** and **20** were chosen as representative test systems. We expected derivative **17** to release acetate directly (Scheme 3-7, top). In contrast, **20** should release the carbamate of aniline which would subsequently thermally decarboxylate to release aniline (Scheme 3-7, bottom). This carbamate/carbonate intermediacy is a common strategy for the photorelease of amines and alcohols since direct release is generally inefficient.[8] The one drawback of releasing *via* the carbamate or carbonate is that release is usually rate limited by thermal decarboxylation of the intermediate.[9]

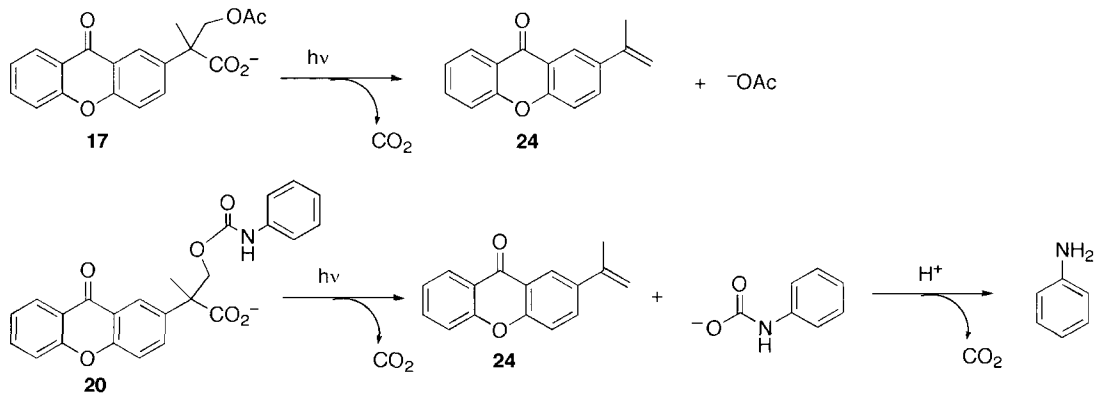

Scheme 3-7. Photorelease of acetate (top) and aniline *via* its carbamate (bottom).

Irradiation of **17** in a 10 mm quartz cuvette (2 UVA lamps, 4.0 x 10^{-5} M in pH 7.4 phosphate buffer solution) led to significant changes in the absorption spectra with peaks characteristic of the starting material decreasing concomitant with the appearance of new peaks at 258, 305, and 354 nm (Figure 3-1). Sharp isosbestic points were observed at 248, 284, 300, 316, and 355 nm, suggesting that irradiation of **17** gives only a single photostable product that absorbs in this region. Such changes are consistent with a clean photochemical reaction that significantly perturbs the chromophore, as might be expected from the exclusive photogeneration of alkene **24** *via* the anticipated elimination pathway. Interestingly, the chromophore is bleached by a factor of 1.5 at the wavelength of a nitrogen laser (337 nm), the excitation source used in many biological applications. This is advantageous for applications using this light source since absorptive screening by the photoproduct would be reduced. At other wavelengths however, this is not the case so linear conversion is limited to low concentrations (< 10^{-3} M).

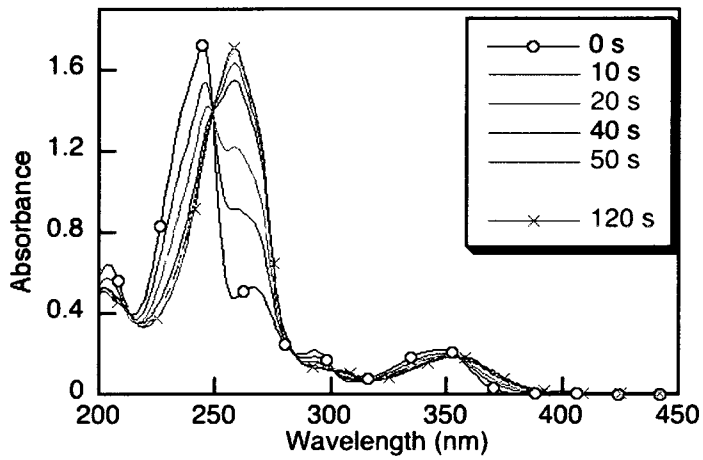

Figure 3-1. UV-Vis traces of **17** in 4.0 x 10^{-5} M solution after times indicated in the legend.

To better characterize the reaction photoproduct, irradiation of preparative scale solutions of **17** were carried out. Following organic extraction from the acidified photolysate, the isolated white solid was analyzed by ^{1}H NMR. Irradiation of **17** (4 UVB lamps, 1.0 x10^{-3} M in pH 7.4 phosphate buffer solution) for 15 minutes resulted in the complete loss of the methylene and acetate ^{1}H NMR signals attributed to **17** (Figure 3-2). New peaks were observed at 5.24 ppm and 5.59 ppm which correspond to the alkene protons of expected photoproduct **24**. HPLC-UV and GC-MS confirmed the complete conversion of **17** to **24** after 15 min. of irradiation with no other photoproducts detected, confirming that the photoreaction proceeds cleanly, and that **24** is photostable under these conditions. Quantitative formation of **24** implies that we have achieved quantitative release of a carboxylic acid in this reaction. Under these conditions the released acetate was lost during the work up due to its volatility.

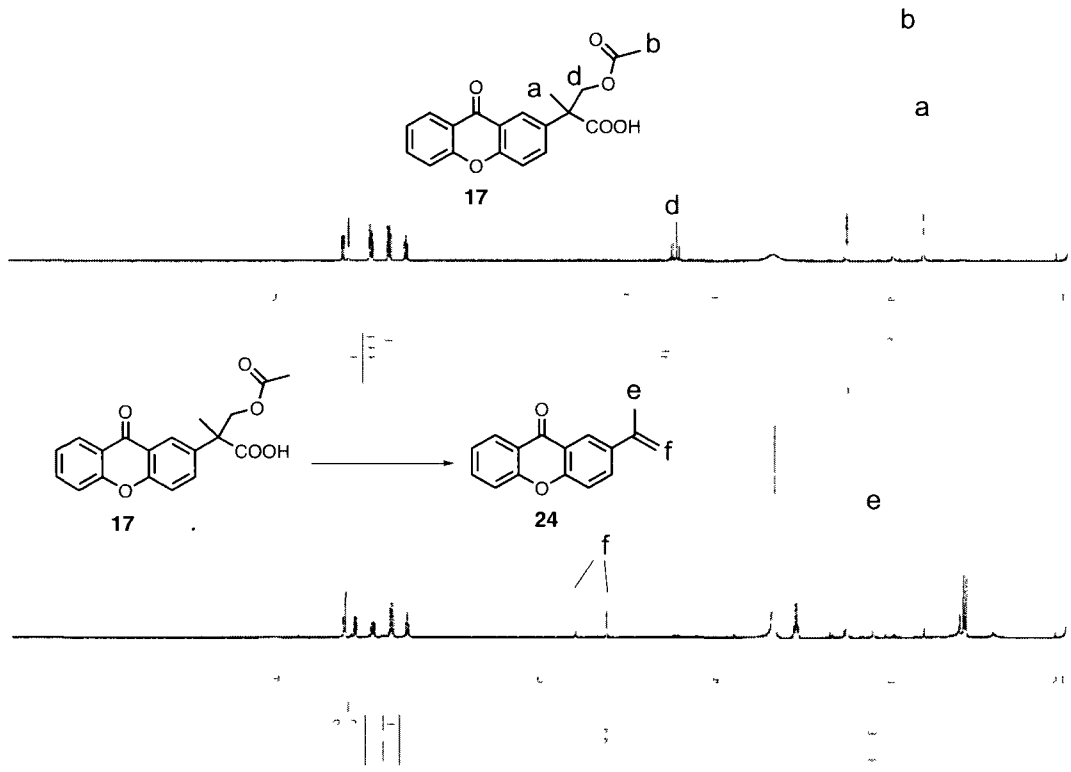

Figure 3-2. Top: ^{1}H NMR of XPA-OAc (**17**) in DMSO-d6. Bottom: ^{1}H NMR of extracted photolysate from irradiation of XPA-OAc (**17**) (4 UVB lamps, 15 min. in pH 7.4 phosphate buffer) in DMSO-d6 showing new peaks attributed to the elimination photoproduct **24**. The unassigned peaks (1.2 and 3.1 ppm) are attributed to a phthalate (confirmed by GC/MS) which likely originated in the solvent used to extract **24** from the photolysate.

To determine the quantum yield of acetate release, three solutions of **17** (2.0 mM) were irradiated for 3 min. in a Luzchem photoreactor with 4 UVB bulbs. All photolysates were analysed by HPLC with UV detection using ketoprofen (Φ = 0.75) as an actinometer. The $\Phi_{release}$ based on disappearance of **17** was determined to be 0.39 ± 0.02, lower than the parent molecule but still quite high.

Irradiation of **20** was conducted under similar conditions as described above for **17**. ^{1}H NMR analysis of the photolysate from a solution of **20** revealed singlets at 5.24 and 5.59 ppm corresponding to alkene **24** as the only new peaks, indicating that we have achieved clean release of the aniline from **20** *via* its carbamate (Figure 3-3).

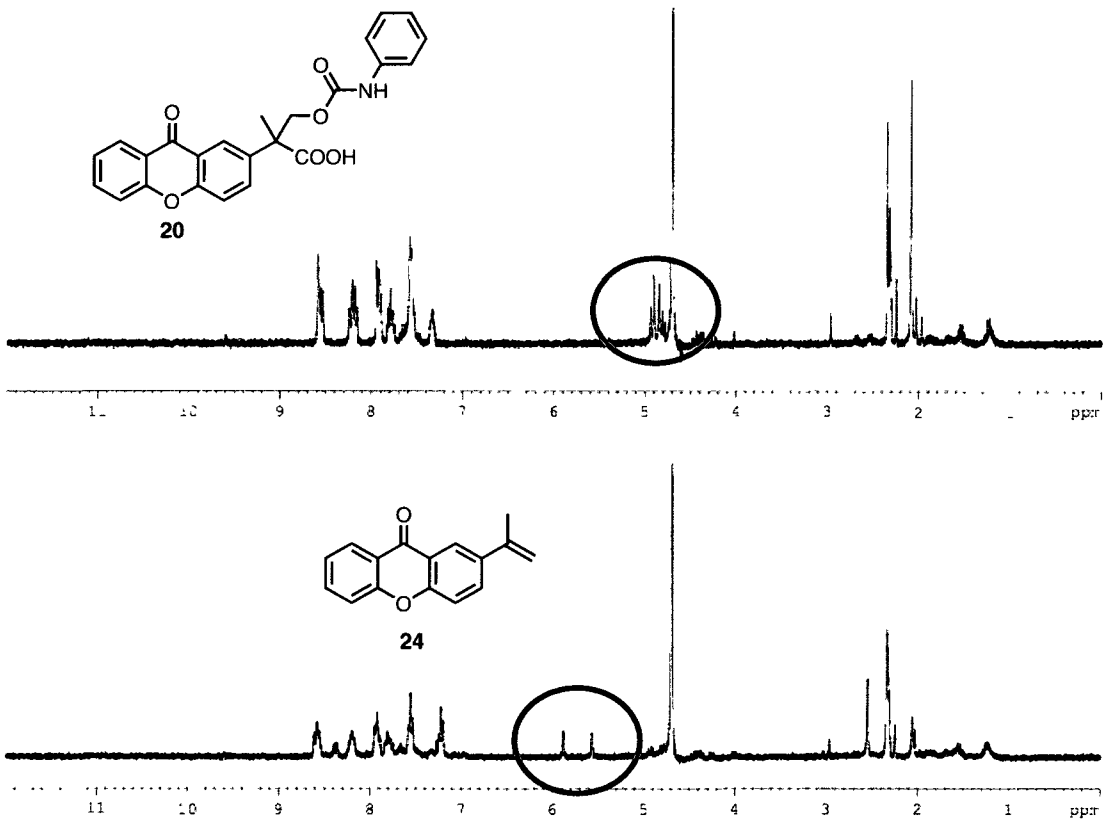

Figure 3-3. Top: ^{1}H NMR of of XPA-OC(O)NHPh (**20**) in D_2O/CD_3CN. Bottom: ^{1}H NMR of extracted photolysate from irradiation of XPA-OC(O)NHPh (**20**) (4 UVB lamps, 15 min. in pH 7.4 phosphate buffer) in D_2O/CD_3CN showing new peaks attributed to the elimination photoproduct **24**.

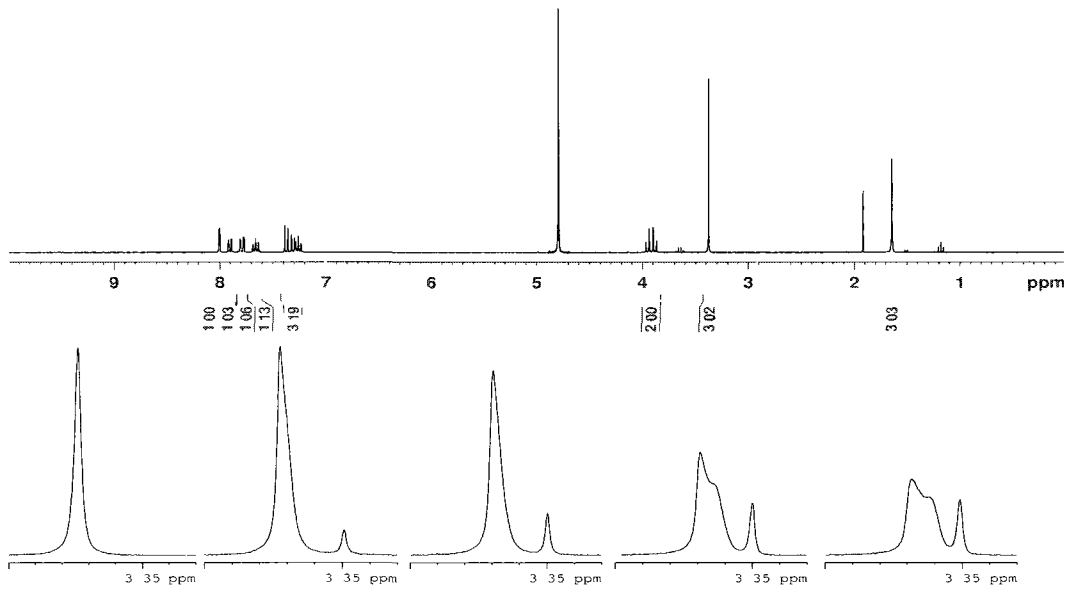

Figure 3-4. Top: ^{1}H NMR spectrum of **22** in D_2O with 0.1 M KOH. Bottom: Appearance of a new peak with irradiation. Irradiation time from left to right = 0 min, 1 min, 2 min, 3 min, 4 min. Irradiation source is a hand-held TLC lamp set to short wavelength (UVB). With irradiation the solution became very cloudy.

We also hoped to release methanol from **22**, as was observed for the ketoprofenate PPG (**2f**). Based on previous results for **2f**, we expected to observe both the release photoproduct **24** and the protonation photoproduct **25**. The ratio of the two would indicate the efficiency of release. Because of the limited amount of **22** synthesized and to avoid contamination, irradiation was performed in D_2O with 0.1 M KOH directly in an NMR tube, thus avoiding the extraction step. By monitoring with ^{1}H NMR (Figure 3-4), we saw the appearance of a new peak with irradiation of the solution by a hand-held TLC lamp. This peak appears at precisely the frequency expected for the CH_3 protons of methanol (3.35 ppm).[10] Unfortunately we were not able to observe the expected peaks of the xanthone

photoproducts **24** and **25** because they precipitated from solution.

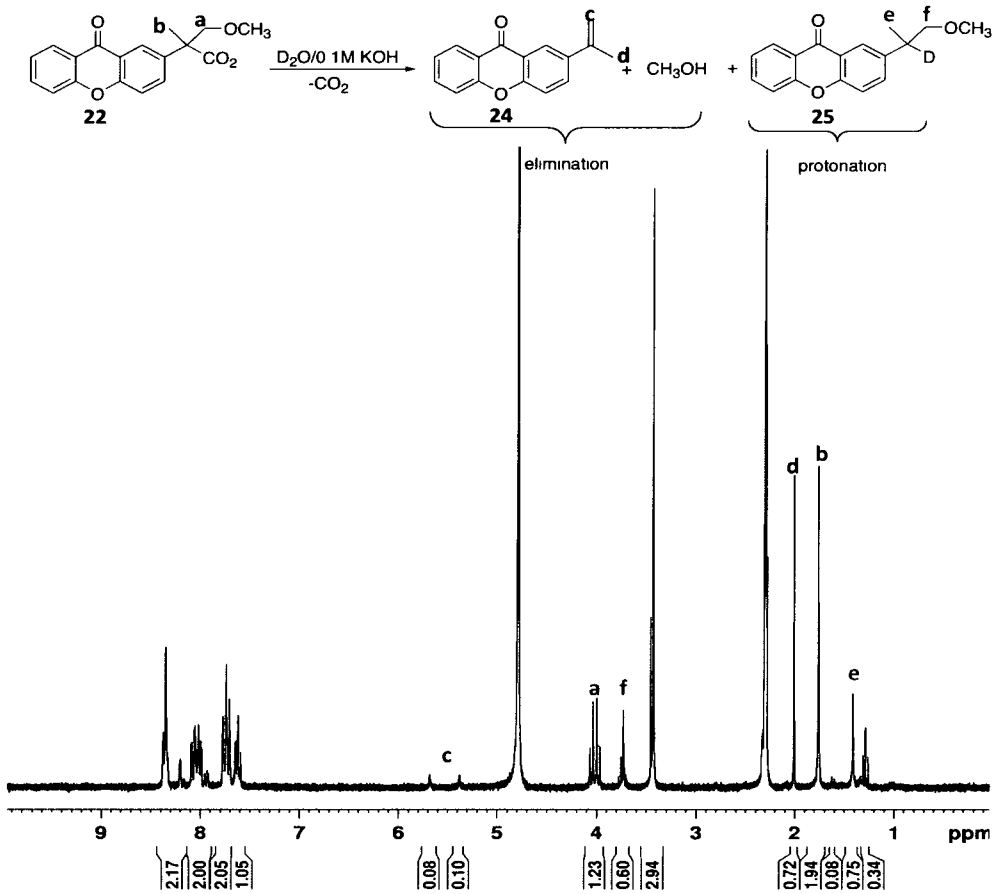

Figure 3-5. ^{1}H NMR spectrum of **22** in D_2O with 0.1 M KOH and 4 min. of irradiation followed by addition of acetone-d6 (D_2O : acetone-d6 = 1:1).

After 4 min. of irradiation, acetone-d6 was added to the NMR tube to dissolve the precipitate. The ^{1}H NMR spectrum of this solution is shown in Figure 3-5. From this spectrum we see that the ratio of **24** to **25** is approximately 1:3 (based on the integration of peaks c and f) or 1:2.5 (based on the integration of peaks c and e). That is, the elimination yield is ~25-30 %, slightly higher than the result obtained for the ketoprofenate derivative **2f**.

3.3.2 Discussion

Initially it was not clear to us whether or not a more reactive carbanion would be beneficial for the photoelimination of leaving groups. On one hand, a rapid trapping of the carbanion by water would provide a formidable competing pathway for the desired elimination. On the other hand, increasing the reactivity of the carbanion should accelerate unimolecular reactions (i.e. elimination) at the expense of bimolecular reactions (i.e., protonation). As we have observed only the elimination byproduct on irradiation of **17** and **20**, it would appear that increasing the reactivity of the carbanion is not deleterious for the elimination of good leaving groups such as carboxylates and carbamates. Since the carbanion intermediates produced on irradiation of **3** and **6** were too short-lived for us to observe by LFP (Chapter 2), we can estimate an upper limit of 20 ns for their lifetimes, which gives us pseudo-first order protonation rate constants of $\geq 5 \times 10^7$ s^{-1}. As we only see elimination photoproducts from **17** and **20**, we can assume that >95 % of the carbanions generated follow the elimination pathway, indicating that the elimination rate constant is at least 20 times that of the protonation rate constant. These assumptions allow us to estimate a *minimum* elimination rate constant of 10^9 s^{-1}, which means that the elimination of leaving groups from **17** and **20** occurs in less than one nanosecond. This represents an improvement in photorelease rates of around five orders of magnitude when compared with the *o*-NB system! It should be noted once more that the leaving group from **20** refers to the intermediate

—$OC(O)NHC_6H_5$ rather than aniline itself. The actual release of aniline is rate limited by the dark decarboxylation step, a common drawback associated with release of amines and alcohols.[9]

One parameter commonly used to describe a PPG is the release cross section, defined as the product of the release quantum yield and the absorptivity coeffecient $\Phi\varepsilon$. This value takes into account both the efficiency of photorelease upon excitation of a PPG and the probability of the PPG to absorb certain wavelengths. To demonstrate the effect of our greatly improved release cross-section (for XPA relative to the ketoprofenate PPG) we can compare the release of acetate from our xanthonate PPG ($\Phi\varepsilon$ = 2700 $M^{-1}cm^{-1}$)[11] and our ketoprofenate PPG ($\Phi\varepsilon \sim 75$ $M^{-1}cm^{-1}$) using UVA irradiation (Figure 3-6).

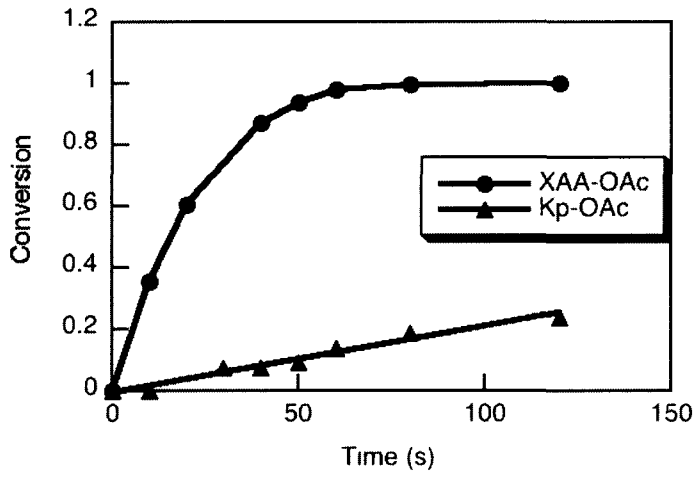

Figure 3-6. Conversion of XPA-OAc and Kp-OAc to their respective photoproducts with UVA irradiation.

The photoprocesses described above are summarized in Scheme 3-8.

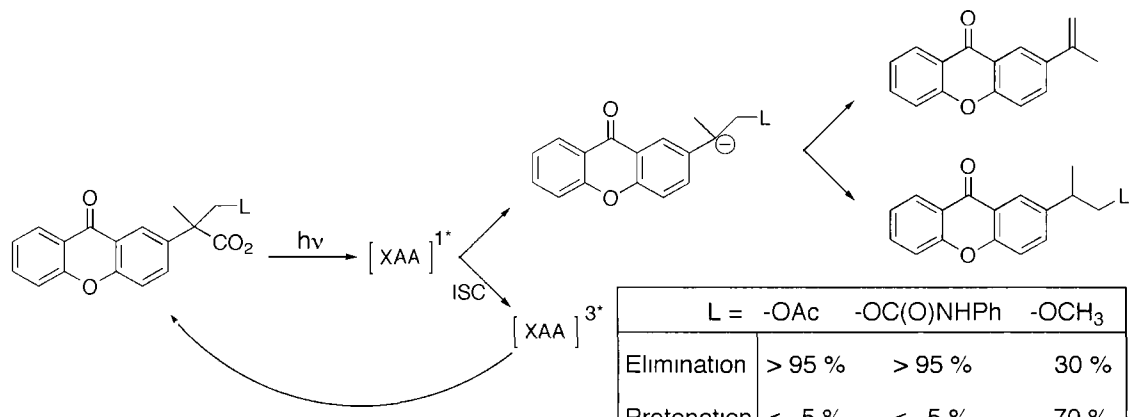

L =	-OAc	-OC(O)NHPh	-OCH_3
Elimination	> 95 %	> 95 %	30 %
Protonation	< 5 %	< 5 %	70 %

Scheme 3-8. Photoprocesses for XPA-OAc (**17**), XPA-OC(O)NHPh (**20**) and XPA-OCH_3 (**22**)

3.4 Summary

In a recent publication,[12] Corrie identified the difficulty in predicting reaction rates or efficiencies as a current challenge in the field of photolabile protecting groups. This difficulty often arises from a lack of information regarding the release mechanism. In fully characterizing the photochemical mechanism of release for this new xanthonate PPG we hope to demonstrate a more predictable release. In particular, we are confident that the 'xanthonate' PPG photorelease of acetate and aniline (*via* the carbamate) can be extended to other carboxylic acids and amines since the key steps of the release mechanism do not involve the substrate and the release occurs so rapidly that interference from the substrate is not likely except in special cases where energy or electron transfer with the substrate is possible .

Xanthonate based PPGs have been shown to have major advantages over *o*-NB and ketoprofenate cages, combining the high quantum yields and chemical yields of the carbanion-mediated photorelease with good UVA absorption properties, ultrafast release, and the formation of fluorescent photoproducts that may find use as reporters in the mapping of release sites in biological systems.

3.5 Experimental

All starting materials used in this work were purchased from Sigma-Aldrich Canada (Oakville, ON) and used without further purification except for Boc-Glu(OtBu)-OH [04-12-0051] which was purchased from Novabiochem. Solvents were dried by the usual methods. DMSO and DMF were purchased as anhydrous grade and stored over molecular sieves. Column chromatography employed Merck silica gel 230-400 mesh. ^{1}H and ^{13}C NMR spectra were recorded at room temperature on a Bruker AVANCE 400 instrument. Chemical shifts are reported relative to internal TMS. Melting points were determined on a Melt-Temp II aparatus from Laboratory Devices.

3.5.1 Synthesis

Benzeneacetic acid, 4-(2-propen-1-yloxy)-, methyl ester (8) [72224-26-1] 4-hydroxyphenylacetic acid (40 g, 0.263 mol) was dissolved in 350 mL methanol in a round bottom flask equipped with a nitrogen inlet, condensor and stir bar. To this, 10 mL H_2SO_4 was added and the solution was brought to reflux. After 2 hours, the reaction solution was cooled to room temperature then transferred to a separatory funnel with 350 mL CH_2Cl_2. The organic solution was washed three times with dilute basic water (0.05 M NaOH) while ensuring that the aqueous solutions were never below pH 7 in order to minimize loss of the phenol to the aqueous layer. The organic layer was dried with $MgSO_4$, filtered, and the solvent was removed yielding 32.6 g of a colourless oil (0.196 mol, 74%). ^{1}H NMR (400 MHz, $CDCl_3$) δ (ppm) 3.55

(2H, s), 3.69 (3H, s), 6.55 (1H, s), 6.7 (2H, m), 7.1 (2H, m). ^{13}C NMR (100 MHz, $CDCl_3$) δ (ppm) 40.30, 52.30, 115.63, 125.42, 130.42, 155.12, 173.53. The 4-hydroxyphenylacetate methyl ester was used as is and 32.5 g was dissolved in dry DMF. To this was added 1.5 equivalents of K_2CO_3 (40.5 g, 0.293 mol, 1.5 eq.) and 3-bromopropene (27.2 g, 0.225 mol, 1.15 eq.). The suspension was stirred at room temperature under positive pressure N_2 overnight. The reaction solution was suction filtered and the filtrate was transferred to a separatory funnel with 200 mL of H_2O and extracted with 200 mL ether. The organic layer was washed with 400 mL brine, dried with $MgSO_4$, filtered and evaporated to dryness yielding 35.2 g of a colourless oil. A second ether extraction of the aqueous layer yielded a further 2.4 g for a combined yield of 37.6 g of pure product (0.182 g, 93%). ^1H and ^{13}C NMR are in good agreement with the literature.[13] ^1H NMR (400 MHz, $CDCl_3$) δ (ppm) 3.54 (2H, s), 3.66 (3H, s), 4.49 (2H, m), 5.2 (1H, m), 5.4 (1H, m), 6.0 (1H, m), 6.85 (2H, dd, J_1= 6.4 Hz, J_2= 2 Hz), 7.17 (2H, dd, J_1= 6.4 Hz, J_2= 2 Hz). ^{13}C DEPTQ NMR (100 MHz, $CDCl_3$) δ (ppm) 40.24 (CH_2), 51.92 (CH_3), 68.77 (CH_2), 114.82 (CH), 117.53 (CH_2), 126.24 (C), 130.26 (CH), 133.32 (CH), 157.75 (C), 172.29 (C).

Benzeneacetic acid, α-methyl-4-(2-propen-1-yloxy)-, methyl ester (9) [1057075-90-7] was made according to a procedure reported by Natarajan et al. for the methylation of *p*-tolylacetic acid methylester.[14] A 500 mL round bottom flask equipped with a magnetic stir bar was charged with potassium hydride (3.93 g, 98.1 mmol). THF (200 mL) was added and the flask was cooled to 0°C in an ice bath. To

this, **8** (18.4 g, 89.2 mmol) dissolved in 200 mL THF was added dropwise with stirring over 20 min. The solution was allowed to warm to room temperature and continued to stir for 30 min. Iodomethane (6.1 mL, 98.1 mmol) was added and the reaction was left to stir overnight (13 hr.) at room temperature under positive pressure N_2. The reaction mixture was quenched with water (400 mL) and the product was extracted twice with ether. The combined organic layers were washed with brine, dried over $MgSO_4$ and filtered. Solvent evaporation yielded 21.6 g of an orange oil. The product was purified by flash chromatography (350 g silica, 8:1 hexanes:ethyl acetate). Purified yield = 65.9 mmol, 74%. ^{1}H NMR (400 MHz, $CDCl_3$) δ (ppm) 1.46 (3H, d, J= 7.2 Hz), 3.64 (3H, s), 3.66 (1H, q, J= 7.2 Hz), 4.49 (2H, dt, J_1= 5.3 Hz, J_2= 1.6 Hz), 5.26 (1H, dq, J_1=9 Hz, J_2= 1.6 Hz), 5.4 (1H, d, J_1=17 Hz, J_2= 1.6 Hz), 6.0 (1H, m), 6.86 (2H, d, J= 8.8 Hz), 7.20 (2H, d, J= 8.6 Hz). ^{13}C DEPTQ NMR (100 MHz, $CDCl_3$) δ (ppm) 18.66 (CH_3), 44.56 (CH), 51.99 (CH_3), 68.84 (CH_2), 114.84 (CH), 117.65 (CH_2), 128.47 (CH), 132.82 (C), 133.32 (CH), 157.75 (C), 175.5 (C).

Benzeneacetic acid, 4-hydroxy-α-methyl-, methyl ester (10) [65784-33-0] was synthesized following a procedure reported by Boss and Scheffold.[15] To a solution of **9** (7.75 g, 35.2 mmol) in anhydrous methanol (435 mL) was added Pd/C (1.5 g) and *p*-toluenesulfonic acid (0.77 g). The suspension was brought to and maintained at reflux for 20 hr. then allowed to cool to room temperature. At this time there was only one spot by TLC. The reaction mixture was filtered through an inch of celite. The filtrate was concentrated to half the original volume, treated with a solution of

brine and ice and extracted 5 times with dichloromethane. The combined organic layers were dried over $MgSO_4$ and filtered. Solvent evaporation yielded 8 g of the crude product which was used in the next step without further purification. ^1H NMR is in good agreement with literature.[16] ^1H NMR (400 MHz, $CDCl_3$) δ (ppm) 1.47 (2.7H, d, CH_3 from **10**), 1.56 (s, 2 x CH_3 from dimethylated product), 3.66(4H, s+t, $CO_2\underline{CH_3}$ from **10** and dimethylated product with CH from **10**), 6.8 (2H, m), 7.2 (2H, m). ^{13}C DEPTQ NMR (100 MHz, $CDCl_3$) δ (ppm) 18.51 (CH_3), 44.62 (CH), 52.20 (CH_3), 115.60 (CH), 12859 (CH), 131.89 (C), 155.41 (C), 176.16 (C).

9H-Xanthene-2-acetic acid, α-methyl-9-oxo- (6) [30087-33-3] 2-Iodobenzoic acid (9.56 g, 38.6 mmol) and **10** (5.79 g, 32.1 mmol) were added to a flame dried 3-neck 250 mL round bottom flask equipped with magnetic stir bar, nitrogen gas inlet and condenser with dry dioxane and Cs_2CO_3 (41.8 g, 128 mmol). The suspension was brought to reflux under positive pressure N_2. After 10 min. freshly recrystallised CuCl (0.38 g, 3.86 mmol) and Tris[2-(2-methoxyethoxy)ethyl]amine (3.86 mmol) were added. The reaction was kept at just below reflux overnight with vigorous stirring. After 20 hr. the reaction was allowed to cool to room temperature. Solvent was removed by rotary-evaporation yielding a green and grey solid. To this a 0.1 M solution of NaOH was added, stirred thoroughly and the suspension was filtered through celite. The filtrate was acidified with 10% HCl and extracted 3 times with ethyl acetate. The organic layers were combined and the volume reduced by half, then added to a separatory funnel. The product was

extracted with 10% NH_4OH, acidified then extracted with ethyl acetate. This final organic layer was dried over $MgSO_4$. Solvent evaporation yielded a beige solid that was dissolved in 40 mL H_2SO_4. The temperature was brought to 85°C for 2.5 hr. After cooling to room temperature the solution was poured on ice resulting in a solid precipitate. Once all of the ice had melted, the product was filtered and rinsed thoroughly with water. Recrystallization from hot toluene yielded 3.4 g (12.7 mmol, ~50% from **9**) of off-white crystals. m.p. 168-170°C. ^1H NMR (400 MHz, DMSO-d6) δ (ppm) 1.46 (3H, d, J=7 Hz), 3.93 (1H, q, J= 7 Hz), 7.49 (1H, dt, J_1= 7 Hz, J_2= 1 Hz), 7.7 (2H, m), 7.8-7.9 (2H, m), 8.10 (1H, d, J= 2 Hz), 8.2 (dd, J_1= 8 Hz, J_2= 1 Hz). DEPTQ ^{13}C NMR (100 MHz, DMSO-d6) δ 18.52, (CH_3), 43.96 (CH), 118.22 (CH), 118.43 (CH), 120.87 (C), 121.05 (C), 124.21 (CH), 124.39 (CH), 126.03 (CH), 135.11 (CH), 135.57 (CH), 137.45 (C), 154.57 (C), 155.60 (C), 175.12 (C=O), 175.97 (C=O). HRMS for $C_{14}H_{10}O_2$ [M^+] calculated 268.0736, found 268.0729.

9H-Xanthene-2-acetic acid, α-methyl-9-oxo-, methyl ester (12) [1134090-41-7] In a round bottom flask equipped with nitrogen inlet, condenser and stir bar, a solution of **6** (1.0 g, 3.7 mmol) in 40 mL CH_3OH with 2 mL H_2SO_4 was refluxed for 4hr. After cooling to room temperature, the solution was transferred to a separatory funnel with 100 mL EtOAc and washed with 100 mL 0.1 M NaOH. The aqueous layer was extracted with 100 mL EtOAc and the combined organic layers were washed twice with 0.1 M NaOH (2 x 100 mL), dried over $MgSO_4$ and the solvent was removed under vacuum yielding 0.98 g of pure **12** (3.5 mmol, 94%). ^1H

NMR (400 MHz, $CDCl_3$) δ (ppm) 1.59 (3H, d, *J*= 7.2 Hz), 3.68 (3H, s), 7.37 (1H, td, J_1= 7.5 Hz, J_2= 1 Hz), 7.5 (2H, m), 7.7 (2H, m), 8.24 (1H, d, *J*= 2.4 Hz), 8.32 (1H, m). ^{13}C NMR DEPTQ (100 MHz, $CDCl_3$) δ (ppm) 18.44 (CH3), 27.94 (CH3), 45.90 (CH), 80.92 (C), 117.96 (CH), 118.20 (CH), 121.58 (C), 121.79 (C), 123.88 (CH), 125.30 (CH), 126.72 (CH), 134.17 (CH), 134.77 (CH), 137.00 (C), 155.19 (C), 156.14 (C), 173.34 (C), 177.12 (C).

9H-Xanthene-2-acetic acid, α-methyl-9-oxo-, *t*-butyl ester (13) 6 (0.50 g, 1.9 mmol) was added to a flask with DMAP (0.068 g, 0.56 mmol), Boc_2O (0.81 g, 3.7 mmol) and *t*-BuOH (45 mL) at 30°C. After 2 hr. stirring at 30°C the reaction was complete by TLC. The solution was transferred to a separatory funnel with 100 mL ethyl acetate and washed with 100 mL 0.1 M NaOH and 2 x 100 mL 10% HCl. The organic layer was dried over $MgSO_4$ and the solvent was removed by roto-evaporation. Methanol was added (70 mL) and final roto-evaporation yielded 0.55 g of an orange oily solid. Flash chromatography (6:1 hexanes:ethyl acetate) yielded 0.39 g of pure product as a colourless oil (1.2 mmol, 64%). ^1H NMR (400 MHz, $CDCl_3$) δ (ppm) 1.41 (9H, s), 1.54 (3H, d, *J*= 7.2 Hz), 3.78 (1H, q, *J*= 7.2 H), 7.37 (1H, td, J_1= 6.8 Hz, J_2= 1.2 Hz), 7.5 (2H, m), 7.7 (2H, m), 8.24 (1H, d, *J*= 2.4 Hz), 8.34 (1H, ddd, J_1= 7.8 Hz, J_2= 1.6 Hz, J_3= 0.4 Hz). ^{13}C NMR DEPTQ (100 MHz, $CDCl_3$) δ (ppm) 18.44 (CH_3), 27.94 (CH_3), 45.90 (CH), 80.92 (C), 117.96 (CH), 118.20 (CH), 121.58 (C), 121.79 (C), 123.88 (CH), 125.30 (CH), 126.72 (CH), 134.17 (CH), 134.77 (CH), 137.00 (C), 155.19 (C), 156.14 (C), 173.34 (C), 177.12 (C).

9H-Xanthene-2-acetic acid, α-(hydroxymethyl)-α-methyl-9-oxo-, methyl ester (14) [1134090-43-9] To a solution of nitrogen purged DMSO with paraformaldehyde and K_2CO_3 (both partially dissolved) **12** (with 16% of the dimethylated impurity) was added. The solution was stirred at room temperature overnight under a positive pressure of nitrogen. After filtering, the reaction was quenched with 1% HCl and extracted with CH_2Cl_2. The combined organic layers were washed with 1% HCl, dried ($MgSO_4$) and concentrated *in vacuo* to give an oil that was further purified by flash chromatography (100 g silica, 30% ethyl acetate in hexanes) yielding **14** as a white solid. ^{1}H NMR (400 MHz, $CDCl_3$) δ (ppm) 1.76 (3H, s, -CH_3), 2.98 (1H, s broad, -OH), 3.74 (3H, s, -CH_3), 3.82 (1H, d, *J*= 11.2 Hz, -CH_2-), 4.10 (1H, d, *J*= 11.2 Hz, -CH_2-), 7.36 (2H, t, *J*= 7.4 Hz), 7.44 (2H, t, *J*= 8.8 Hz), 7.73-7.66 (2H, m), 8.25 (1H, d, *J*= 2.4 Hz), 8.30 (1H, dd, *J*= 1.6 Hz). ^{13}C DEPTQ NMR (100 MHz, $CDCl_3$) δ (ppm) 20.4 (CH_3), 52.3 (C), 52.5 (CH_3), 69.4 (CH_2), 117.9, 118.3 (aromatic CH), 121.6, 121.4, (aromatic C), 124.0, 124.1, 126.7, 133.5 (aromatic CH), 136.6, 155.2, 156.0 (aromatic C), 176.0 (C=O), 176.9 (C=O).

9H-Xanthene-2-acetic acid, α-(hydroxymethyl)-α-methyl-9-oxo-, *t*-butyl ester (15) was made in the same way as **14** using **13** (0.39 g, 1.2 mmol) instead of **12**. The yield after flash chromatography purification was 0.4 g (1.1 mmol, 94%) as a white crystalline solid. ^{1}H NMR (400 MHz, $CDCl_3$) δ (ppm) 1.45 (9H, s, *t*-Bu), 1.71 (3H, s, -CH_3), 3.06 (1H, t broad, *J*= 6 Hz, -OH), 3.78 (1H, dd, J_1= 11 Hz, J_2= 6 Hz), 4.02 (1H, dd, J_1= 11 Hz, J_2= 6 Hz), 7.35 (1H, t, *J*= 7.5 Hz), 7.4 (2H, m), 7.7 (2H, m), 8.3 (2H,

m). ^{13}C DEPTQ NMR (100 MHz, $CDCl_3$) δ (ppm) 20.5 (CH_3), 27.9 (CH_3), 52.7 (C), 69.5 (CH_2), 81.9 (C), 117.9, 118.0 (aromatic CH), 121.4, 121.7 (aromatic C), 123.9, 124.1, 126.6, 133.4, 134.8 (aromatic CH), 137.3, 155.1, 156.0 (aromatic C), 174.8 (C=O), 177.0 (C=O). HRMS for $C_{16}H_{13}O_3$ [M^+ – $CO_2C(CH_3)_4$] calculated 253.0865, found 253.0857.

9H-Xanthene-2-acetic acid, α-(hydroxymethyl)-α-methyl-9-oxo- (16) A solution of **12** (0.25 g, 0.80 mmol) in 25 mL CH_3CN with 25 mL 0.1 M KOH was stirred for 4 hr. The reaction solution was then washed with CH_2Cl_2 (2 x 25 mL), acidified with 10% HCl (20 mL) and extracted with 3 x 25 mL EtOAc. The combined organics were dried with $MgSO_4$, filtered and the solvent was removed under vacuum yielding pure **16** (0.23 g, 0.77 mmol, 96%). HRMS for $C_{17}H_{14}O_5$ [M^+] calculated 298.0841, found 298.0848.

9H-Xanthene-2-acetic acid, α-[(acetyloxy)methyl]-α-methyl-9-oxo- (XPA-OAc) (17) [1134090-36-0] To a 100 mL round bottom flask **16** (0.46 mmol) was added with 50 mL of CH_2Cl_2, 0.3 mL pyridine and 0.6 mL acetic anhydride. The mixture was stirred for 3 hr. at room temperature, transferred to a separatory funnel and washed with 1% HCl (50 mL) then concentrated under vacuum. The residue was dissolved in 100 mL of a 1:1 CH_3CN-H_2O mixture, and stirred overnight at room temperature to decompose any remaining anhydride. The mixture was diluted with 50 mL CH_2Cl_2 then washed with 50 mL 1% HCl. The organic layer was dried with $MgSO_4$ and the solvent was removed under vacuum to yield a white solid (0.33 mmol,

72%). ^{1}H NMR (400 MHz, acetone-d6) δ (ppm) 1.77 (3H, s), 1.98 (3H, s), 4.50 (1H, d, *J*= 10.8 Hz), 4.60 (1H, d, *J*= 10.8 Hz), 7.47 (1H, t, *J*= 7.6 Hz), 7.62 (2H, t, *J*= 8.8 Hz), 7.8-8.0 (2H, m), 8.26 (1H, dd, J_1= 8 Hz, J_2= 1.6 Hz), 8.31 (1H, d, *J*= 2.4 Hz). ^{13}C DEPTQ NMR (100 MHz, acetone-d6) δ (ppm) 19.77 (-CH_3), 20.34 (-CH_3), 49.5 (quaternary), 68.7 (-CH_2-), 118.1, 118.4 (aromatic CH), 121.3, 121.6 (aromatic quaternary), 123.8, 124.2, 126.2, 133.6, 135.2 (aromatic CH), 169.7 , 175.5 (CO), 205.3 (aromatic CO). HRMS for $C_{19}H_{16}O_6$ [M^+] calculated 340.0947, found 340.0939.

1,3-Diphenylurea (18) [102-07-8] was isolated as a byproduct of the synthesis of **19**. m.p. 234-235°C. ^{1}H NMR (400 MHz, DMSO-d6) δ (ppm) 6.97 (2H, tt, J_1= 7.4 Hz, J_2= 1.1 Hz), 7.28 (4H, m), 7.46 (4H, m), 8.66 (s). ^{13}C DEPTQ NMR (100 MHz, DMSO-d6) δ (ppm) 118.18 (CH), 121.80 (CH), 128.78 (CH), 139.70 (C), 152.53 (C=O). HRMS for $C_{13}H_{12}N_2O$ [M^+] calculated 212.0950, found 212.0944.

9H-Xanthene-2-acetic acid, α-methyl-9-oxo-α-[[[(phenylamino)carbonyl]oxy] methyl]- methyl ester (19) [1134090-47-3] Triphosgene (0.49 mmol, 0.145 g) was dissolved in 3 mL CH_2Cl_2. Aniline and triethylamine were dissolved in 7 mL CH_2Cl_2 then added dropwise over 1 hour to triphosgene at room temperature under N_2. To this was added **10** (0.23 g, 0.74 mmol) dissolved in 2 mL CH_2Cl_2. The solution was stirred under nitrogen for 15 hr. then quenched with water. The solvent was removed under vacuum followed by extraction with EtOAc. Combined organics were washed with saturated $NaHCO_3$, then brine, then dried with $MgSO_4$. The solvent was removed under vacuum to yield an oil. Pure **12** was isolated by column

chromatography. ^{1}H NMR (400 MHz, $CDCl_3$) δ 1.77 (3H, s), 3.73 (3H, s), 4.60 (1H, d, *J*= 10.8 Hz), 4.71 (1H, d, *J*= 10.8 Hz), 6.95 (s broad, NH), 7.03 (1H, t, *J*= 8.4 Hz), 7.38 (5H, m with broadening possibly due to rotational hindrance), 7.47 (2H, t, *J*= 8.8 Hz), 7.73 (2H, m), 8.3 (2H, dd J_1= 2.4 Hz, J_2= 1.6 Hz). ^{13}C DEPTQ NMR (100 MHz, $CDCl_3$) δ 20.9 (CH_3), 50.5 (C), 52.7 (CH_3), 69.4 (CH_2), 118.0, 118.5 (aromatic CH), 121.5, 121.7 (aromatic C), 123.5, 124.1, 124.3, 126.8, 129.0, 133.2, 135.0 (aromatic CH), 135.9, 137.7, 155.4, 156.1 (aromatic C), 174.0, 176.9 (C=O).

9H-Xanthene-2-acetic acid, α-methyl-9-oxo-α-[[[(phenylamino)carbonyl]oxy] methyl]- (XPA-OC(O)NHPh) (**20**) [1134090-38-2] A solution of **19** in CH_3CN and 0.1 M KOH (1:1) was stirred for 2 hr. The reaction solution was then washed with CH_2Cl_2, acidified with 10% HCl and extracted with 3 x 25 mL EtOAc. The combined organics were dried with $MgSO_4$, filtered and the solvent was removed under vacuum yielding pure **20**. ^{1}H NMR (400 MHz, D_2O/CD_3CN) δ 2.1 (s), 4.9 (d,d), 7.2 – 8.6 (m).

Methyl 3-methoxy-2-methyl-2-(9-oxo-*9H*-xanthen-2-yl)propanoate (**21**) A solution of **12** (0.11 g, 0.39 mmol) in dry THF (10 mL) was cooled in a dry ice/acetone bath. To this, LDA was added (0.42 mL of a 1.0 M solution prepared from nBuLi and diisopropylamine) and the dark purple colour of the carbanion was observed. Upon addition of CH_3OCH_2I the solution became yellow. The reaction was left to stir overnight under a positive pressure of nitrogen gas. The reaction was quenched with water and extracted with ethylacetate (x 3). The combined

removed under vacuum. Purification by column chromatography (3:1 hexanes: EtOAc) yielded 30 mg of pure **21** (0.092 mmol, 24 %). ^{1}H NMR (400 MHz, $CDCl_3$) δ (ppm) 1.73 (3H, s), 3.39 (3H, s), 3.71 and 3.75 (4H, s + d, *J*= 8.8 Hz), 3.96 (1H, d, *J*= 8.8 Hz), 7.39 (dt, J_1=7.5 Hz, J_2= 0.8 Hz), 7.5 (2H, m), 7.7 (2H, m), 8.29 and 8.34 (2H, 2 x d, *J*= 2Hz). ^{13}C DEPTQ NMR (100 MHz, $CDCl_3$) δ (ppm) 21.30 (CH_3), 51.27 (C), 52.46 (CH_3), 59.53 (CH_3), 78.26 (CH_2), 117.98, 118.17 (aromatic CH), 121.46, 121.78 (aromatic C), 123.97, 124.00, 126.80, 133.63, 134.89 (aromatic CH), 137.19, 155.24, 156.14 (aromatic C), 174.74 (C=O), 177.14 (C=O).

3-Methoxy-2-methyl-2-(9-oxo-*9H*-xanthen-2-yl)propanoic acid (XPA-OCH_3) (**22**) A solution of **21** in 10 mL ACN:0.1 M KOH (1:1) was left to stir overnight. The solution was then acidified with 10% HCl and extracted with EtOAc. The solid obtained following removal of solvent was dissolved in 0.1 M KOH, washed with EtOAc then acidified with 10% HCl and extracted with EtOAc. Finally, the organic layer was dried over $MgSO_4$ and the solvent was removed under vacuum. ^{1}H NMR (400 MHz, $CDCl_3$) δ 1.64 (3H, s), 3.37 (3H, s), 3.90 and 3.93 (2H, 2 x d), 7.3 (3H, m), 7.66 (1H, m), 7.8 (1H, dd, J_1= 11.6 Hz, J2= 3.2 Hz), 7.9 (1H, dd, J_1= 10.8 Hz, J_2= 2 Hz), 8.00 (1H, d, *J*= 3.2 Hz).

(**23**) Boc-Glu(OtBu)-OH [04-12-0051] (0.086 g, 0.28 mmol) and **15** (0.10 g, 0.28 mmol) were dissolved in 3 mL dry CH_2Cl_2 and cooled in an ice bath. EDCI (0.0.059 g, 0.31 mmol) dissolved in 1 mL CH_2Cl_2 was added to the solution. After stirring for 1 hour under positive pressure argon, the reaction was allowed to warm to room

temperature and then left to stir for 20 hours. Purification by column chromatography (3:1 Hexanes: EtOAc) yielded 0.15 g of a white solid (0.23 mmol, 83%). ^{1}H NMR (400 MHz, $CDCl_3$) δ 1.4 (27H, m), 1.72 (3H, s), 2-3 (4H, m), 4.3 (0.89H, sb), 4.6, (2H, m), 5.1 (0.86H, mb), 7.40 (1H, t, J= 7.2 Hz), 7.5 (2H, two overlapping d, J= 7.2 Hz, J= 8.8 Hz), 7.7-7.8 (2H, m), 8.3-8.4 (2H, m) ^{13}C DEPTQ NMR (100 MHz, $CDCl_3$). δ 20.81, 20.95 (CH_3); 27.55, 27.69 (CH_2); 27.85, 28.00, 28.04, 28.28 (tBu CH_3); 31.47 (CH_2); 50.63, 50.67 (C); 53.05 (CH); 69.99(CH_2); 82.02, 82.06(tBu C); 117.99 (CH); 118.31, 118.34 (CH); 121.56 (C); 121.59 (C); 121.84 (C); 124.04 (CH); 124.14 (CH); 126.80 (CH); 133.10, 133.17 (CH); 134.90 (CH), 136.18 (C); 136.23 (C); 155.31 (C=O); 156.15 (C=O); 171.87 (C=O); 172.16 (C=O); 176.96 (C=O). Many peaks are doubled due to the presence of multiple stereoisomers.

3.5.2 Absorption Coefficient

The absorption coefficient for **17** was measured in 0.1 M pH 7.4 phosphate buffer. 10 absorbance measurements were taken for concentrations ranging from 1.4 x 10^{-5} M to 1.3 x 10^{-4} M in quartz cells with a pathlength of 1.00 cm. Plots of absorbance *vs.* concentration were linear within this region.

3.5.3 Photoproduct Studies

For the semi-preparative scale irradiation of **17**, a 1.0 mM solution of **16** in 40 mL phosphate buffer solution (pH 7.4) with acetonitrile (1:1) was purged with nitrogen gas in a quartz round bottom flask with a magnetic stir bar. The flask was irradiated with stirring in a Luzchem photoreactor with 4 UVB lamps (2 per side).

The solution was monitored by UV-vis absorption spectroscopy. Once the photolysis was complete (i.e. no further change in the absorption spectrum) the solution was transferred to a separatory funnel with 20 mL 10% HCl and 20 mL brine. The organic component was extracted with 3 x 50 mL dichloromethane. The combined organics were dried over $MgSO_4$ and the volatile components were removed under vacuum. The extracted solid was confirmed to be purely the elimination photoproduct (**24**) by ^1H NMR, DEPTQ NMR and MS. The small amount of impurity observed in the NMR spectra (1.2, 3.1 ppm) was determined by MS to be a phthalate, likely present in the extraction solvent. (dichloromethane). The same procedure was used for photolysis of **20**, however characterisation of the photolysis solution was achieved with ^1H NMR analysis alone. Irradiation of **22** (~40 mM) was conducted in glass NMR tubes using a hand held TLC lamp (λ_{max} = 368 nm, 6.2 Watt m^{-2}, FWHM = 16 nm). The photolysis was monitored by ^1H NMR using a Bruker AVANCE 400 instrument.

The quantum yield of release from **17** was measured by irradiating three solutions of **17** (2 mL, 2.0 mM) and four solutions of ketoprofen (2mL, 2.0 mM) in PB (pH 7.4) for 3 minutes. The irradiation was performed in a merry-go-round apparatus within a Luzchem photoreactor (2 UVB lamps per side). After irradiation 6.00 mL of an internal standard (0.21 mM 9-hydroxyfluorene in CH_3CN) was added to each tube and the contents were diluted to 20 % PB 80 % CH_3CN with 0.1% acetic acid for HPLC analysis (method described in Chapter 2, monitoring λ=300 nm).

3.6 References

1. Blake, J. A.; Lukeman, M.; Scaiano, J. C., Photolabile Protecting Groups Based on the Singlet State Photodecarboxylation of Xanthone Acetic Acid. *J. Am. Chem. Soc.* **2009,** *131* (11), 4127-4135.

2. Cosa, G.; Lukeman, M.; Scaiano, J. C., How Drug Photodegradation Studies Led to the Promise of New Therapies and Some Fundamental Carbanion Reaction Dynamics along the Way. *Acc. Chem. Res.* **2009,** *42* (5), 599-607.

3. Lukeman, M.; Scaiano, J. C., Carbanion-mediated Photocages: Rapid and Efficient Photorelease with Aqueous Compatibility. *J. Am. Chem. Soc.* **2005,** *127*, 7698-7699.

4. Turro, N. J.; Ramamurthy, V.; Scaiano, J. C., *Modern Molecular Photochemistry of Organic Molecules*. University Science Books: Sausalito, California, 2010.

5. Kottani, R.; Roman, A. V.; Kutateladze, A. G., Direct screening of solution phase combinatorial libraries encoded with externally sensitized photolabile tags. *PNAS* **2006,** *103* (38), 13917-13921.

6. Sundararajan, C.; Falvey, D. E., Photorelease of carboxylic and amino acids from *N*-methyl-4-picolinium esters by mediated electron transfer. *Photochem. Photobiol. Sci.* **2006,** *5*, 116-121.

7. Rewcastle, G. W.; Atwell, G. J.; Baguley, B. C.; Calveley, S. B.; Denny, W. A., Potential antitumour agents. 58. Synthesis and structure-activity relationships of substituted xanthenone-4-acetic acids active against the codon 38 tumor in vivo. *J. Med. Chem.* **1989,** *32* (4), 793-799.

8. Goeldner, M.; Givens, R., *Dynamic Studies in Biology*. Wiley-VCH: Weinheim, 2005.

9. Papageorgiou, G.; Barth, A.; Corrie, J. E. T., Flash photolytic release of alcohols from photolabile carbamates or carbonates is rate-limited by decarboxylation of the photoproduct. *Photochem. Photobiol. Sci.* **2005,** *4*, 216-220.

10. Gottlieb, H. E.; Kotlyar, V.; Nudelman, A., NMR Chemical Shifts of Common Laboratory Solvents as Trace Impurities. *J. Org. Chem.* **1997,** *62*, 7512-7515.

11. Calculated based on the absorption coefficient at 347 nm.

12. Corrie, J. E. T., In *Dynamic Studies in Biology*, Goeldner, M.; Givens, R., Eds. Wiley-VCH: Weinham, 2005; Vol. 1.

13. Bose, D. S.; Narsaiah, A. V., An efficient asymmetric synthesis of (*S*)-atenolol: using hydrolytic kinetic resolution. *Bioorg. Med. Chem.* **2005,** *13*, 627-630.

14. Natarajan, A.; Ng, D.; Yang, Z.; Garcia-Garibay, M. A., Parallel syntheses of (+)- and (-)-alpha-cuparenone by radical combination in crystalline solids. *Angew. Chem. Int. Ed.* **2007,** *46* (34), 6485-6487.

15. Boss, R.; Scheffold, R., Cleavage of Allyl Ethers with Pd/C. *Angew. Chem. Int. Ed.* **1976,** *15* (9), 558-559.

16. Hazeldine, S. T.; Polin, L.; Kushner, J.; White, K.; Corbett, T. H.; Horwitz, J. P., Synthetic modification of the 2-oxypropionic acid moiety in 2-{4-[7-chloro-2-quinoxalinyl)oxy]phenoxy}propionic acid (XK469), and consequent antitumour effects. Part 4. *Bioorg. Med. Chem.* **2005,** *13*, 3910-3920.

4. Photochemistry of Nitro, Amine and Amide Substituted Xanthone Acetic Acids and Thioxanthone Acetic Acids

Graphical Abstract

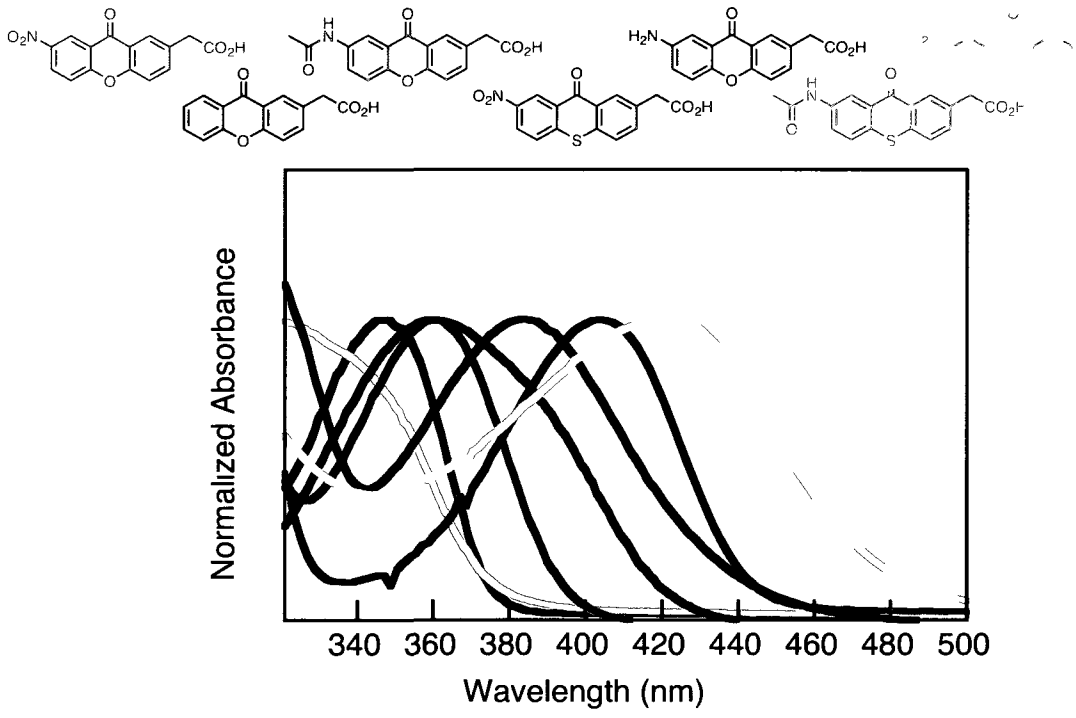

4.1 Introduction

Having demonstrated that efficient photorelease is possible from xanthone propionic acid (XPA) derivatives (Chapter 3), it would be advantageous to examine further modifications to the chromophore and their effect on the photochemistry in order to determine the versatility of this new class of photolabile protecting group (PPG). For example, one may wish to red-shift the absorption spectrum (shift to higher wavelengths) for certain applications requiring a lower excitation energy. Substitution of sulfur at the ether oxygen position (i.e. exchange thioxanthone for xanthone) is expected to lower the energy of the lowest energy excitation, but what effect does it have on the photodecarboxylation mechanism? We are also interested in designing XPA PPGs with a 'handle' that can be used to attach the group to a substrate (e.g. nanoparticle surface, polymer, protein) in order to release interesting molecules from said substrate. One option is to incorporate a functionalizable group (e.g. an amine) on the xanthone core, distal to the site of photodecarboxylation. This would allow attachment to surfaces functionalized with a complementary group (e.g. a carboxylic acid) as illustrated in Scheme 4-1. Although the proposed funtionalization is on the opposite side of the xanthone core from the site of decarboxylation, it is still directly attached to the chromophore and therefore could significantly influence the photochemistry. For this reason, we chose to evaluate the effect by studying the photochemistry of a model compound with just a simple amide substituent (**4** in Chart 1). As a first step towards evaluating the versatility of

XPA based PPGs and the potential to attach them to substrates as proposed in Scheme 4-1 we have synthesized and examined the photochemistry of a series of xanthone acetic acid and thioxanthone derivatives with substituents in position 7 on the aromatic ring, distal to the carboxylic acid (Chart 4-1).

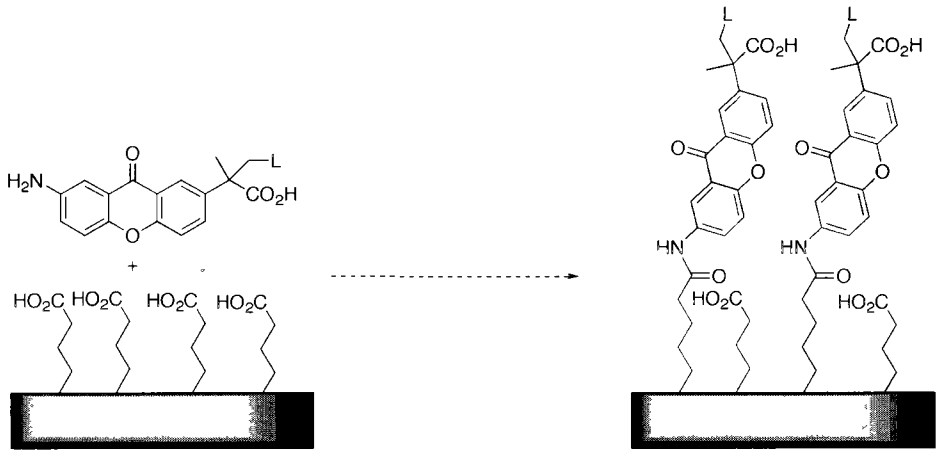

Scheme 4-1. An illustration of one potential way to attach an XPA PPG to a surface. Coupling of the aromatic amine and the surface carboxylic acid could be achieved using a diimide coupling agent. Protection and subsequent deprotection of the XPA carboxylic acid would likely be necessary as well.

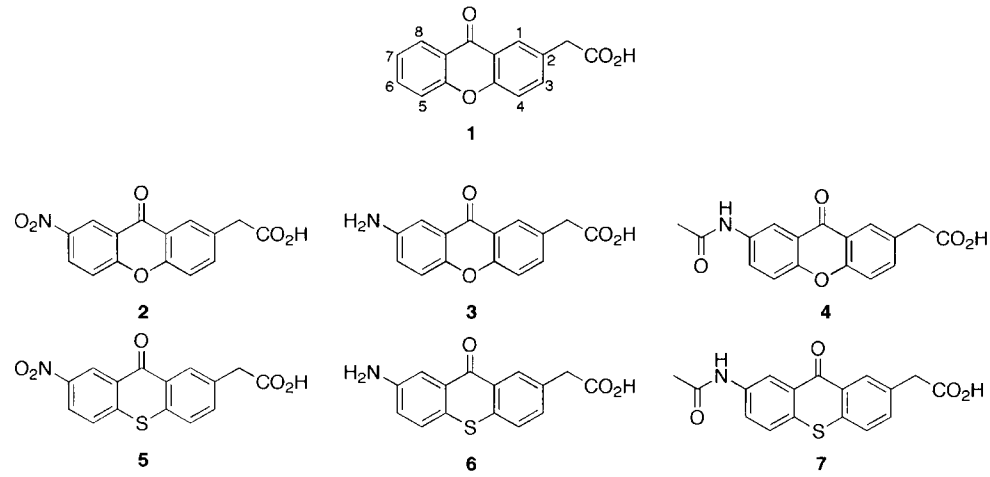

Chart 4-1.

This work has been undertaken in collaboration with M. J. Yorke, a fellow graduate student in our group. My contribution focused on a comparison of the basic photochemistry of **1** – **7** including quantum yield measurements, photoproduct characterization for **2** and **5**, and the laser flash photolysis results described. The more in-depth photochemistry and photophysics of **3**, **4**, **6**, and **7** as well as photorelease from derivatives of **4** both in solution and from surfaces were the focus of M. J. Yorke. The synthesis of derivatives **2** and **5** was developed collaboratively by both Mr. Yorke and myself, however synthesis of **3**, **4**, **6** and **7** was undertaken entirely by him and further details regarding these results can be found in his M.Sc. thesis.

4.2 The effect of altering the chromophore

4.2.1 Synthesis

Initially we synthesized **2** by nitrating the methyl ester of 2-xanthone acetic acid using standard nitration conditions.[1, 2] While this method, shown in Scheme 4-2, worked sufficiently to produce a small amount of pure test compound, it is a difficult reaction to scale up; the substrate itself was obtained from another reaction that was difficult to achieve on a large scale (the xanthone acetic acid synthesis described in Chapter 2). Overall, this route was not very practical for anything more than initial photochemical studies.

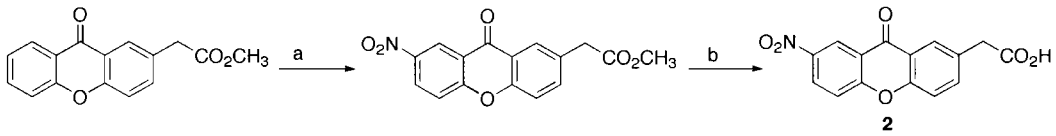

Scheme 4-2. Initial synthesis of **2**. a) HNO_3/H_2SO_4 b) 0.1 M KOH/CH_3CN

Fortunately we came across an alternative synthesis that avoids both the Ullmann coupling xanthone synthesis and the nitration reaction. Rarick et al. demonstrated that the fluorine atom in *p*-nitrofluorobenzene is quite labile, allowing for reactions with phenols in alkaline solution forming diaryl ethers in near quantitative yields.[3] We were able to successfully adapt this synthesis using commercially available 2-fluoro-5-nitrobenzoic acid and 4-hydroxyphenylacetic acid (Scheme 4-3). Ring closure in concentrated sulfuric acid afforded **2** in high yield. As an additional benefit, this synthesis could also be used to obtain the thio derivative (**5**). Previous attempts to synthesize thio-xanthone acetic acid *via*

Ullmann coupling had failed, likely due to the reduced acidity of the thiol as compared to the alcohol.

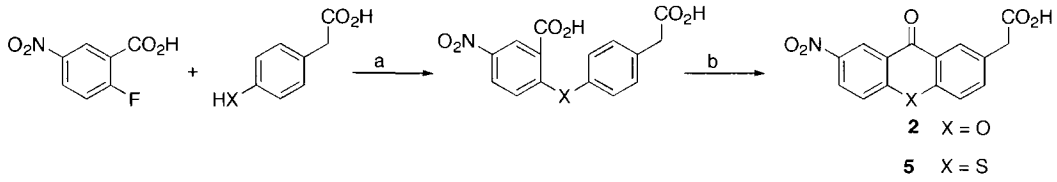

Scheme 4-3. Synthesis of **2** and **5** *via* direct arylation. a) KOH/DMSO b) H_2SO_4/85°C

4.2.2 Characterization

The ^{1}H NMR spectra for **1**, **2**, and **5** are shown in Figure 4-1. The inclusion of a nitro group on the xanthone ring is very apparent in the aromatic region of the spectrum. To start, the spectra of **2** and **5** possess one less aromatic proton than that of **1**. In addition, the coupling to the position 7 proton is lost in the spectra for **2** and **5**. Finally, consistent with the incorporation of an electron withdrawing substituent, the signals for all protons have shifted slightly to lower frequencies.

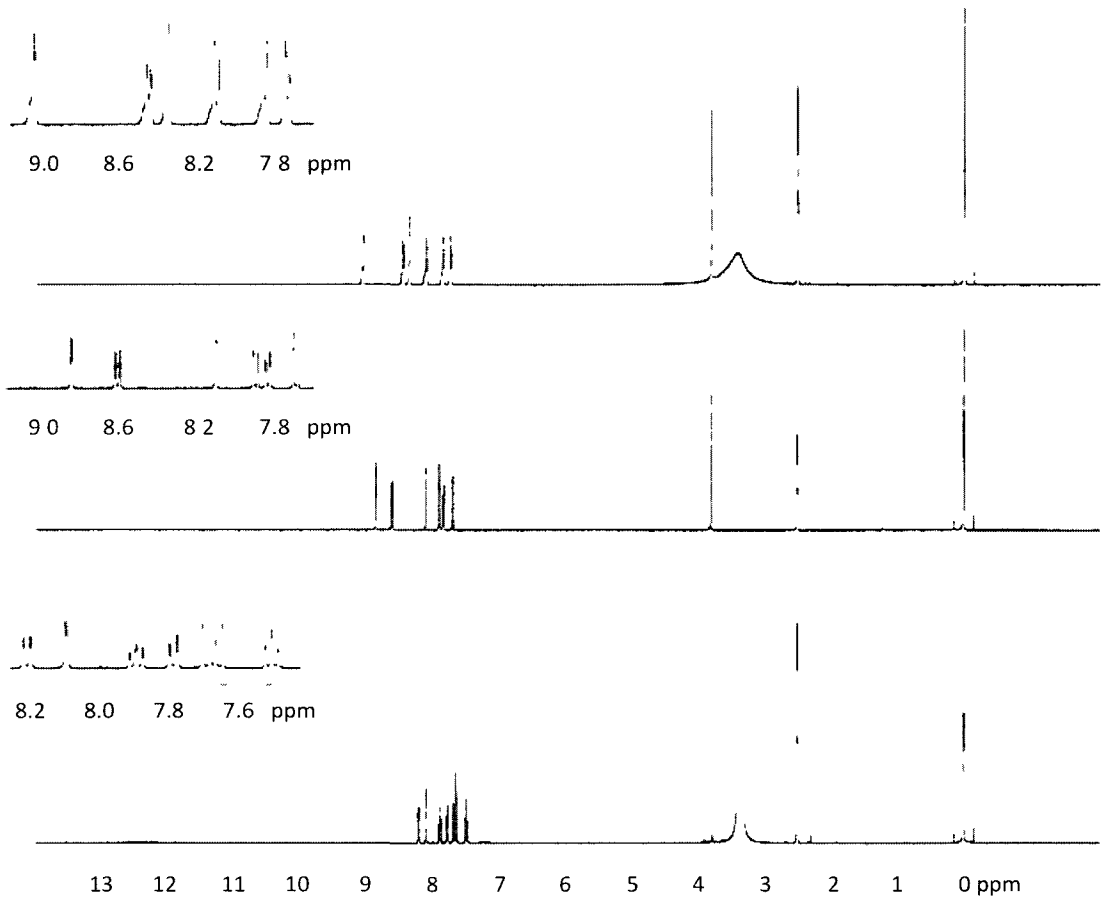

Figure 4-1. ^{1}H NMR of **5** (Top), **2** (Middle), and **1** (Bottom) in DMSO-d6.

All derivatives (**1** – **7**) were also characterized by either ^{13}C or DEPTQ NMR and HRMS.

4.2.3 Absorbance of 1 – 7

One obvious effect of changing the chromophore is a change in the UV-vis absorption spectra, which can be seen in Figure 4-2. As expected amine and amide substitution red shift the absorption of the xanthone chromophore (Figure 4-2 Top) with the energy of the $S_0 \rightarrow S_1$ band following the trend **1** ~ **2** > **3** > **4**. Substitution

of thioxanthone for xanthone significantly red shifts the absorption (Figure 4-2 Bottom).

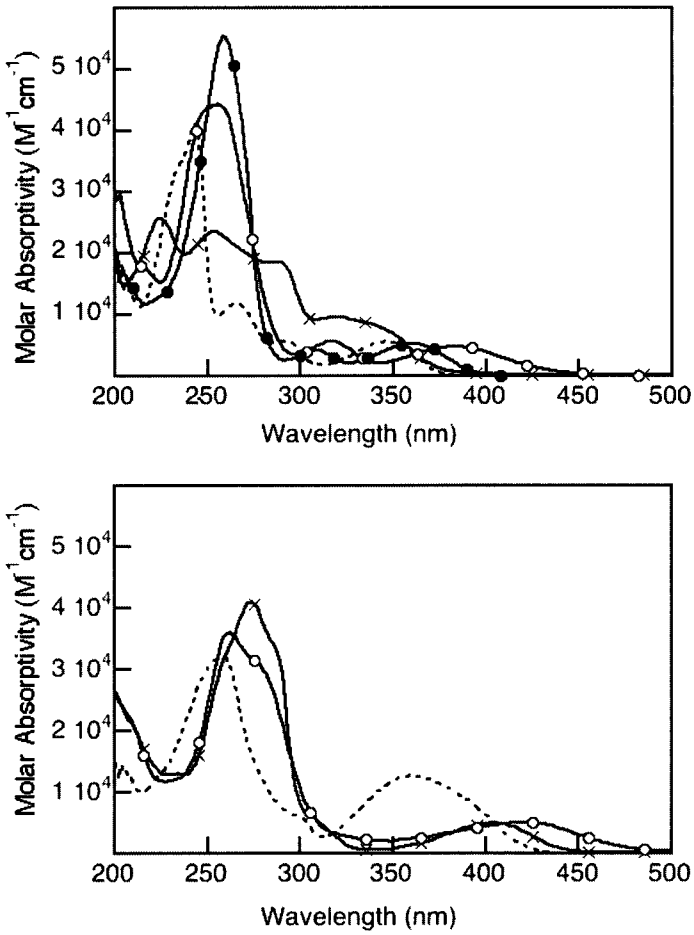

Figure 4-2. Top: Absorbance spectra of xanthone derivatives **1** (---), **2** (×), **3** (o) and **4**(•). Bottom: Absorbance spectra of thioxanthone derivatives **5** (×), **6** (o) and **7** (•). Spectra for **1**, **2**, and **5** were measured in phosphate buffer solution. Spectra for **3**, **4**, **6**, and **7** were measured in phosphate buffer solution with 20% acetonitrile by M.J. Yorke.

4.2.4 Photochemistry of 1 - 7

By measuring the photochemical decarboxylation quantum yields of **2** - **7** using ketoprofen (Φ_{PDC} = 0.75)[4] as an actinometer (Table 4-1), we have determined that nitro substitution decreases the quantum yield of photochemical reaction by approximately half with respect to the unsubstituted derivative (based on disappearance of **2**). In addition, we find that the photochemistry of **2** is not as clean as that of 2-xanthone acetic acid (**1**). The expected product resulting from protonation of the photochemically generated carbanion is observed, but it is not the only photoproduct. When non-deaerated solutions of **2** in pH 7.4 phosphate buffer solution (PB) were irradiated to low conversion, HPLC-UV traces of the photolysates show four photoproducts (Figure 4-3 Top). When conversion is higher, there are even more absorbing photoproducts observed (Figure 4-4). Using preparative thin layer chromatography to separate the photoproducts from a higher conversion preparative scale photolysis, we were able to identify three of the photoproducts based on ^{1}H NMR and GC-MS as **8**, **9**, and **10.** Photoproduct **8** is the product expected from protonation of the photochemically generated carbanion. Oxidation products **9** and **10** can be attributed to reaction of the carbanion with oxygen. This is supported by the observation that irradiation of **2** after purging with nitrogen (Figure 4-4 bottom) produces much lower amounts of **9** and **10.**

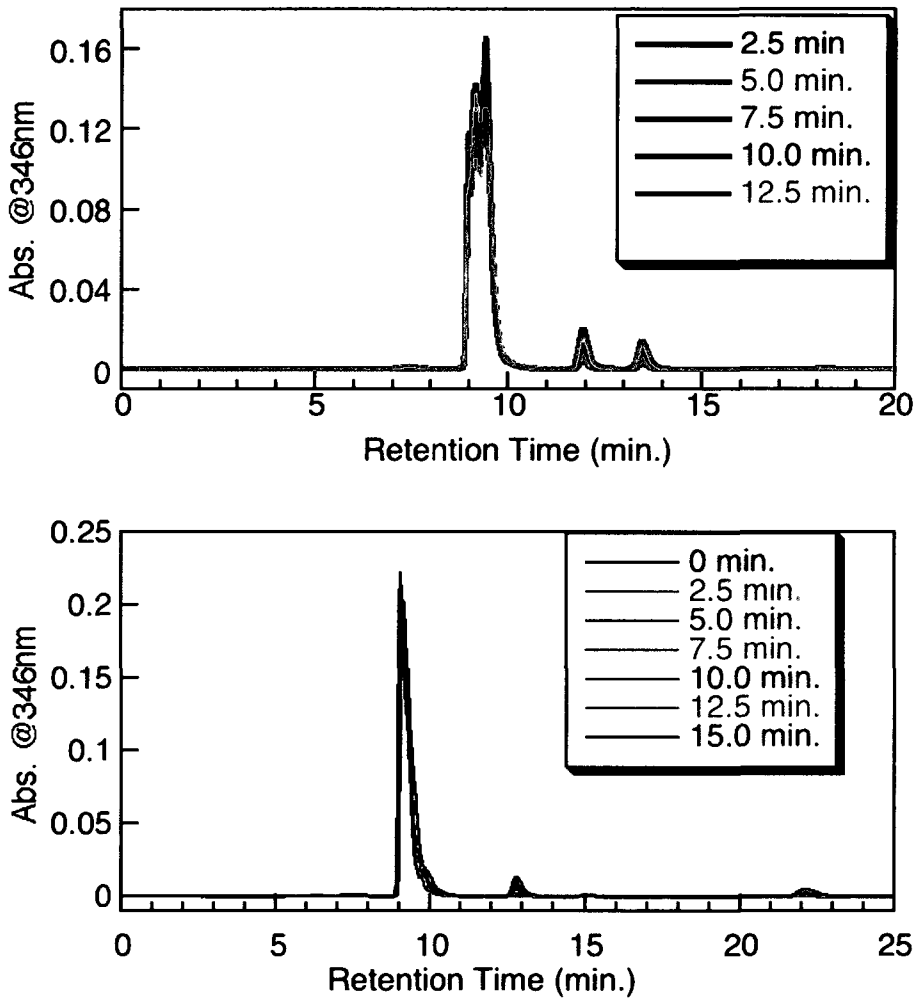

Figure 4-3. HPLC traces for irradiation of **2** (top) and **5** (bottom) in phosphate buffer solution. The largest peaks in both graphs correspond to **2** and **5** respectively. They are split because of the carboxylate group. In later experiments 0.1 % acetic acid in the HPLC mobile phase resolved this problem.

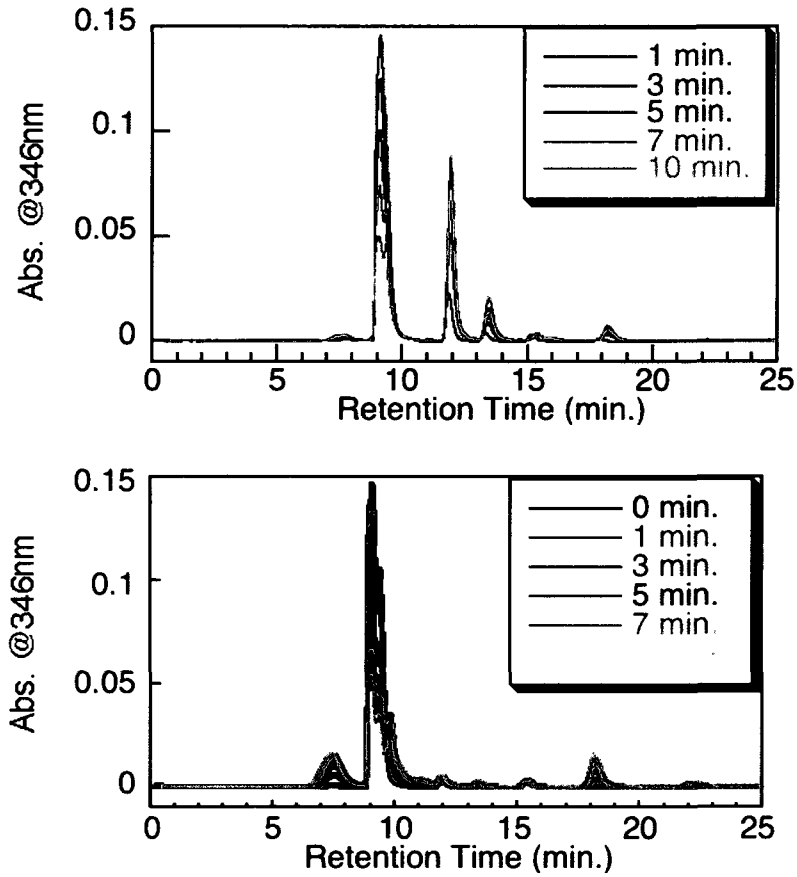

Figure 4-4. HPLC traces for irradiation of **2** in PB with (bottom) and without (top) nitrogen gas purging.

The oxidation photoproducts **9** and **10** observed from photodecarboxylation of **2** under air may indicate a longer carbanion lifetime for the nitro-substituted derivative relative to the parent xanthone derivative **1**, long enough for the reaction of the carbanion with oxygen to compete with protonation. This is supported by the fact that ketoprofen photodecarboxylation under the same conditions (ketoprofen carbanion lifetime = 200 ns)[5] produces the analogous aldehyde and alcohol.[4] In contrast, the carbanion generated from **1** (τ < 20 ns) yields only the protonation product.

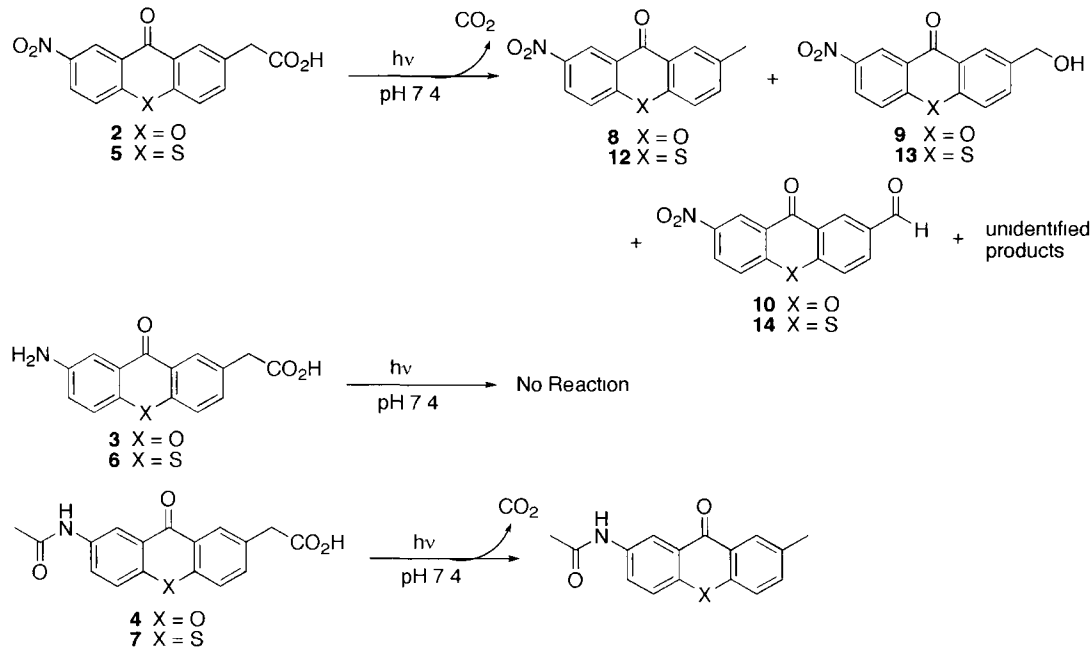

Scheme 4-4. Photolysis of **2** – **7** in PB. Irradiated **2** and **5** yield four absorbing photoproducts. Deaerated solutions of **2** and **5** produce mainly **8** and **12** respectively as well as the unidentified products. **3** and **6** are photostable under the same conditions. Irradiation of **4** and **7** yield only one photoproduct.

Table 4-1. Photochemistry of **1 – 7** with UVB irradiation.

	In pure phosphate buffer (pH 7.4)		Phosphate buffer:acetonitrile (1:1)	
Derivative	$\Phi_{photoreaction}$[a] Deaerated	$\Phi_{photoreaction}$[a] Non-deaerated	$\Phi_{photoreaction}$[a] Deaerated	$\Phi_{photoreaction}$[a] Non-deaerated
1	0.62 ± 0.07	0.64 ± 0.06	0.65 ± 0.08	0.68 ± 0.06
2	0.35 ± 0.05	0.33 ± 0.06	0.27 ± 0.05	0.30 ± 0.07
3	-	0[b]	-	-
4	-	0.01[b]	-	0.17[b]
5	0.38 ± 0.04	0.29 ± 0.11	0.33 ± 0.09	(0.54 ± 0.05)[d]
6	-	0	-	
7	-	~0.0004[b,c]	-	0.004[b]

Errors are estimated for a 95% confidence interval using a student's t test (t=4.303) (a) by HPLC-UV using ketoprofen as an actinometer (b) Measured by M.J. Yorke (c) in 90:10 buffer:acetonitrile (d) There may be additional error for this value since the internal standard area was unusually high.

Amine substitution completely quenches the photodecarboxylation pathway as determined by HPLC-UV analysis following extensive irradiation of solutions of **3** and **6** in pH 7.4 PB. Given that amine groups are known to quench excited states,[6] this is not at all surprising.

In the case of amide substitution, analysis by HPLC-UV and ^{1}H NMR show clean conversion of **4** to **8** as the only photoproduct in both deaerated and non-deaerated solutions. However, the quantum yield of this reaction (Φ = 0.01) is significantly decreased relative to the unsubstituted compound (**1**) and the nitro substituted compound (**2**). We were initially discouraged by this result, but upon investigation

into the influence of acetonitrile (CH_3CN), we discovered a very interesting solvent effect on the quantum yield of photodecarboxylation. The observed trend is shown in Figure 4-5 Overall there is a 24-fold increase in quantum yield from 0 % CH_3CN to 70 % CH_3CN

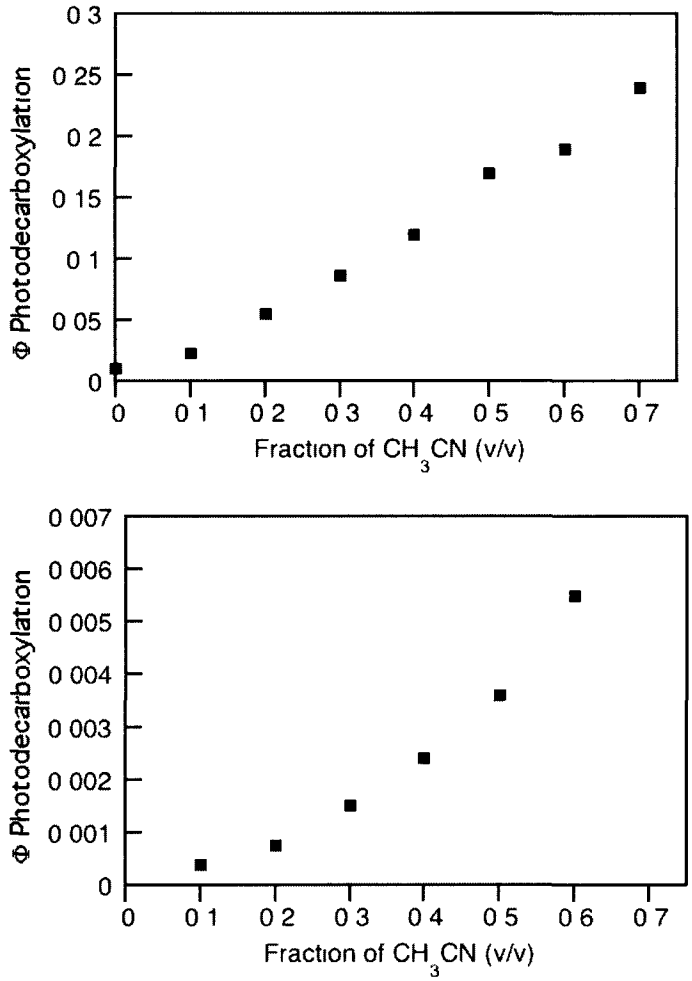

Figure 4-5 [7] Increase in photodecarboxylation Φ for **4** (top) and **7** (bottom) with increasing fraction of CH_3CN in PB CH_3CN solutions A value could not be measured for 0 % CH_3CN for **7** due to solubility constraints

Thioxanthone derivatives (**5** - **7**) behave in much the same way as their

xanthone counterparts (compare Figure 4-3 top and bottom for the nitro derivatives **2** and **5**) with the exception that the quantum yield of reaction for **7** is significantly lower than for the xanthone derivative **4**. Derivative **7** also displays a solvent effect on the photochemical quantum yield (14-fold increase from 10 % to 60 % CH_3CN for **7** compared to an 8-fold increase when comparing the same solvent compositions for **4**) as shown in Figure 4-5.

4.2.5 Nanosecond Laser Flash Photolysis (LFP)

We have had some success observing the carbanion intermediate from ketoprofen photodecarboxylation using LFP.[8] In the case of **1** however, the carbanion is too short lived to be seen using our system ($\tau < 20$ ns).[9] Suspecting that the carbanion generated from photodecarboxylation of **2** may be longer lived, we employed this technique. Flowed solutions of **2** dissolved in 0.1 M KOH with 20 % CH_3CN purged with nitrogen gas (N_2) produced a signal with two absorption maxima, 440 nm and 600 nm (Figure 4-6 A). Given that solvated electrons have been detected by ns LFP during ketoprofen photodecarboxylation and that triplet signals are common for xanthone derivatives,[10] we needed to determine if the signal observed could in fact be attributed to the carbanion intermediate or if it belonged instead to solvated electrons or the xanthone triplet. Nitrous oxide, well known to scavenge electrons,[11] had no observable effect on this signal (Figure 4-6 B) thus ruling out the possibility of solvated electrons contributing to the signal. Sorbate, a conjugated diene, was successfully used previously to completely quench the triplet

signal of **1**, but in this case it had no effect (Figure 4-6 C). Purging of the solution with oxygen on the other hand quenched both absorbance maxima significantly (Figure 4-6 D).

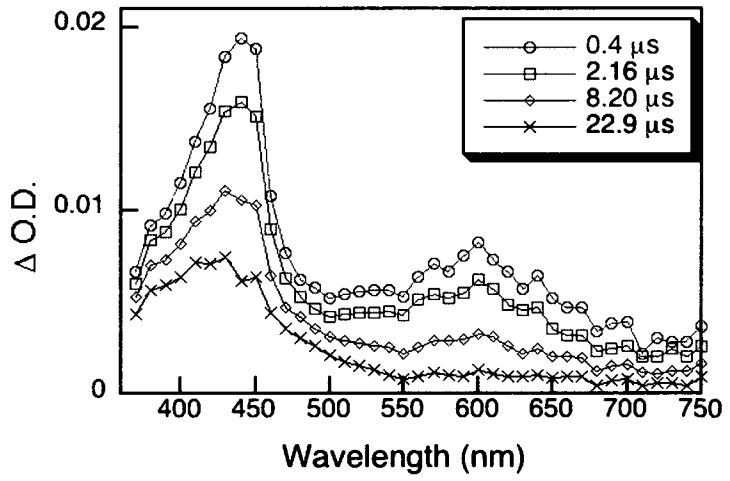

A

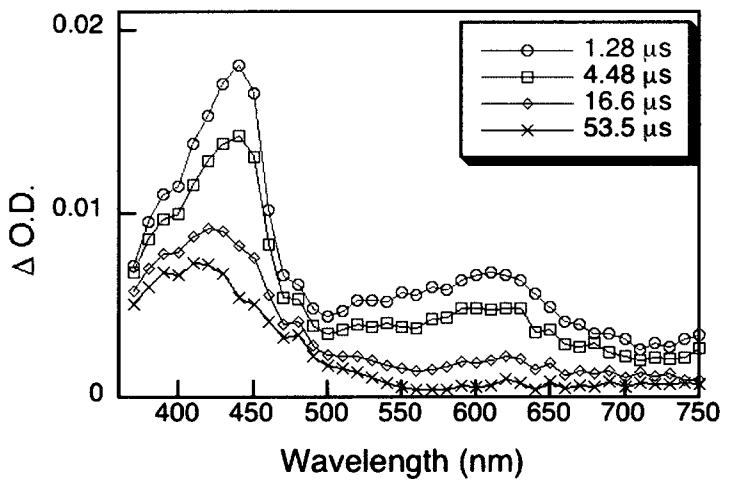

B

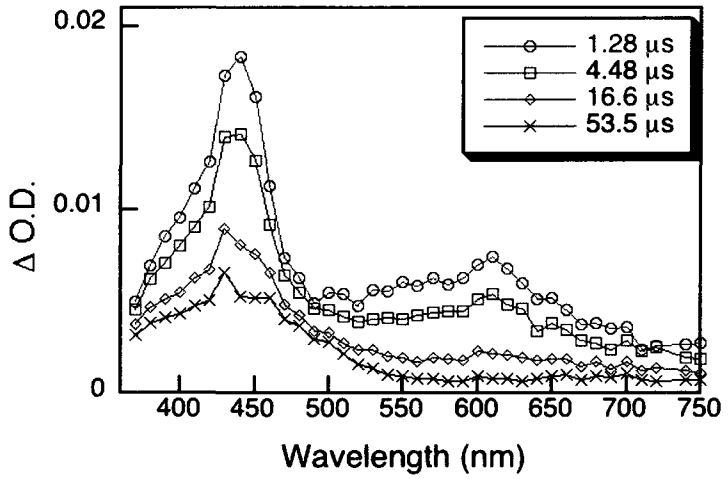

C

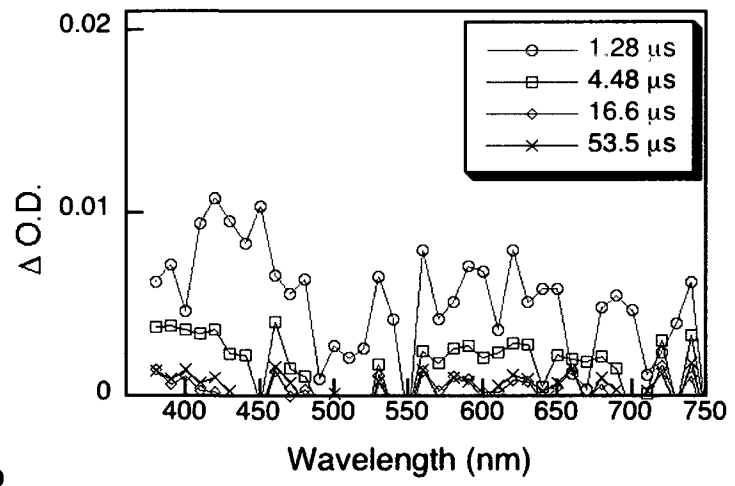

D

Figure 4-6. Time resolved absorption spectra for a flowed solution of **8** (Abs. = 0.3) dissolved in 0.1 M KOH with 20% CH_3CN **A**: purged with N_2, **B**: purged with N_2O, **C**: with 0.05 M sorbic acid, purged with N_2, **D**: purged with oxygen.

Taken in combination, these results leave us with two possibile intermediates that could be assigned to the observed signal. The first is a low lying triplet (i.e. not quenchable by sorbate (E_T ~ 247 kJ/mol)[12], but still quenchable by O_2 (E_T required to undergo energy transfer to ground state oxygen is equal to the energy of the O_2 transition $^1\Delta\Lambda \leftarrow ^3\Sigma_g^-$ = 94 kJ/mol).[12] The second possibility is the carbanion

intermediate, which we know from the observed photoproducts **8** and **9** reacts with oxygen. If the first of these options were true we should observe singlet oxygen from the $^1\Delta\Lambda \leftarrow ^3\Sigma_g^-$ transition. However, time-resolved near infrared measurements demonstrated no singlet oxygen generation from **8** under identical conditions to those used in our LFP experiments, confirming that the signal we see which is quenched by oxygen is in fact the carbanion intermediate.

When the signal at 440 nm for a nitrogen purged sample is fitted with 1st order + shift decay kinetics, a lifetime of 1860 ± 90 ns is obtained (Figure 4-7, Top). The lifetime from the signal at 600 nm is 3280 ± 160 ns. While it may seem that these signals originate from two different species, there is a great deal of error in the lifetimes for a number of reasons. For one, the decays are complicated by a shift (i.e. the ΔO.D. does not return to zero) likely due to the formation of high absorbing photoproducts. The magnitude of the shift is highly dependent on the flow rate and therefore difficult to reproduce. In addition, it is notoriously difficult to completely eliminate oxygen from flowed solutions. Since we know both signals were significantly quenched by oxygen, the degree to which oxygen was eliminated from the solution would likely have a large influence on the decays observed. Finally, the intensity of the 600 nm signal is fairly low. As a further complication, there may be a second order contribution to the decay of the carbanion since carbanions of this type have been shown to dimerize.[13] That said, we can at least say for certain that either signal is significantly longer lived than either the ketoprofen or the xanthone

acetic acid carbanion. Long lived carbanion intermediates for nitro aromatics are certainly not unprecedented. For *p*-nitrophenylacetic acid photodecarboxylation the carbanion lifetime is on the order of seconds.[13] While the nitro group in derivative **2** is not expected to have as strong of an effect given that it is not positioned on the same ring as the carboxylate this powerful EWG should still have a stabilizing effect on the ground state carbanion.

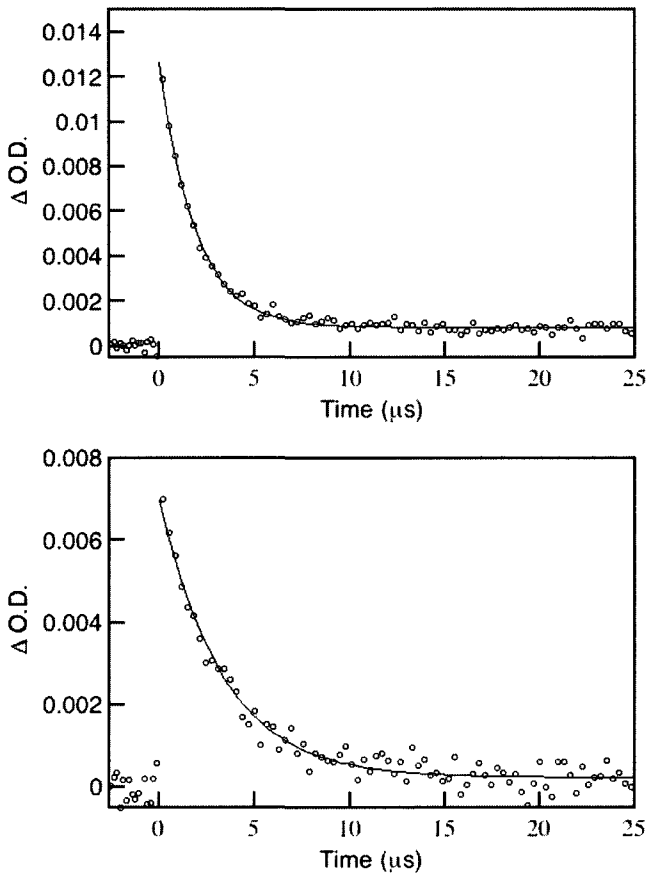

Figure 4-7. Decay traces for a flowed solution of **2** in 0.1 M KOH with 20 % CH_3CN monitored at 440 nm (top) and 600 nm (bottom). Each trace is fitted with 1st + shift decay kinetics. When monitored at 440 nm (top) τ = 1860 ± 90 ns. When monitored at 440 nm (top) τ = 3280 ± 160 ns.

4.2.6 Fluorescence

Given that the quantum yields of photodecarboxylation for the amide derivatives are quite low, we were interested in determining what else is happening to the singlet excited state. To probe this we measured fluorescence quantum yields (Φ_F)[7] for both **4** and **7** and found them to be significantly higher than that of **1** (Table 4-2). Interestingly, though the reaction quantum yield for **4** depends significantly on solvent composition, the fluorescence quantum yield did not exhibit the same trend (values ranged from 0.31 to 0.38, with the highest Φ_F measured at 30% CH_3CN). As such, we cannot fully attribute the decreased Φ_{PDC} to an increase in Φ_F.

The fluorescence quantum yield for the amine derivatives was also measured and found to be very low. This is consistent with rapid singlet state quenching by the amine substituent

Table 4-2. Fluorescence quantum yields (Φ_F) for **1 – 7.**

	Φ_F PB at pH 7.4	Φ_F 80 % PB at pH 7.4 with 20 % CH_3CN
1	0.008	-
3	0.03	-
4	0.31	0.37
6	~ 0	-
7	-	0.25

4.3 Discussion

The results we have presented provide some insights into the effect of nitro, amine and amide substitution on xanthone and thioxanthone acetic acid photodecarboxylation, and therefore the effect on release potential for PPGs derived from these molecules.

It would seem that as the first excited singlet energy decreases (estimated by a shift in the absorbance spectra to higher wavelengths), along the series of R = H, $NHC(O)CH_3$, NH_2 the quantum yield also decreases. These observations can be rationalized if we assume that lowering the singlet state energy decreases the chance of surpassing the ground state energy barrier to the carbanion intermediate. That is, stabilization of S_1 favours internal conversion and fluorescence over photodecarboxylation. Amine substitution is a special case because not only is the excited state energy decreased, but the amine quenches this excited state once it is formed, probably by charge transfer, as evidenced by the very low fluorescence quantum yield.

The same trend is true (lower first excited singlet energy leading to lower $\Phi_{reaction}$) when the xanthone core is exchanged for thioxanthone for R = $NHC(O)CH_3$ (**4** *vs.* **7**) but not for R = NO_2 (**2** *vs.* **5**). In this latter case, the thioxanthone chromophore significantly red shifts the lowest energy absorption, however the quantum yield relative to **2** is not decreased. It may be that while the singlet state energy is decreased, the nitro substituent has lowered the ground state barrier to

carbanion formation enough that the quantum yield is not affected.

The decreasing Φ_{PDC} from **4** with decreasing fraction of acetonitrile is not accompanied by a red shift in the absorbance spectra[7] as might be expected from the above discussion. This may indicate that the solvent effect is related more to the ground state energy surface than the excited singlet surface. This is supported by the absence of an effect on the fluorescence of **4**. Interestingly, the solvent effect on Φ_{PDC} is only observed for derivatives **4** and **7**. We propose that the sensitivity of the quantum yield is related to the position of the intersection of S_1 and S_0 relative to the transition state and that for **4** and **7** these two points are relatively close (and therefore sensitive) while for derivatives **1**, **2** and **5** the intersection is further to the carbanion side of the S_0 transition state and therefore less sensitive.

4.4 Summary

We have demonstrated fairly efficient photodecarboxylation from nitro-substituted xanthone and thioxanthone acetic acid yielding a longer lived, less reactive carbanion. It should be noted that the multiple photoproducts observed do not necessarily mean that photorelease would not be clean since all identified photoproducts originate from the carbanion intermediate. It is possible that intramolecular elimination (the release pathway) would compete effectively with both oxidation and protonation. That is, the carbanion intermediate of a derivative of **2** able to eliminate a good leaving group may have a significantly shorter lifetime as a result of the intramolecular reaction. However, a less reactive carbanion would certainly be a disadvantage when attempting to release poor leaving groups such as alcohols.

We have also shown that an amine substituent in the 7 position quenches both fluorescence and photodecarboxylation. This may prove to be an advantage in terms of PPG applications as it provides a photostable state that can be stored and handled under light until the amine is converted to an amide.

The amide also quenches the photodecarboxylation but not completely. Unfortunately, given the significant solvent effect, a PPG based on either **4** or **7** would require separate quantum yield determination for the application conditions if it is important to know the quantum yield accurately. Considering the high solvent dependency and the low quantum yield relative to derivative **2**, we may

wish to find an alternative method to attach our PPGs to surfaces.

The exchange of thioxanthone for xanthone dramatically extends the excitation wavelength range into the visible which would be advantageous for some applications, but poses its own problems. If a photoreactive molecule absorbs visible light, special care needs to be taken during experiments to avoid reaction induced by ambient light. In addition, the use of a coloured PPG (yellow in this case) could be undesirable in some cases. For many applications of PPGs, the absorbance spectrum of xanthone is ideal. That said, it would be appealing to generate a series of similar PPGs with different profiles so that an appropriate one could be chosen based on the individual application. If a synthetic route to thioxanthone acetic acid was discovered, PPGs based on this derivative would be worth investigating. Also, if photochemical elimination from a PPG derived from the nitro derivative **5** turned out to be clean, this would be an attractive next generation group in our series of carbanion mediated photolabile protecting groups, further extending the range of possible excitation wavelengths. However, the dramatic decrease in photodecarboxylation quantum yield with derivative **7** make this an unlikely candidate for future PPGs.

4.5 Experimental

All ^{1}H NMR and ^{13}C NMR spectra were recorded at room temperature on Bruker AVANCE 300, 400, or 500 instruments. Chemical shifts are reported relative to internal TMS. Melting points were determined on a Melt-Temp II aparatus from Laboratory Devices. Water was purified through a Millipore MilliQ system. CH_3CN was HPLC grade. DMSO was reagent grade from Aldrich and was dried and stored over molecular sieves. All other solvents are reagent grade from Aldrich and used as received. 2-Nitro-5-fluorophenylacetic acid was purchased from Fluorochem. All other chemicals were purchased from Aldrich.

4.5.1 Synthesis

The synthesis of **1** was reported in Chapter 2. Derivatives **3**, **4** and **6**, **7** were synthesized by M.J. Yorke. The details of these syntheses can be found in his M.Sc. thesis.

(7-nitro-9-oxo-9H-xanthen-2-yl)acetic acid (2) – To a flame dried 50 mL round bottom flask under N_2 was added 2-nitro-5-fluorobenzoic acid (1.0 g, 5.4 mmol), 4-hydroxyphenylacetic acid (0.90 g, 5.9 mmol, 1.1 eq.), KOH (crushed, 1.0 g), and dry, nitrogen purged DMSO (50 mL). This solution was stirred overnight under a nitrogen atmosphere at room temperature. The reaction was dissolved in 50 mL CH_2Cl_2 and washed with 100 mL 10% HCl. The aqueous layer was then extracted with EtOAc and the combined organics were dried over $MgSO_4$ and evaporated under reduced pressure to yield 2.12 g of a powder. The powder was dissolved in

20 mL conc. H_2SO_4 at 85°C and stirred at this temperature for 1 hr. then poured over ice. Once the ice had melted, the precipitated solid was isolated by filtration and washed thoroughly with 1% HCl. Recrystallization from hot toluene yielded off-white crystals. Crude yield (pure by ^1H NMR): 0.81 g, 2.7 mmol, 50 %. Recrystallized yield: 0.19 g, 0.63 mmol, 12 %. Crude yield reported by M.J. Yorke = 91%. m.p. 244-246 °C (decomposes), ^1H NMR (400 MHz, DMSO-d_6) δ (ppm) 3.81 (2H, s), 7.69 (1H, d, J= 8.6 Hz), 7.84 (1H, dd, J_1= 2.5 Hz, J_2= 8.6 Hz), 7.90 (1H, d, J= 9.2 Hz), 8.11 (1H, d, J= 2.1 Hz), 8.62 (1H, dd, J_1= 2.8 Hz, J_2= 9.4 Hz), 8.86 (1H, d, J= 2.8 Hz). ^{13}C NMR (100 MHz, DMSO-d_6) δ (ppm) 39.5 (CH_2 under DMSO peak), 118.3, 120.3, 120.4, 121.0, 122.0, 126.4, 129.4, 132.6, 137.8, 143.3, 154.3, 158.8, 172.4 (C=O), 175.1(C=O). HRMS for $C_{15}H_9NO_6$ [M^+] calculated 299.0430, found 299.0414.

(7-nitro-9-oxo-*9H*-thioxanthen-2-yl)acetic acid (5) - To a flame dried 100 mL round bottom flask under N_2 was added 2-nitro-5-fluorobenzoic acid (1.21 g, 6.54 mmol), 4-mercaptophenylacetic acid (1.00 g, 5.94 mmol), K_2CO_3 (1.0 g), and dry, nitrogen purged DMSO (50 mL). This solution was stirred overnight under a nitrogen atmosphere at room temperature. The reaction was quenched with 100 mL 1% HCl and extracted with 100 mL EtOAc. The organic layer was washed with 4 x 100 mL 1% HCl then dried with $MgSO_4$, filtered, and the solvent was removed under reduced pressure to yield 2.14 g of a yellow powder. This powder was dissolved in conc. H_2SO_4 at 85°C and stirred at this temperature for 3 hr. then poured over ice. Once the ice had melted, the precipitated solid was isolated by

filtration and washed thoroughly with 1% HCl. Recrystallization from hot toluene yielded a yellow crystalline solid (0.3 g, 0.95 mmol, 16 %). m.p. 265 °C (decomposes). ^{1}H NMR (400 MHz, DMSO-d6) δ (ppm) 3.82 (2H, s), 7.74 (1H, dd, J_1= 8.0 Hz, J_2= 2.0 Hz), 7.86 (1H, d, J= 8.4 Hz), 8.11 (1H, d, J= 9.0 Hz), 8.36 (1H, d, J= 1.6 Hz), 8.46 (1H, dd, J_1= 8.8 Hz, J_2= 2.8 Hz), 9.06(1H, d, J= 2.6 Hz), 12.55 (1H, bs). ^{13}C NMR (100 MHz, DMSO-d6) δ (ppm) 39.8, 123.87, 126.0, 126.7, 127.4, 128.3, 128.5, 129.7, 133.8, 135.1, 135.2, 143.8, 145.5, 172.2 (C=O), 177.7 (C=O).

4.5.2 Initial photolysis

Solutions of **2** (2 mM in 80% pH 7.4 PB: 20% ACN) and **5** (0.6 mM in 80% pH 7.4 PB: 20% ACN) were irradiated for varying lengths of time with 333 nm light from the excitation beam of a PTI fluorimeter using slit widths 3 mm and 10 mm. Following irradiation each sample was analysed by HPLC with UV detection yielding the traces in Figure 4-3.

4.5.3 Quantum yield measurements

The quantum yields reported in Table 4-1 for **1**, **2** and **5** were determined as follows. Solutions of each xanthone derivative (2.1 mM of **1**, 1.0 mM of **2**, 1.2 mM of **5** in PB, and 2.0 mM of **5** in PB/CH_3CN 1/1 (v/v)) were prepared and 2 mL of each were added to quartz test tubes then capped with rubber septa. For each derivative 12 tubes were prepared: triplicate tubes of each PB under air, PB deaerated with nitrogen gas, PB/CH_3CN 1/1 (v/v) under air and PB/CH_3CN 1/1 (v/v) deaerated

with nitrogen gas. The deaerated samples were head space purged with nitrogen gas for 10 min. prior to irradiation. All 12 tubes were irradiated for 3 min. in a merry-go-round apparatus within a Luzchem photoreactor (2 UVB lamps per side) along with 4 tubes containing 2 mL of 2.1 mM ketoprofen in deaerated PB as the actinometer. After irradiation 6.00 mL of an internal standard solution (0.21 mM 9-hydroxyfluorene) was added to each tube and the contents were diluted to 20 % PB 80 % CH_3CN with 0.1% acetic acid for HPLC analysis. The HPLC method is described in Chapter 2.

The error estimates were calculated based on a 95% confidence interval according to Equation 4-1 and propagated according to Equation 4-2 where x is the value of $n_{photolysed}$ measured by HPLC and m is the degree of freedom.

$$x = x_{avg} \pm \frac{ts}{\sqrt{m}} = x_{avg} \pm \frac{4.303s}{\sqrt{2}} \tag{4-1}$$

$$= \Phi \sqrt{\left(\frac{u_x}{x_{avg}}\right)^2 + \left(\frac{u_{Kp}}{x_{Kp}}\right)^2} \tag{4-2}$$

4.5.4 Photoproduct Identification

A 0.8 mM solution of **2** (50 mL) in 80 % pH 7.4 PB with 20 % CH_3CN in a quartz round bottom flask was irradiated for 10 min. The solution was sampled at 1, 3, 5, 7, and 10 min. These samples were analysed by HPLC, yielding Figure 4-4. Following irradiation, the remaining solution was acidified with 10 % HCl and extracted with

EtOAc. The combined organic layers were dried over $MgSO_4$ and the solvent was removed *in vacuo*. The remaining residue was separated by preparative TLC and each spot was analysed by ^1H NMR and GC-MS. The same procedure was repeated for a solution that was purged with nitrogen gas prior to irradiation.

4.5.5 Nanosecond Laser Flash Photolysis

The laser flash photolysis system is a customized system operated with Luzchem software. Kinetics and spectra were obtained by exciting with the third harmonic of a Surelite Nd:YAG laser generating pulses at 355 nm of 8 ns duration and 15 mJ output. Spectra and kinetic experiments employed 7x7 mm^2 quartz flow cells with solutions flowed at a high rate with constant bubbling of either nitrogen, nitrous oxide or oxygen as specified. Each compound was dissolved in 80% 0.1 M KOH 20% CH_3CN to A = 0.3 and purged with the specified gas for 40 minutes prior to data acquisition.

The kinetics were fit with a 1st order decay + a shift to account for the absorbance of photoproducts formed in the laser pulse. The kinetic equation used for this fit is:

$$y = m_3 e^{-m_2 m_0} + m_1 \qquad (4\text{-}3)$$

Where m_1 is the shift (i.e. the final ΔOD), m_2 is the rate constant of the decay, and m_3 is the weight for m_2. The error in each lifetime is estimated as 5 % of the value.

4.5.6 Time-resolved Near Infrared Emission Spectroscopy

For the detection of singlet oxygen phosphorescence, the identical system described above (Section 4.5.5) was used with NIR detection[14] (Peltier-cooled (-62.8°C) Hamamatsu NIR detector (Model H10330-75) operating at 900 V coupled with a computer-controlled grating monochromator). A long pass filter, type FEL1150 filter from Thorlabs was placed in front of the monocromator. The photocurrent signal from the PMT was stored on a digital oscilloscope (Tektronix TDS 2012B). Dilute solutions (A = 0.028, 0.049, and 0.11) of methylene blue in D_2O in a 1 x 1 cm^2 quartz cuvette capped with septum gave strong signals (Top OD = 0.66, 0.84, and 1.08 respectively) under the same conditions that gave no signals for flowed solutions of **8** in D_2O with 0.01M KOH in a 0.7 x 0.7 cm^2 quartz flow cell.

4.5.7 Fluorescence

All solutions under study were thoroughly deaerated with dry nitrogen prior to fluorescence measurements. Spectra were collected with a luminescence spectrometer from Photon Technology International (PTI).

4.6 References

1. Goldberg, A. A.; Walker, H. A., Synthesis of Diaminoxanthones. *J. Chem. Soc.* **1953**, 1348-1357.

2. Pace, T. C. S.; Monahan, S. L.; MacRae, A. I.; Kaila, M.; Bohne, C., Photophysics of aminoxanthone derivatives and their application as binding probes for DNA. *Photochem. Photobiol.* **2006,** *82* (1), 78-87.

3. Rarick, M. J.; Brewster, R. Q.; Dains, F. B., The formation of aromatic ethers from p-nitrofluorobenzene. *J. Am. Chem. Soc.* **1933,** *55*, 1289-1290.

4. Costanzo, L. L.; De Guidi, G.; Condorelli, G.; Cambria, A.; Fama, M., Molecular mechanism of drug photosensitization. II. Photohemolysis sensitized by ketoprofen. *Photochem. Photobiol.* **1989,** *50* (3), 359-365.

5. Cosa, G.; Llauger, L.; Scaiano, J. C.; Miranda, M. A., Absolute Rate Constants for Water Protonation of 1-(3-Benzoylphenyl)alkyl Carbanions. *Org. Lett.* **2002,** *4* (18), 3083-3085.

6. Cohen, S. G.; Parola, A.; Parsons, G. H. J., Photoreduction by Amines. *Chem. Rev.* **1973,** *73* (2), 141-161.

7. Yorke, M. J., M.Sc. Thesis. **2010**.

8. Cosa, G.; Lukeman, M.; Scaiano, J. C., How Drug Photodegradation Studies Led to the Promise of New Therapies and Some Fundamental Carbanion Reaction Dynamics along the Way. *Acc. Chem. Res.* **2009,** *42* (5), 599-607.

9. Blake, J. A.; Gagnon, E.; Lukeman, M.; Scaiano, J. C., Photodecarboxylation of xanthone acetic acids: C-C bond heterolysis from the singlet excited state. *Org. Lett.* **2006,** *8* (6), 1057-1060.

10. Scaiano, J. C., Solvent effects in the photochemistry of xanthone. *J. Am. Chem. Soc.* **1980,** *102* (26), 7747.

11. Buxton, G. V.; Greenstock, C. L.; Helman, W. P.; Ross, A. B., Critical review of Rate Constants for Reactions of Hydrated Electrons, Hydrogen-atoms and Hydroxyl radicals (•OH/•O-) in Aqueous Solution. *J. Phys. Chem. Ref. Data* **1988,** *17* (2), 513-886.

12. Turro, N. J.; Ramamurthy, V.; Scaiano, J. C., *Modern Molecular Photochemistry of Organic Molecules*. University Science Books: Sausalito, California, 2010.

13. Craig, B. B.; Atherton, S. J., Kinetic and Spectral Properties of the Photogenerated para-Nitrobenzyl carbanion in aqueous-media. *J. chem. Soc., Perkin Trans. 2* **1988,** (11), 1929-1935.

14. Cojocaru, B., Laferrière, M., Carbonell, E., Parvulescu, V., García, H., Scaiano, J. C., Direct Time-Resolved Detection of Singlet Oxygen in Zeolite-Based Photocatalysts. *Langmuir* **2008,** *24* (9), 4478-4481.

5. Xanthone Propionate PPGs for Drug Delivery

Graphical Abstract

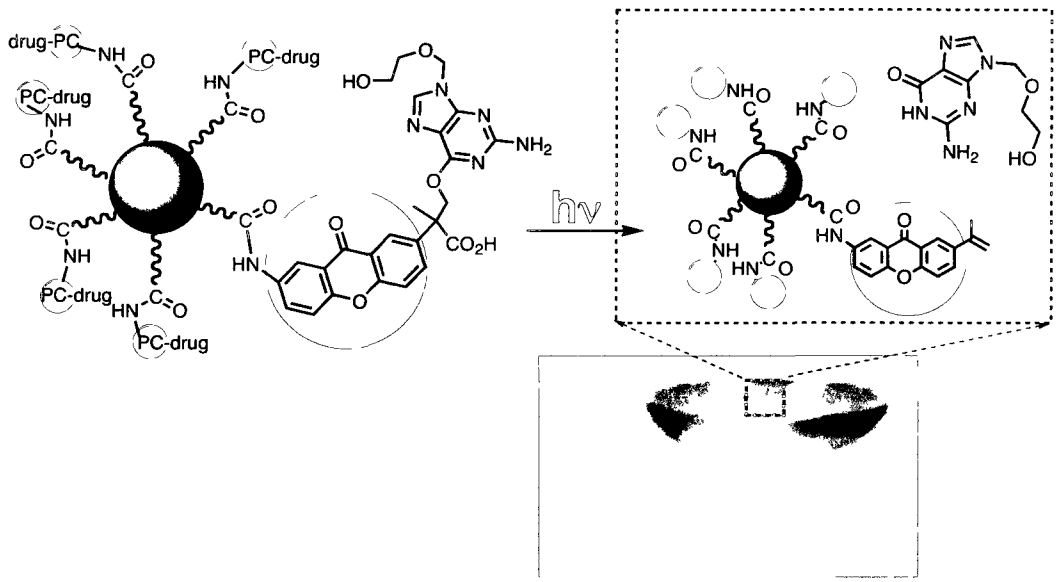

5.1 Corneal Herpes Simplex Virus; Treatment and Challenges

5.1.1 Corneal Herpes Simplex Virus (HSV-1)

The Herpes simplex virus (HSV) commonly infects the skin and mucous membranes of the mouth, genitalia, and eye. HSV-1 is the strain associated with corneal infections and is currently the most frequent cause of corneal blindness in North America.[1-3] Initial exposure to the virus results in a primary infection leading to a range of damaging symptoms including surface ulceration, nerve damage, damage to deep stromal structures, corneal perforation, and both necrotizing and non-necrotizing stromal disease.[4] With anti-viral treatment, the symptoms generally subside but the virus remains latent in the ocular nerve[1] and likely within the cornea.[5] As such, the virus can be reactivated by a variety of triggers such as stress, immunosuppression, sunlight, and ingestion of certain foods.[4, 6]

If the symptoms of a corneal HSV-1 infection are left untreated the result is often severe corneal damage and scarring leading to corneal blindness. Much like a window that is scratched too many times, the cornea becomes opaque. At this stage the treatment of choice is corneal transplantation.[6] Unfortunately, the success rate for HSV related transplants is much lower than for non-HSV grafts (22 %[3] compared to 73 %[6] at 5 years after the operation). It would appear that surgery reactivates the virus leading to a rejection of the transplant.

5.1.2 Acyclovir

Acyclovir (ACV) (**1**), a guanine derivative containing an acyclic side chain, is an antiviral that is widely employed as a therapy for HSV-1.[7] This antiviral, which was

first reported by Elion and Schaeffer et al.[8, 9] can be considered as a guanosine or deoxyguonosine analogue in which the 2 and 3 carbon atoms of the sugar moiety are missing. Acyclovir's mechanism of action, which results in viral DNA polymerase inhibition by acyclovir triphosphate, is highly specific to HSV-1 because the first event is phosphorylation by HSV-1-specified thymidine kinase (Scheme 5-1). Elion *et al.* have demonstrated that while phosphorylation activity by this kinase is very high, phosphorylation levels by other kinases are extremely low.[8] In addition, inhibition of HSV-1 DNA polymerase by acyclovir triphosphate is 30 to 50 times stronger than inhibition of human cellular alpha-DNA polymerase.[10] Thus, acyclovir activity in healthy cells and even in the presence of other DNA viruses is very low (except varicella-zoster virus and cytomegalovirus, which each have similar specificity with acyclovir)[10] .

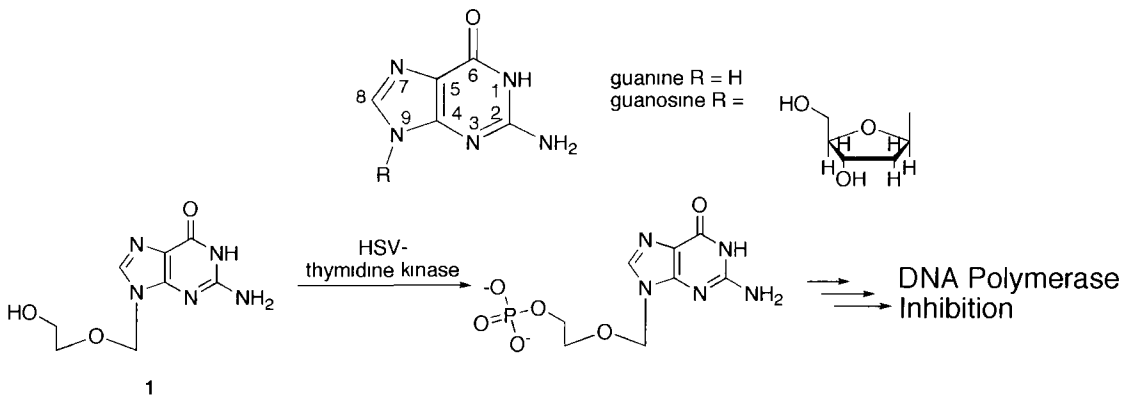

Scheme 5-1. Acyclovir's mechanism of action is activated by HSV-specified thymidine kinase. The first event is phosphorylation of the guanosine analogue (**1**). Cellular enzymes then add a second and a third phosphate group to form acyclovir triphosphate which competes with 2'-deoxyguanosine triphosphate as a substrate for DNA polymerase. In this way DNA polymerization is inhibited.[10]

While acyclovir is effective against HSV-1 there are a number of problems

associated with its delivery. With orally delivered ACV, only a small fraction of the drug reaches the target site and long term use can lead to gastrointestinal upset and suppression of the immune system,[11, 12] not to mention the expense of administering large doses so that a sufficient amount reaches the target. Delivery *via* eye drops is also inefficient mostly due to the poor solubility and lack of penetration by acyclovir.[11, 13] In addition, a great deal of the drug is lost to blinking and tears.[11]

5.1.3 Our approach

In order to improve the success rate of corneal transplants for HSV patients, it is necessary to develop a mechanism to suppress the virus immediately after transplant surgery. Given the problems associated with acyclovir delivery, this would be best accomplished by embedding the antiviral directly in the corneal transplant in a manner that would allow for its controlled release. The ideal release profile would combine a 'burst' release (i.e. a large dose of antiviral at a controlled time) to initially suppress the virus from reactivation followed by a slow release to keep the virus at bay (Figure 5-1).

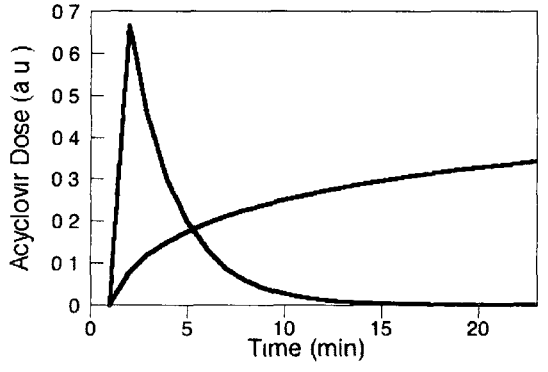

Figure 5-1. Illustration of two components of a theoretical ideal release profile. The red trace represents an initial 'burst' dose while the blue trace represents a slow, release.

For the envisioned therapeutic applications we would like to use a photolabile protecting group (PPG) to provide the controlled burst. The xanthone propionic acid (XPA) PPG is particularly well suited to this application because of the extremely clean photochemistry, lack of free radical intermediates and the ability to release using wavelenths of light above 350 nm. This design will require either covalent attachment of XPA-ACV to an appropriate frame (such as natural or artificial tissue) or incorporation as part of a composite (*e.g.* based on nanoparticles) that can be fully integrated into these materials. Our approach represents a two part goal: i) to attach acyclovir to our PPG in a way that allows the photorelease of acyclovir and ii) the incorporation of a 'handle' on the PPG, which could be used to attach it to the selected material. This is illustrated in the target molecule shown in Figure 5-2.

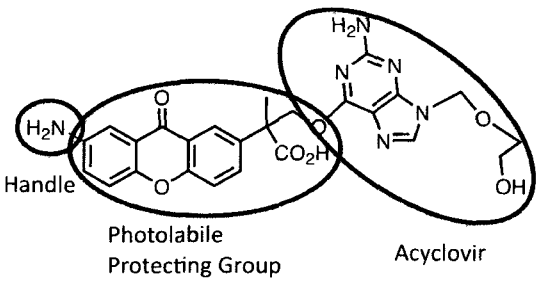

Figure 5-2. Illustration of the target molecule for PPG-based drug delivery.

The work described in this chapter was part of a large collaborative project with Prof. May Griffith from the University of Ottawa Eye Institute and Prof. James Harden from the University of Ottawa Department of Physics. All of the studies performed in cell models and the experiments with silica nanoparticles were done with Bettina Bareiss, a M.Sc. student from May Griffith's group. I would also like to

acknowledge the work of Liliana Jimenez, a post-doctoral associate from our own group. While the successful synthesis of XPA-Acyclovir was my own work, her initial attempts were helpful in ruling out other synthetic possibilities.

5.2 Synthesis of XPA-Acyclovir

As a first step towards the goal of acyclovir delivery in artificial corneas we hoped to demonstrate clean photorelease of acyclovir from our XPA PPG. This of course required a synthetic route to XPA-ACV.

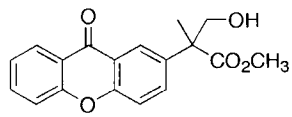

2

Chart 5-1.

5.2.1 Initial synthetic design and results

Given our success in synthetically attaching aniline and photoreleasing *via* a carbamate linkage (Chapter 3), we initially attempted a similar synthesis to attach acyclovir through the guanosine amine group (*N2* position). Once again our photolabile protecting group is the alcohol **2** (Chart 5-1). Attempts with both acyclovir and guanosine, using the same method for carbamate formation described in Chapter 3 (Scheme 5-2, top), were both unsuccessful in that only the starting materials were recovered. When we reversed the order of addition, combining **2** with triphosgene first, then adding acyclovir, we were able to form and isolate the chloroformate intermediate, but no reaction was observed with acyclovir even after 2 days at room temperature. Instead, the chloroformate decomposed in this time period (Scheme 5-2, bottom).

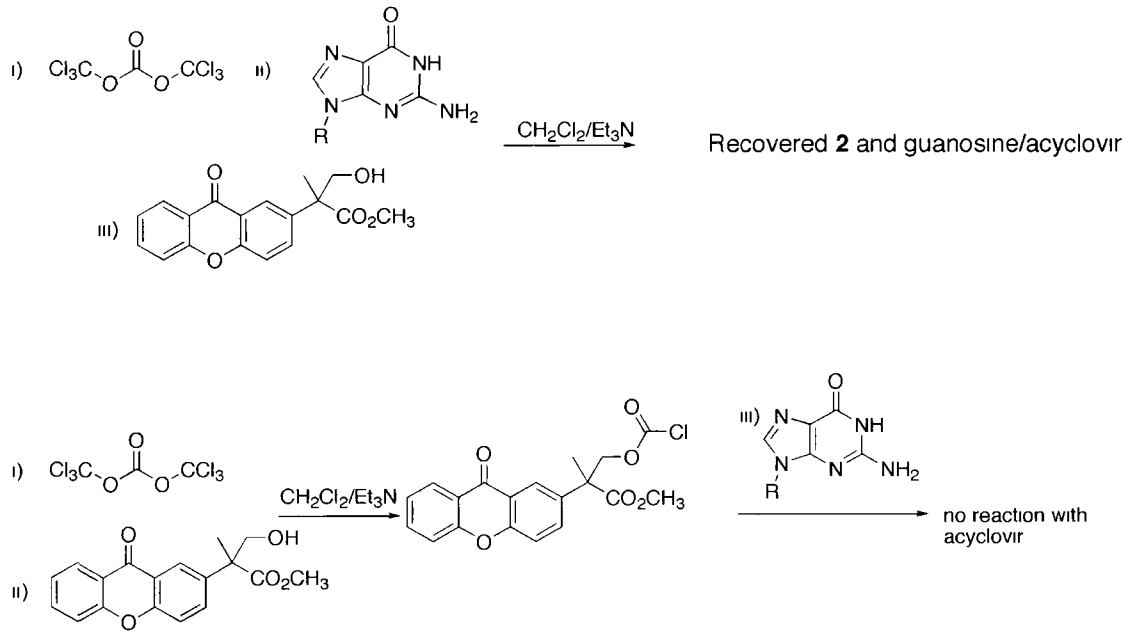

Scheme 5-2. Top: attempted synthesis of XPA-ACV following the procedure described in Chapter 3 for carbamate formation. Guanosine, R = H; Acyclovir, R = $CH_2OCH_2CH_2OH$. Bottom: Synthesis of the chloroformate of **2** followed by attempted attachment of acyclovir. R = $CH_2OCH_2CH_2OH$.

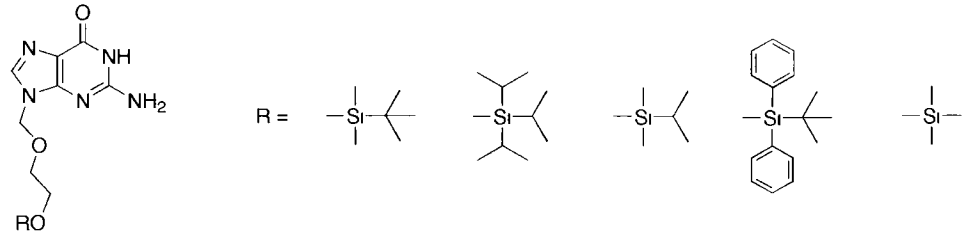

Chart 5-2.

We first thought the problem lay with acyclovir's (and guanosine's) poor solubility in dichloromethane. Acyclovir is only soluble in very polar solvents (DMSO, DMF, H_2O). However we found that the chloroformate intermediate used to form the carbamate is not stable in these solvents. For this reason we tried a number of protecting groups for the acyclovir alcohol in an attempt to improve solubility (Chart 5-2) but still were not able to dissolve these derivatives in

dichloromethane. Our lack of success sent us back to the literature. A search for alternate carbamate syntheses with guanine derivatives led us to a report of Fmoc protection of guanosine in anhydrous pyridine using 9-fluorenylmethyl chloroformate by Hagen et al.[14] We attempted the same conditions with both acyclovir and acyclovir-TBDMS; unfortunately we were still unsuccessful. Eventually we concluded that the acyclovir amine group is not reactive enough to react with the chloroformate of **2** before this intermediate decomposes. This is supported by the scarcity of reactions at the amine site of acyclovir present in the literature, aside from amide formation.

We also attempted to attach acyclovir to our photolabile protecting group *via* the alcohol of acyclovir. In theory we could do this directly, however we predicted (based on our results with methoxide presented in Chapter 3) direct release of the primary alcohol would not completely compete with protonation of the carbanion intermediate so irradiation would lead to a combination of elimination and protonation photoproducts. Instead, we tried to attach through a carbonate linkage. This strategy is very similar to the use of carbamates for releasing amines. Unfortunately, we ran into the same problems with acyclovir solubility and considered derivatizing the *O6* position to improve organic solubility. One attempt (Scheme 5-3) using nitrophenylcloroformate in acetonitrile (a solvent the acyclovir is moderately soluble in) showed initial promise, but was both low yielding (20% by ^{1}H NMR) and not reproducible. We eventually abandoned this route when a colleague's results suggested the carbonate would not be sufficiently stable to the

hydrolysis conditions required to deprotect the methyl ester.[15]

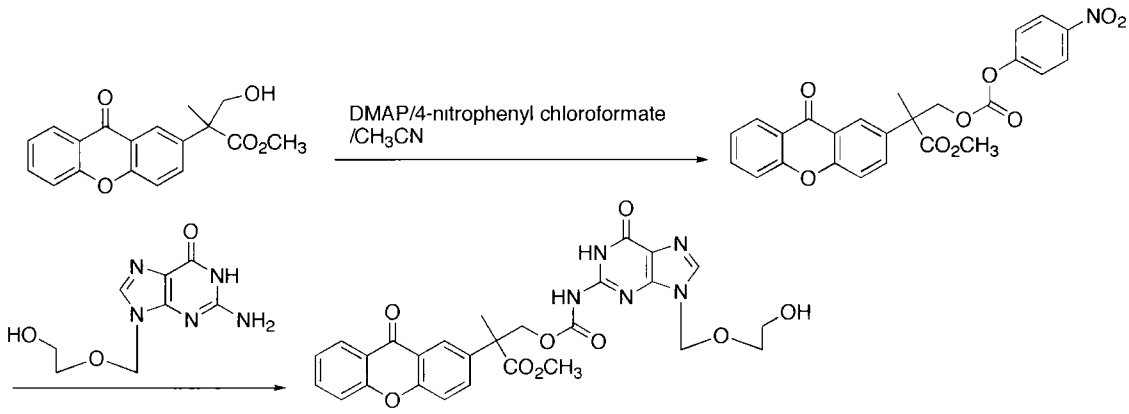

Scheme 5-3. Attempted XPA-ACV carbonate synthesis.

5.2.2 Successful synthesis

The consideration to protect the *O6* position for solubility reasons led us to the realization that we could photorelease *via* this amide group (Scheme 5-6). Pletsas *et al.* have reported functionalization of the O6 position of acyclovir with alcohols[16] using a synthesis adapted from Harrison *et al.*[17] We were able to successfully adapt this synthesis using **2** as the alcohol. The first step was a simple protection of acyclovir using TBDMS-Cl, a common protecting group for alcohols. This was followed by incorporation of the 6-mesitylene sulfonyl leaving group at the *O6* position of the purine ring (Scheme 5-4) by reaction of the purine enolate form with the electron poor sulfur centre. Although a relatively simple reaction, this step was initially a struggle because of an error in the Pletsas paper. The authors reported that 0.47 equivalents of triethylamine were used for the synthesis but inspection of the earlier synthesis revealed that 4.7 equivalents were required.[17] Once this issue was resolved, **4** was achieved in moderate yield (56% purified yield). This

intermediate allowed the introduction of nucleophilic groups to the *O6* position. Prior to introduction of **2**, the mesitylene group was replaced with DABCO generating a quaternary DABCO salt and a more reactive site for nucleophilic substitution. Replacement of the mesitylene sulfonyl group with DABCO also avoided reaction of the nucleophile with the sulfur centre in the next step. Pletsas *et al.* were able to introduce a variety of groups to the *O6* position in relatively high yields by using a 10-fold excess of sterically unhindered nucleophiles. Our disadvantage at this stage was two-fold, first because our nucleophile (**2**) is more sterically hindered and second because we were unable to synthesize enough of **2** to add such a large excess. Nonetheless, we obtained **5** in 26% isolated yield and removal of the TBDMS and ester protecting groups left us with a sufficient amount of photolabile protected acyclovir purified by preparative high performance liquid chromatography (HPLC) and obtained in ~4 % overall yield from **1**.

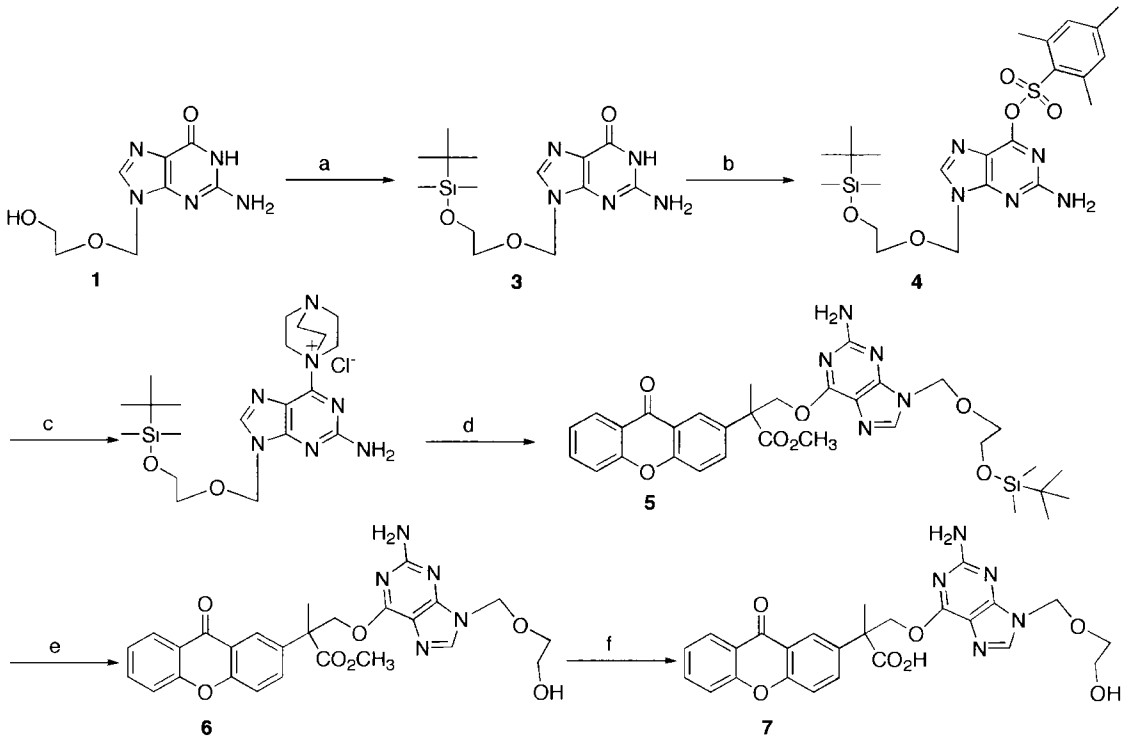

Scheme 5-4. Successful synthesis of XPA-ACV (**7**). (a) TBDMS-Cl/Imidazole/DMAP/DMF (quantitative); (b) 2-mesitylensulfonyl chloride/DMAP/Et_3N/CH_3CN (56%); (c) DABCO/THF; (d) **2**/DBU/THF (26%); (e) TBAF/THF (73%); (f) 0.1 M NaOH/CH_3CN (40%)

5.2.3 Characterization

^{1}H NMR was extremely useful both for following our attempted syntheses (by monitoring the frequency of the CH_2 adjacent to the alcohol for alcohol functionalization and the amine frequency for amine functionalization) and in confirming the products of Scheme 5-4. Addition of a silyl group to the alcohol position of acyclovir was accompanied by the appearance of two new peaks in the ^{1}H NMR (relative to the ^{1}H NMR for acyclovir) corresponding to the *tert*-butyl and methyl groups of TBDMS. This addition had a very small effect (< 0.1 ppm) on the

acyclovir ^{1}H NMR frequencies except for the CH_2 adjacent to the silyl group which shifted downfield by 0.16 ppm. The NMR solvent had a large effect on the amine ^{1}H frequency. Changing from DMSO-d6 to $CDCl_3$ shifted it upfield by 1.54 ppm. This is consistent with a consideration of contributing resonance structures (Scheme 5-5) since DMSO, more so than chloroform, would stabilize resonance structures II and III.

Both functionalization of the purine ring to make **4** and substitution by **2** to form **5** had very little effect on the acyclovir proton frequencies. However, all of the new frequencies expected from addition of the mesitylene group followed by the xanthone group were observed including the very characteristic doublet of doublets assigned to the methylene group connecting our PPG to acyclovir which is split as a result of the adjacent chiral centre (Figure 5-3).

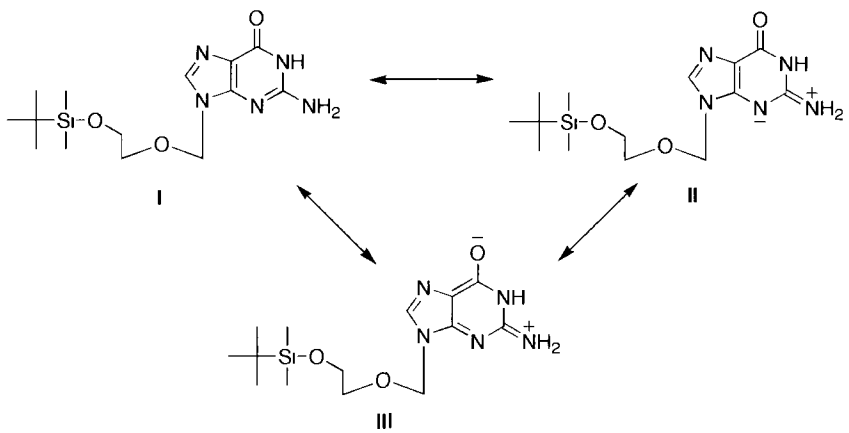

Scheme 5-5. Resonance structures of product **3**.

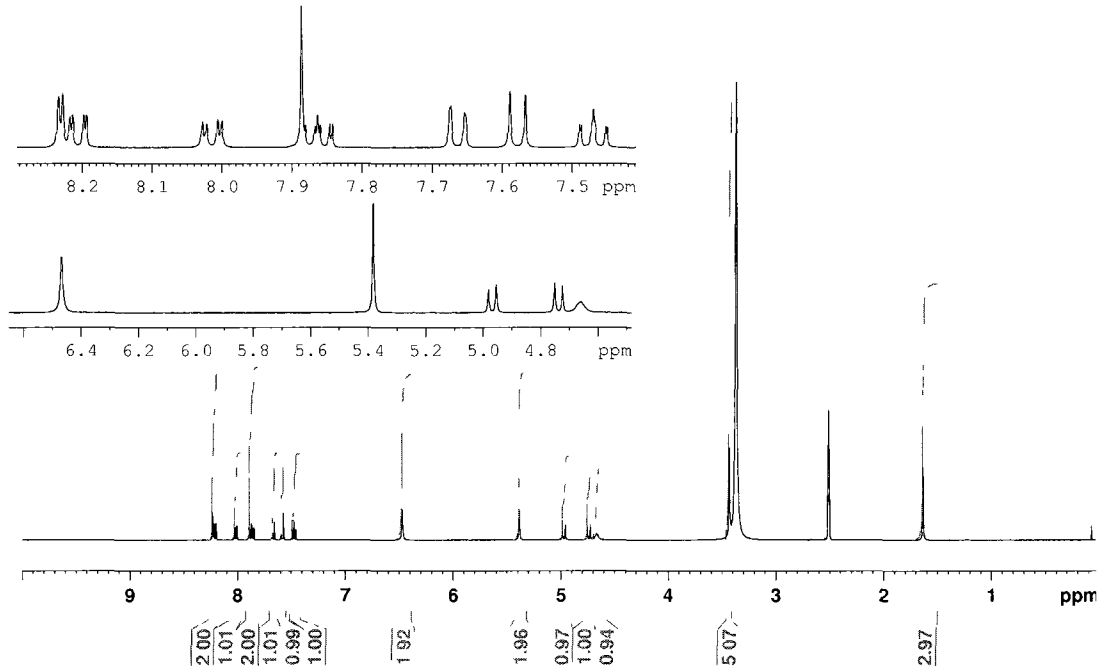

Figure 5-3. ^{1}H NMR of XPA-ACV (**7**) in DMSO-d6.

5.3 Solution phase release of acyclovir from XPA-ACV

The UV-vis absorbance spectrum of **7** in Figure 5-4 demonstrates that the absorption characteristics of the parent molecule, 2-xanthone acetic acid, have been retained and the absorption coefficient is still quite high (4500 $M^{-1}cm^{-1}$) at 350 nm. With irradiation in pH 7.4 phosphate buffer (Figure 5-5 A), the absorption spectrum shows a clean conversion that is complete within 270 s. The spectral changes, particularly the red shift in the peak near 250 nm are consistent with release of free acyclovir from **7** (Scheme 5-6) since the new maximum near 250 nm corresponds exactly with the absorption spectrum of acyclovir at this pH (Figure 5-5 D)

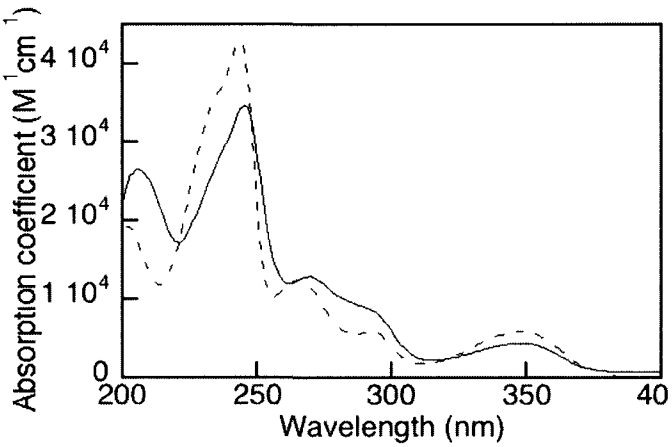

Figure 5-4 Absorbance spectra of 2-xanthone acetic acid (---) and XPA-ACV (**7**) (—) in pH 7 4 phosphate buffer

UVA irradiation in buffer with increasing amounts of acetonitrile reveals a slight solvent effect on the efficiency of conversion. With 20% CH_3CN conversion was complete within 150 s while in 50% CH_3CN, 50% buffer solution conversion was complete within 90 s Given that no such effect was observed for the parent molecule (2-xanthone acetic acid), the solvent effect may be related to the ability of

the free amine (from the acyclovir moiety) to quench the excited states.

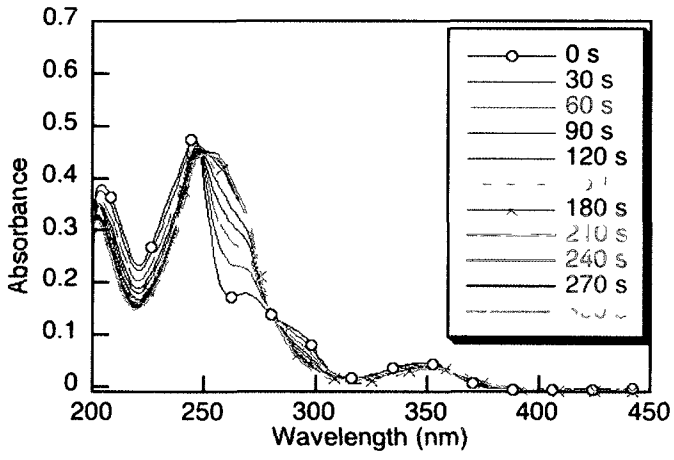

A

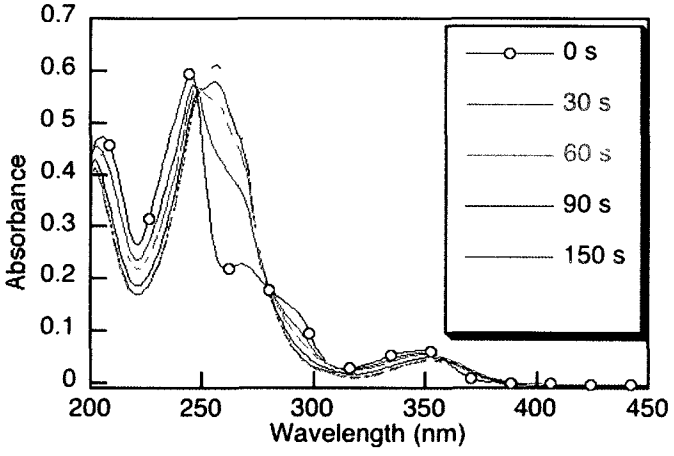

B

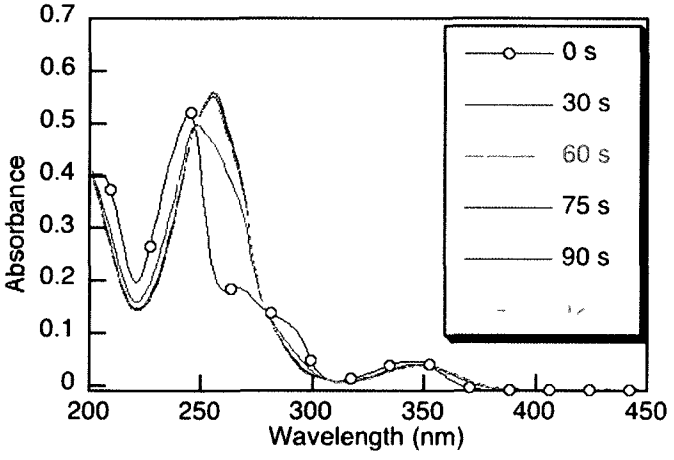

C

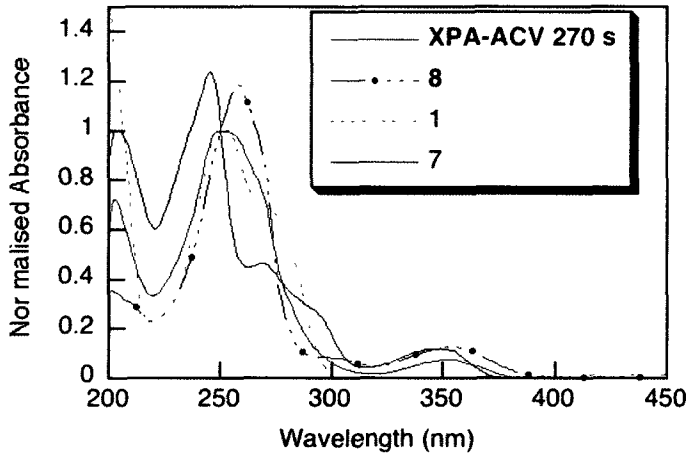

D

Figure 5-5. Absorbance of XPA-ACV with irradiation. **A**: in pH 7.4 phosphate buffer. **B**: in 80 % buffer, 20% acetonitrile. **C**: in 50 % buffer, 50% acetonitrile. Each solution was photolysed to completion as indicated by no further change in the absorbance. This point was verified by continued photolysis for at least 5 min. with no observed change. Only the two earliest traces with identical spectra are shown for each solution. **D**: an overlay of normalized spectra in pH 7.4 phosphate buffer showing that the spectral shift of XPA-ACV with irradiation corresponds to the release of free acyclovir (**1**).

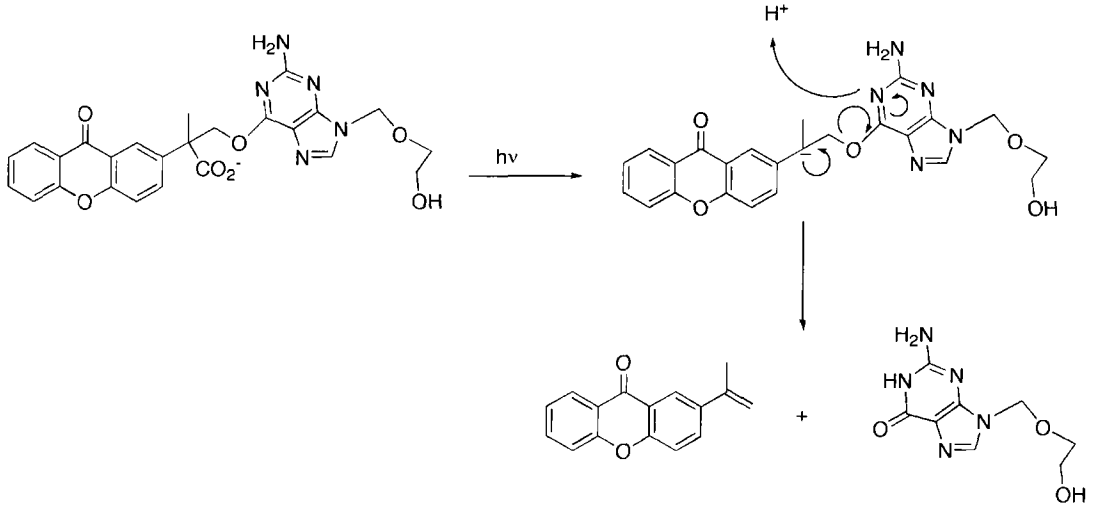

Scheme 5-6. Proposed mechanism of amide release from XPA-ACV.

We were also able to follow the photolysis and confirm that acyclovir is being released using reverse phase HPLC (Figure 5-6). The peak at 12 min. was confirmed to be acyclovir (**1**) by comparison of the absorbance spectrum and retention time to

a standard solution. This peak is split at low concentrations of **1** due to the different pK_as of acyclovir, but the calibration curve (peak area *vs.* concentration) is still linear in this region. Using HPLC we measured the quantum yield for release in pH 7.4 phosphate buffer to be 0.08 based on the appearance of acyclovir and 0.11 based on the disappearance of XPA-ACV. This is much lower than expected but can be rationalized if we consider the free amine on acyclovir; amines are well known to quench excited states.[18] We also confirmed the Φ solvent effect by measuring the quantum yield of release in 1:1 PB:CH_3CN to be 0.28.

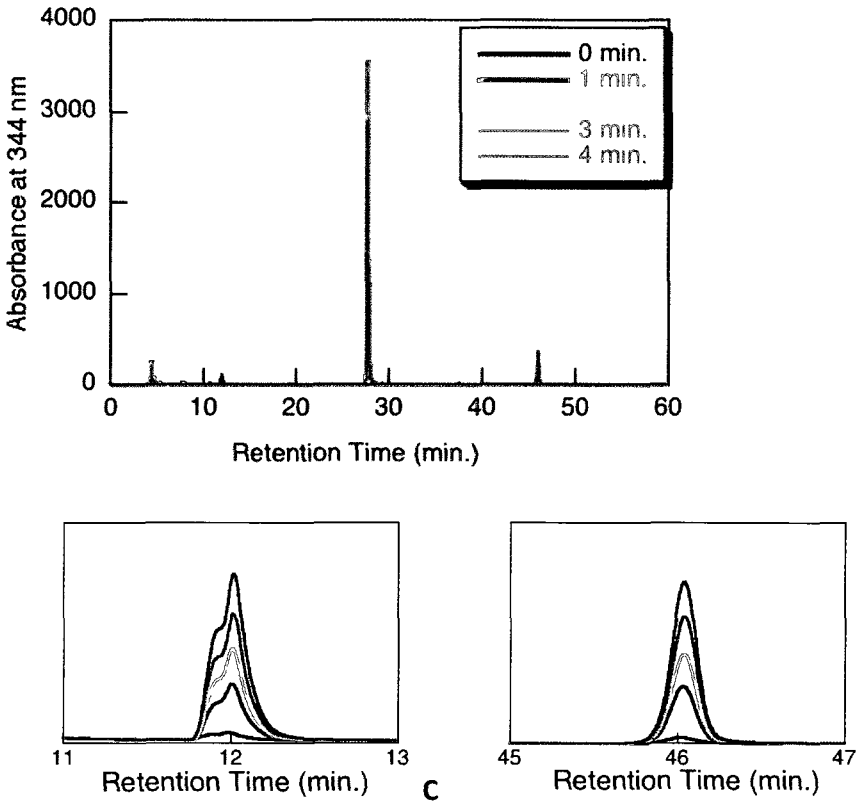

Figure 5-6. A: HPLC trace with irradiation showing XPA-ACV (**7**) (retention time (RT) = 28 min.), acyclovir (**1**) (RT = 12 min.) and photoproduct **8** (RT = 46 min.). **B**: Expanded view of the peak at 12 min. showing the increase with irradiation time. Peak splitting is due to the multiple possible protonation states for **1**. **C**: Expanded view of the peak at 46 min. showing the increase with irradiation time.

Although we have lost a great deal of efficiency, the release of acyclovir is still very clean. In addition, given the observed solvent dependence of the efficiency, it is difficult to predict what the quantum yield in our artificial cornea will be; it may very well be higher in the hydrogel environment. The main concern with low efficiency is that the dose of light required to release a sufficient amount of antiviral will be too high. The only way to really determine if this is true is to test the release in a model for the transplanted artificial cornea.

5.4 Release of acyclovir in corneal cells from XPA-ACV

As an initial model for the human cornea we used a line of human corneal epithelial cells (HCEC) to test acyclovir release from **7**. Our aim was to determine the toxicity of **7** as well as the ability of **7** to release acyclovir in a cellular environment and the subsequent viral (HSV-1) suppression.

5.4.1 Relevant information for the non-biologist reader

To evaluate toxicity under different conditions, we used one of two standard detection methods, either live-dead staining or an MTT assay. Live-dead staining, as the name implies, involves simultaneous staining of the live cells and the dead cells. Once stained, each population is counted to determine the percent of dead cells. Typically, 5% cell death is acceptable. An MTT assay is a colorimetric assay that uses the reduction of 3-(4,5-dimethylthiazol-2-yl)-2,5-diphenyltetrazolium (MTT) to detect enzyme activity. The enzymes in live cells will reduce MTT, which is yellow, to formazan, which is purple. As such, the absorbance at 570 nm is a measure of the number of living cells. For the latter technique, controls of live and dead cells are always used as a reference for the signal at 570 nm.

We also evaluated the ability of **7** to suppress viral proliferation when HSV-1 was added to HCEC using two techniques: real-time polymerase chain reaction (RT-PCR) and plaque assays. PCR is commonly used to amplify small amounts of DNA copies. By thermally cycling a sample in the presence of nucleotides, a DNA polymerase and DNA primers, each DNA sequence in the sample is replicated and amplified by orders of magnitude to a detectable level. RT-PCR uses fluorescently

labelled oligonucleotides so that the amplification can be monitored in 'real time'.

One standard unit used for the quantity of virus is the plaque forming unit (pfu) because a plaque is formed once a virus particle infects a host cell. Plaque assays are based on this process. If the virus particle is present it infects only the cells immediately surrounding it (the high viscosity of the medium prevents viral spreading). When the cell culture is stained with crystal violet, all of the living cells in the plate appear violet. In the regions of dead cells (i.e. surrounding the virus particle) nothing is stained, and these regions appear as white circles. (see picture below). The white circles are referred to as plaques and one plaque stands for one virus particle. To quantify the amount of virus present in the original sample, the plaques formed in a diluted sample (typically 1:10, 1:100, and 1:1000 to avoid overlap of plaques) are simply counted.

Figure 5-7. Image of a typical well containing HCEC stained with crystal violet. The white circles are viral plaques, each corresponding to one viral particle.

5.4.2 Preliminary Results

The results described in this section are preliminary only. These experiments were undertaken in order to determine which conditions to test more thoroughly.

Because of the high cost associated with both the cell line used and our compound **7**, many of the results were only tested once (i.e. n = 1). However, in Section 5.4.3 I will describe experiments repeated in triplicate (i.e. n = 3) with our chosen conditions.

Before attempting any release, we first needed to determine the dose limits within which the cells are viable, both for concentration of **7** and the dose of light. Cells were irradiated by placing a well plate containing the cell culture under a Luzchem exposure panel with 5 UVA bulbs (Irradiance = 65 W/m^2) for varied lengths of time. Figure 5-8 shows the toxicity results for this irradiation. Based on an MTT assay, cell death due to irradiation up to 5 minutes was negligible. In fact, the irradiated cells survived more than the living control; however without a measure of error we can only determine that 5 minutes of irradiation under our condition is not harmful to the cells. The same was true for concentrations of **7** up to 750 μg/mL based on live-dead staining (for the concentrations tested, the percentage of dead cells is generally under 5 %).

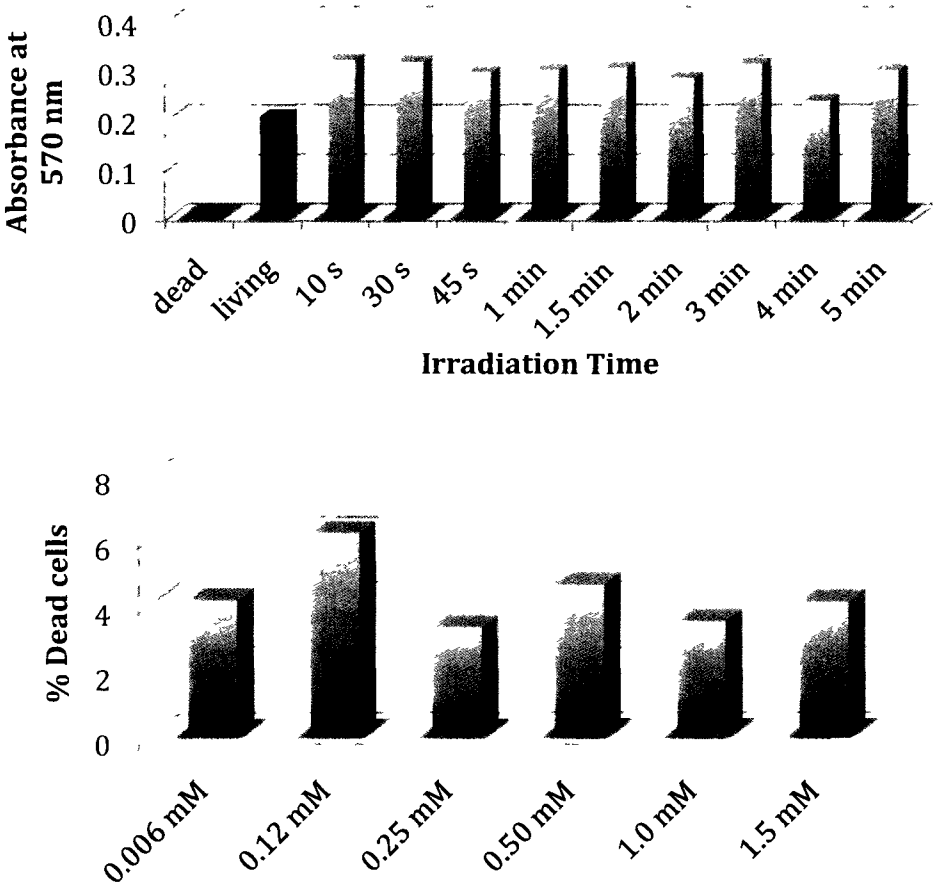

Figure 5-8. Top: MTT assay for HCEC with irradiation up to 5 min. The y-axis is proportional to the number of living cells. None of the samples (blue) showed significant difference from the control of non-irradiated living cells (green). Bottom: Live-dead staining results for HCEC with varied doses of XPA-ACV (unirradiated). For each sample, 1 mL of a prepared solution of the specified concentration was added to the cells.

We then chose to test the effect of irradiating healthy corneal cells for 5 minutes with varying concentrations of **7** which had either been incubated with the cells for 24 hours prior to irradiation or added directly before irradiation. As can be seen in Figure 5-9, cell death was below 5 % for all samples except when the highest

concentration of **7** was incubated before irradiation. For concentrations below 2.0 mM there seems to be no significant difference between the samples which were incubated and those that were not. This indicates either that **7** is not toxic at these concentrations or that it does not penetrate the cell membrane.

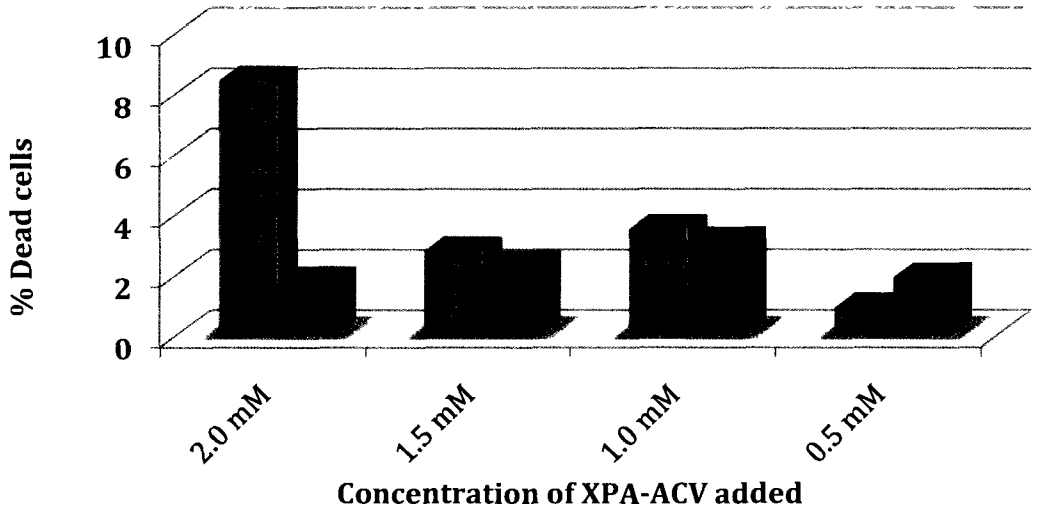

Figure 5-9. Toxicity of XPA-ACV (based on live-dead staining) with irradiation when incubated with cells for 24 hr. before irradiation (orange) and when added directly before irradiation (red). For each sample, 1 mL of a prepared solution of the specified concentration was added to the cells.

We also wished to determine if acyclovir was in fact being released during the irradiation and if the cells or the cell medium affected the efficiency of release. To this end, we irradiated **7** in phosphate buffer saline (PBS) and in cell medium simultaneously in a well plate with the irradiation of cells described above (samples corresponding to the results in Figure 5-9). We then removed the supernatants from each well post irradiation (including the wells with HCEC), treated them to remove large biological molecules (e.g. proteins) and analysed the solutions by HPLC. From the results shown in Figure 5-10 we can conclude that i) the cell

medium does not significantly affect the efficiency of ACV release (as compared to the release in PBS), ii) a similar amount of ACV is released within 5 min. of irradiation for the concentration range 1.0 – 2.0 mM, and iii) the majority of ACV released in the presence of cells remains in the supernatent (based on a comparison of the amount of ACV released in the presence of cells (orange and red bars) to the amount released in PBS and cell medium. This latter result implies that either most of **7** never penetrates the cells (even when incubated for 24 hr., orange bars) or once released, ACV exits the cells. It is also possible that the release efficiency is higher outside of the cells, but given the high level of released ACV when cells are present, this option would still indicate that the majority of **7** is outside of the cells.

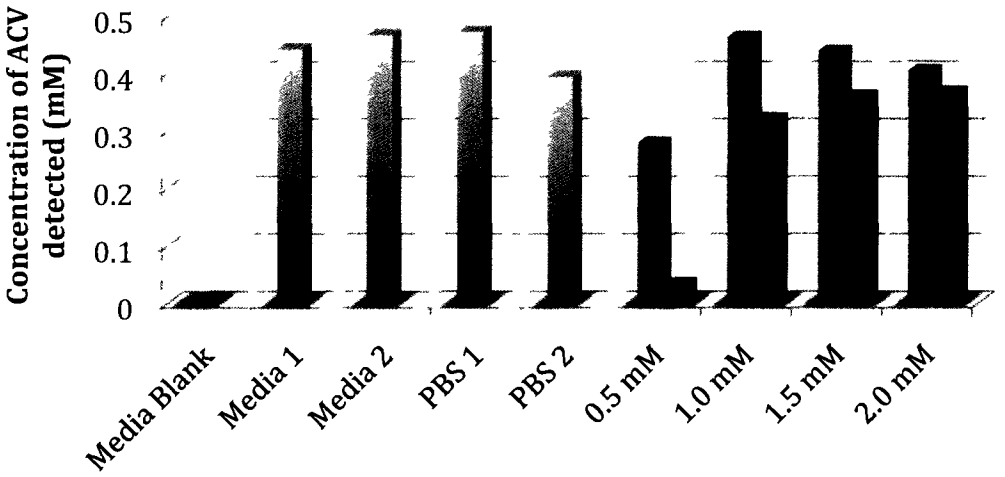

Figure 5-10. Amount of ACV detected in the supernatent for irradiation of 1 mg/mL XPA-ACV in cell medium and PBS (blue), and for irradiation of 0.5, 1.0, 1.5, 2.0 mM of XPA-ACV in the presence of cells with XPA-ACV incubated for 24 hr prior to irradiation (orange) and with XPA-ACV added just prior to irradiation (red). The absolute values detected may not reflect those present in solution due to the necessary treatment before analysis, rather they are relative values.

Given that cell death was minimal for 5 minutes of irradiation, we tested the same conditions for cells infected with HSV-1 (both for 10^4 pfu and 10^5 pfu of virus) using two concentrations of **7** that were each non-toxic (1.5 mM and 0.5 mM). Interestingly, without any irradiation **7** had some protecting effect against the virus (i.e. more infected cells lived in the presence of unirradiated **7** as compared to infected cells with no **7** added, although this difference may simply be within error). Conversely, infected cells irradiated with **7** were less viable than those irradiated in the absence of **7** (Figure 5-11).

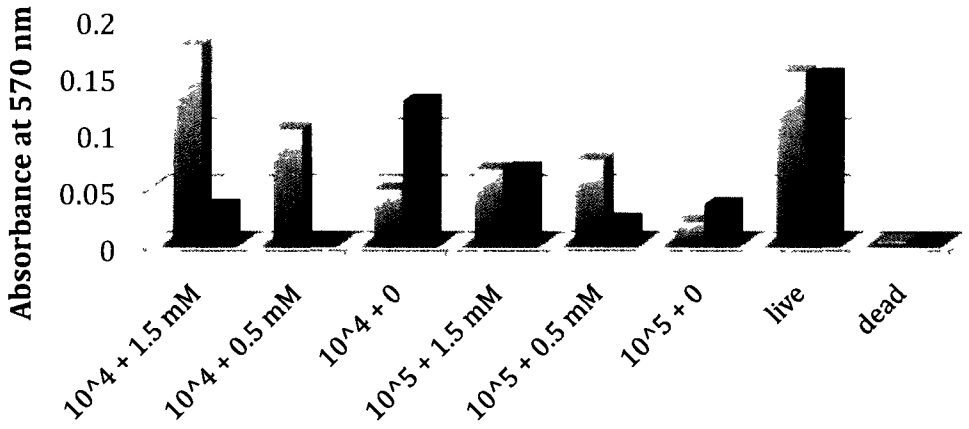

Figure 5-11. MTT assay for unirradiated (blue) and irradiated (red) HCEC with HSV-1 (0, 10^4, or 10^5 pfu) and XPA-ACV (0, 0.5, or 1.5 μM).

We were also able to evaluate the antiviral activity of **7** (irradiated and unirradiated) using both RT-PCR and a plaque assay to quantify the amount of HSV-1. These results are shown in in Figure 5-12.

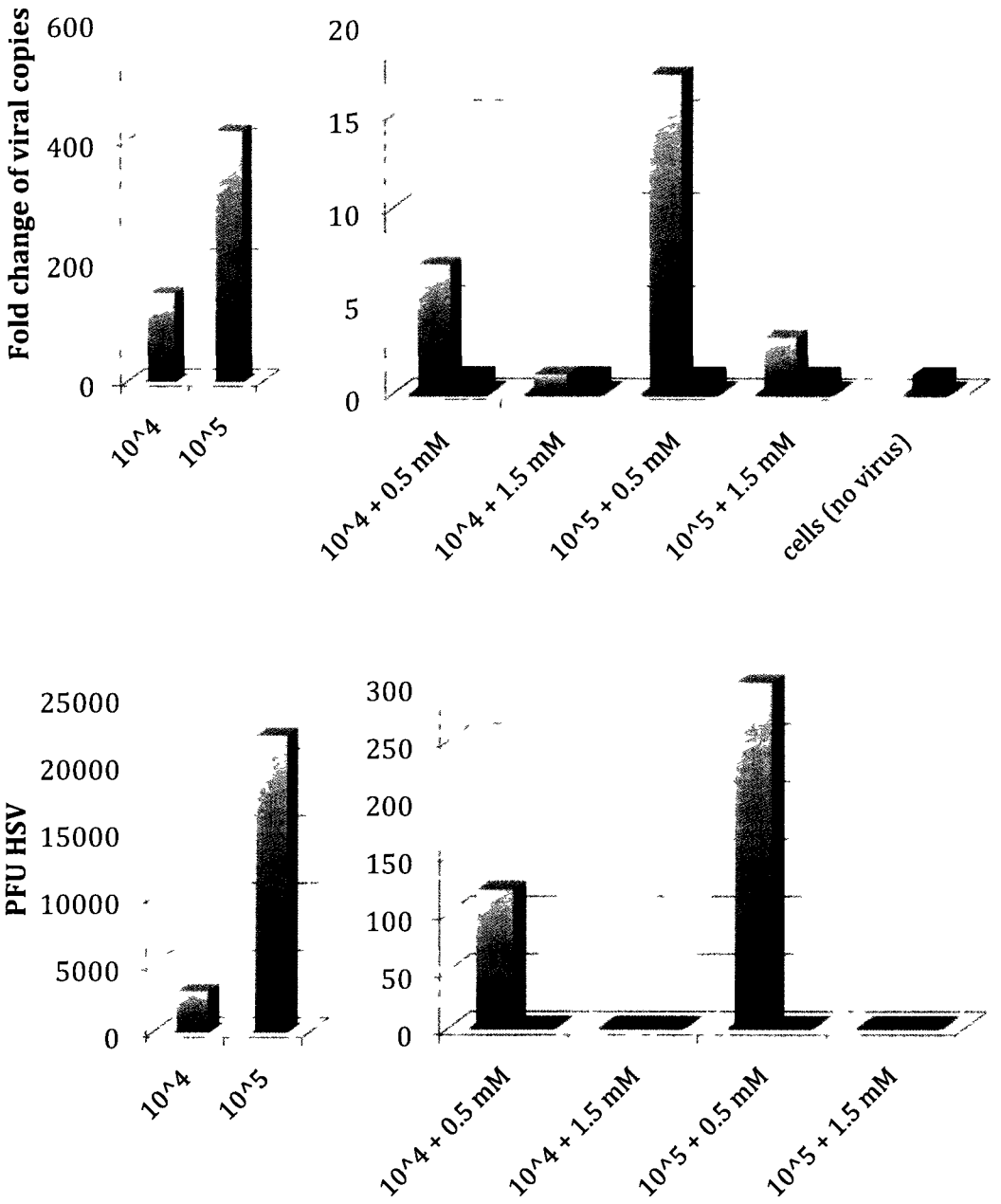

Figure 5-12. Top: RT-PCR results for unirradiated (blue) and irradiated (red) HCEC with HSV-1 (0, 10^4, or 10^5 pfu) and XPA-ACV (0, 0.5, or 1.5 mM). The y-axis is proportional to the amount of HSV-1 DNA and therefore a measure of viral proliferation. Bottom: Plaque assay for unirradiated (blue) and irradiated (red) HCEC with HSV-1 (10^4 or 10^5 pfu) and XPA-ACV (0, 0.5, or 1.5 mM). The y-axis is proportional to the number of viral particles present and therefore also a measure of viral proliferation.

From these preliminary results it seems that **7** has some antiviral activity on its own, however the antiviral activity is higher when **7** is irradiated, consistent with photorelease of acyclovir. Unfortunately the results of our toxicity studies were less positive. Overall it would appear that the toxicity of 1.5 mM of **7** with and without irradiation (for 5 min.) is minimal in healthy cells but significant in infected cells.

It has been shown that HSV-1 increases the permeation of acyclovir into cells.[8] This may also be true for XPA-ACV (**7**), in which case the toxicity we observed may be due to the irradiation of **7** inside the cells. Remember that the low toxicity observed for **7** irradiated with healthy cells (Figure 5-9) may be attributed to the possibility that **7** does not permeate the cells significantly. To evaluate this possibility we compared the effect of irradiating the cells in the presence of **7** before and after adding HSV-1 (Figure 5-13). We also took this opportunity to compare the effect of **7** with an equal concentration of acyclovir. We found, as expected, that any 'protective' ability that unirradiated **7** offers is not as high as from acyclovir itself (Figure 5-13 A). When the cells are first infected with HSV-1 (10^4 or 10^5 pfu) and then irradiated (as was done in the previous experiment) we see once again that fewer cells survive when **7** is present (green *vs.* blue bars in Figure 5-13 B). However, if we first irradiate the cells and then infect with HSV-1, **7** (or presumably, the acyclovir released from **7**) protects the cells to a similar magnitude as free acyclovir (Figure 5-13 C).

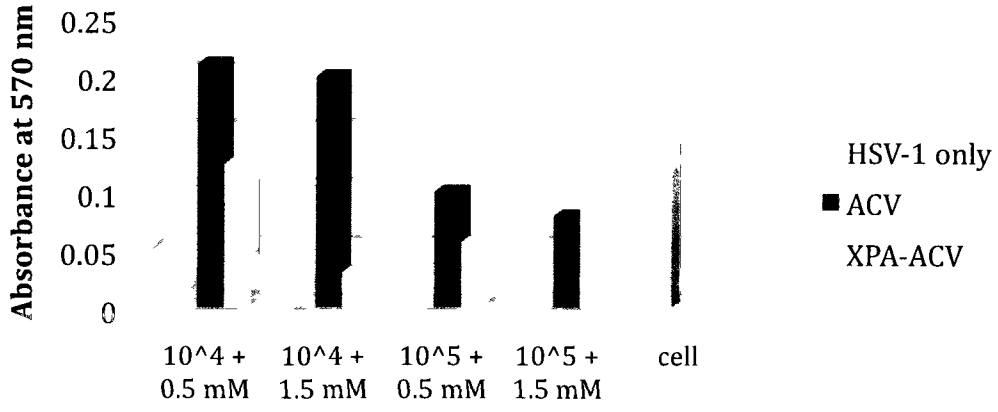

A

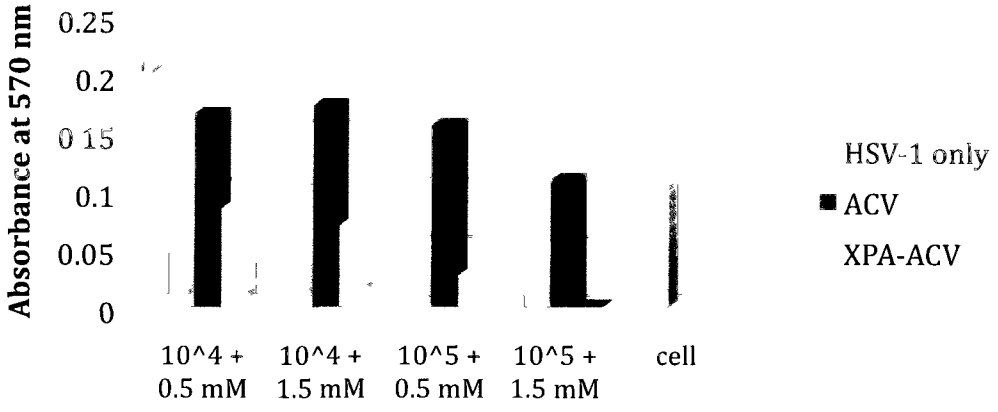

B

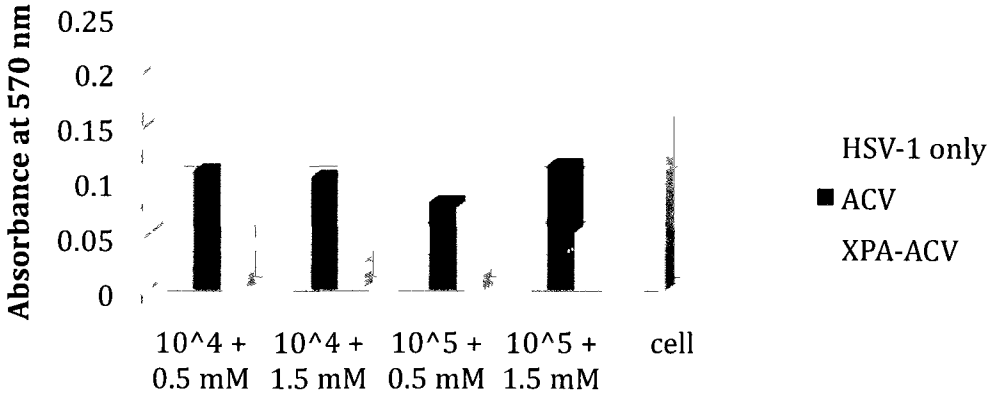

C

Figure 5-13. MTT results for HCEC with XPA-ACV (0.5 or 1.5 mM) infected with HSV-1 (10^4 or 10^5 pfu) **A**: Unirradiated. **B**: Infected then Irradiated. **C**: Irradiated then infected

The results from RT-PCR and a plaque assay (Figure 5-14) on these samples show that regardless of the order of irradiation and infection, irradiated **7** suppresses viral proliferation whereas unirradiated **7** does not.

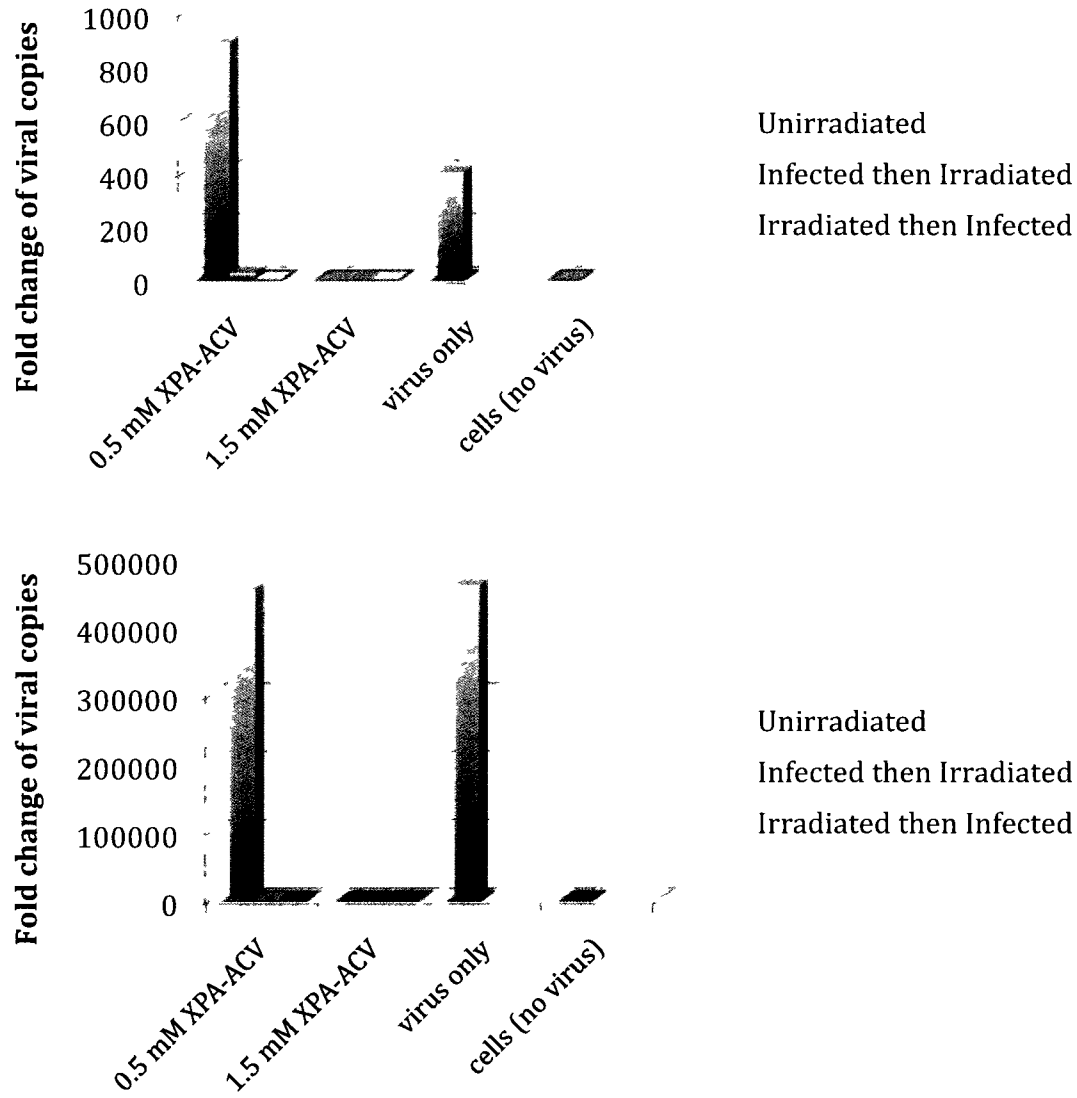

Figure 5-14. Viral proliferation for 10^4 pfu HSV-1 (top) and 10^5 pfu HSV-1 (bottom) with 0.5 mM, 1.5 mM and 0 mM of XPA-ACV as measured by RT-PCR.

To summarize, we have determined conditions that appear to be unharmful to

our cell model in the absence of HSV-1 (1.5 mM of XPA-ACV with 5 minutes of UVA irradiation) and we seen viral suppression by XPA-ACV in infected cells. Our initial studies suggest that XPA-ACV does not likely penetrate healthy cells to a significant extent based on i) similar levels of released acyclovir measured for incubated samples compared to non-incubated samples as well as samples with no cells, and ii) the increased toxicity resulting from XPA-ACV in infected cells compared to healthy cells. However, without a measure of error, we cannot really draw any conclusions from these results.

5.4.3 Confirmed Results

Based on our preliminary results, it would seem that irradiating up to 1.5 mM of XPA-ACV in the presence of cells for 5 min. is not harmful to the cells, however we observed formation of a significant number of crystals upon irradiation of this concentration (Figure 5-15), likely due to crystallization of the xanthone photoproduct, which is very poorly soluble in water. Although these crystals did not seem to harm the cells (likely because they are formed outside of the cells, *vide supra*), we were concerned they may interfere with our measurements. For this reason we proceeded with the lower concentration of 0.5 mM for which the crystals were not observed.

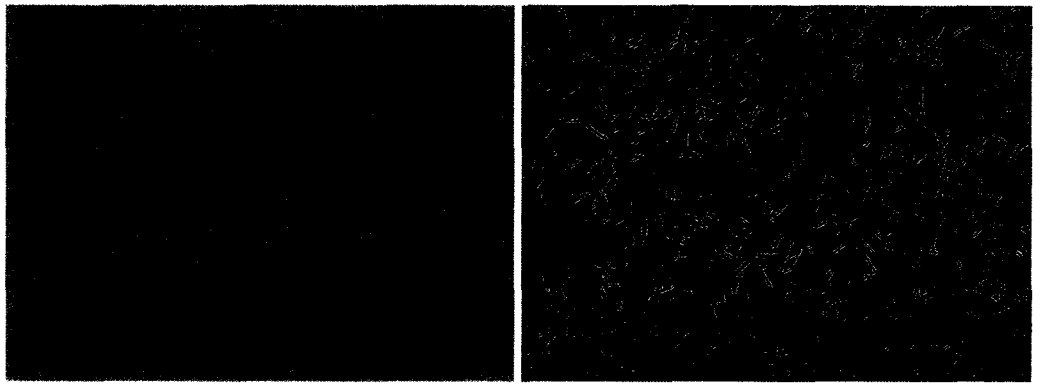

Figure 5-15. An optical microscope image of cells with 1.5 mM XPA-ACV before irradiation (left) and after irradiation (right).

Our results in triplicate confirmed the earlier result that 5 min. of irradiation, 0.5 mM of **7**, and the combination of both are all non-toxic to HCEC (Figure 5-16). With this in mind, we proceeded to test the same conditions with infected cells, once again testing if there is an effect of releasing acyclovir with light before infecting the cells as compared to irradiating after infecting the cells with HSV-1. We now see that while irradiated **7** does protect the infected cells more so than unirradiated **7**, any effect from the order of irradiation and infection is not significant with respect to toxicity (Figure 5-17).

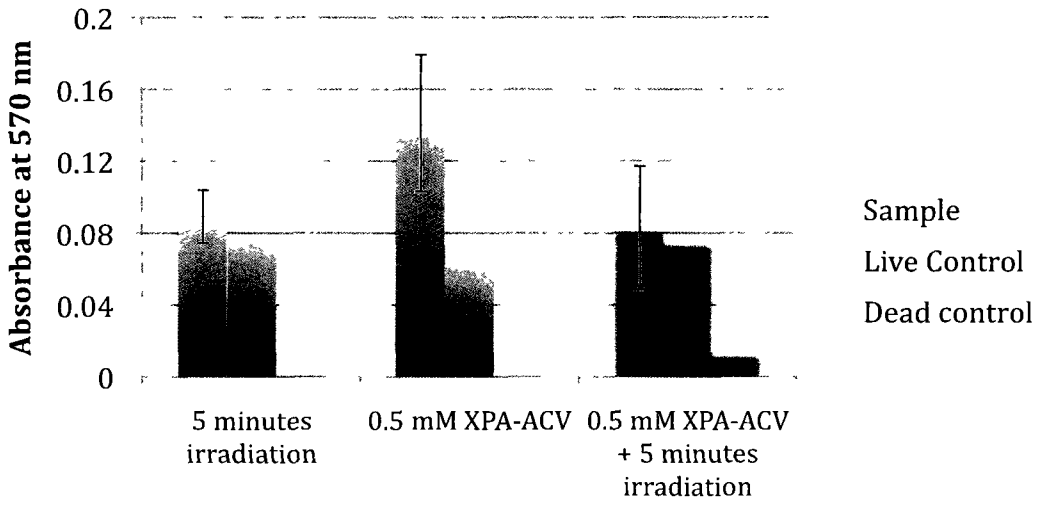

Figure 5-16. MTT Assay results for 5 min. irradiation, 0.5 mM XPA-ACV and the combination of both. Each result is shown with a live and a dead control for comparison. Error bars refer to a 95% confidence interval calculated from n = 3.

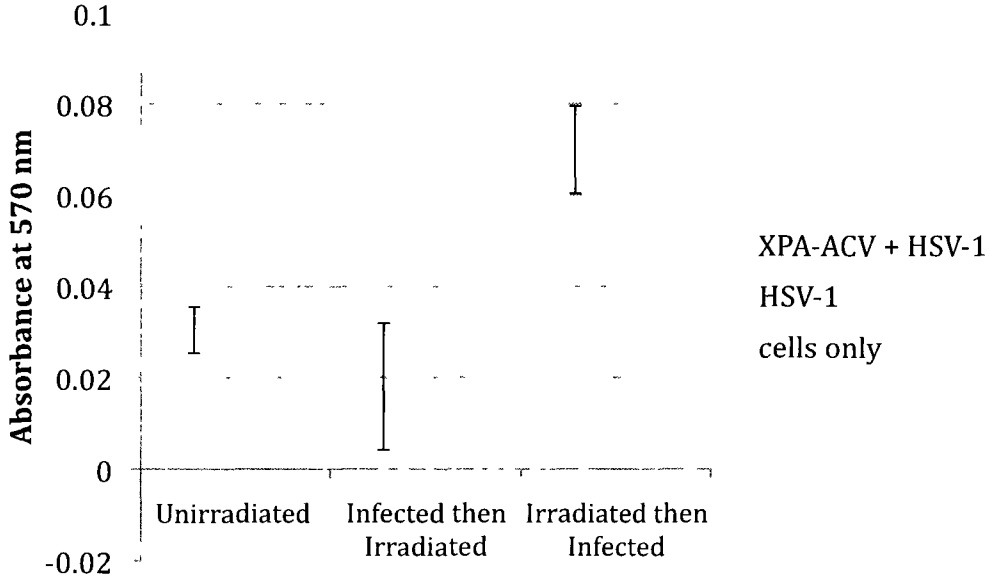

Figure 5-17. MTT Assay for 0.5 mM XPA-ACV with cells infected with HSV-1. Each result (blue) is shown with a control of infected cells with no XPA-ACV and a control of healthy cells with no XPA-ACV. Error bars refer to a 95% confidence interval calculated from n = 3.

We were also able to confirm the ability of irradiated **7** to suppress HSV-1 in HCEC. This is shown in Figure 5-18 where we see a significant decrease in viral proliferation relative to the control with just the virus. However, we also see significant viral suppression from unirradiated **7** implying that **7** has antiviral activity itself, and is not just a 'carrier' of the antiviral. Another feature of these results is that viral proliferation is slightly higher when acyclovir is released after infection. The difference may reflect the extent of viral replication in the time delay between infection and irradiation.

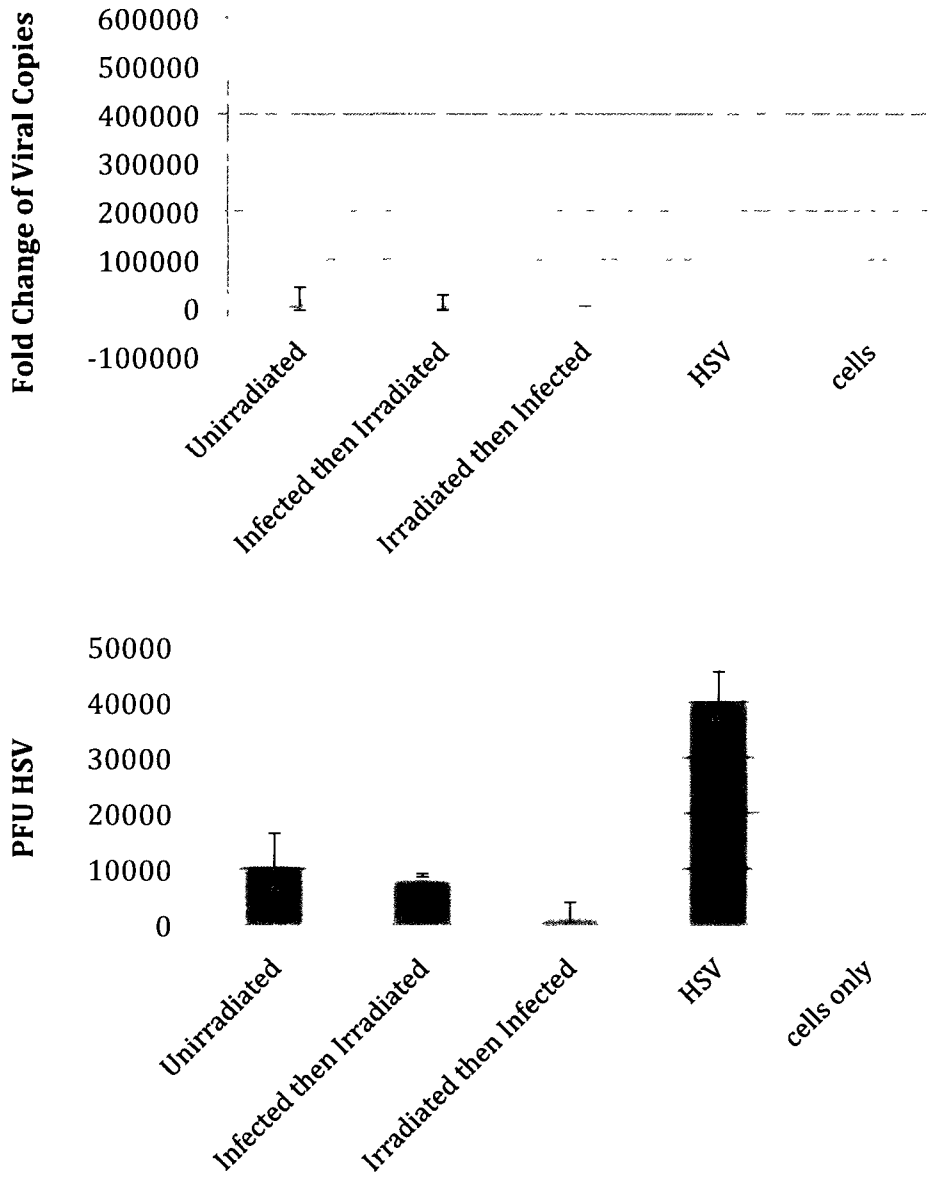

Figure 5-18. Suppression of HSV-1 by XPA-ACV as shown by RT-PCR (top) and a plaque assay (bottom). Error bars refer to a 95% confidence interval calculated from n = 3.

5.5 Release of acyclovir from silica nanoparticles

One option to achieve the slow release of acyclovir (blue line in Figure 5-1) is to encapsulate acyclovir into porous nanoparticles (NP) embedded in the artificial corneas such that the nanoparticles gradually release the antiviral over a span of days. We did just that with SiO_2 NP, chosen because they are easy to make and are known to encapsulate organic molecules.

Silica nanoparticles were prepared in the presence of acyclovir such that acyclovir was directly encapsulated during the synthesis. Hydrogels containing either free acyclovir or encapsulated acyclovir were placed in PBS and the surrounding solution was tested over a span of 12 days for the concentration of free acyclovir (Figure 5-19). My main contribution to this work involved the analysis of these solutions and quantification of acyclovir released. Since in each case, the solution was removed and replaced with fresh PBS, the concentrations in Figure 5-19 represent the amount of acyclovir released (into 15 mL) for each time span. As this figure shows, when acyclovir was embedded in the hydrogel alone it was completely released into the surrounding solution within the first day. Conversely, detectable levels of acyclovir released from SiO_2 NP were measured even after 12 days.

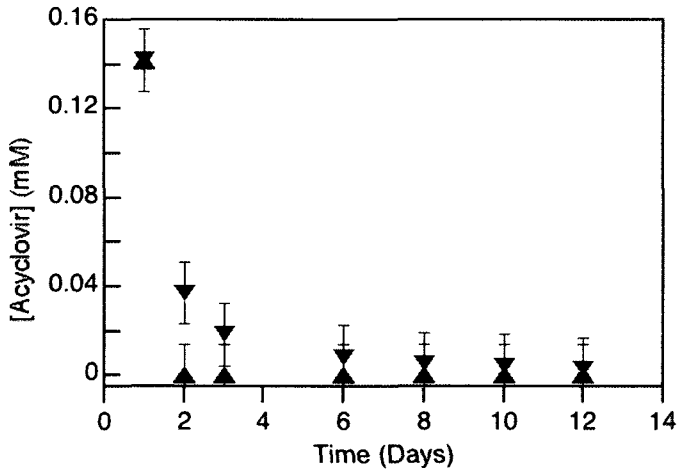

Figure 5-19. Concentration of acyclovir released from hydrogel artificial corneas when acyclovir is freely embedded in the hydrogel (▲) and when acyclovir is encapsulated in SiO_2 nanoparticles embedded in the hydrogel (▼).

When the hydrogels containing SiO_2 NP encapsulated acyclovir were used to treat HSV infected cells, a similar trend was observed (Figure 5-20). For the first day, both hydrogels (with encapsulated ACV and with free ACV) are effective at keeping the infected cells alive. After the first day however, only the hydrogel with initially encapsulated ACV has an effect on cell viability. Even after ten days there is a significantly higher number of living cells when acyclovir is initially encapsulated.

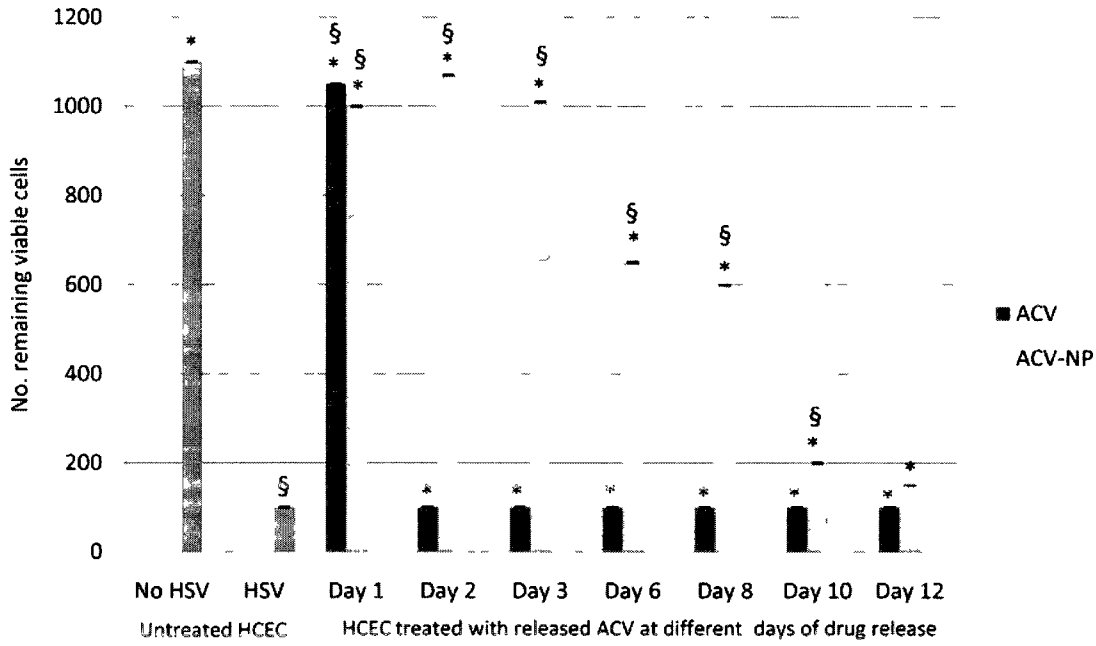

Figure 5-20. Comparison of efficacy in inhibiting HSV-1 viruses of free vs. SiO_2 nanoparticle-encapsulated ACV released from collagen-MPC hydrogels over 12 days. Hydrogels were placed in PBS to allow release of ACV. At different time points after the start of release (days 1,2, 3, 6, 8, 10 and 12) they were placed on top of corneal epithelial cells that were infected with 10^4 pfu of HSV-1. *, § indicates significant difference between each sample and the negative control of uninfected HCEC, or positive control of HSV-1 infected, untreated HCEC, respectively.

5.6 Summary

We have managed to synthetically attach the antiviral acyclovir to our XPA PPG in a manner that allows the clean photorelease of acyclovir; that is, from XPA-ACV (**7**). Although the quantum yield of release is fairly low (Φ_{ACV} release = 0.1), complete release of the drug is theoretically possible given a sufficient dose of light. Our hope is that the dose of light required to release a sufficient amount of acyclovir for viral suppression will be low enough to avoid photodamage to the cornea and surrounding tissue. The experiments we have undertaken with a cell model of the cornea support this possibility; cells remained viable under the same conditions (0.5 mM **7** and 5 min. irradiation) that lead to near complete viral suppression.

In our attempts to study the photorelease of acyclovir in a cell model we have learned that **7** also has antiviral activity towards HSV-1, at least under the conditions studied. This may imply that functionalization with XPA at the *O6* position does not interfere with phosphorylation by HSV-1-specified thymidine kinase or with subsequent DNA polymerase inhibition, however further studies would be necessary to confirm this.

Although we have demonstrated the ability to suppress HSV-1 with photoreleased acyclovir, XPA-ACV does not likely provide any advantage over acyclovir itself for the described application. Since XPA-ACV is also water soluble it would likely leach from the hydrogel artificial corneas at a similar rate to acyclovir itself and so the majority would be lost before its intended release (i.e. during the transplant surgery before the transplant is fully in place). To achieve the full goal of

this collaborative project it will be necessary to attach XPA-ACV to the hydrogel, potentially using the strategy described in Chapter 4. That is, it should be possible to functionalize the hydrogel by amide formation with an amine substituted version of XPA-ACV as illustrated in Figure 5-1.

While our initial aim is a treatment for HSV-1 through the release of acyclovir, I would like to note that the end goal is a broad based technology for a novel drug delivery method. It should be possible to extend this strategy to any small molecule drug. As such, this strategy could provide a very controlled release of the drug of choice to any region where light can reach.

5.7 Experimental

All ^{1}H NMR and ^{13}C NMR spectra were recorded at room temperature on a Bruker AVANCE 400 instrument. Chemical shifts are reported relative to internal TMS unless otherwise specified. Melting points were determined on a Melt-Temp II aparatus from Laboratory Devices. Column chromatography employed Merck silica gel 230-400 mesh. Water was purified through a Millipore MilliQ system. Acetonitrile was HPLC grade. All other solvents are reagent grade from Aldrich; THF was distilled over Na metal and DMF was dried and stored over molecular sieves. All chemicals (except acyclovir) were purchased from Aldrich and used as received.

Acyclovir (**1**) was extracted from pills containing 200 mg (from Laboratorios CENTRUM, Spain) by taking advantage of acyclovir's relative solubility at high and low pH, and insolubility in neutral water.[7] One pill containing 200 mg acyclovir was crushed with a mortar and pestle and the powder was stirred in 10 mL of a 0.1 M NaOH aqueous solution for at least 1 hour at 50°C. The suspension was then filtered and the filtrate was neutralized with a 10% HCl solution. The white precipitate was isolated by centrifuging the suspension, removing the supernatant and washing twice with THF. The white solid was dried in an oven at 50°C for 5 min. ^{1}H and ^{13}C NMR correlate well with those reported in the literature.[19] ^{1}H NMR (400 MHz, DMSO-d6) δ (ppm) 3.4 (overlapping with H_2O, s), 4.78 (1H, s), 5.34 (2H, s), 6.50 (2H, s), 7.81 (1H, s), 10.68 (1H, s, broad).

5.7.1 Synthesis

The synthesis of **2** was described in Chapter 3.

6H-Purin-6-one, 2-amino-9-[[2-[[(1,1-dimethylethyl)dimethylsilyl]oxy] ethoxy]methyl]-1,9-dihydro- (3) [139767-68-3] Imidazole (2.13 g, 31.3 mmol, 5 eq.), DMAP (0.306 g, 2.51 mmol, 0.4 eq.) and **1** (1.41 g, 6.26 mmol) were added to a round bottom flask containing 30 mL DMF and equipped with a magnetic stir bar and a nitrogen gas inlet. The suspension was stirred and TBDMS-Cl (2.36 g, 15.6 mmol, 2.5 eq.) was added. The suspension was left to stir under positive pressure N_2 overnight. ^{1}H-NMR in good agreement with those reported.[16] ^{1}H NMR (400 MHz, DMSO-d6, reported relative to DMSO chemical shift 2.50 ppm) δ (ppm) -0.01 (6H, s), 0.82 (9H, s), 3.52 (2H, t, *J*= 5 Hz), 3.63 (2H, t, *J*= 5 Hz), 5.34 (2H, s), 6.49 (2H, s, broad), 7.80 (1H, s), 10.66 (0.85H, s, v. broad). EI (MS) m/z (%) 339.2, (0.3) (M^+); 282.1, (9.3) ($M^+ - C_4H_9$); 225.1, (2.9) (M^+ - TBDMS); 208.1, (25.4) ($M^+ - C_6H_{15}OSi$); 164.1, (100) ($M^+ - C_8H_{19}O_2Si$). HRMS for $C_{14}H_{25}N_5O_3Si$ [M^+] calculated 339.1727, found 339.1710.

Benzenesulfonic acid, 2,4,6-trimethyl-, 2-amino-9-[[2-[[(1,1-dimethylethyl) dimethylsilyl]oxy]ethoxy]methyl]-9H-purin-6-yl ester (4) [888498-37-1] 2-mesitylsulfonyl chloride (2.07 g, 9.48 mmol, 2 eq.), DMAP (0.29 g, 2.37 mmol, 0.5 eq.) and **3** (1.61 g, 4.74 mmol) were suspended in 7 mL of freshly distilled CH_3CN in a 2-neck 30 mL round bottomed flask equipped with magnetic stir bar and N_2 inlet. To the white, cloudy solution was added triethylamine (3.10 mL, 22.3 mmol, 4.7 eq.) dropwise. After 2 hrs, solvent was removed by rotary evaporation and the product

was purified by flash chromatography (120 g silica, 3:97 CH_3OH:$CHCl_3$). Yield: 1.38 g, 2.64 mmol, 56 % (some was lost due to poor column separation). ^1H NMR in good agreement with those reported with minor differences due to the difference in solvent.[16] ^1H NMR (400 MHz, $CDCl_3$, reported relative to $CHCl_3$ chemical shift 7.26 ppm) δ (ppm) 0.03 (6H, s), 0.86 (9H, s), 2.30 (3H, s), 2.74 (6H, s), 3.57 (2H, t, *J*= 4.8 Hz), 3.72 (2H, t, *J*= 5 Hz), 4.97 (2H, s, broad), 5.5 (2H, s), 6.98 (2H, s), 7.83 (1H, s). ^{13}C NMR (100 MHz, $CDCl_3$, reported relative to $CDCl_3$ chemical shift 77.0 ppm) δ (ppm). -5.33 (CH_3), 18.33 (C), 21.14 (CH_3), 22.79 (CH_3), 25.88 (CH_3), 62.53 (CH_2), 70.98 (CH_2), 72.98 (CH_2), 131.71 (CH), 140.39 (C), 141.77 (CH), 143.96 (C), 155.16 (C), 156.35 (C), 158.88 (C).

(5) Acyclovir derivative **4** (1.4 g, 2.7 mmol) was dissolved in 30 mL dry THF. To this, DABCO (1.5 g, 13.4 mmol, 5 eq.) was added and after ~10 min. a precipitate formed. DBU (1.2 mL, 8.1 mmol, 3 eq.) and **2** (1.26 g, 4.03 mmol, 1.5 eq.) were added and the solution was left to stir under positive pressure N_2 overnight. The volatile components were removed *in vacuo* and the residue was purified by column chromatography. Yield: 0.45 g, 0.71 mmol, 26%. ^1H NMR (400 MHz, $CDCl_3$, reported relative to $CHCl_3$ chemical shift 7.26 ppm) δ (ppm) 0.029 (6H, s), 0.86 (9H, s), 1.92 (3H, s), 3.56 (2H, dd, J_1= 5.4 Hz, J_2= 4.2 Hz), 3.7 (5H, m), 4.87 (1H, d, *J*= 10.8 Hz), 4.95 (2H, s), 5.05 (1H, d, *J*= 10.8 Hz), 5.48 (2H, s), 7.38 (1H, m), 7.48 (2H, m), 7.72 (2H, m), 7.86 (1H, dd, J_1= 8.8 Hz, J_2= 2.6 Hz), 8.33 (1H, dd, J_1= 8 Hz, J_2= 1.6 Hz), 8.41 (1H, d, *J*= 2.4 Hz). ^{13}C NMR (100 MHz, $CDCl_3$, reported relative to $CDCl_3$ chemical shift 77.0 ppm) δ (ppm). -5.32 (CH_3), 20.92 (CH_3), 25.90 (CH_3), 50.60 (C), 52.70 (CH_3), 62.54

(CH_2), 70.70 (CH_2), 71.28 (CH_2), 72.78 (CH_2), 117.99 (CH), 118.38 (CH), 121.56 (C), 121.79 (C), 124.03 (CH), 124.31 (CH), 126.79 (CH), 133.67 (CH), 134.92 (CH), 136.26 (C), 139.52 (CH), 154.49 (C), 155.41 (C), 156.13 (C), 159.47 (C), 160.96 (C), 174.10 (C=O), 177.06 (C=O). EI (MS) m/z (%) 633.3, (1.1) (M^+); 576.2, (7.1) (M^+ - C_4H_9); 458.1, (100) (M^+ - $C_8H_{19}O_2Si$).

(6) 5 (0.45 g, 0.71 mmol) was dissolved in 10 mL dry THF. TBAF (0.76 mL of a 1.0 M solution in THF, 0.76 mmol) was added and the solution was left to stir under positive pressure N_2 for 3 hr. At this time a white precipitate had formed. Distilled water (5 mL) was added to quench the reaction and the precipitate dissolved. When the THF was removed under vacuum a white precipitate formed. Filtration washing with water and ethyl acetate yielded **6** (0.27 g, 0.52 mmol, 73%) which was used as is. ^{1}H NMR (400 MHz, DMSO) δ (ppm) 1.80 (3H, s), 3.45 (overlapping with H_2O, s), 3.69 (3H, s), 4.85 (1H, d), 5.0 (1H, d), 5.41 (2H, s), 6.57 (2H, s), 7.5 (1H, t), 7.7-7.8 (2H, m), 7.9-8.0 (3H, m), 8.2 (2H, m).

XPA-ACV (7) To a 250 mL round bottom flask equipped with stir bar was added **6** (0.26 g) and equal parts CH_3CN and 0.1M NaOH (aqueous) to a total volume of 200 mL. The solution was left to stir overnight protected from ambient light. After filtering the small amount of white solid (~0.05 g) the solution was neutralized with a 10% HCl solution. Evaporation of CH_3CN led to the precipitation of a white solid. The water was removed by lyophilization and **7** was purified by preparative HPLC. The purified yield was 0.1 g, 0.2 mmol, 40%. ^{1}H NMR (400 MHz, DMSO) δ (ppm) 1.63 (3H, s), 3.43 (overlapping with H_2O signal, s), 4.66 (1H, s, broad), 4.74 (1H, d,

J=11 Hz), 4.97 (1H, d, J=11 Hz), 5.38 (2H, s), 6.47 (2H, s), 7.47 (1H, m), 7.58 (1H, d, J=9 Hz), 7.66 (1H, d, J=8 Hz), 7.86 (m) and 7.89 (s) (2H overlapping), 8.02 (1H, d of ds, J=9 Hz, J=2.6 Hz), 8.21 and 8.23 (2H overlapping, d of ds, J=8 Hz, J=1.6 Hz and d, J=2.4 Hz) . ^{13}C NMR (100 MHz, DMSO-d6) δ (ppm) 21.71 (CH_3), 50.73 (C), 59.89 (CH_2), 70.37 (CH_2), 71.93 (CH_2), 73.50 (CH_2), 113.53 (C), 117.10 (CH), 118.19 (CH), 120.18 (C), 121.12 (C), 123.10 (CH), 124.17 (CH), 126.06 (CH), 134.86 (CH), 135.32 (CH), 139.57 (CH), 153.84 (C), 154.27 (C), 155.61 (C), 160.12 (C), 161.12 (C), 174.49 (C=O), 176.20 (C=O). MALDI m/z (%) 528.2 (47%) $[M+Na]^+$; 506.3 (100%) $[M+H]^+$.

5.7.2 Irradiation conditions

Solution phase irradiation was performed in a Luzchem photoreactor with 2 UVA bulbs per side. The quantum yield of release based on appearance of acyclovir was determined by irradiating solutions of XPA-ACV (Abs. > 2) for 0, 1, 2, 3, and 4 min. simultaneously with 4 mM solutions of ketoprofen followed by HPLC analysis. Concentrations of ACV in each photolysis solution were determined from a calibration curve. The quantum yield was calculated by comparing the slopes of $n_{photolysed}$ vs. irradiation time for XPA-ACV and ketoprofen.

The quantum yield for loss of XPA-ACV was determined by irradiating four solutions of XPA-ACV, two in pure phosphate buffer and two in buffer with acetonitrile (1:1) simultaneously with four solutions of ketoprofen in phosphate buffer (4 mM) for 10 minutes. To each photolysate, 6.00 mL of an internal standard (9-hydroxyfluorene) in acetonitrile was added and the solution was diluted to 80% acetonitrile 20% buffer to ensure solubility of all products. Quantification of XPA-

ACV concentration was based on a calibration curve and the quantum yields were calculated by comparing the average value for $n_{photolysed}$ to that of ketoprofen.

For the irradiation of cells, a Luzchem exposure panel equipped with 5 UVA bulbs was utilized (Irradiance = 65 W/m^2).

5.7.3 High performance liquid chromatography conditions

High performance liquid chromatography (HPLC) was performed using an Agilent 1100 Series apparatus (G1379A Degasser, G1312A Binary Pump, G1387A Autosampler, G1315B Diode Array Detector). Separations were achieved on a reversed-phase C-18 column (Zorbax SB C-18 4.6 mm x 25 cm) at room temperature.

The mobile phase, flowing at a rate of 0.5 mL/min., consisted of acetonitrile and water with 1% acetic acid added to improve peak shape. It was ramped from 0% to 50% acetonitrile over 25 min., then to 100% acetonitrile over 20 min., then back to 100% water with acetic acid over 10 min. with a final 5 minutes at this composition. The injection volume was 10.0 μL. Absorbance signals were monitored at 254 nm using 400 nm as a baseline reference. Under these conditions, acyclovir was detected at 11.9 min. and was sufficiently separated from the background peaks. XPA-ACV, the xanthone photoproduct, ketoprofen and 9-hydroxyfluorene were detected at 27.6, 45.6, 35.0, and 34.4 minutes respectively and each peak was well resolved. Quantification was based on peak area using a calibration curve constructed by analyzing standard samples of acyclovir, XPA-ACV

and ketoprofen with the identical HPLC method.

For samples that likely contained large biological molecules (i.e. the supernatents from cell irradiation and cell media controls) 0.5 mL of sample was added to a vortex tube with 0.25 mL perchloric acid and 0.25 mL acetonitrile. The tubes were vortexed for 10 s then centrifuged for 10 min. at a speed of 36670 g (22343 rpm). The resulting supernatents were analysed by HPLC as described above.

5.7.4 Cell source

Immortalized human corneal epithelial cells (HCEC) that possess key morphological and physiological characteristics of primary cells were cultured with Keratinocyte Serum-Free Medium (KSFM; Invitrogen, Burlington, Canada) in a humidified tissue culture incubator.[20]

5.7.5 MTT assay

Briefly, MTT (1 mg/mL) was added to KSFM. 300 µl of this MTT solution was added per well and the wells were incubated for 3 hr at 37°C. Following incubation 300 µl/well of stop solution (isopropanol containing 0.1 M HCl, and 10% Triton X-100) was added and the wells were left for 1 hr at room temperature. Controls were non-treated cells and cells killed with concentrated HCl. The background control was a well with no cells and only MTT mixed with stop solution. Each sample was transferred into a 96 well plate (100 µl/well) and the absorbance at 570 nm was measured in a Synergy HT Multi-Mode Microplate Reader (Bio Tek, Winooski,

United States).[21] The signal from the background control was subtracted from each sample signal.

5.7.6 Live/dead staining

Following the protocol from Bio Tek., 24 hr. after cell treatment, live/dead mix containing DAPI was added to cells 300 µl/well and the cells were incubated for 20 min. at 37°C. Cells were then washed twice in PBS and investigated under a reverse fluorescent Nikon microscope with FITC channel for living cells and TRITC channel for dead cells. DAPI channel was used to investigate the cell nuclei. Living and dead cells were counted to calculate the % of dead cells.

5.7.7 Plaque assay

Human corneal fibroblast cells were seeded in 12 well tissue culture treated plates (Corning) and were cultured to 50-60 % confluence. Cells were washed in PBS prior to infection, in order to remove remaining culture media. Virus solutions and dilutions (from the samples being tested) were prepared in keratinocyte serum free media (KSFM, Invitrogen) and added as 200 µL/well. One known concentration of virus was added in one well as a positive control and 200 µl KSFM was added without virus as a negative control. Plates were incubated at 37°C for 30 min. Virus solutions and dilutions were then aspired and 2 mL/well of 2% methylcellulose in Dulbecco's modified eagle medium (DMEM), 10% Fetile Bovine Serum (FBS), 1% penicillin/streptomycin (pen/strep) (1:1 v/v, 4% methylcellulose : 2 x DMEM, 20% FBS, 2 % pen/strep) was added on top of the cell monolayer. After 5 days of

incubation at 37°C, the cells and over layer were fixed by adding 1 ml of methanol: acetic acid (3:1) per well followed by incubation for 30 min. at room temperature. The colour change of the overlay from red to yellow due to pH change is an indication of fixation. The overlays were aspired and the fixed cells were washed twice with H_2O, before incubation with 1 mL/well 1 % crystal violet stain for 3 hr. at room temperature. After washing off the crystal violet stain with H_2O, plaques were counted. The values reported are calculated as the amount of virus present in the original solution (i.e. prior to dilution).

5.7.8 Real-time Polymerase Chain Reaction (RT-PCR)

After 3 days of infection and treatment with XPA-ACV and irradiation, the supernatants from each sample were collected and 5 µl were used per RT-PCR reaction. RT-PCR was performed in special optical tubes in 96-well microtitre plates (Perkin-Elmer/Applied Biosystems) using an iCycler (Bio-Rad). Fluorescent signals were generated using a Quantitect SYBR Green PCR kit. The HSV gene was analyzed using HSV-1 sense and antisense primer sequences 5-CCGTCAGCACCTTCATCGA-3 and 3-CTGATGTGCCTCCAGGTCGC-5 obtained from the diagnostic laboratory at CHEO (Children's Hospital of Eastern Ontario). The HSV genes were amplified using the above mentioned primers and a viral DNA template from the different treatment groups. Target samples were added in individual reactions to a total volume of 25 µL and no DNA was added to the negative control. For each amplification, the protocol included 10 min. at 95 °C and 40 cycles of 15 s at 95 °C, 1 min. at 55 °C and 1 min. at 72 °C, followed by a melting curve. All RT-PCR

experiments were run in triplicate. The iCycler software (Bio-Rad) detected the threshold cycle (CT) for each amplicon.

5.8 References

1. Toma, H. S.; Murina, A. T.; Areaux, R. G. J.; Neumann, D. M.; Bhattacharjee, P. S.; Foster, T. P.; Kaufman, H. E.; Hill, J. M., Ocular HSV-1 Latency, Reactivation and Recurrent Disease. *Semin. Ophthalmol.* **2008,** *23* (4), 249-273.

2. Cleator, G. M.; Klapper, P. E., *Herpes Simplex*. 4 ed.; John Wiley & Sons: 2000.

3. Prepose, J. S.; Leib, D. A.; Stuart, P. M.; Easty, D. L., *Herpes simplex virus diseases: anterior segment of the eye*. Mosby: St. Louis, 1996.

4. Khan, B. F.; Pavan-Langston, D., Clinical Manifestations and Treatment Modalities in Herpes Simplex Virus of the Ocular Anterior Segment. *Int. Ophthalmol. Clin.* **2004,** *44* (3), 103-133.

5. Liesegang, T. J., Herpes simplex virus epidemiology and ocular importance. *Cornea* **2001,** *20* (1), 1-13.

6. Liesegang, T. J.; Melton, L. J.; Daly, P. J.; Ilstrup, D. M., Epidemiology of ocular herpes simplex. Incidence in Rochester Minn. 1950 through 1982. *Arch. Ophthalmol.* **1989,** *107*, 1155-1159.

7. O'Brien, J. J.; Campoli-Richards, D. M., Acyclovir. An updated review of its antiviral activity, pharmacokinetic properties and therapeutic efficacy. *Drugs* **1989,** *37* (3), 233-309.

8. Elion, G.; Furman, P. A.; Fyfe, J. A.; de Miranda, P.; Beauchamp, L.; Schaeffer, H. J., Selectivity of action of an antiherpetic agent, 9-(2-hydroxyethoxymethyl)guanine. *PNAS* **1977,** *74* (12), 5716-5720.

9. Schaeffer, H. J.; Beauchamp, L.; de Miranda, P.; Elion, G.; Bauer, D. J.; Collins, P., 9-(2-Hydroxyethoxymethyl)guanine Activity Against Viruses of Herpes Group. *Nature* **1978,** *272*, 583.

10. Balfour, H. H., Antiviral drugs. *New Engl. J. Med.* **1999,** *340* (16), 1255-1268.

11. Le Bourlais, C.; Acar, L.; Zia, H.; Sado, P. A.; Needham, T.; Leverge, R., Ophthalmic drug delivery systems - Recent advances. *Prog. Retin. Eye Res.* **1998,** *17* (1), 33-58.

12. Nagarsenker, M. S.; Londhe, V. Y.; Nadkarni, G. D., Preparation and evaluation of liposomal formulations of tropicamide for ocular delivery. *Int. J. Pharm.* **1999,** *190* (1), 63-71.

13. Gulsen, D.; Chauhan, A., Ophthalmic drug delivery through contact lenses. *Invest. Ophth. Vis. Sci.* **2004,** *45* (7), 2342-2347.

14. Hagen, M. D.; Scalfi-Happ, C.; Happ, E.; Chládek, S., Synthesis of 2'(3')-O-(Aminoacyl) Trinucleotides Incorporating All Four Common Bases. *J. Org. Chem.* **1988,** *53*, 5040-5045.

15. M. Liras was attempting to synthesize photoreleasable alcohols for a photolithography project but was unsuccessful.

16. Pletsas, D.; Wheelhouse, R. T.; Pletsa, V.; Nicolaou, A.; Jenkins, T. C.; Bibby, M. C.; Kyrtopoulos, S. A., Polar, functionalized guanine-O6 derivatives resistant to repair by O6-alkylguanine-DNA alkyltransferase: implications for the design of DNA-modifying drugs. *Eur. J. Med. Chem.* **2006,** *41*, 330-339.

17. Harrison, K. L.; Fairhurst, N.; Challis, B. C.; Shuker, D. E. G., Synthesis, Characterization, and Immunochemical Detection of O6-(Carboxymethyl)-2'-deoxyguanosine: A DNA Adduct Formed by Nitrosated Glycine Derivatives. *Chem. Res. Toxicol.* **1997,** *10*, 652-659.

18. Cohen, S. G.; Parola, A.; Parsons, G. H. J., Photoreduction by Amines. *Chem. Rev.* **1973,** *73* (2), 141-161.

19. Gao, H.; Mitra, A. K., NMR spectral data for acyclovir prodrugs. *Magn. Reson. Chem.* **1999,** *37*.

20. Araki-Sasaki, K. O. Y.; Sasabe, T., An SV-40 immortalized human corneal epithelial cell line and its characterization. *Invest. Ophth. Vis. Sci.* **1995,** *36*, 614-21.

21. Ngamwongsatit, P. B. P.; Panbangred, W.; Bhunia, A. K., WSt-1 based cell cytotoxicity assay as a substitute for MTT-based assay for rapid detection of toxigenic Bacillus species using CHO cell line. *J. Microbiol. Methods* **2008,** *73*, 211-215.

6. Final Comments and a Look to the Future

6.1 Final Comments

The work described in this thesis represents the development of a novel photolabile protecting group (PPG); from initial photochemical mechanistic studies to the demonstration of release ability to the application of this PPG towards a new drug delivery method. We have demonstrated that 2-xanthone acetic acid (2-XAA and 4-XAA), like ketoprofen, photodecarboxylates efficiently to form a carbanion intermediate that is rapidly protonated in aqueous solution and we have taken advantage of this highly efficient photochemistry in the form of our xanthone propionate (XPA) PPG.

From a mechanistic point of view, this work has extended the series of electron poor arylacetic acids that undergo efficient photodecarboxylation. Among this series, the xanthone acetic acids described in Chapter 2 exhibit the highest contrast in Φ_{PDC} when comparing *meta* to *para* substitution; that is, they are the strongest example of Zimmerman's 'meta-ortho effect'. In addition, the carbanion intermediate formed from 2- and 4-xanthone acetic acid photodecarboxylation is remarkably short lived (< 20 ns relative to ~200 ns for the carbanion from ketoprofen). The enhanced reactivity of the carbanion is likely due to ground state electron donating from the xanthone ether oxygen, which is *para* to the carbanion for 2-xanthone acetic acid and *ortho* to the carbanion for 4-xanthone acetic acid. Taken together, these observations led to new insight into the governing factors of the general photodecarboxylation mechanism. It would seem that *meta-ortho*

substitution on the aryl ring, being strongest in the excited state, dictates the photodecarboxylation efficiency as predicted by the 'meta-ortho effect', while *para-ortho* substitution, being strongest in the ground state, dictates the reactivity and lifetime of the carbanion. The longer lifetime observed for nitro-substituted 2-xanthone acetic acid implies that even distal substitution on the xanthone ring can affect the carbanion intermediate. In this case, a strong electron withdrawing group stabilizes the carbanion.

Our results from fluorescence studies and triplet quenching experiments demonstrate conclusively that the xanthone acetic acid photodecarboxylation occurs from the singlet excited state, supporting (though not proving) the earlier proposal of ketoprofen's singlet mediated photodecarboxylation. With respect to the evaluation of a PPG based on this photochemistry, the short timescale for singlet state photodecarboxylation and the short lifetime of the carbanion are highly appealing not only because they imply the release rate should be fast, but also because there are no intermediates long-lived enough to react with substrates that may be present in the surrounding media.

Through the release of acetate and aniline (*via* the carbamate), we have demonstrated the ability of the XPA PPG to release simple molecules that are good leaving groups. By extention, it should be possible to release many biologically relevant small molecules that possess either a carboxylic acid or an amine with the *caveat* that free amines on the small molecule may quench the photochemistry. If

we return to the list of criteria for PPGs outlined in Chapter 1, we see that our new PPG measures up quite well:

1) *Clean and efficient photochemistry.* For good leaving groups, release is the only photochemical path and the quantum yield of release is quite high (Φ = 0.4 for XPA-OAc).

2) *High absorption coefficient at wavelengths above 300 nm.* The xanthone chromophore absorbs significantly with a band of $\lambda_{max} \sim 350$ nm. For XPA-OAc, $\varepsilon_{347nm} = 6960\ M^{-1}cm^{-1}$.

3) *Non-interfering photoproducts.* Extended photolysis of XPA-OAc leads to no photoproducts other than those expected which tells us that the photoproducts themselves are photostable. While we do not know the toxicity of the xanthone alkene photoproduct from release, the methylxanthone photoproduct from 2-xanthone acetic acid photodecarboxylation was shown to be non-toxic. In addition, the absorbance at 337 nm (a wavelength commonly used in biological studies) decreases by a factor of 1.5 when converting from XPA to its photoproduct.

4) *Fast release rate.* We estimate a *minimum* elimination rate constant of $10^9\ s^{-1}$ for good leaving groups which means groups like acetate would be released in less than one nanosecond. In addition, since we can monitor both the singlet state and the carbanion intermediate (assuming they live long enough) by time resolved emission and absorption respectively, we have a relatively easy way to determine the release

rate for different released groups and different conditions (solvent, pH, temperature). Recall from Chapter 1 that this is a challenge for *o*NB groups because of the complex photochemistry leading to release.

5) *Solubility*. All of the compounds studied are soluble in water at physiological pH. Unfortunately, the photoproduct, which has lost the carboxylate group, is not. This could be overcome by substitution of the xanthone ring with additional solubilizing groups. For example, the photoproduct from amide substituted xanthone acetic acid (Chapter 4) is water soluble.

6) *Low background activity*. All of the XPA caged groups studied are thermally stable for days at physiological pH.

One criteria that was not included in this list, but is particularly relevant to the XPA PPG is the synthetic accessibility. While our PPG performs very well, it is not likely to become a favourite of biochemists any time soon simply because of the multistep synthesis required. As such, we chose to focus on applications where the XPA PPG could accomplish something other groups could not. The first of these areas is the release of poor leaving groups like alcohols. Our results with XPA-OCH_3 show the potential to directly release primary alcohols, a particular challenge for most PPGs. Even phenols like serotonin usually cannot be directly released and most applications rely on the carbonate release strategy. If we could demonstrate the direct release of alcohols and phenols like serotonin, this would represent a

significant advancement in the field. Our second 'specialty' area is the possibility to release with two photon excitation. The two photon excitation cross section measured by T. Dore is very promising and we hope to continue this collaboration.

Finally, we directed our new PPG to the field of drug delivery. PPGs have previously been limited in this field possibly due to the toxicity associated with the photoproducts and byproducts generated. Two major advantages of the XPA group is the remarkably clean the photochemistry and the short lifetimes of the intermediates. Because of these characteristics we do not have to worry about reactive intermediates in a biological environment, and the only toxicity concern is with the initial XPA-drug compound and the xanthone-alkene photoproduct, both of which seem to be non-toxic based on our studies with a cell model.

Another reason the application of PPGs to drug delivery has been limited is that the drug delivery must warrant their use. That is, a health problem must require a significant level of either spatial or temporal control. The post-transplant delivery of acyclovir within the eye is one such example. In this case, it is necessary to somehow hold the antiviral to the corneal transplant until the right moment at which point it is released efficiently. Our initial results demonstrate the ability of XPA to release acyclovir with light in a way that is not toxic to a cell model. This work is part of an ongoing collaboration with researchers at the Ottawa Eye Institute and we hope it continues towards the end goal that will improve the success rate of corneal transplants for HSV-1 patients.

6.2 Future Directions

6.2.1 Mechanistic photochemistry

Since we were unable to observe the carbanion from 2-XAA and 4-XAA photodecarboxylation, it is desirable to study this process using femtosecond techniques. A. Stolow from the National Research Council of Canada is currently exploring this possibility.

Further extention of the electron poor aryl acetic acid series would confirm (or disprove) the insights suggested in this thesis. For example, 2-anthraquinone acetic acid, which has a carbonyl in place of the ether oxygen of 2-xanthone acetic acid possesses an electron withdrawing group *meta* and *para* to the site of decarboxylation, should photodecarboxylate efficiently, but have a longer lived carbanion.

A more in depth study of the effect of substitution on PDC may lead to further insights into the mechanism. For example, it would be interesting to examine the effect on Φ_{PDC} and the carbanion τ of a series of EDG and EWG substituted on the XAA ring.

6.2.2 Release applications

Given the potential suggested by our study of XPA-OCH_3, a continued study of the release of alcohols would be highly advantageous. At this time, it is necessary to confirm the ratio between protonation and elimination photoproducts and to

characterize the photochemistry by laser flash photolysis. Although it is most likely that the carbanion will be too short lived to see, confirmation of this is necessary. A knowledge of the carbanion lifetime and the ratio of photoproducts can allow us to determine the elimination rate constant for $-OCH_3$. Given that $-OCH_3$ is such a poor leaving group, this would give us the lower limit of release rate constants for XPA PPGs in general. Further to this, a demonstration of serotonin release (or another biologically relevant alcohol) would likely be faster than from any PPG yet reported and may lead to very interesting collaborations.

An evaluation of the two photon cross section for XPA release is currently being investigated by T. Dore. If successful, it would be desirable to release neurotransmitters such as glutamate from XPA with two photon excitation since this could be used in signalling studies that require very high spatial resolution. Two photon excitation would also open the door to release using wavelengths of light that biological tissue is transparent to. As such, we could extend the use of this PPG to drug delivery applications beyond just the cornea.

6.2.3 Drug delivery

To fully achieve the full goal of controlled corneal acyclovir delivery with our XPA PPG it is necessary to:

1. Synthesize XPA-PPG with a 'handle' such as the amide handle described in Chapter 4 and evaluate the release efficiency. We have demonstrated the

photochemical and synthetic possibility of both release and incorporation of a handle. Now the two need to be combined.

2. When an appropriate handle has been chosen (i.e. one that does not quench the release), attach XPA-PPG to the synthetic cornea hydrogel or to nanoparticle composite that can be embedded in the hydrogel.

3. Evaluate the thermal and photochemical release of acyclovir from a hydrogel containing photocaged acyclovir and test the ability of this hydrogel to suppress the herpes simplex virus in a cell model as well as any potential toxicity.

4. If the above experiments are successful, extend these studies to animal models and finally to clinical trials.

The reader may recall from Chapter 5 that current delivery of acyclovir is quite inefficient. This applies to regular delivery as well as post surgical delivery. In order to avoid the potential damage caused by reactivation of HSV-1, patients must take large oral doses so that a sufficient dose reaches the eye. This can lead to a number of negative side effects. Once a protocol for attaching XPA-ACV to a hydrogel is developed, it may prove advantageous to apply this method towards attaching photocaged acyclovir to therapeutic contact lenses, thus providing an alternative to oral administration of the drug for corneal HSV-1 infected patients.

6.3 Claims to Original Research

1. The elucidation of the photodecarboxylation mechanism for 2- and 4-xanthone acetic acid (pH > pK_a) is reported. This is a singlet state mediated reaction which occurs within the laser pulse of our ns LFP system with a Φ_{PDC} of 0.6. The large contrast with 3-xanthone acetic acid, which is photostable, is attributed to the 'meta' effect common amongst electron poor aryl acetic acids. The very short lifetime of the carbanion intermediate (pseudo-first order protonation rate constants of $\geq 5 \times 10^7$ s^{-1}) is attributed to the ground state electron donating effect of the ether oxygen. The Φ_F for 2- and 4-xanthone acetic acids increase 30- and 15-fold, respectively, upon photochemical conversion to the methylxanthone photoproduct.

2. The photodecarboxylation mechanism for these same derivatives when pH < pK_a was determined to be triplet mediated. This acid catalysed mechanism involves a protonated excited state.

3. A photolabile protecting group based on the photochemistry of 2-xanthone acetic acid (abbreviated XPA) was demonstrated to release acetate and aniline (*via* the carbamate) by an elimination mechanism from the carbanion intermediate that competes completely with protonation of the carbanion. Release of methoxide was also demonstrated but in this case protonation was favoured over elimination. The minimum rate constant for release of acetate was determined to be 1×10^9 s^{-1} and the uncaging cross section was

determined to be $\Phi\varepsilon = 2700\ M^{-1}cm^{-1}$ at 347 nm.

4. The Φ_{PDC} for nitro, amine and amide substituted 2-xanthone acetic acids were measured to be 0.3, 0, and 0.01 respectively in phosphate buffer solution (pH 7.4). For nitro, amine and amide substituted thioxanthone acetic acids, the Φ_{PDC} under these same conditions was determined to be 0.3, 0, < 0.001. A significant solvent effect was measured for both amide substituted derivatives as Φ_{PDC} increases with increasing fraction of acetonitrile in aqueous solutions. (Joint work with M.J. Yorke) The carbanion intermediate for nitro-substituted 2-xanthone acetic acid was measured to be significantly longer than the carbanion from either 2-xanthone acetic acid or ketoprofen. This is attributed to the electron withdrawing effect of the nitro group.

5. Photorelease of acyclovir (ACV) from the XPA PPG was demonstrated in phosphate buffer solutions and in a cell model for the human cornea. In phosphate buffer solution, release proceeds cleanly with a quantum yield of 0.1. In the cell model, irradiation of XPA-ACV suppressed the proliferation of HSV-1 as did unirradiated XPA-ACV to a lesser extent. Both XPA-ACV and the dose of light used were determined to be non-toxic to the cell model. (Joint work with B. Bareiss)

6.4 Publications

6.4.1 Published

Bareiss, B.; Ghorbani, M.; Li, F.; **Blake, J.A.**; Scaiano, J.C.; Zhang, J.; Deng, C.; Merrett, K.; Harden, J.; Diaz-Mitoma, F.; Griffith, M. Controlled Release of Acyclovir Through Bioengineered Corneal Implants with Silica Nanoparticle Carriers. *The Open Tissue Engineering and Regenerative Medicine Journal*, **2010**, *3*,

Scaiano, J.C.; **Blake, J.A.**; Griffith, M. Use of Ketoprofenate and Xanthonate Photocages for Antiviral Release. In *Extreme Photonics & Applications*, Proceedings of the NATO Advanced Study Institute on Laser Control & Monitoring New Materials, Biomedicine, Environment, Security & Defense, Ottawa, Ontario, Canada, November 24 – December 5, 2008; Hall, T.J.; Gaponenko, S.V., Eds.; Springer: Dordrecht, The Netherlands, 2010.

Blake, J.A.; Lukeman, M.; Scaiano, J.C. Photolabile Protecting Groups Based on the Singlet State Photodecarboxylation of Xanthone Acetic Acid. *Journal of the American Chemical Society*. **2009**, *131*(11), 4127-4135

Blake, J.A.; Gagnon, E.; Lukeman, M.; Scaiano, J.C. (2006) Photodecarboxylation of Xanthone Acetic Acids: C-C Bond Heterolysis from the Singlet Excited State. *Organic Letters*. **2006**, *8*(6), 1057-1060

6.4.2 In Preparation

Blake, J.A.; Bareiss, B.; Jimenez, L.; Griffith, M.; Scaiano, J.C. Photoactivated Drug Delivery: Photorelease of Acyclovir from the Xanthone Propionic Acid Photolabile Protecting group.

Blake, J.A.; Yorke, M.J.; Scaiano, J.C. Photochemistry of Nitro, Amine and Amide Substituted Xanthone Acetic Acids and Thioxanthone Acetic Acids.

Blake, J.A.; Wilson, H.; Dore, T.; Scaiano, J.C. Rapid and Efficient Photorelease of a Carboxylate by Two Photon Excitation.

Appendix

^{1}H and ^{13}C or DEPTQ NMR Spectra of Products

Chapter 2 - ^{1}H and ^{13}C or DEPTQ NMR Spectra of Products

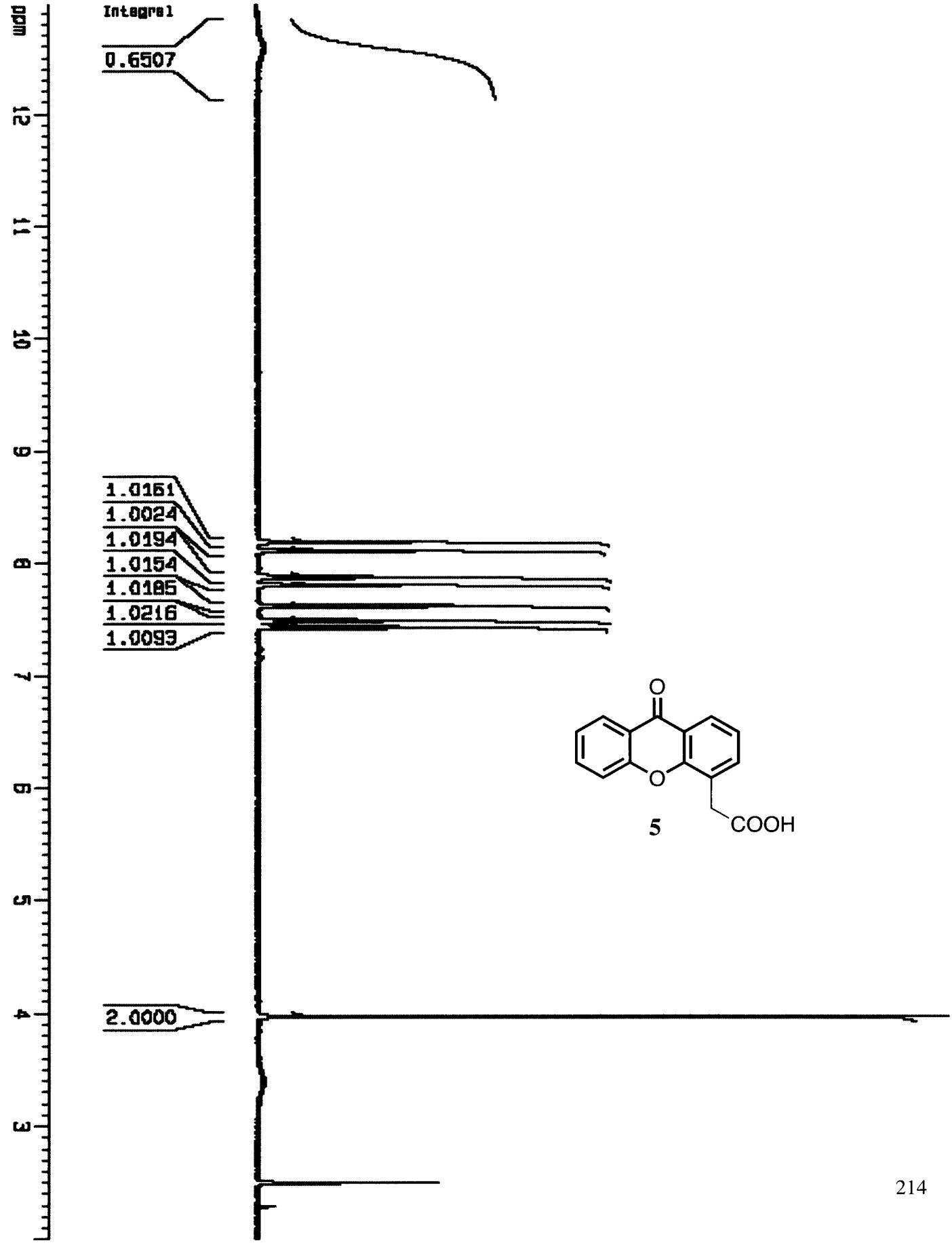
Integral
0.6507
1.0161
1.0024
1.0194
1.0154
1.0185
1.0216
1.0093
2.0000
ppm
12
11
10
9
8
7
6
5
4
3
O
O
COOH

5

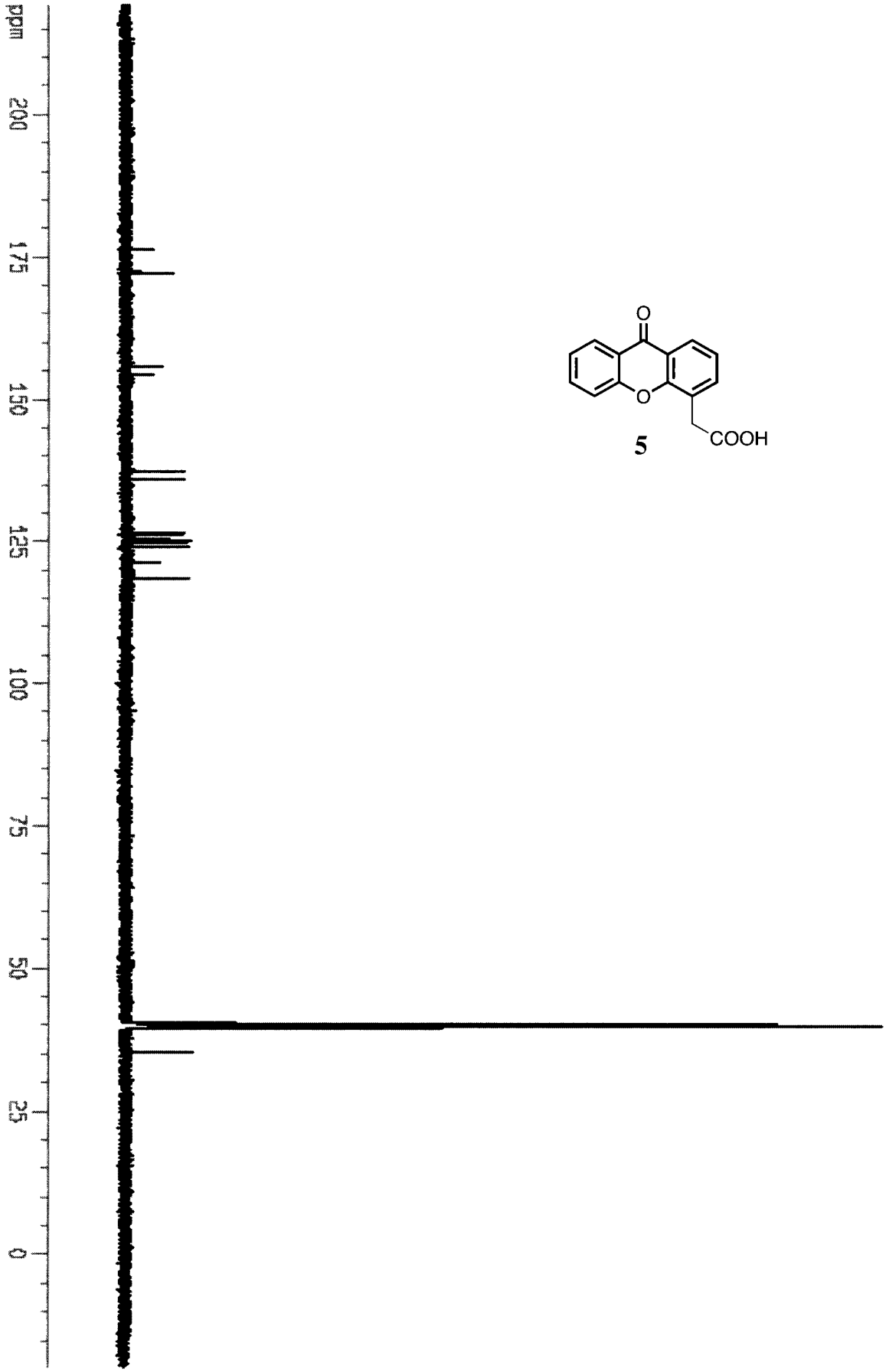

5

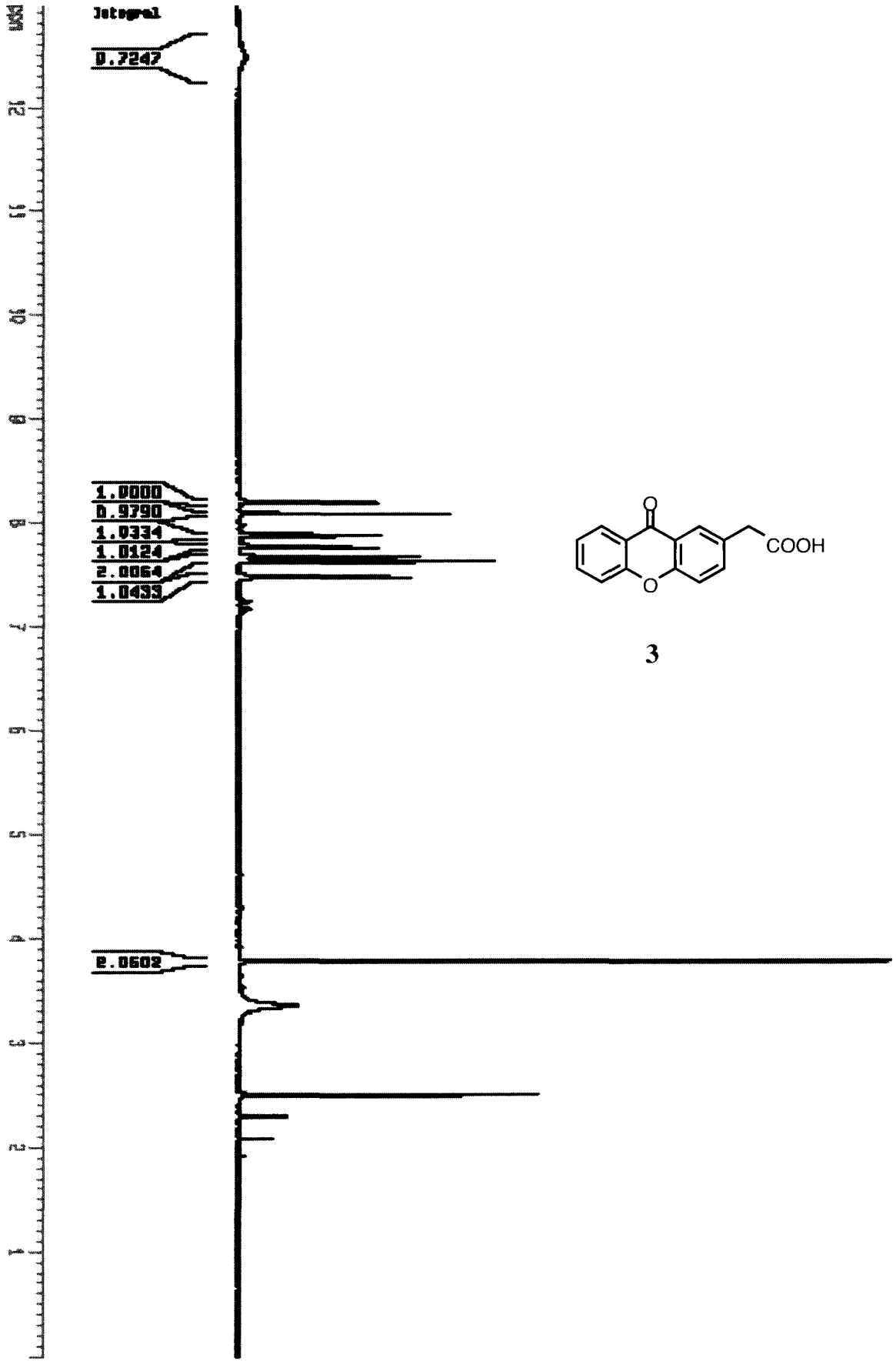
Integral
0.7247
1.0000
0.9790
1.0334
1.0124
2.0064
1.0433
2.0602
COOH
O
O

3

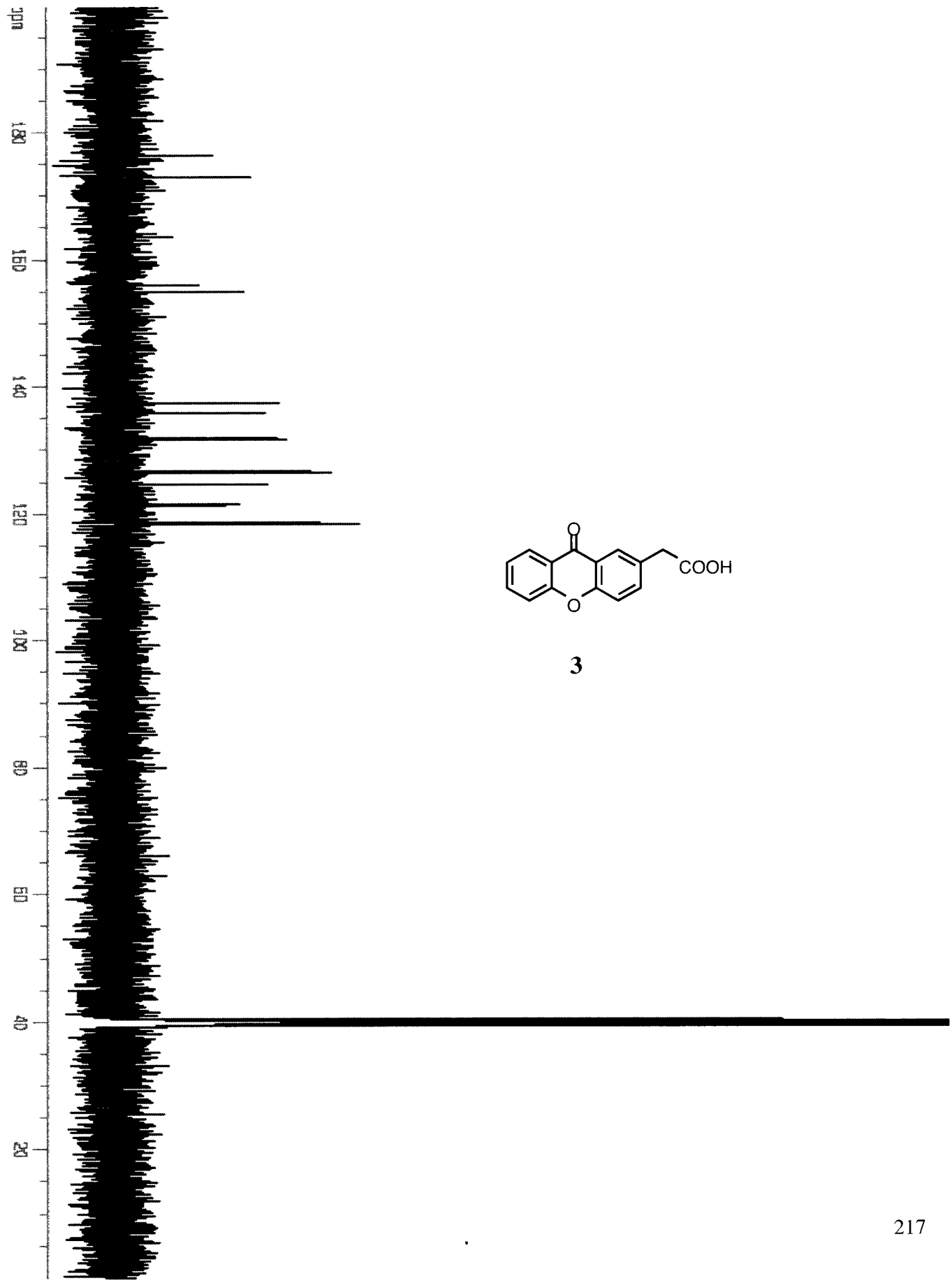

3

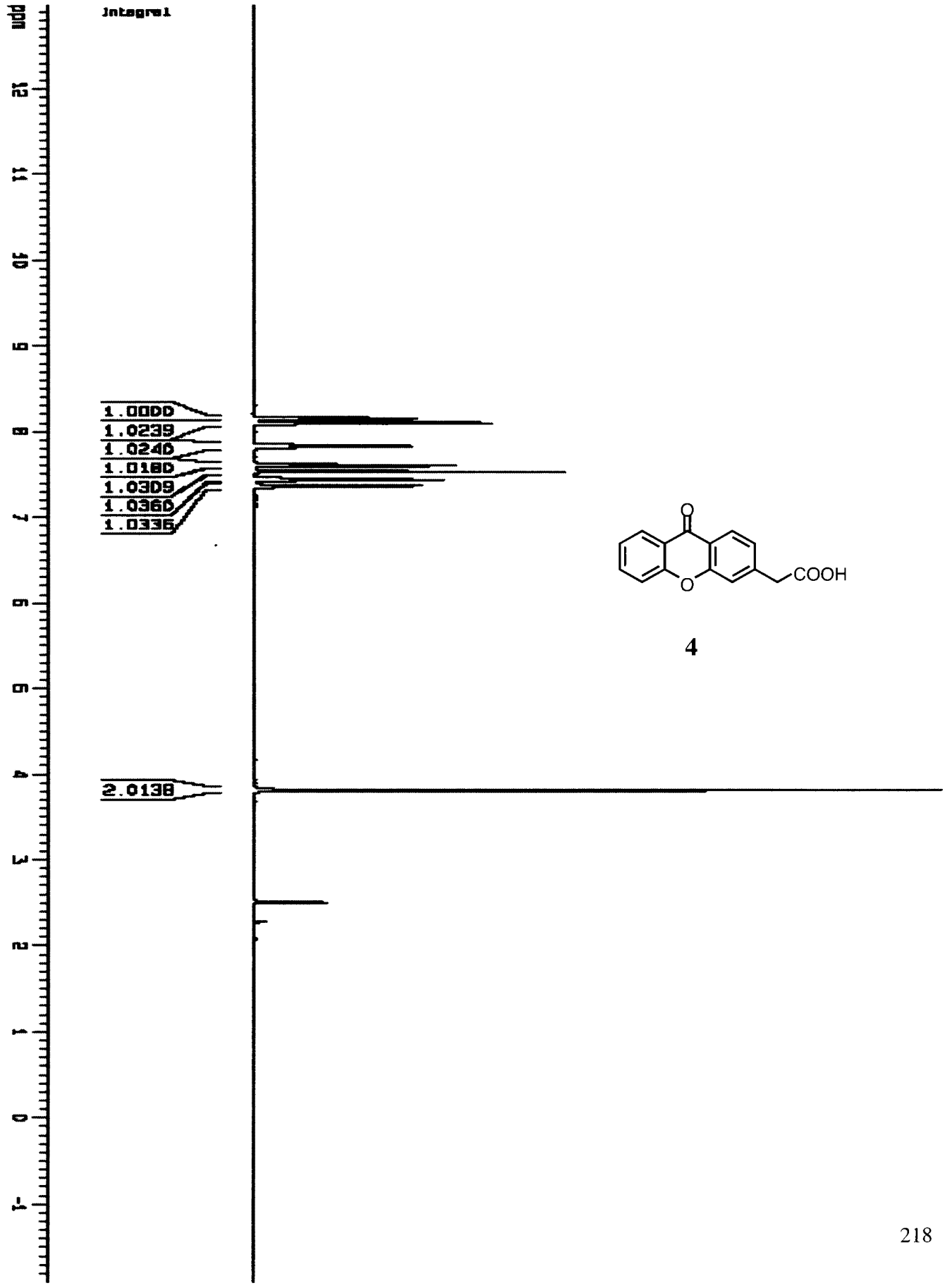
Integral
1.0000
1.0239
1.0246
1.0180
1.0309
1.0360
1.0336
2.0138
O
O
COOH

4

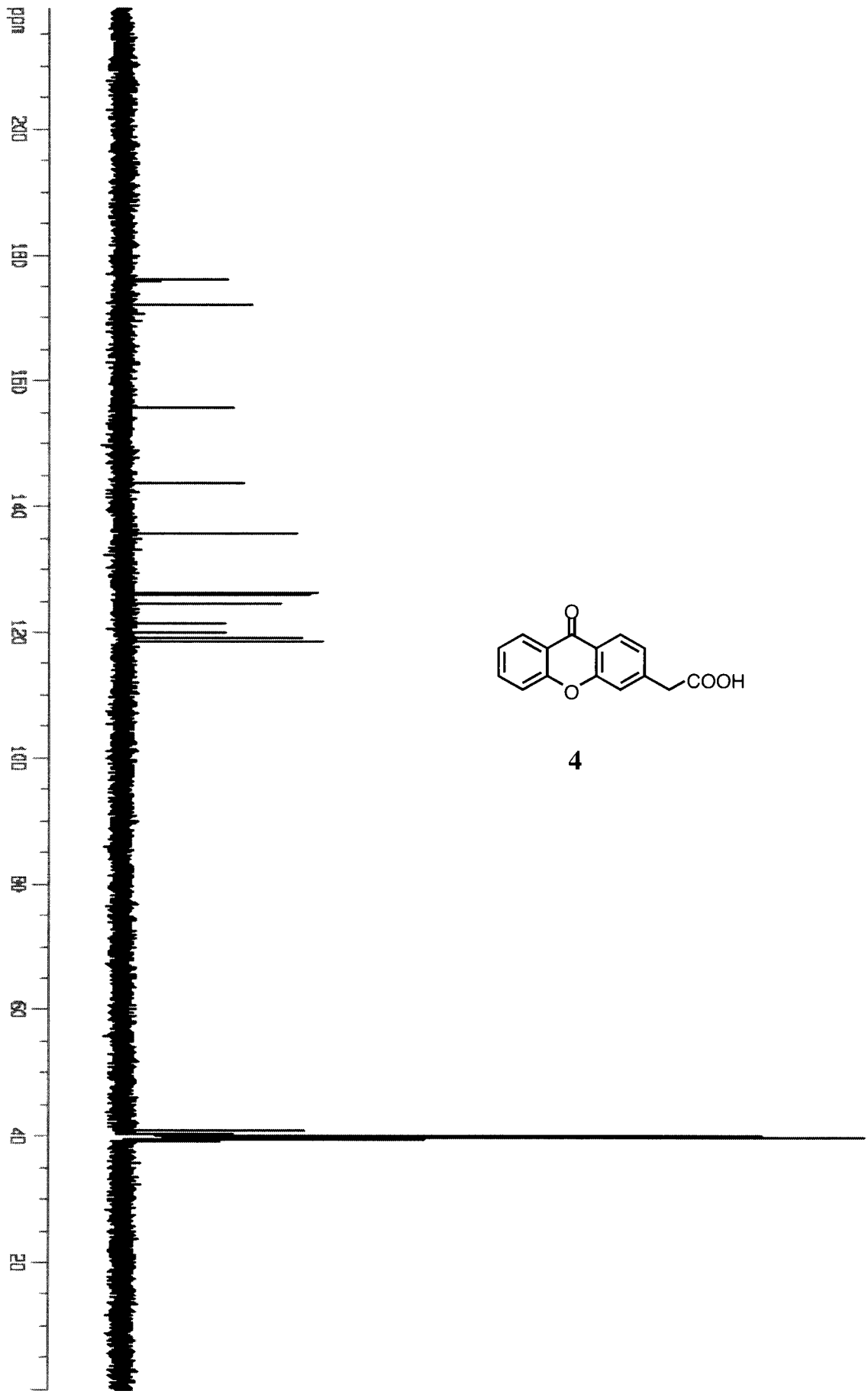

4

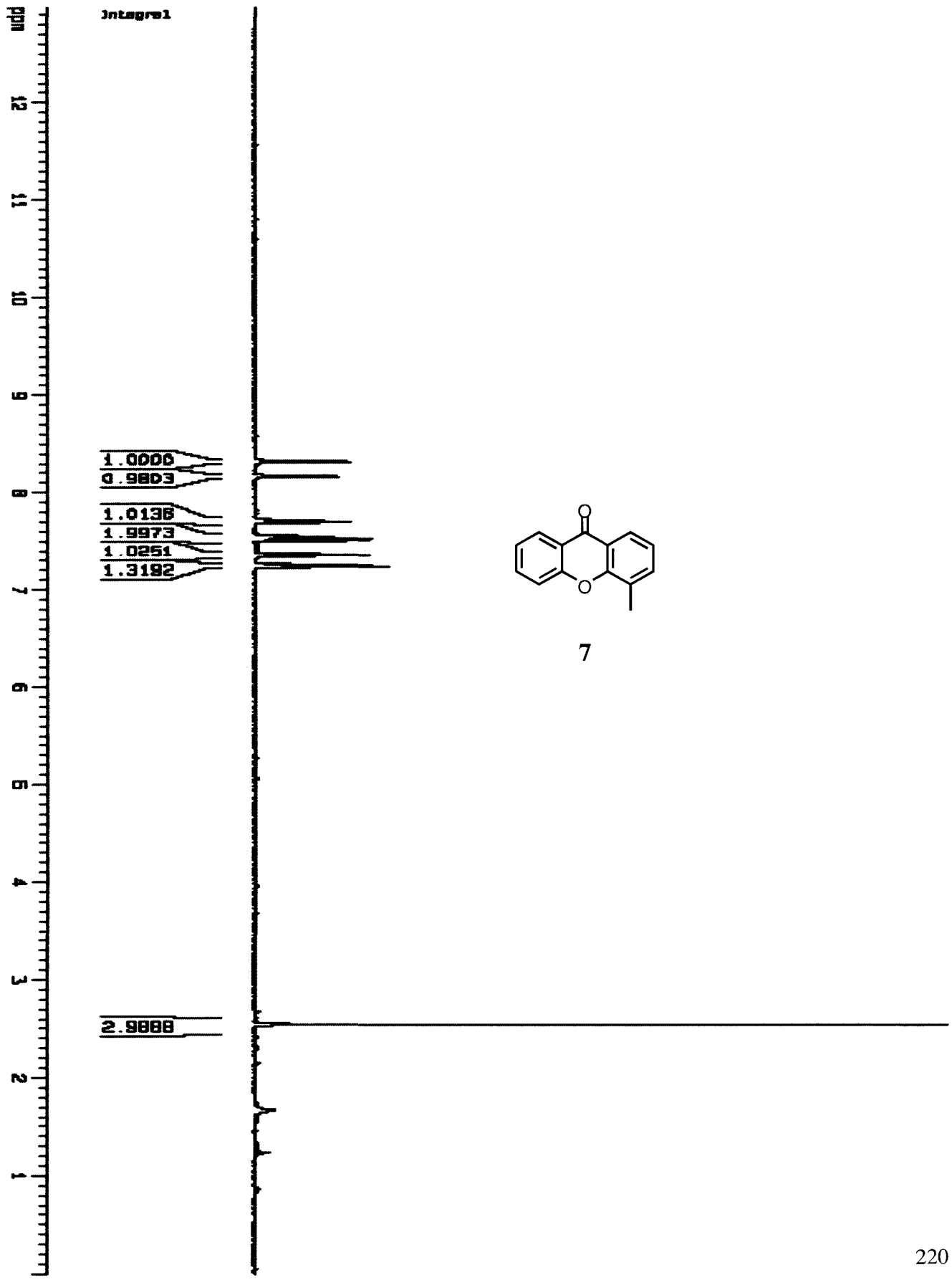

7

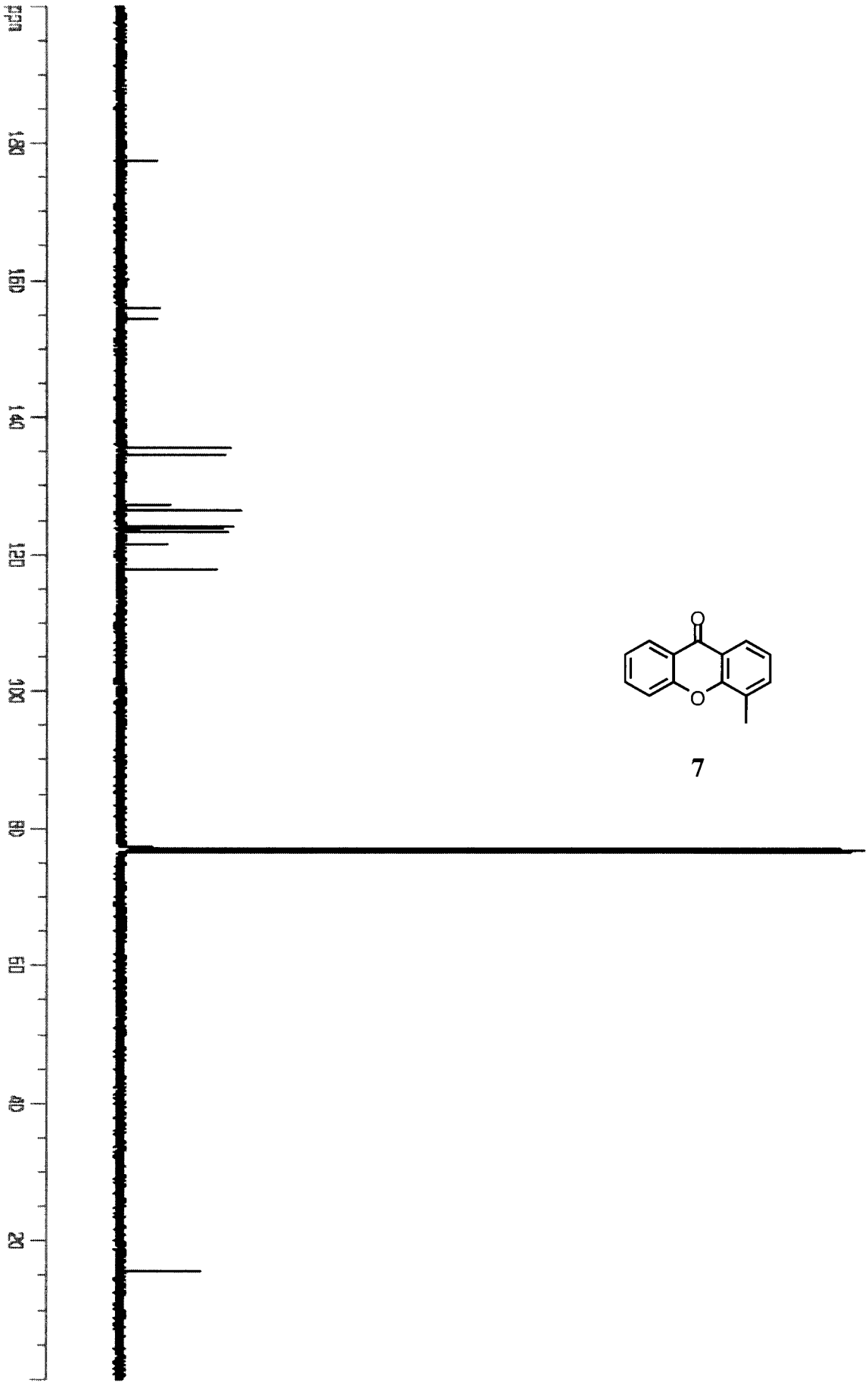

7

Chapter 3 - ^{1}H and ^{13}C or DEPTQ NMR Spectra of Products

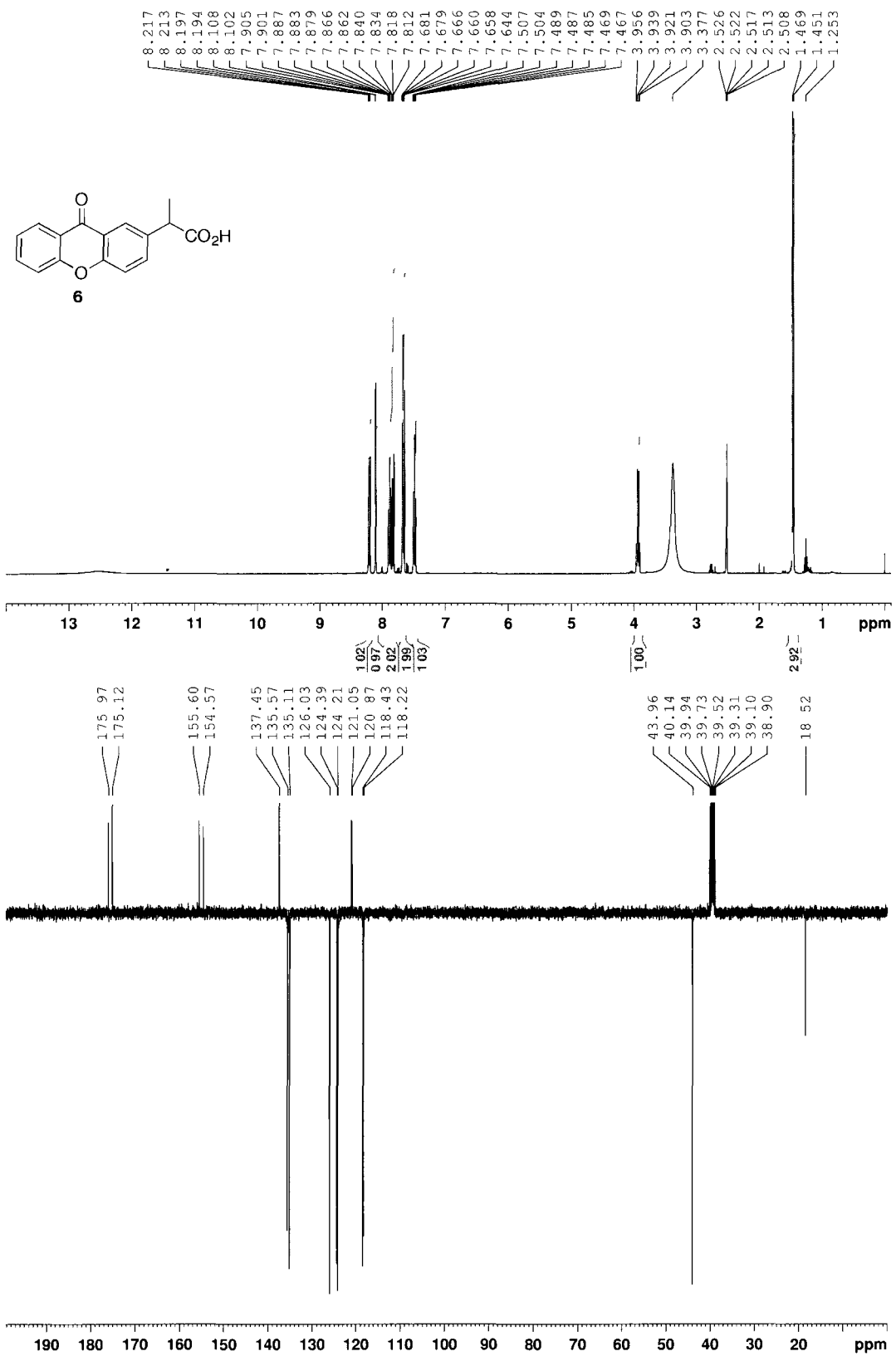
8.217
8.213
8.197
8.194
8.108
8.102
7.905
7.901
7.887
7.883
7.879
7.866
7.862
7.840
7.834
7.818
7.812
7.681
7.679
7.666
7.660
7.658
7.644
7.507
7.504
7.489
7.487
7.485
7.469
7.467
3.956
3.939
3.921
3.903
3.377
2.526
2.522
2.517
2.513
2.508
1.469
1.451
1.253
O
CO2H
O
6
13 12 11 10 9 8 7 6 5 4 3 2 1 ppm
1.02
0.97
2.02
1.99
1.03
1.00
2.92
175.97
175.12
155.60
154.57
137.45
135.57
135.11
126.03
124.39
124.21
121.05
120.87
118.43
118.22
43.96
40.14
39.94
39.73
39.52
39.31
39.10
38.90
18.52
190 180 170 160 150 140 130 120 110 100 90 80 70 60 50 40 30 20 ppm

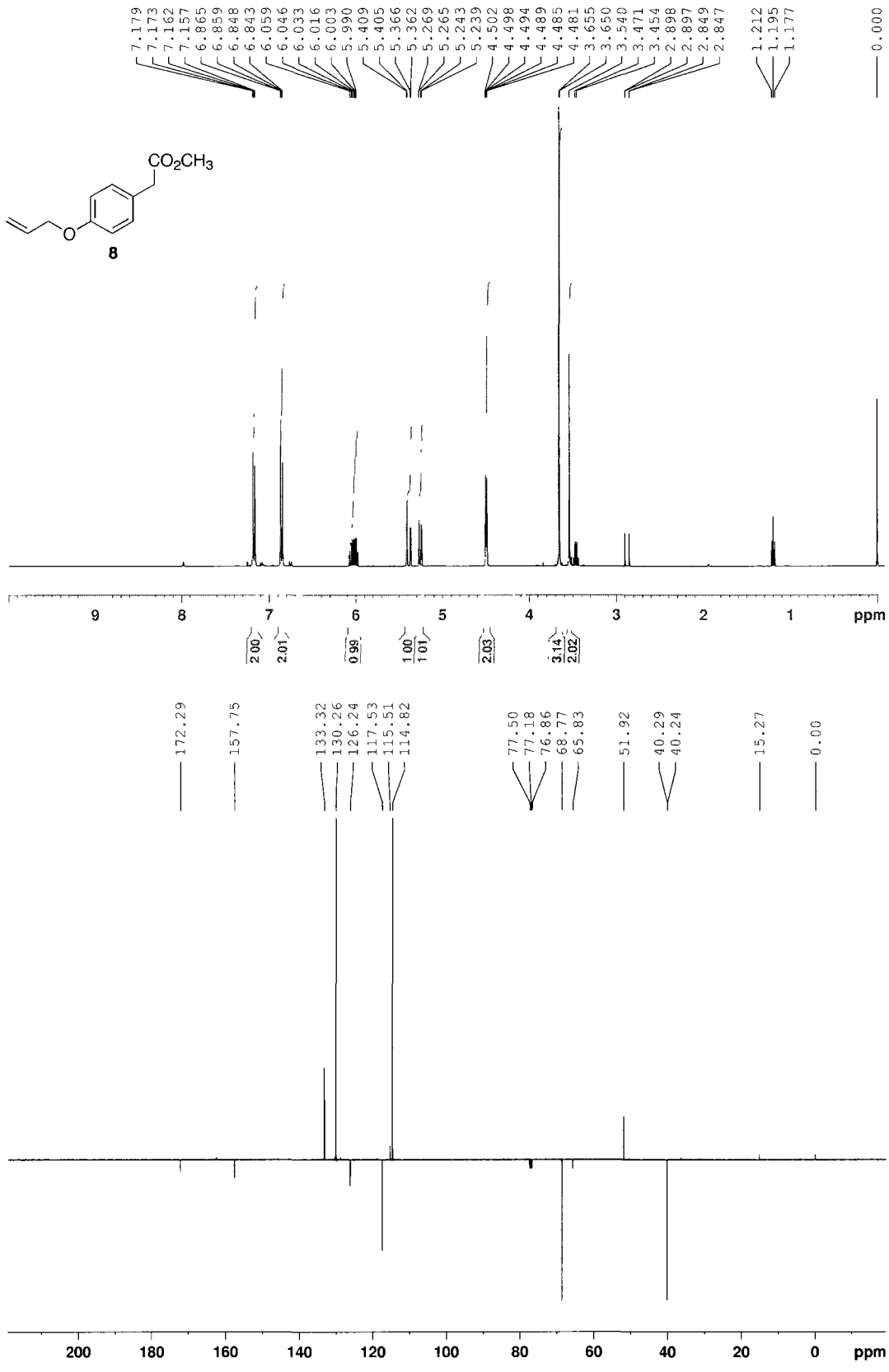
7.179
7.173
7.162
7.157
6.865
6.859
6.848
6.843
6.059
6.046
6.033
6.016
6.003
5.990
5.409
5.405
5.366
5.362
5.269
5.265
5.243
5.239
4.502
4.498
4.494
4.489
4.485
4.481
3.655
3.650
3.540
3.471
3.454
2.898
2.897
2.849
2.847
1.212
1.195
1.177
0.000
CO2CH3
O
8
9
8
7
6
5
4
3
2
1
ppm
2.00
2.01
0.99
1.00
1.01
2.03
3.14
2.02
172.29
157.75
133.32
130.26
126.24
117.53
115.51
114.82
77.50
77.18
76.86
68.77
65.83
51.92
40.29
40.24
15.27
0.00
200
180
160
140
120
100
80
60
40
20
0
ppm

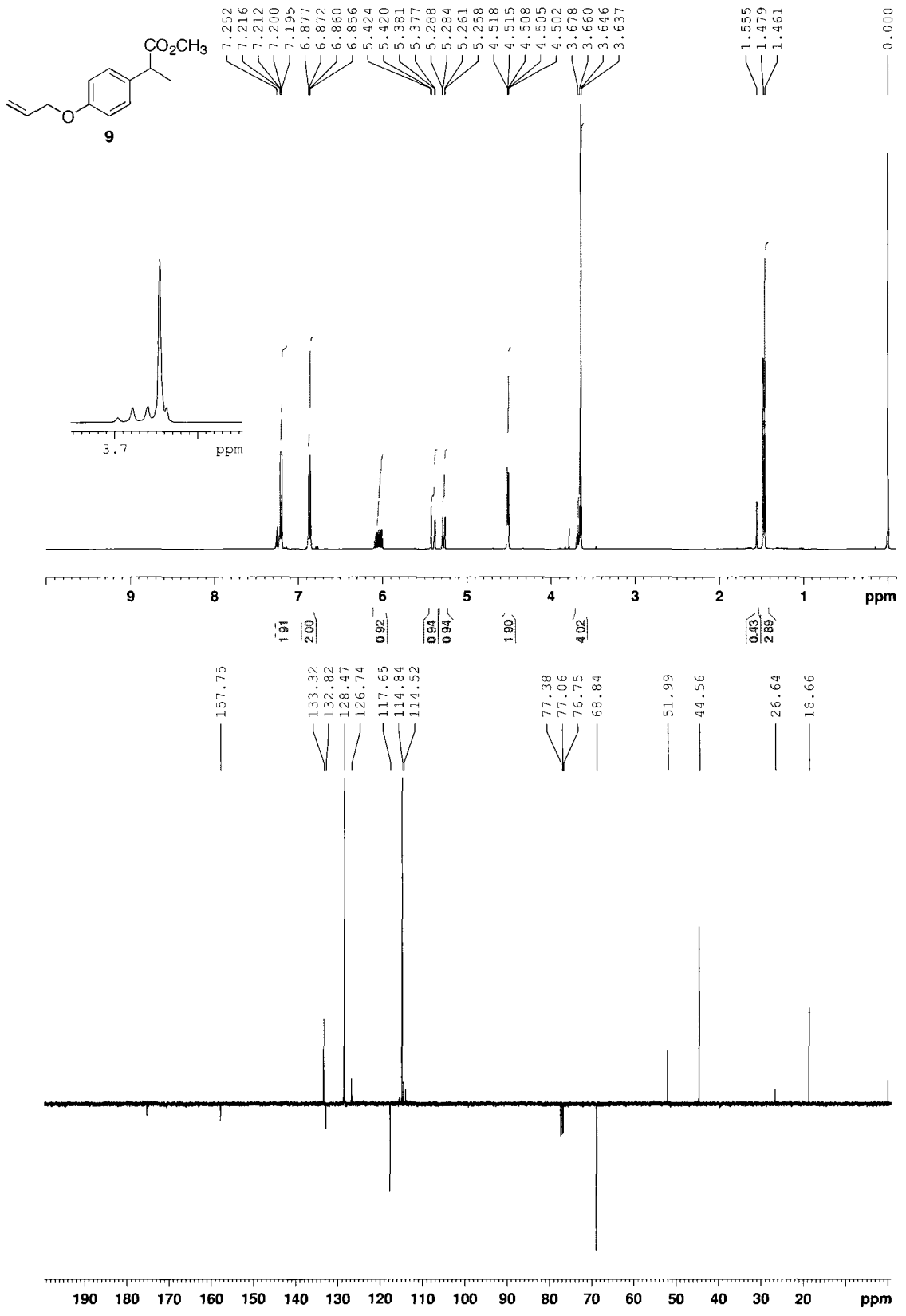
CO2CH3
O
9
7.252
7.216
7.212
7.200
7.195
6.877
6.872
6.860
6.856
5.424
5.420
5.381
5.377
5.288
5.284
5.261
5.258
4.518
4.515
4.508
4.505
4.502
3.678
3.660
3.646
3.637
1.555
1.479
1.461
0.000
3.7
ppm
9
8
7
6
5
4
3
2
1
ppm
1.91
2.00
0.92
0.94
0.94
1.90
4.02
0.43
2.89
157.75
133.32
132.82
128.47
126.74
117.65
114.84
114.52
77.38
77.06
76.75
68.84
51.99
44.56
26.64
18.66
190
180
170
160
150
140
130
120
110
100
90
80
70
60
50
40
30
20
ppm

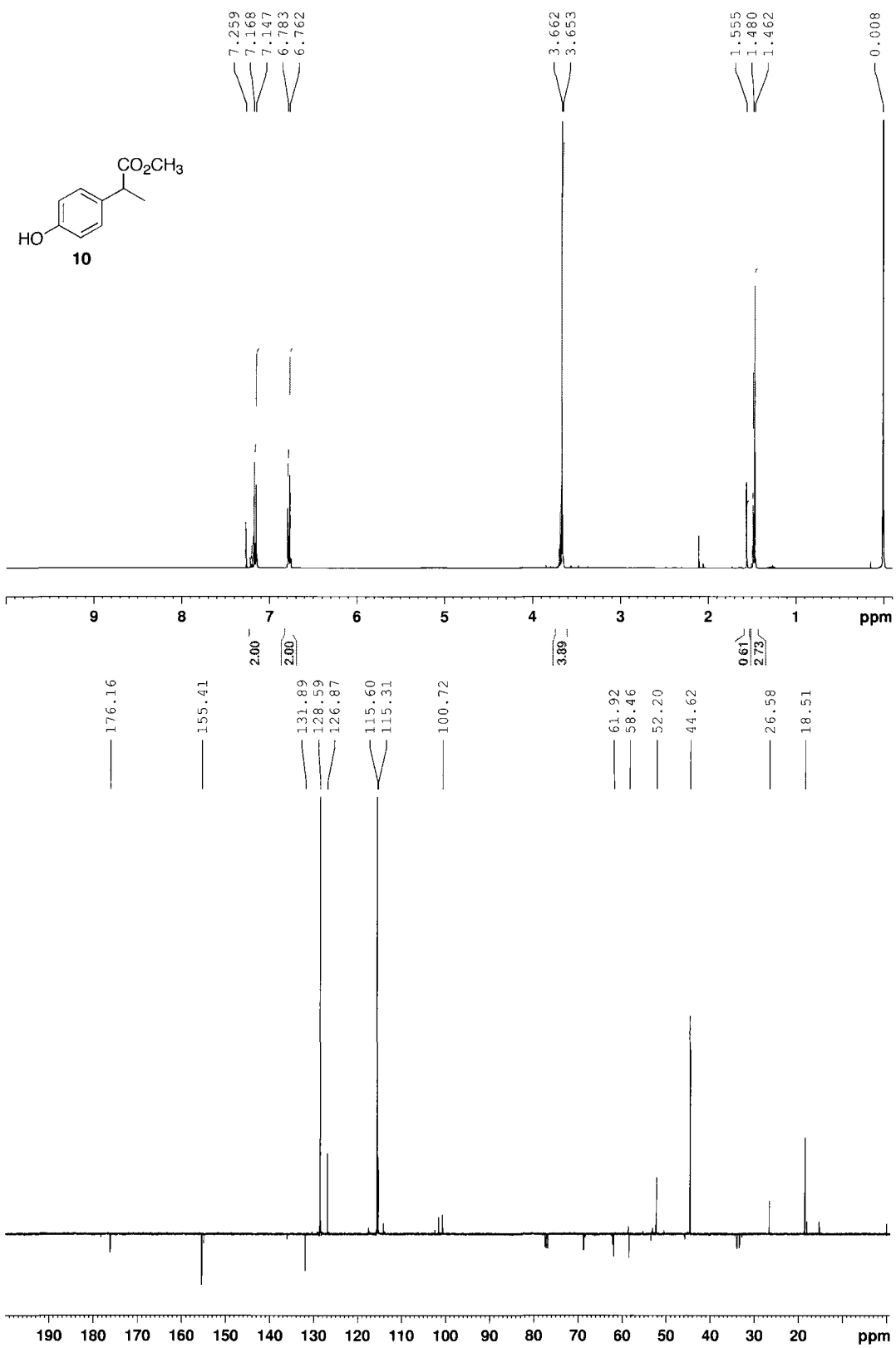
7.259
7.168
7.147
6.783
6.762
3.662
3.653
1.555
1.480
1.462
0.008
CO2CH3
HO
10
9
8
7
6
5
4
3
2
1
ppm
2.00
2.00
3.09
0.61
2.73
176.16
155.41
131.89
128.59
126.87
115.60
115.31
100.72
61.92
58.46
52.20
44.62
26.58
18.51
190
180
170
160
150
140
130
120
110
100
90
80
70
60
50
40
30
20
ppm

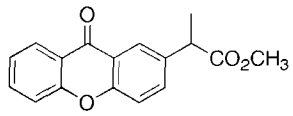
O
CO2CH3
O

12

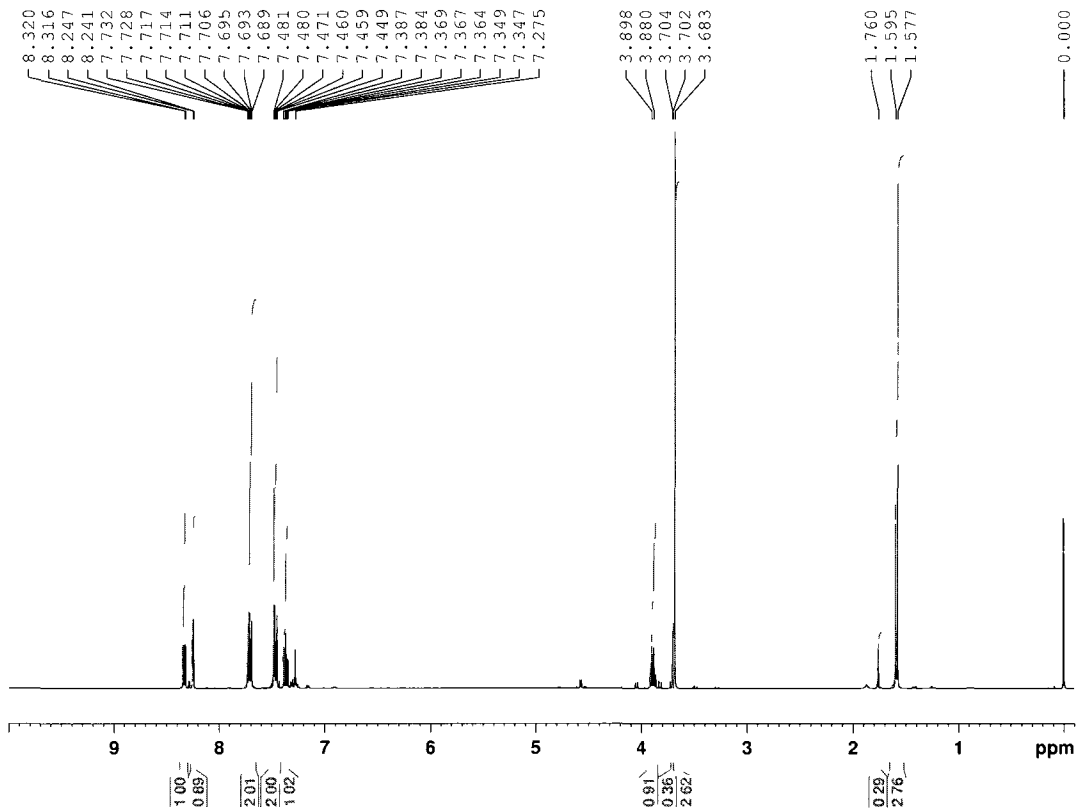
8.320
8.316
8.247
8.241
7.732
7.728
7.717
7.714
7.711
7.706
7.695
7.693
7.689
7.481
7.480
7.471
7.460
7.459
7.449
7.387
7.384
7.369
7.367
7.364
7.349
7.347
7.275
3.898
3.880
3.704
3.702
3.683
1.760
1.595
1.577
0.000
9
8
7
6
5
4
3
2
1
ppm
1.00
0.89
2.01
2.00
1.02
0.91
0.36
2.62
0.29
2.76

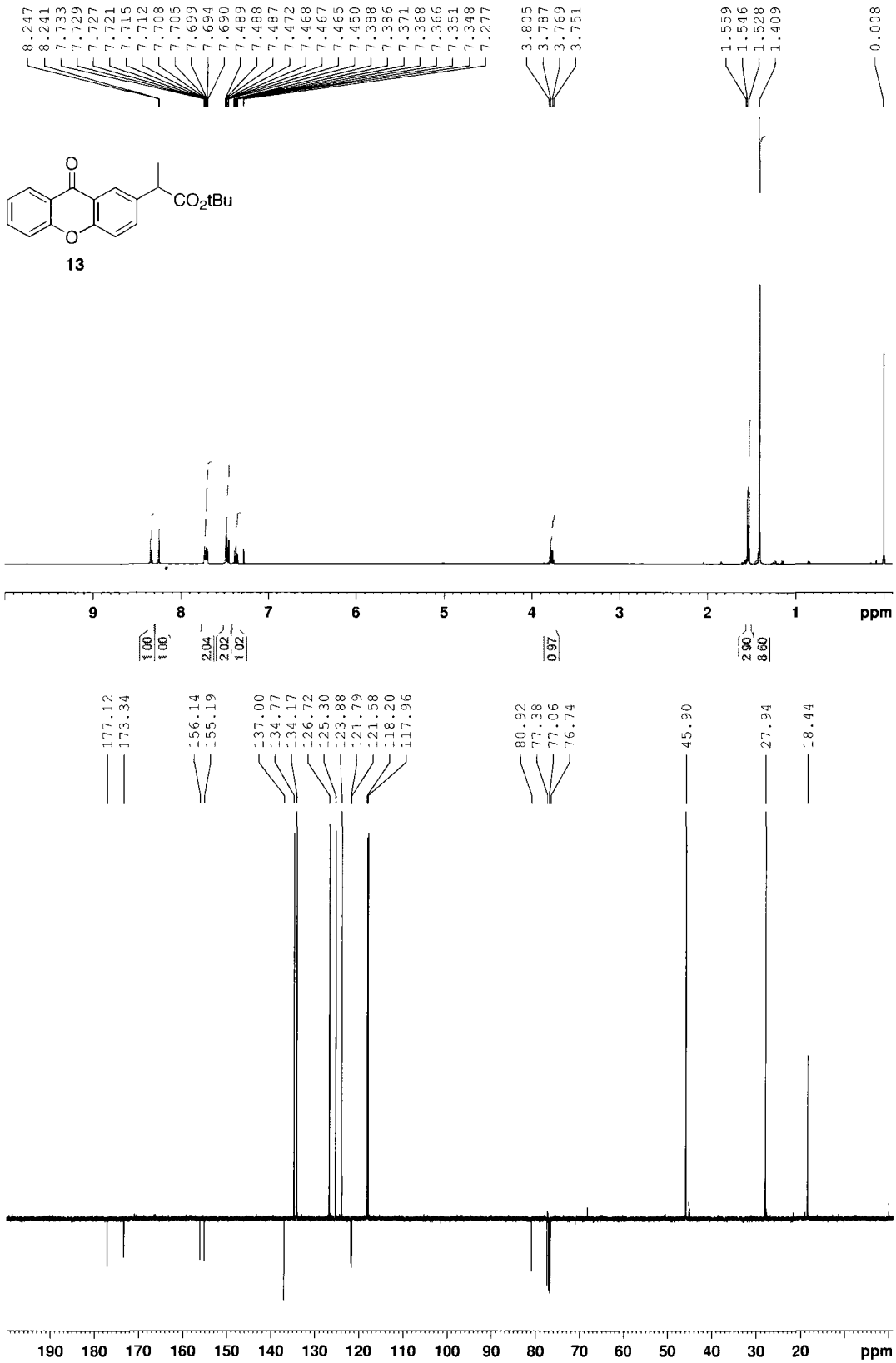
8.247
8.241
7.733
7.729
7.727
7.721
7.715
7.712
7.708
7.705
7.699
7.694
7.690
7.489
7.488
7.487
7.472
7.468
7.467
7.465
7.450
7.388
7.386
7.371
7.368
7.366
7.351
7.348
7.277
3.805
3.787
3.769
3.751
1.559
1.546
1.528
1.409
0.008
O
O
CO2tBu
13
9
8
7
6
5
4
3
2
1
ppm
1.00
1.00
2.04
2.02
1.02
0.97
2.90
8.60
177.12
173.34
156.14
155.19
137.00
134.77
134.17
126.72
125.30
123.88
121.79
121.58
118.20
117.96
80.92
77.38
77.06
76.74
45.90
27.94
18.44
190
180
170
160
150
140
130
120
110
100
90
80
70
60
50
40
30
20
ppm

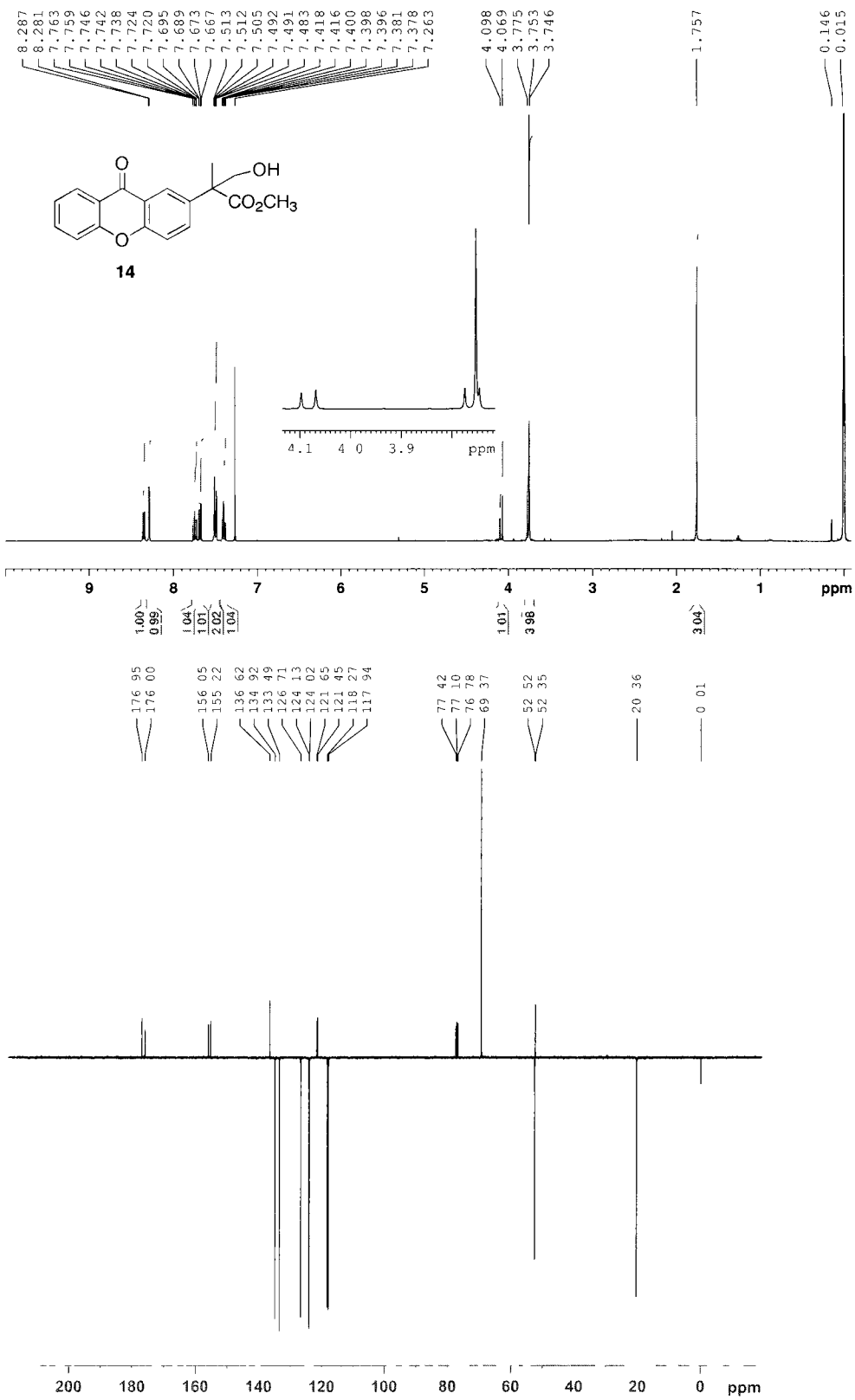
8.287
8.281
7.763
7.759
7.746
7.742
7.738
7.724
7.720
7.695
7.689
7.673
7.667
7.513
7.512
7.505
7.492
7.491
7.483
7.418
7.416
7.400
7.398
7.396
7.381
7.378
7.263
4.098
4.069
3.775
3.753
3.746
1.757
0.146
0.015
OH
CO2CH3
O
O
14
4.1
4.0
3.9
ppm
9
8
7
6
5
4
3
2
1
ppm
1.00
0.99
1.04
1.01
2.02
1.04
1.01
3.98
3.04
176.95
176.00
156.05
155.22
136.62
134.92
133.49
126.71
124.13
124.02
121.65
121.45
118.27
117.94
77.42
77.10
76.78
69.37
52.52
52.35
20.36
0.01
200
180
160
140
120
100
80
60
40
20
0
ppm

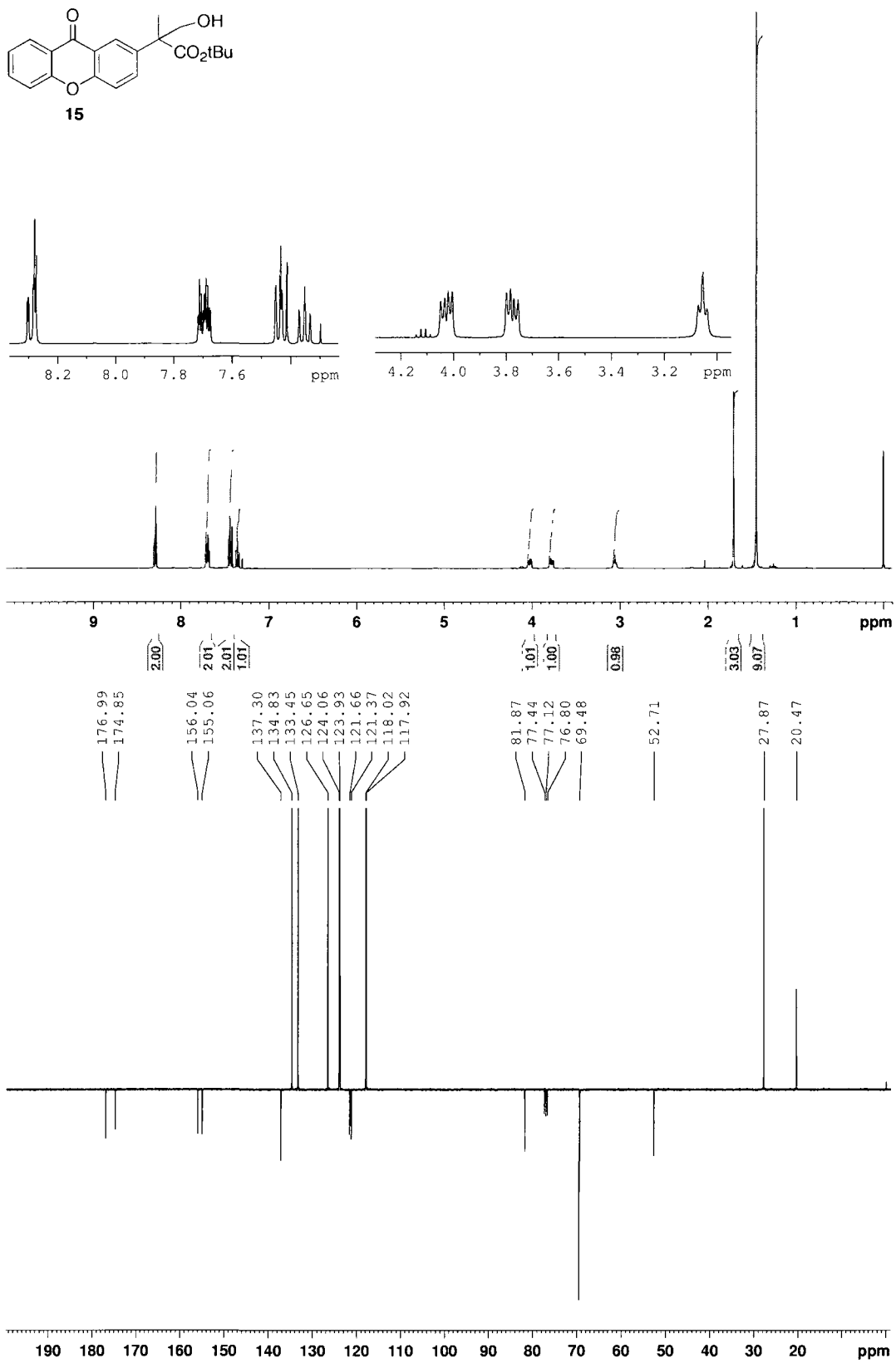
O
OH
CO2tBu
O
15
8.2
8.0
7.8
7.6
ppm
4.2
4.0
3.8
3.6
3.4
3.2
ppm
9
8
7
6
5
4
3
2
1
ppm
2.00
2.01
2.01
1.01
1.01
1.00
0.98
3.03
9.07
176.99
174.85
156.04
155.06
137.30
134.83
133.45
126.65
124.06
123.93
121.66
121.37
118.02
117.92
81.87
77.44
77.12
76.80
69.48
52.71
27.87
20.47
190
180
170
160
150
140
130
120
110
100
90
80
70
60
50
40
30
20
ppm

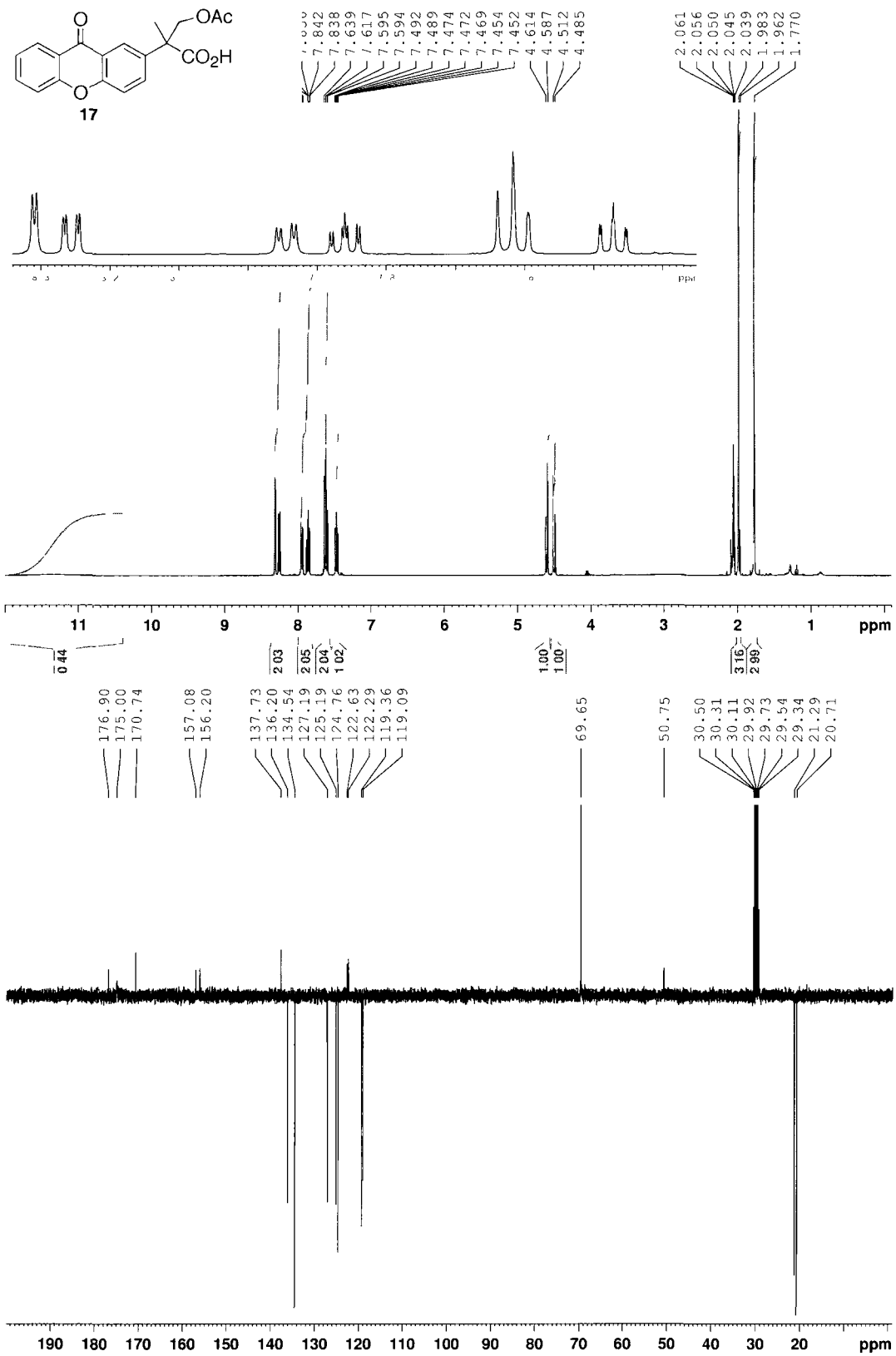
OAc
CO2H
O
O
17
7.842
7.838
7.639
7.617
7.595
7.594
7.492
7.489
7.474
7.472
7.469
7.454
7.452
4.614
4.587
4.512
4.485
2.061
2.056
2.050
2.045
2.039
1.983
1.962
1.770
ppm
0.44
2.03
2.05
2.04
1.02
1.00
1.00
3.16
2.90
176.90
175.00
170.74
157.08
156.20
137.73
136.20
134.54
127.19
125.19
124.76
122.63
122.29
119.36
119.09
69.65
50.75
30.50
30.31
30.11
29.92
29.73
29.54
29.34
21.29
20.71
ppm

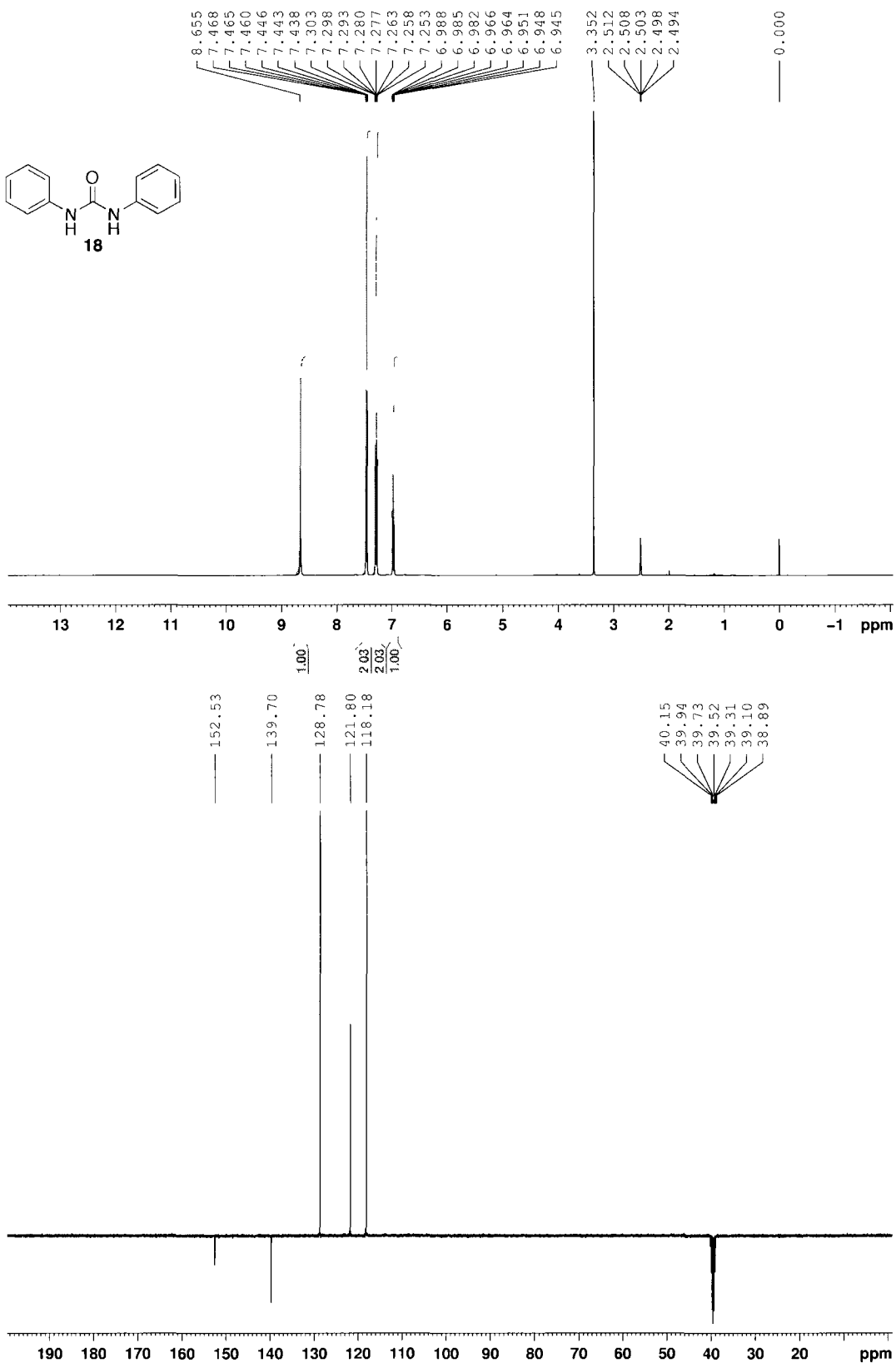
8.655
7.468
7.465
7.460
7.446
7.443
7.438
7.303
7.298
7.293
7.280
7.277
7.263
7.258
7.253
6.988
6.985
6.982
6.966
6.964
6.951
6.948
6.945
3.352
2.512
2.508
2.503
2.498
2.494
0.000
18
13 12 11 10 9 8 7 6 5 4 3 2 1 0 −1 ppm
1.00
2.03
2.03
1.00
152.53
139.70
128.78
121.80
118.18
40.15
39.94
39.73
39.52
39.31
39.10
38.89
190 180 170 160 150 140 130 120 110 100 90 80 70 60 50 40 30 20 ppm

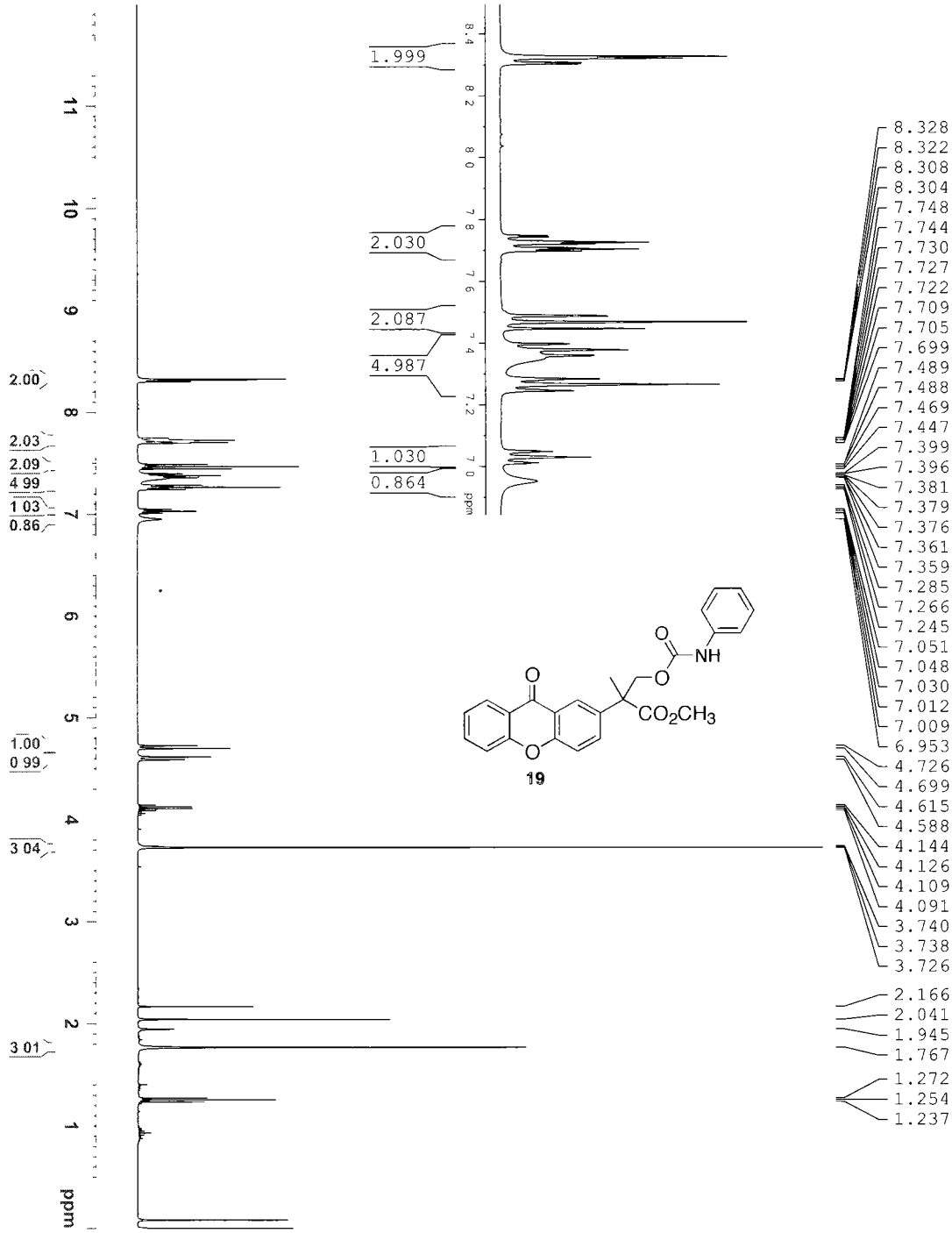
1.999
2.030
2.087
4.987
1.030
0.864
2.00
2.03
2.09
4.99
1.03
0.86
1.00
0.99
3.04
3.01
ppm
8.328
8.322
8.308
8.304
7.748
7.744
7.730
7.727
7.722
7.709
7.705
7.699
7.489
7.488
7.469
7.447
7.399
7.396
7.381
7.379
7.376
7.361
7.359
7.285
7.266
7.245
7.051
7.048
7.030
7.012
7.009
6.953
4.726
4.699
4.615
4.588
4.144
4.126
4.109
4.091
3.740
3.738
3.726
2.166
2.041
1.945
1.767
1.272
1.254
1.237
NH
CO2CH3
19

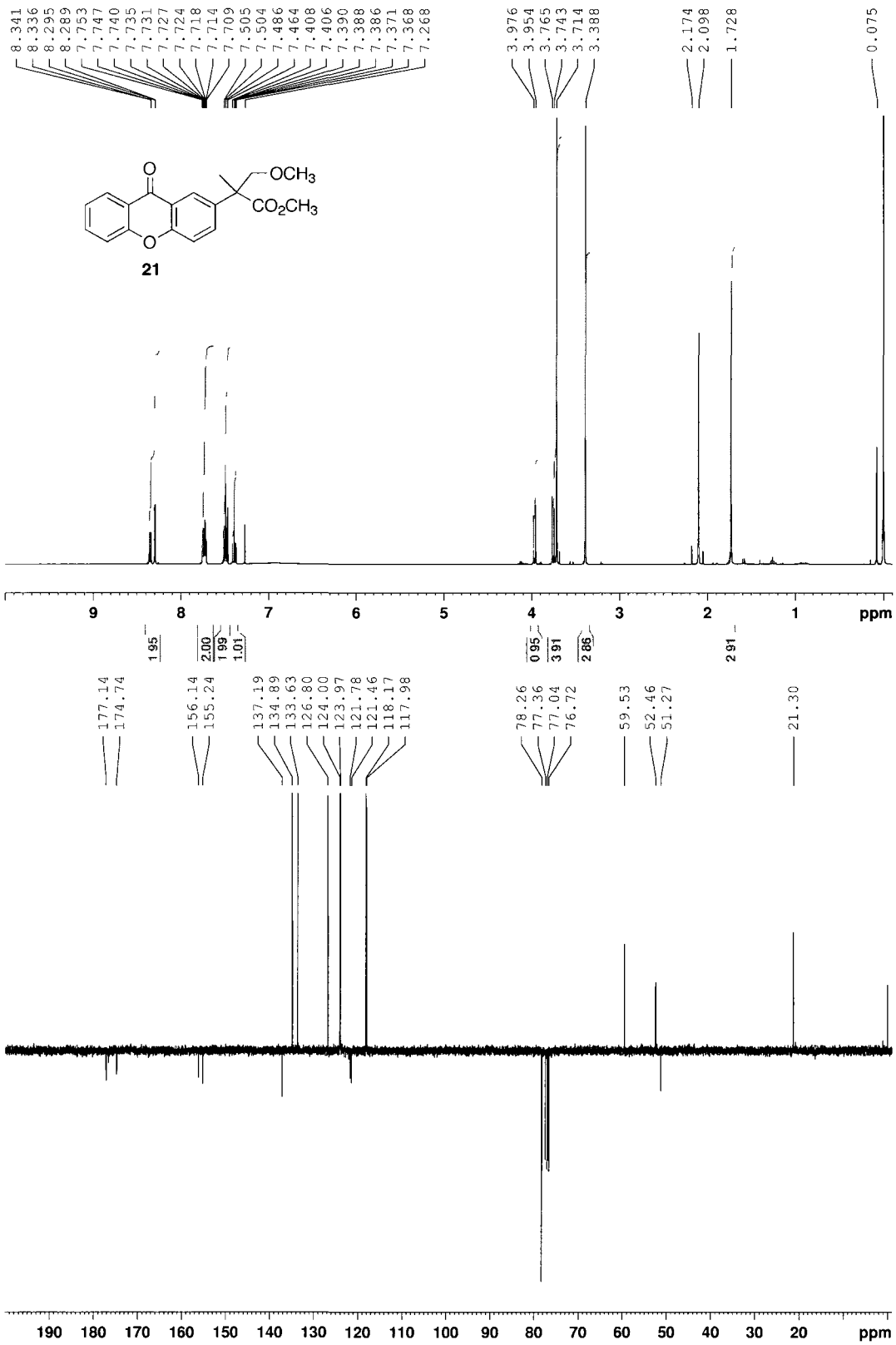
8.341
8.336
8.295
8.289
7.753
7.747
7.740
7.735
7.731
7.727
7.724
7.718
7.714
7.709
7.505
7.504
7.486
7.464
7.408
7.406
7.390
7.388
7.386
7.371
7.368
7.268
3.976
3.954
3.765
3.743
3.714
3.388
2.174
2.098
1.728
0.075
OCH3
CO2CH3
O
O
21
ppm
1.95
2.00
1.99
1.01
0.95
3.91
2.86
2.91
177.14
174.74
156.14
155.24
137.19
134.89
133.63
126.80
124.00
123.97
121.78
121.46
118.17
117.98
78.26
77.36
77.04
76.72
59.53
52.46
51.27
21.30
ppm

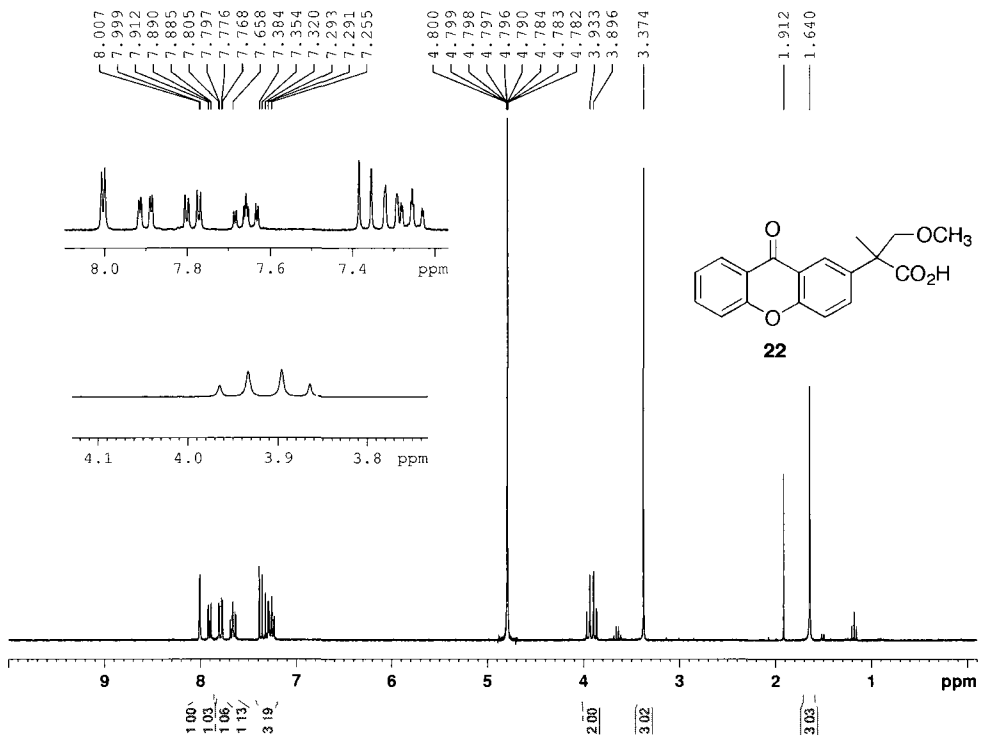
8.007
7.999
7.912
7.890
7.885
7.805
7.797
7.776
7.768
7.658
7.384
7.354
7.320
7.293
7.291
7.255
4.800
4.799
4.798
4.797
4.796
4.790
4.784
4.783
4.782
3.933
3.896
3.374
1.912
1.640
8.0
7.8
7.6
7.4
ppm
4.1
4.0
3.9
3.8
ppm
O
OCH3
CO2H
O
22
9
8
7
6
5
4
3
2
1
ppm
1.00
1.03
1.06
1.13
3.19
2.00
3.02
3.03

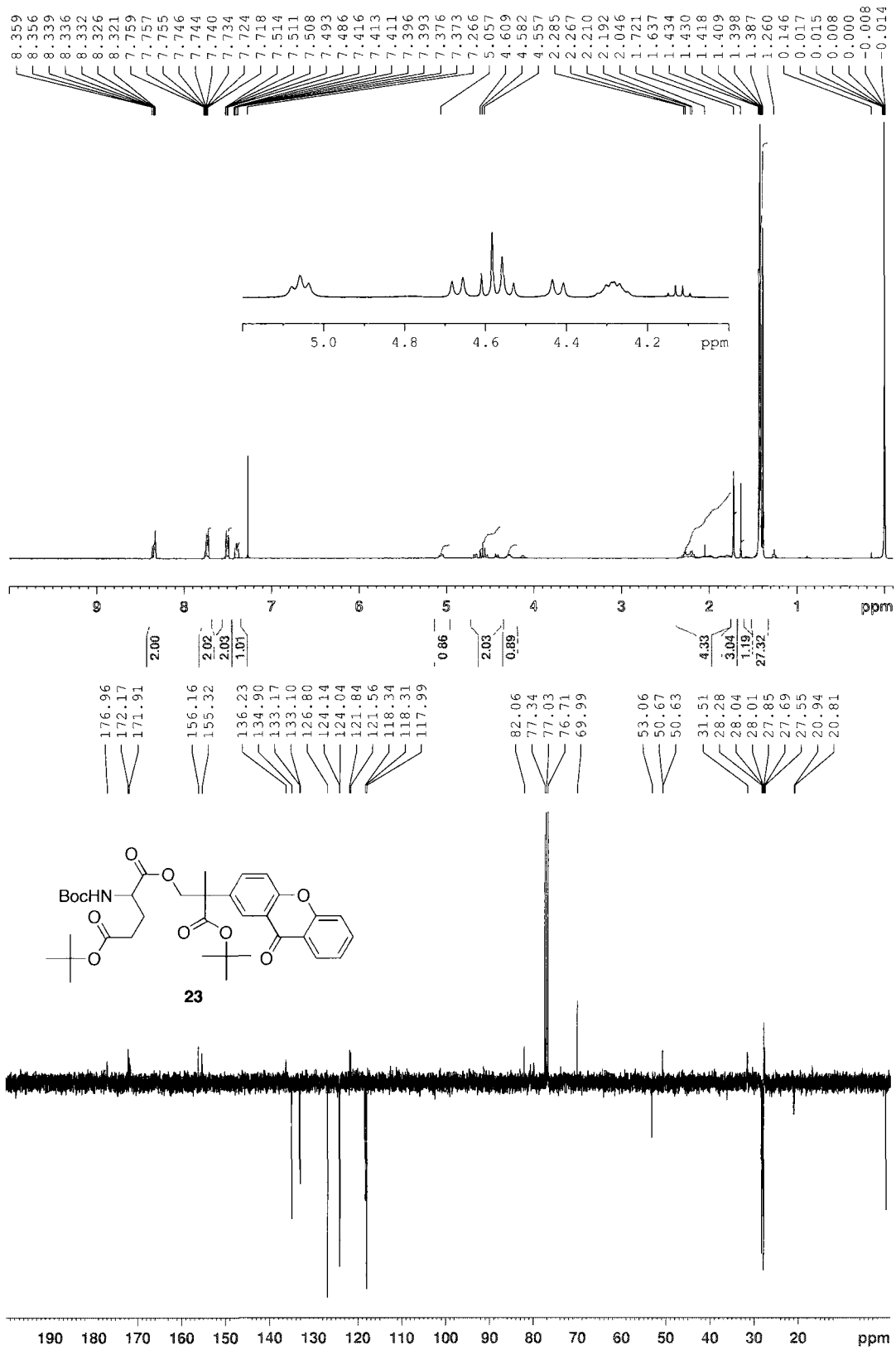
8.359
8.356
8.339
8.336
8.332
8.326
8.321
7.759
7.757
7.755
7.746
7.744
7.740
7.734
7.724
7.718
7.514
7.511
7.508
7.493
7.486
7.416
7.413
7.411
7.396
7.393
7.376
7.373
7.266
5.057
4.609
4.582
4.557
2.285
2.267
2.210
2.192
2.046
1.721
1.637
1.434
1.430
1.418
1.409
1.398
1.387
1.260
0.146
0.017
0.015
0.008
0.000
-0.008
-0.014
5.0
4.8
4.6
4.4
4.2
ppm
9
8
7
6
5
4
3
2
1
ppm
2.00
2.02
2.03
1.01
0.86
2.03
0.89
4.33
3.04
1.19
27.32
176.96
172.17
171.91
156.16
155.32
136.23
134.90
133.17
133.10
126.80
124.14
124.04
121.84
121.56
118.34
118.31
117.99
82.06
77.34
77.03
76.71
69.99
53.06
50.67
50.63
31.51
28.28
28.04
28.01
27.85
27.69
27.55
20.94
20.81
BocHN
O
O
O
O
O
O
O
O
23
190
180
170
160
150
140
130
120
110
100
90
80
70
60
50
40
30
20
ppm

Chapter 4 - ^{1}H and ^{13}C or DEPTQ NMR Spectra of Products

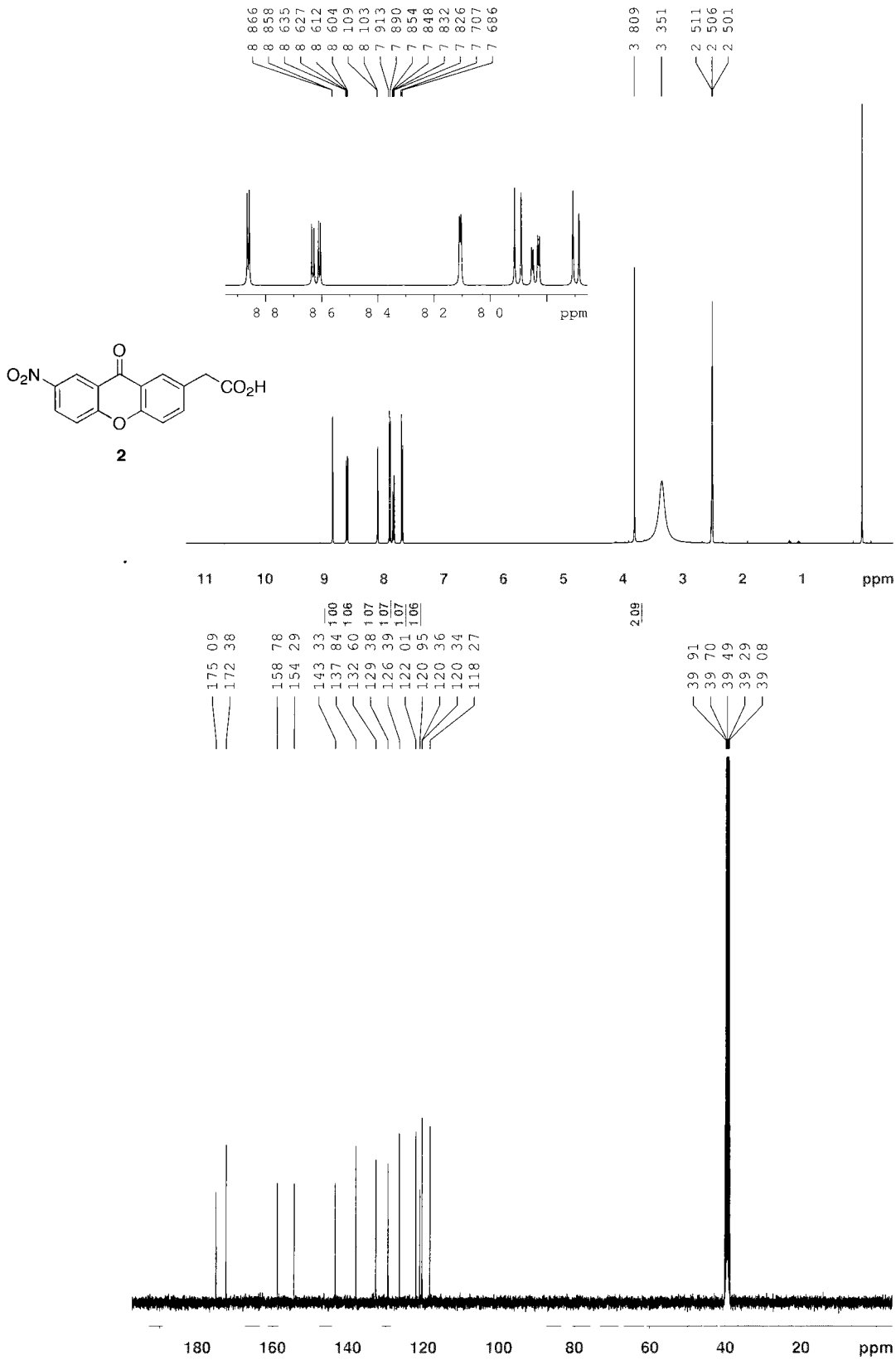
8.866
8.858
8.635
8.627
8.612
8.604
8.109
8.103
7.913
7.890
7.854
7.848
7.832
7.826
7.707
7.686
3.809
3.351
2.511
2.506
2.501
O2N
CO2H
O
O
2
ppm
11 10 9 8 7 6 5 4 3 2 1 ppm
175.09
172.38
158.78
154.29
143.33
137.84
132.60
129.38
126.39
122.01
120.95
120.36
120.34
118.27
100
106
107
107
106
2.09
39.91
39.70
39.49
39.29
39.08
180 160 140 120 100 80 60 40 20 ppm

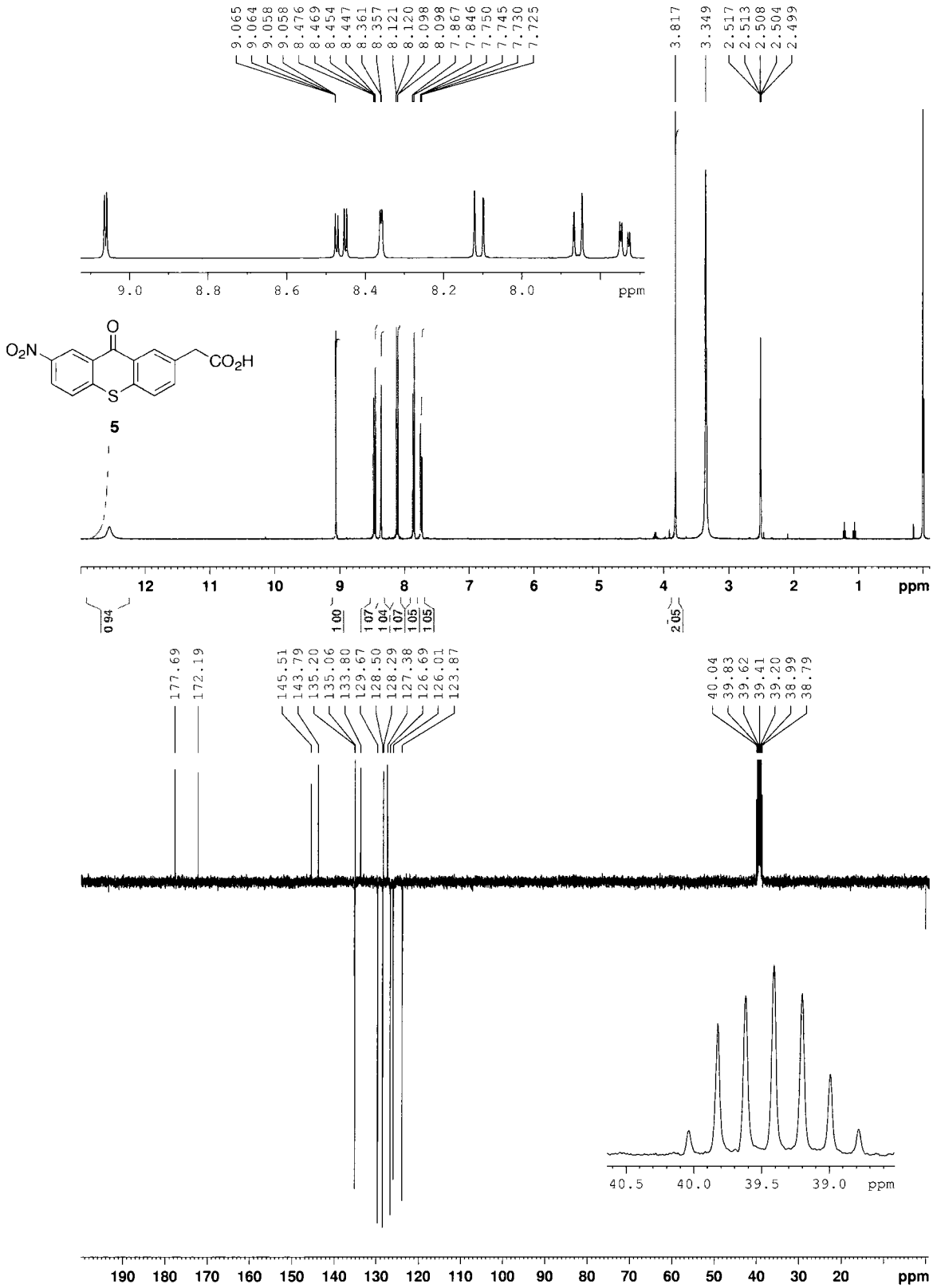
9.065
9.064
9.058
9.058
8.476
8.469
8.454
8.447
8.361
8.357
8.121
8.120
8.098
8.098
7.867
7.846
7.750
7.745
7.730
7.725
3.817
3.349
2.517
2.513
2.508
2.504
2.499
9.0
8.8
8.6
8.4
8.2
8.0
ppm
O
O2N
CO2H
S
5
12
11
10
9
8
7
6
5
4
3
2
1
ppm
0.94
1.00
1.07
1.04
1.07
1.05
1.05
2.05
177.69
172.19
145.51
143.79
135.20
135.06
133.80
129.67
128.50
128.29
127.38
126.69
126.01
123.87
40.04
39.83
39.62
39.41
39.20
38.99
38.79
40.5
40.0
39.5
39.0
ppm
190
180
170
160
150
140
130
120
110
100
90
80
70
60
50
40
30
20
ppm

Chapter 5 - ^{1}H and ^{13}C or DEPTQ NMR Spectra of Products

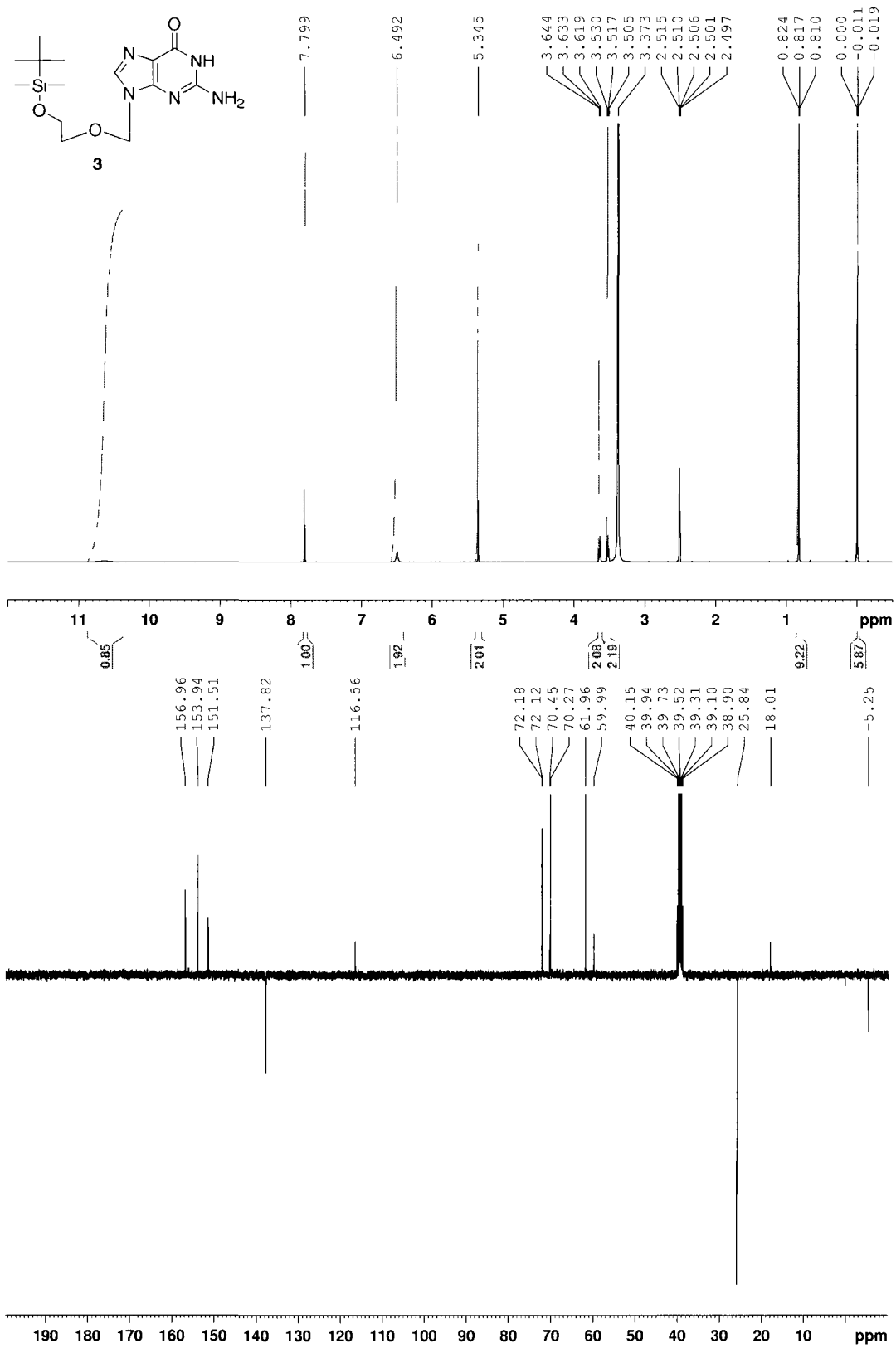
3
7.799
6.492
5.345
3.644
3.633
3.619
3.530
3.517
3.505
3.373
2.515
2.510
2.506
2.501
2.497
0.824
0.817
0.810
0.000
-0.011
-0.019
ppm
0.85
1.00
1.92
2.01
2.08
2.19
9.22
5.87
156.96
153.94
151.51
137.82
116.56
72.18
72.12
70.45
70.27
61.96
59.99
40.15
39.94
39.73
39.52
39.31
39.10
38.90
25.84
18.01
-5.25
ppm

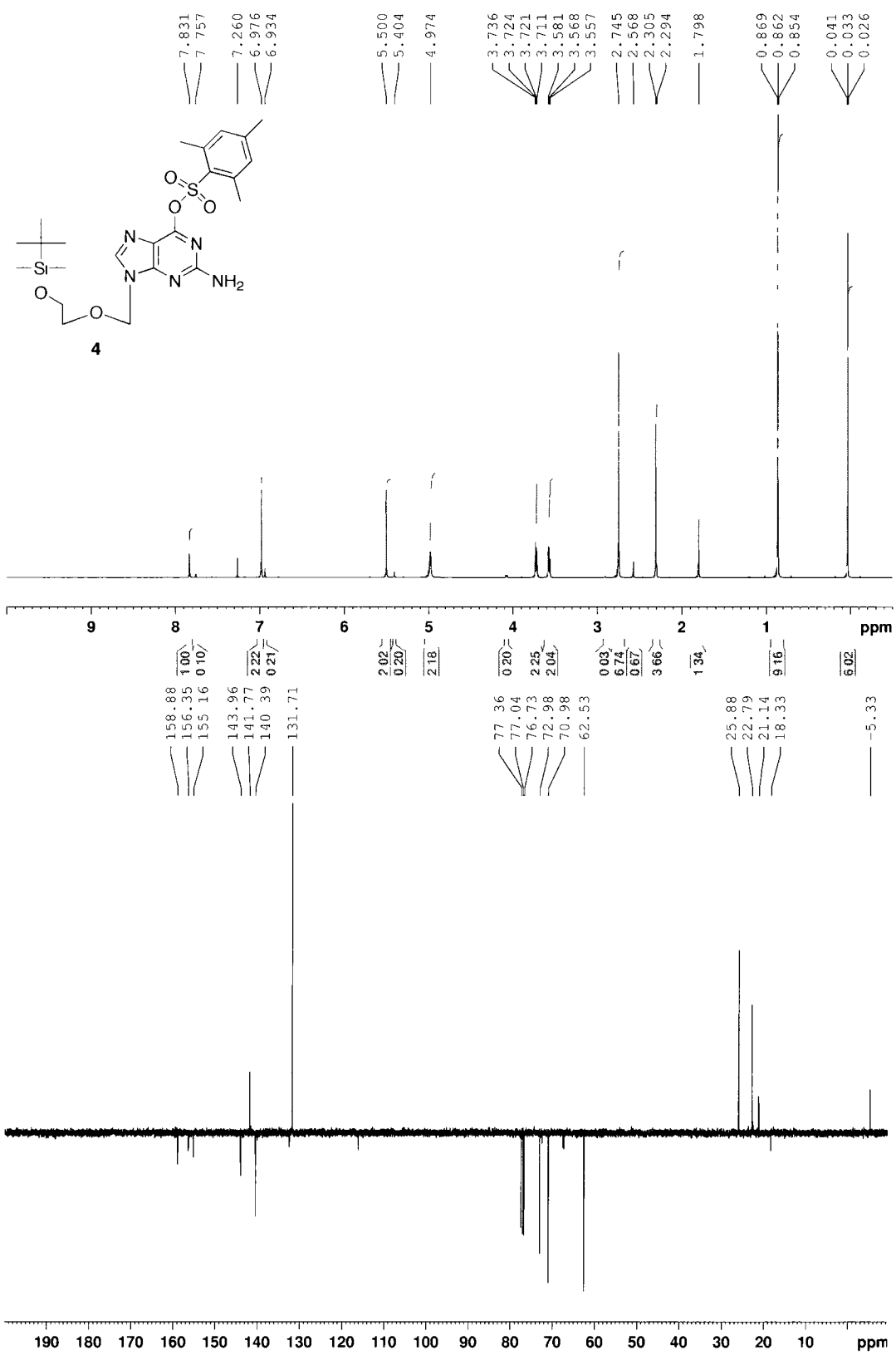
7.831
7.757
7.260
6.976
6.934
5.500
5.404
4.974
3.736
3.724
3.721
3.711
3.581
3.568
3.557
2.745
2.568
2.305
2.294
1.798
0.869
0.862
0.854
0.041
0.033
0.026
4
ppm
158.88
156.35
155.16
143.96
141.77
140.39
131.71
77.36
77.04
76.73
72.98
70.98
62.53
25.88
22.79
21.14
18.33
-5.33
ppm

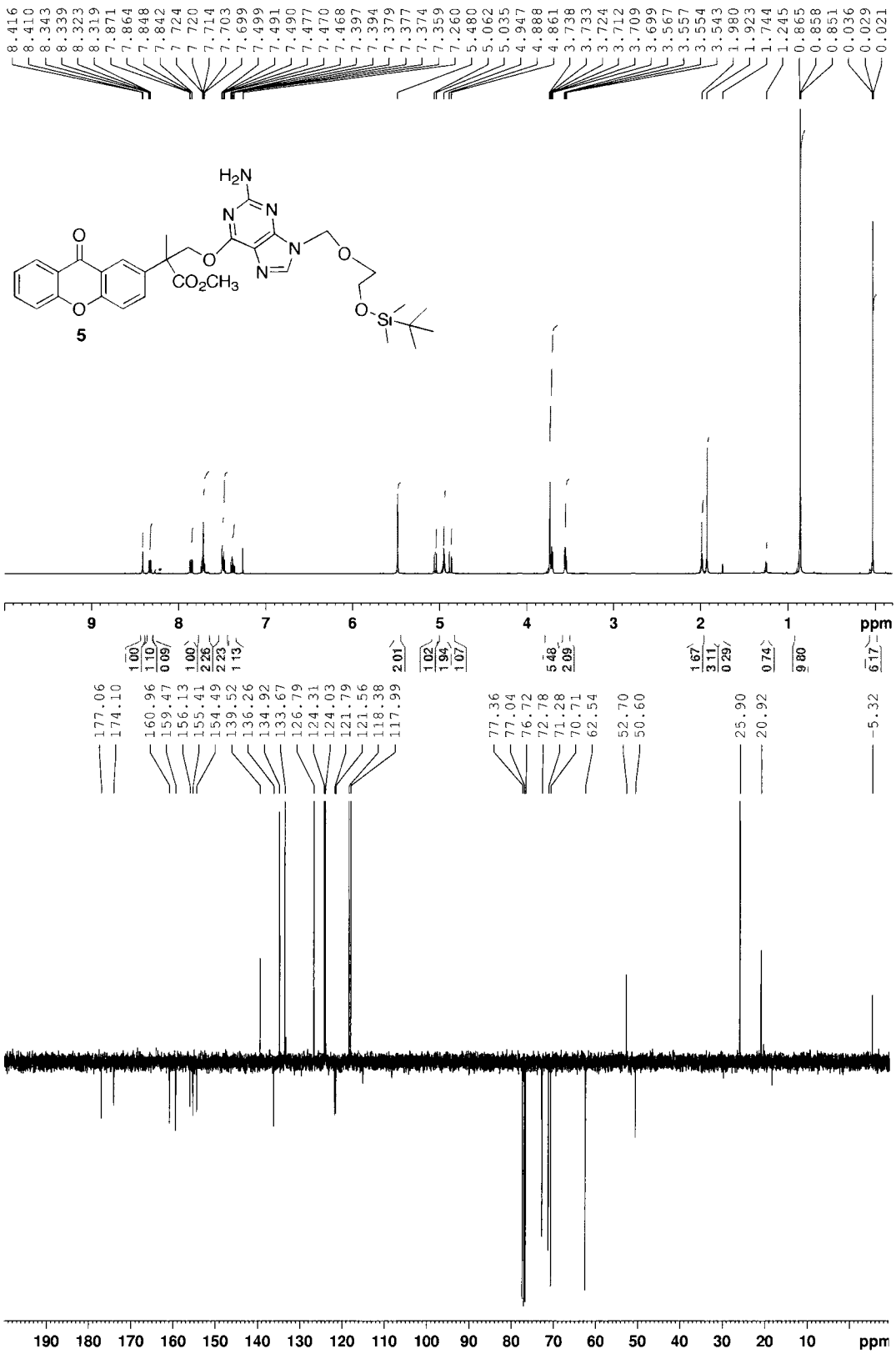
8.416
8.410
8.343
8.339
8.323
8.319
7.871
7.864
7.848
7.842
7.724
7.720
7.714
7.703
7.699
7.499
7.491
7.490
7.477
7.470
7.468
7.397
7.394
7.379
7.377
7.374
7.359
7.260
5.480
5.062
5.035
4.947
4.888
4.861
3.738
3.733
3.724
3.712
3.709
3.699
3.567
3.557
3.554
3.543
1.980
1.923
1.744
1.245
0.865
0.858
0.851
0.036
0.029
0.021
H2N
N
N
N
N
O
O
O
O
CO2CH3
O
Si
5
9
8
7
6
5
4
3
2
1
ppm
1.00
1.10
0.09
1.00
2.26
2.23
1.13
2.01
1.02
1.94
1.07
5.48
2.09
1.67
3.11
0.29
0.74
9.80
6.17
177.06
174.10
160.96
159.47
156.13
155.41
154.49
139.52
136.26
134.92
133.67
126.79
124.31
124.03
121.79
121.56
118.38
117.99
77.36
77.04
76.72
72.78
71.28
70.71
62.54
52.70
50.60
25.90
20.92
5.32
190
180
170
160
150
140
130
120
110
100
90
80
70
60
50
40
30
20
10
ppm

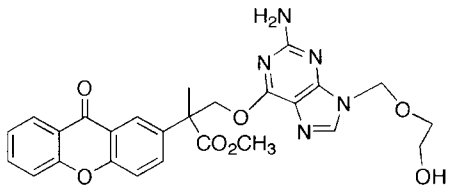
H2N
N
N
O
O
N
O
N
CO2CH3
OH

6

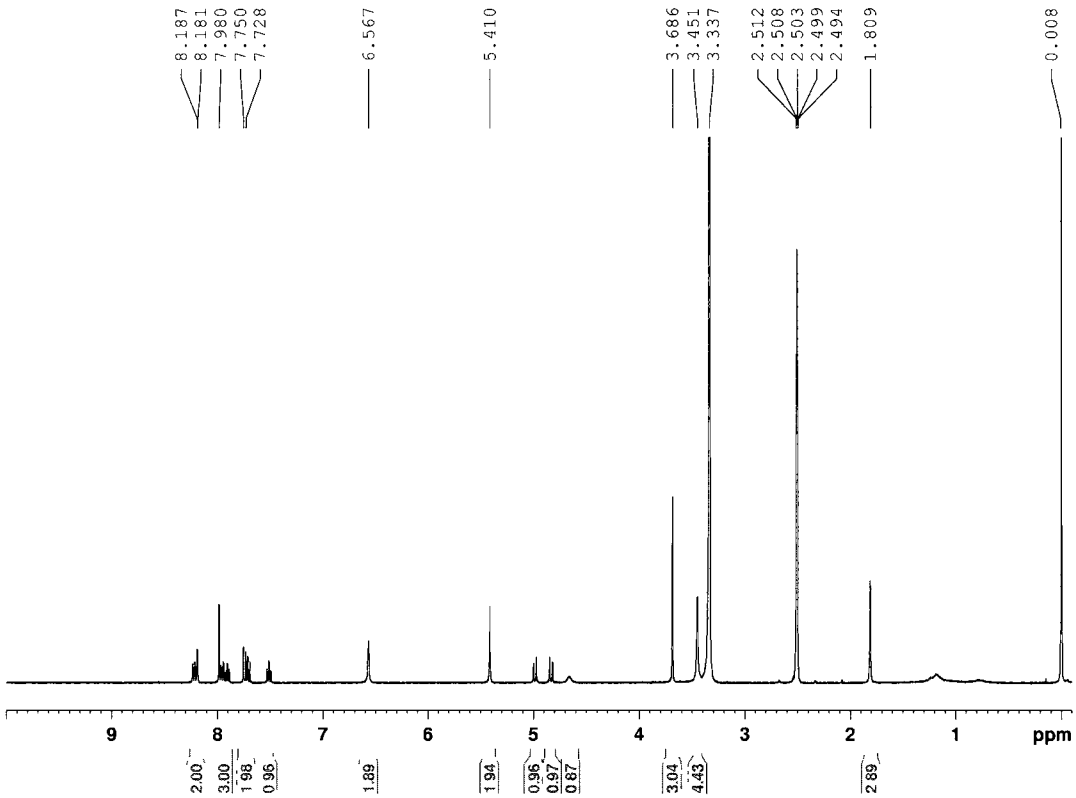
8.187
8.181
7.980
7.750
7.728
6.567
5.410
3.686
3.451
3.337
2.512
2.508
2.503
2.499
2.494
1.809
0.008
9
8
7
6
5
4
3
2
1
ppm
2.00
3.00
1.98
0.96
1.89
1.94
0.96
0.97
0.87
3.04
4.43
2.89

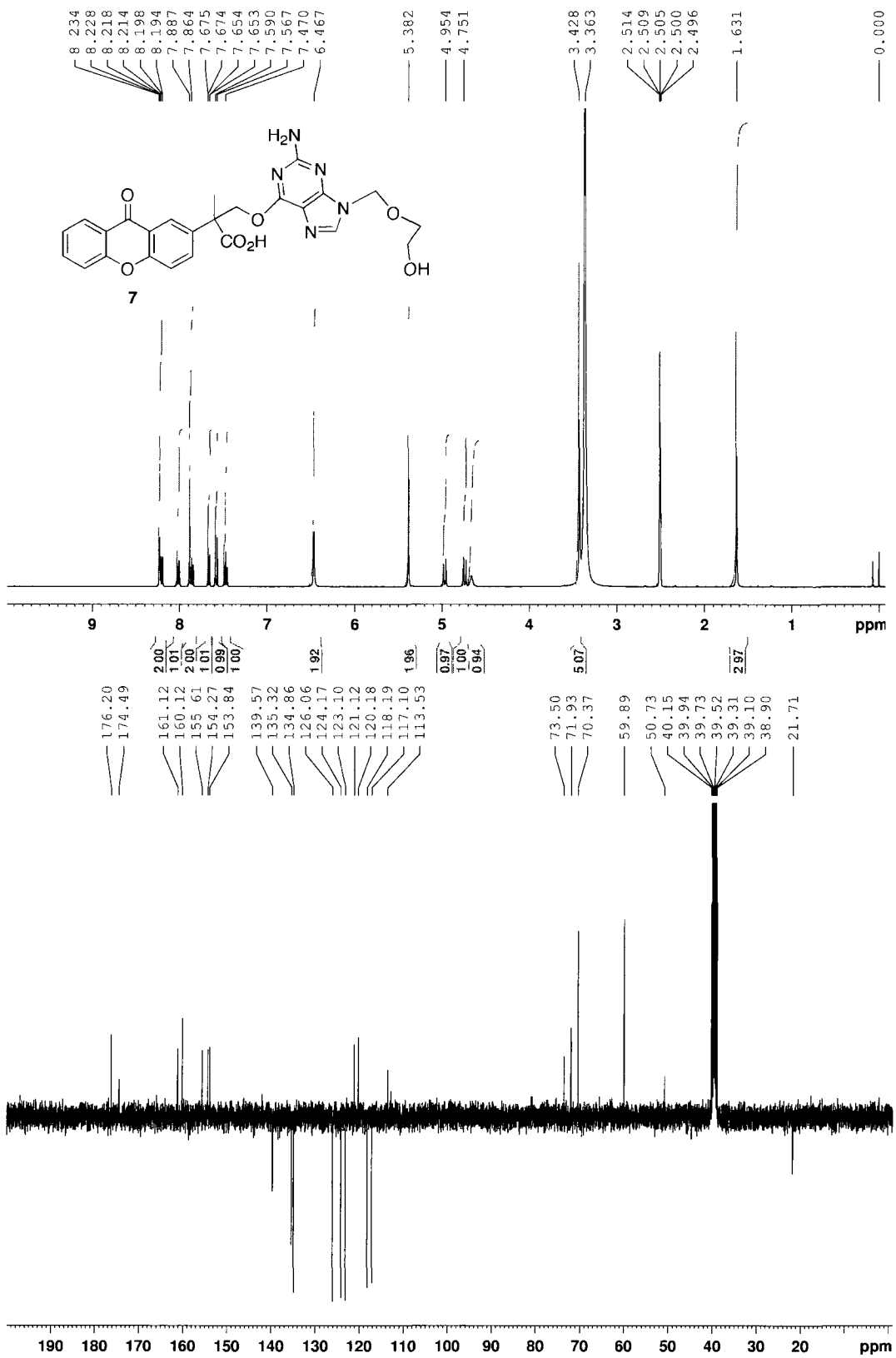
8.234
8.228
8.218
8.214
8.198
8.194
7.887
7.864
7.675
7.674
7.654
7.653
7.590
7.567
7.470
6.467
5.382
4.954
4.751
3.428
3.363
2.514
2.509
2.505
2.500
2.496
1.631
0.000
H2N
N
N
O
O
N
N
O
CO2H
O
OH
7
9
8
7
6
5
4
3
2
1
ppm
2.00
1.01
2.00
1.01
0.99
1.00
1.92
1.96
0.97
1.00
0.94
5.07
2.97
176.20
174.49
161.12
160.12
155.61
154.27
153.84
139.57
135.32
134.86
126.06
124.17
123.10
121.12
120.18
118.19
117.10
113.53
73.50
71.93
70.37
59.89
50.73
40.15
39.94
39.73
39.52
39.31
39.10
38.90
21.71
190
180
170
160
150
140
130
120
110
100
90
80
70
60
50
40
30
20
ppm